Performance comparison of wind park configurations

Stefan Lundberg

Department of Electric Power Engineering
CHALMERS UNIVERSITY OF TECHNOLOGY
Göteborg, Sweden 2003

Technical Report

Performance comparison of wind park configurations

Stefan Lundberg

Department of Electric Power Engineering
CHALMERS UNIVERSITY OF TECHNOLOGY
Göteborg, Sweden 2003

Performance comparison of wind park configurations

Stefan Lundberg

Technical Report No. 30R
ISSN 1401-6176

Department of Electric Power Engineering
School of Electrical Engineering
Chalmers University of Technology
SE-412 96 Göteborg
Sweden
Telephone + 46 (0)31 772 1000

Department of Electric Power Engineering
Göteborg, Sweden 2003

Abstract

In this report, layouts of various large-scale wind parks, both AC as well as DC, are investigated. Loss modelling of the wind park components as well as calculations of the energy capture of the turbines using various electrical systems are performed, and the energy production cost of the various park configurations is determined.

It was found that from an energy capture point of view, the difference in energy production between various wind turbine systems is very small. In addition, a study of the suitability of various DC/DC-converters is made. Three DC/DC-converters, Boost, Full Bridge and Full Bridge Isolated Boost, are found to be interesting candidates as the "transformer" component in potential DC-based wind parks.

Of all the investigated wind park configurations, the wind park with the series connected DC wind turbines seems to have the best potential to give the lowest energy production cost, if the transmission distance is longer then 10-20km.

Acknowledgement

This work has been carried out at the Department of Electric Power Engineering at Chalmers University of Technology. The financial support given by the Swedish National Energy Agency and ABB Power Technologies is gratefully acknowledged.

Many thanks also goes to the steering and reference group of this project: Torbjörn Thiringer, CTH, Tore Undeland, CTH, Mats Hyttinen, ABB, Jan Svensson, ABB, Pehr Hjalmarsson, ABB, Anders Lasson, ABB, Peter Christensen, NVE, Kent Søbrink, Eltra and Christer Liljegren, CLEPS AB.

Contents

Chapter 1

Introduction

1.1 Problem background

Wind energy converters are becoming larger and larger and more and more erected in groups rather than one by one. Today wind farms up to a size of 160 MW are being built and several plans on 1000 MW-parks exist. These larger wind parks are mainly considered to be located out in the sea, preferably at such a distance that they cannot be observed from the shore. The size of the wind parks has led to a problem of finding a suitable grid connection point, which is strong enough to take care of the power from the wind parks. This leads to that in many cases the distance between the grid connection point and the wind park is so long, that a DC-transmission may become more favorable than a conventional AC-transmission. This is due to the well known problem with capacitive current generation of AC-cables, which makes the possible length of an AC-cable limited. This is further stressed by the fact that it is extremely difficult to get permission to build new over-head lines, and therefore it must be taken into consideration that it might be necessary to use DC-cables also for the land transmission.

All of this lead to interesting issues like: When is DC-transmission more feasible than AC-transmission? If DC is used, how far down in the wind park can we have DC? How should DC/DC converters be designed? How should large-scale parks be designed?

1.2 Overview of previous work

Wind park design studies have been presented in several papers, for instance [2, 24, 26, 31, 42, 43, 45, 54]. The most detailed study was made by Bauer, Haan, Meyl and Pierik [6]. In [30] some interesting DC solutions for offshore wind parks are presented and especially the proposal of a wind park with wind turbines connected in series, is of great interest. The energy production of various wind parks is calculated in [31, 39, 47], and in [24, 31, 44, 47, 49] the estimated cost of the produced electric energy is presented. In [5] the economics of some offshore wind farms that are build and are planned to be built, are presented.

Of importance when determining the energy capture is to have detailed blade data as well as detailed loss models of components. Relevant blade data is not trivial to obtain, but previous authors have most likely used the same method as here: By

not revealing the origin of the blade description, it is possible to obtain such data. Generator loss models has for instance been presented in [22, 44], gear-box losses have been found in [22]. However, available loss models of existing high power DC/DC-converters are very crude.

Cost data is another large problem area. Here the same principle seems to be dominant: Data can be obtained providing that the sources are not revealed. However, in [10, 32, 38, 47, 49] valuable cost information is given which can be utilized.

Energy capture calculations of wind turbine systems and wind farms is a subject in which it is possible to find much information in the literature. However, detailed comparisons between different electric generating systems for wind turbines are not so common. As a part of the present work article [36] was published where a detailed comparison between electric generating systems for wind turbines was studied.

1.3 Purpose of the report

The purpose of this report is to investigate the energy capture and energy loss of different wind park configurations and also to compare the energy production cost of the configurations.

1.4 Layout of report

In chapter 2 the six different wind park configurations that are investigated in this work are presented. Some of the general boundary conditions are presented in this chapter also.

In chapter 3 the principle of converting kinetic energy of the air flow through the rotor disc to mechanical power on the wind turbine shaft is explained.

In chapter 4 different wind turbine systems are investigated, both AC and DC systems. The energy capture of the different wind turbine systems are compared in order to make the selection of which wind turbine system that shall be used in the study of the wind parks.

In chapter 5 the energy production cost of the six wind park configurations are shown for some different cases. The energy production cost of the configurations are compared and the wind park selection is discussed depending on the transmission distance and the rated power of the wind park.

In chapter 6 the conclusions are presented.

In appendix A different DC/DC converter topologies are investigated. The investigation focuses on choosing the DC/DC converter topology that utilizes the semiconductors best.

In appendix B the loss models of the components in the wind park are derived.

In appendix C the cost models of the components in the wind park are presented.

Chapter 2

Wind park configuration

In this chapter, the different wind park configurations that are investigated in this work are described. The boundary conditions for the investigation are explained and the different transmission systems are described.

2.1 General wind park layout

Generally, the wind parks investigated in this work can be represented by the sketch presented in figure 2.1. As seen in figure 2.1 the wind park consists of a number of

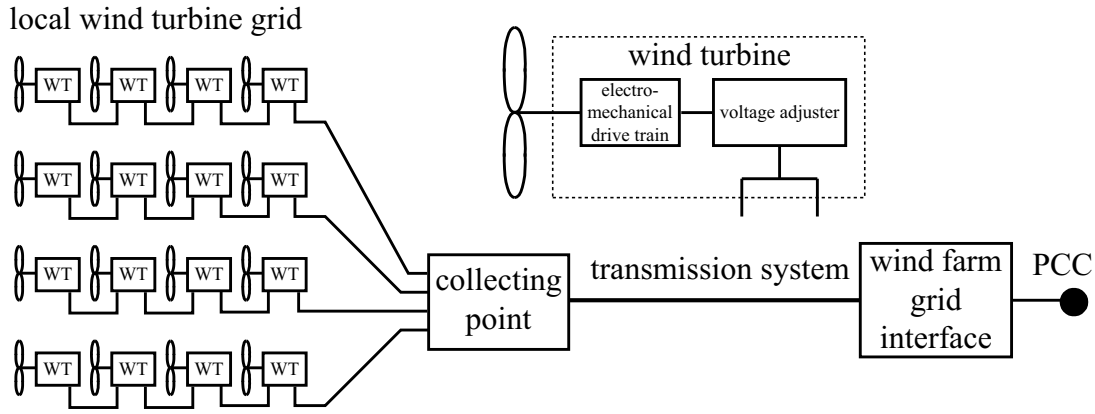

Figure 2.1: General wind park layout.

elements, wind turbines (WT), local wind turbine grid, collecting point, transmission system, wind park interface to the point of common connection (PCC). It shall be noticed that all wind turbines in this work have a voltage adjusting unit (AC or DC transformer) included in the wind turbine unit itself. The local wind turbine grid connects the wind turbine units to the collecting point. The wind turbine units are connected in parallel to radials, unless otherwise is specified in this work. In the collecting point, the voltage is increased to a level suitable for transmission. The energy is then transmitted to the wind park grid interface over the transmission system. The wind park grid interface adapts the voltage, frequency and the reactive power of the transmission system to the voltage level, frequency and reactive power demand of the grid in the PCC.

2.1.1 Rated power of the wind park, Number of turbines

The size of the wind turbines has in this project been selected to 2MW, since these turbines are available for all kinds of wind energy systems today. However, it should be pointed out that the main results of this study would most likely not be very different if another turbine size would have been selected. Almost all wind turbines considered in this work has a rated generator voltage of 690V. Most likely, the generator voltage will be increased when the rated power of the generator is increased in order to decrease the losses. For example NEG Micon has chosen 960V in their 2MW wind turbine [34].

This work focuses on four sizes of wind parks

- 60MW
- 100MW
- 160MW
- 300MW

Although most wind parks today are much smaller then 60MW, 60MW is used as a small wind park here. Horns Ref is one example of a 160MW offshore wind park $14-20$km out of the west coast of Denmark [4]. It is today (2003) the largest built sofar. No larger wind parks than 300MW is taken under consideration in this work due to the fact that if a larger wind park is going to be build it will probably be divided into smaller modules, where a maximum module size of 300MW seems appropriate. Two advantages using modular building of wind parks are, that the investment cost of the whole wind park is spread out over a longer period and that part of the production can start before the whole park has been built. Another advantage of this division is that if cross connections between the modules are made, the park can be more fault tolerate.

2.1.2 Distances between the wind turbines

In this work the wind power plants will be placed in a grid with 7 rotor diameters between the turbines in both directions. This seems to be a commonly used distance and at Horns Rev the distance is 7 rotor diameters [4]. The distance between wind turbines in the wind direction can not be too small. This is due to the fact that when the wind passes through the rotor of the wind turbine it gets very turbulent and the wind speed is decreased. This means that if the wind turbines are located to close to each other, the wind will be more and more turbulent after it passes each wind turbine. This would lead to that wind turbines downstream in the wind park, are subjected to aerodynamical stresses, may even have to be shut down due to that the mechanical loading gets to high during difficult conditions. In addition, the energy losses due to the reduced wind speed will be significant if the wind turbines are put to close to each other. The minimum length to avoid this is approximately 5-7 rotor diameters.

Of course, if the wind is mainly coming from one direction, the wind turbines can be placed closer in the direction perpendicular to the prevailing winds. But for the Nordic countries, wind directions from northwest to south are quit normal, which means that the wind turbines should be placed with an equal distance in all directions.

In this work, it is thus assumed that the wind turbines are put in a grid with 7 rotor diameters between. The distance from the column nearest the collecting point to the collecting point is also 7 rotor diameters, see figure 2.1.

Since 7 rotor diameters was used, it was possible to neglect the wake effects. Anyway, if wake effects were taken into account, it would not affect the comparison between different wind park configurations very much. In addition, there is a lack of available, simple and good models for calculating the wake effect in steady-state.

2.2 Electrical system configuration

In this section, the different electrical systems for the wind parks are described. For all systems, the main grid voltage in the PCC is assumed to be constant.

2.2.1 AC/AC

All wind parks that have been build today have an AC electrical system from the wind turbines to the PCC. In this work, two different AC-systems are investigated, referred to as the small and the large AC wind park. Three core cables are used for AC transmission throughout this work.

The first configuration to be discussed is the small AC wind park. The idea with the small AC wind park, is that it should be suitable for small wind parks with a short transmission distance. In the small AC wind park, the local wind park grid is used both for connecting all wind turbines in a radial together and to transmit the generated power to the wind park grid interface, which is shown in figure 2.2. For this system

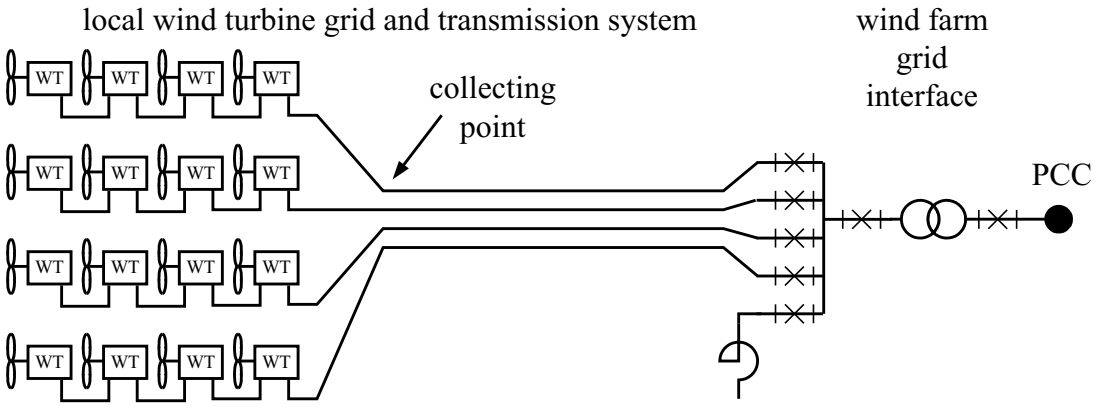

Figure 2.2: The electrical system for the small AC wind park.

the cables in the local wind park grid are assumed to be installed one and one from the wind turbines to the collecting point. From the collecting point to the wind farm grid interface all cables are assumed to be installed together. This means that there is one cable installation cost per cable from the wind turbines to the collecting point and only one cable installation cost for all cables from the collecting point to the wind park grid interface.

Let us now study a slightly different configuration, the large AC wind park. The large AC wind park system is a more traditional system, based on the general system

in figure 2.1. This system has a local wind park grid with a lower voltage level (20-30kV) connected to a transformer and a high voltage transmission system. This system requires an offshore platform for the transformer and switch gear, as can be seen in figure 2.3. Horns Rev wind park is build according to this principle. For this system

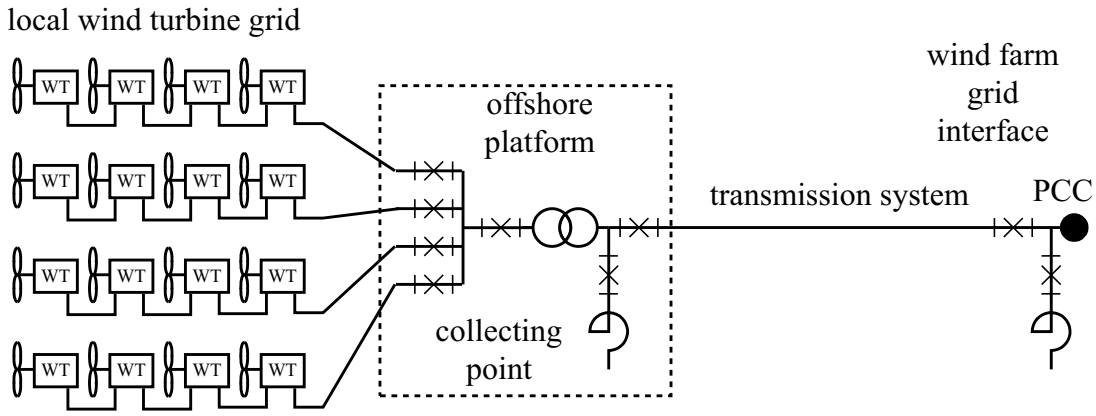

Figure 2.3: The electrical system for the large AC wind park.

there is one cable installation cost per cable, due to the fact that all cables have different routes.

2.2.2 AC/DC

In this system the AC transmission in figure 2.3 has been replaced with a DC transmission, this wind park will be referred to as the AC/DC wind park. This type of system does not exist today but is frequently proposed when the distance to the PCC is long, or if the AC grid that the wind park is connected to is weak. The system is shown in figure 2.4. In this system we have an independent local AC system in which both the voltage and the frequency are fully controllable with the offshore converter station. This can be utilized for a collective variable speed system of all wind turbines in the park. The benefits with this are that the aerodynamic and electrical efficiency can be increased.

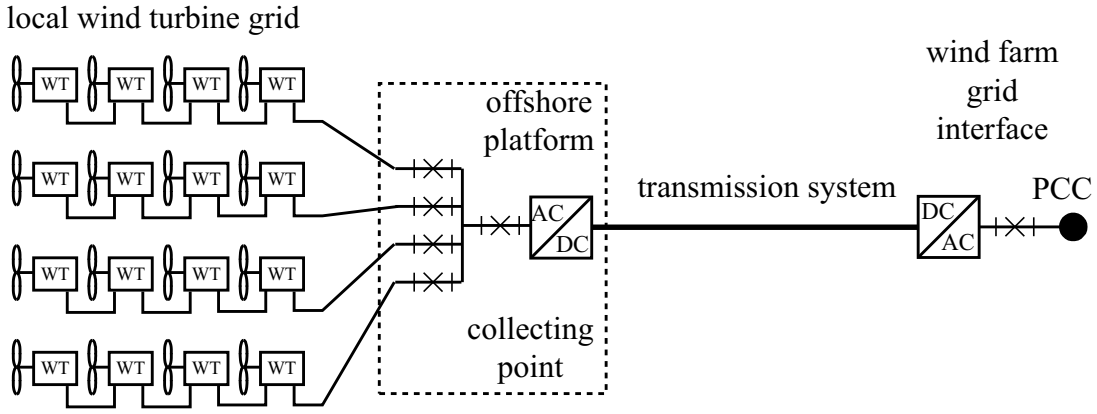

Figure 2.4: The electrical system for the AC/DC wind park.

The installation cost of the cables are the same as for the large AC wind park. The two DC transmission cables, one for the positive pole and one for the negative pole, are assumed to be installed together and therefore there is only one cable installation cost for these two cables.

2.2.3 DC/DC

For the pure DC wind park, three different configurations are investigated. Two that are based on the two layouts of the AC systems, referred to as the small DC wind park and the large DC wind park, and one configuration with the turbines in series, as shown in [30]. In all DC configurations in this work, the two cables, one for the positive pole and one for the negative pole, are assumed to be installed together and are therefore referred to as one cable.

The electrical system for the small DC wind park is shown in figure 2.5. As can be

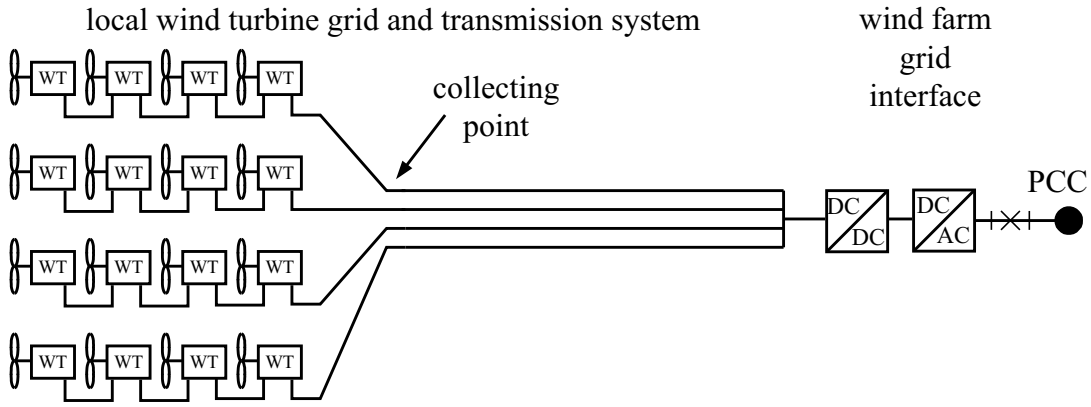

Figure 2.5: The electrical system for the small DC wind park.

noticed, the electrical system for the small DC wind park is identical to the system of the small AC wind park. The only difference is that the transformer in the wind park grid interface is replaced with a DC transformer and an inverter. Of course, a rectifier is needed in each wind turbine. The advantage of the small DC park compared to the large DC park is, as for the small versus large AC park, that it does not require an offshore platform. The installation cost of the cables are assumed to be the same as for the small AC wind park.

The configuration of the electrical system for the large DC wind park can differ somewhat from the configuration of the large AC wind park. The difference is if it requires one or two transformations steps to increase the DC voltage from the wind turbines to a level suitable for transmission. It is assumed that if the DC voltage from the wind turbines is high enough (20-40kV) only one transformation step is required. But if the output voltage of the wind turbine is lower (5kV), two steps are required. In figure 2.6 this system is presented with two DC transformer steps. For the large DC wind farm with two transformation steps, all wind turbines are divided into smaller clusters. All wind turbines within one cluster are connected one by one to the first transformation step. The high-voltage side of the first DC transformer step are then connected to the second step, as can be noticed in figure 2.6. If only one step is used, the wind turbines are connected in radials directly to the second DC transformer step,

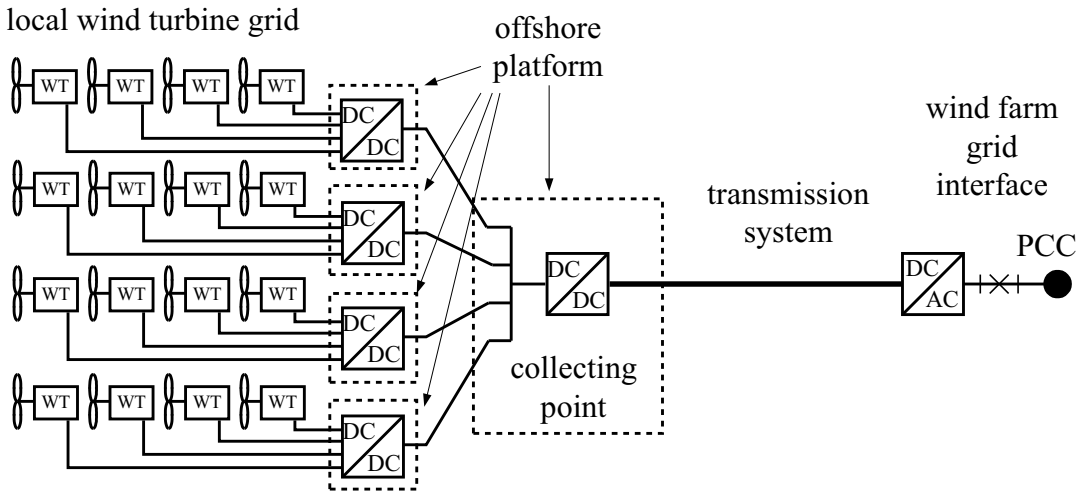

Figure 2.6: The electrical system for the large DC wind park with two DC transformer steps.

similarly as for the large AC wind park in figure 2.3. For this system there is one cable installation cost per cable, due to the fact that all cables have different routes.

In the third DC system shown in figure 2.7 the wind turbines are connected in series, as mention before, in order to obtain a voltage suitable for transmission directly. This system is referred to as the series DC wind park. The benefit of this system is that

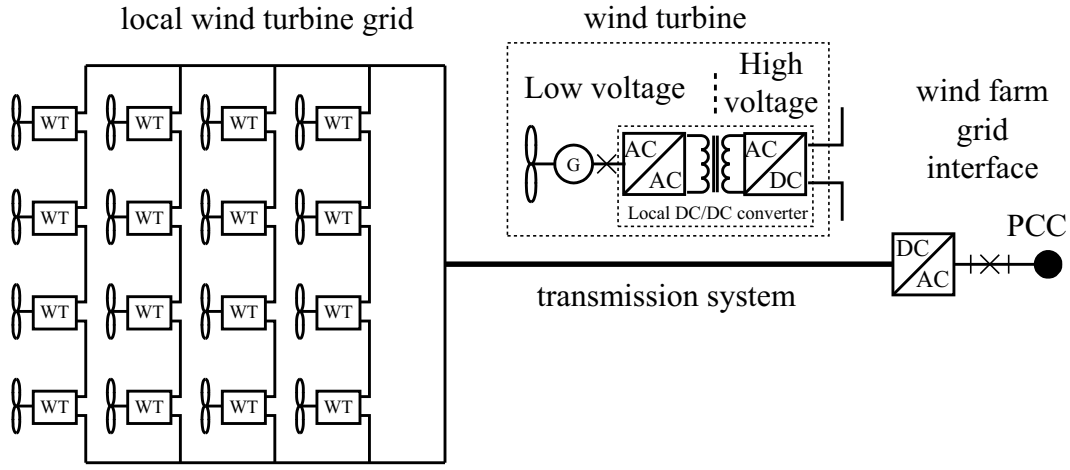

Figure 2.7: DC electrical system with series connected wind turbines.

it, in spite of a relatively large possible size, does not require large DC-transformers and offshore platforms. The voltage insulation in the wind turbines is taken by the transformer in the local DC/DC converter. The drawback with this configuration is that the DC/DC converters in the wind turbines must have the capability to operate towards a very high voltage. This is due to the fact that if one wind turbine does not feed out energy and therefore it fails to hold the output voltage, then the other turbines must compensate for this by increasing their output voltage.

For this system, there is one cable installation cost per cable, due to the fact that all cables have different routes, as can be noticed in figure 2.7.

Chapter 3

Short about aerodynamic energy conversion of wind turbines

3.1 Wind speed distribution

The wind speed can be treated as a continuous random variable. The probability that a given wind speed shall occur can be described with a density function. There are several density functions which can be used to describe how the wind speed is distributed. The two most common are the Weibull and the Rayleigh functions. The Rayleigh distribution, or chi-2 distribution, is a subset of the Weibull distribution. The Weibull distribution is described by [25]

$$f(w_s) = \frac{k}{c}(\frac{w_s}{c})^{k-1}\mathrm{e}^{-(w_s/c)^k}. \tag{3.1}$$

Where:

$f(w_s)$	Probability density
w_s	Wind speed > 0 [m/s]
k	Shape parameter > 0
c	Scale parameter > 0

Comparisons with measured wind speeds over the world show that the wind speed can be reasonably well described by the Weibull density function if the time period is not too short. Periods of several weeks to a year or more is usually reasonably well described by the Weibull distribution but for shorter time periods the agrement is not so good [25]. The average wind speed can be calculated by using the equation for calculating the expectation value of a continuous random variable, which gives

$$w_{s,AVG} = \int_0^\infty w_s f(w_s)\mathrm{d}w_s = \frac{c}{k}\Gamma(\frac{1}{k}) \tag{3.2}$$

where Γ is Euler's gamma function

$$\Gamma(z) = \int_0^\infty t^{z-1}\mathrm{e}^{-t}\mathrm{d}t. \tag{3.3}$$

If the shape parameter, k, is equal to 2 the Weibull distribution is equal to the Rayleigh distribution. The advantage of the Rayleigh function is that it only depends on the scale

parameter, which is dependent only on the average wind speed. The scale parameter, c, can be calculated by equation 3.4 for a given average wind speed

$$c = \frac{2}{\sqrt{\pi}} w_{s,AVG} \quad \text{for} \quad k = 2, \quad \Gamma(\frac{1}{2}) = \sqrt{\pi}. \tag{3.4}$$

In figure 3.1 the Rayleigh distribution function is shown for different average wind speeds. Average wind speeds of 5.4m/s and 7.2m/s correspond to a medium and high

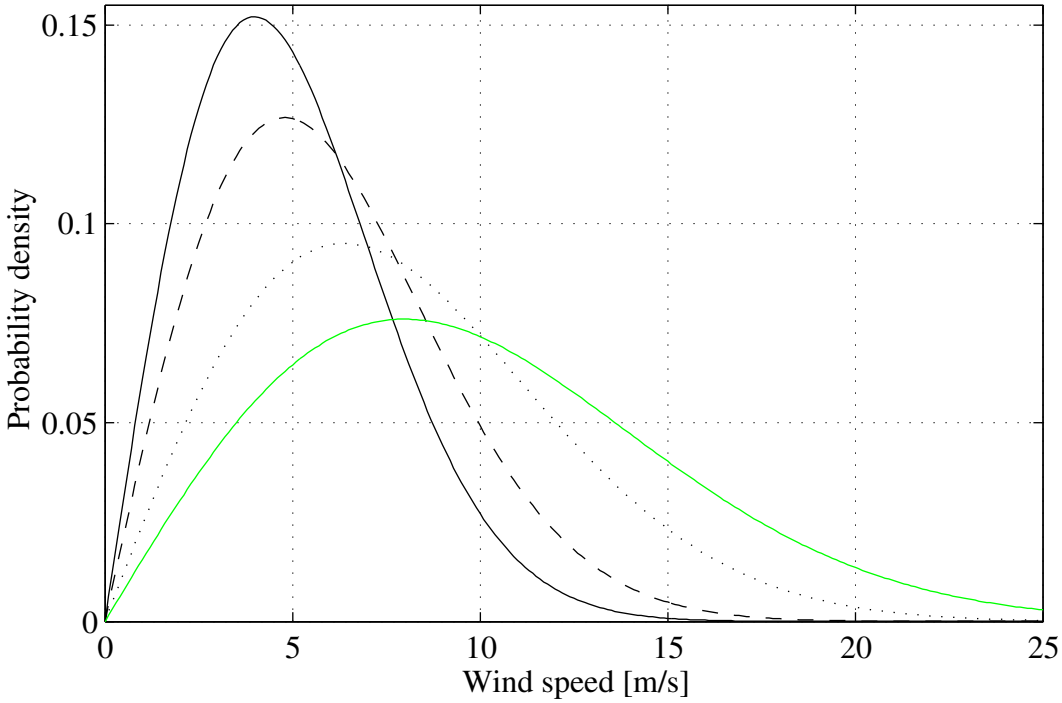

Figure 3.1: Rayleigh distribution function for different average wind speeds, solid 5m/s, dashed 6m/s, dotted 8m/s and grey 10m/s.

wind site in Sweden respectively, according to [50], and an average wind speed of 9.7m/s is found at Horns Rev [4]. The Rayleigh distribution is used in this work to describe the distribution of the wind speed.

3.2 Operating principle of a wind turbine

A wind turbine consists of a tower, a nacelle and a rotor. The rotor converts wind energy to mechanical energy. In the hub, the drive train is located. In the drive train, the mechanical energy is converted into electrical energy. The drive train consists of one or several shafts, generator and usually a gear-box.

A wind turbine has a specific rating. Sizes year 2003 are up to 4.5MW [16]. The rated power level is reached at a wind speed of 12-15m/s, and the wind speed when the rated power is reached is referred to as rated wind speed. Below rated wind speed the turbine tries to capture as much energy as possible from the wind, a value of the electric output power of about 40% of the available power in the wind is what can be obtained. Below 3-4m/s there is so little energy available in the wind so the turbine stops. At

wind speeds above rated, the operation principle is different. The wind turbine rotor must now limit the incoming power to the rated shaft power. This is done by utilizing the blades. Either the blades are turned out of the wind, pitch control, or the blades are designed in such a way that the flow becomes disturbed and the blades loose their efficiency, stall control.

As mention before, the rotor blades convert some of the kinetic energy of the wind to mechanical energy on the rotor shaft. The efficiency of this conversion depends on several factors such as blade profiles, pitch angle, tip speed ratio and air density. The pitch angle, β, is the angle of the blades towards the rotational plane. If the pitch angle is low, the blades are almost perpendicular to the wind and if it is high (near 90 degrees) the blades are almost in parallel with the hub direction. The tip speed ratio, λ, is the ratio between the tip speed of the blades and the wind speed, equation 3.6. The conversion from wind speed to mechanical power can in steady state be described by [25]

$$P_{mec} = \frac{\pi \rho w_s^3 R^2}{2} C_p(\lambda, \beta) \tag{3.5}$$

$$\lambda = \frac{\omega_t R}{w_s}. \tag{3.6}$$

Where:

R	rotor radius [m]
ω_t	rotor speed [rad/s]
ρ	air density = 1.225 [kg/m^3]
w_s	wind speed [m/s]
λ	tip speed ratio
β	pitch angle
$C_p(\lambda, \beta)$	aerodynamic efficiency

In figure 3.2 the mechanical power and the aerodynamic efficiency for the blade profile used in this report is shown for different pitch angles and for a fixed rotor speed.

3.2.1 Stall control

From figure 3.2 it can be noted that if the pitch angle is kept at 0^o the turbine automatically limits the output power to a maximum of 1.2 p.u., for -1^o the power is limited to a maximum of 1.0 pu using the same rotor speed in the whole wind speed interval. As can be noted, the power reaches a maximum around 15 m/s and then decreases for higher wind speeds.

Stall control in combination with fixed speed was the dominating concept for wind turbines earlier. The reason is, of course, that it is cheaper to have blades that do not need a pitching mechanism. Moreover, power electronic equipment was too expensive earlier and therefore induction generators connected to the grid without power electronic equipment were used.

However, for MW size turbines, stall control has been considered to be unfeasible. One important reason is the emergency breaking of the turbine. If the blades can not be turned, the turbine must have a very large brake on the primary shaft. But if turnable blades are used, and in particular if each blade has its own emergency pitching system, this can replace the large main shaft brake. Instead it is sufficient to only have a much smaller parking brake.

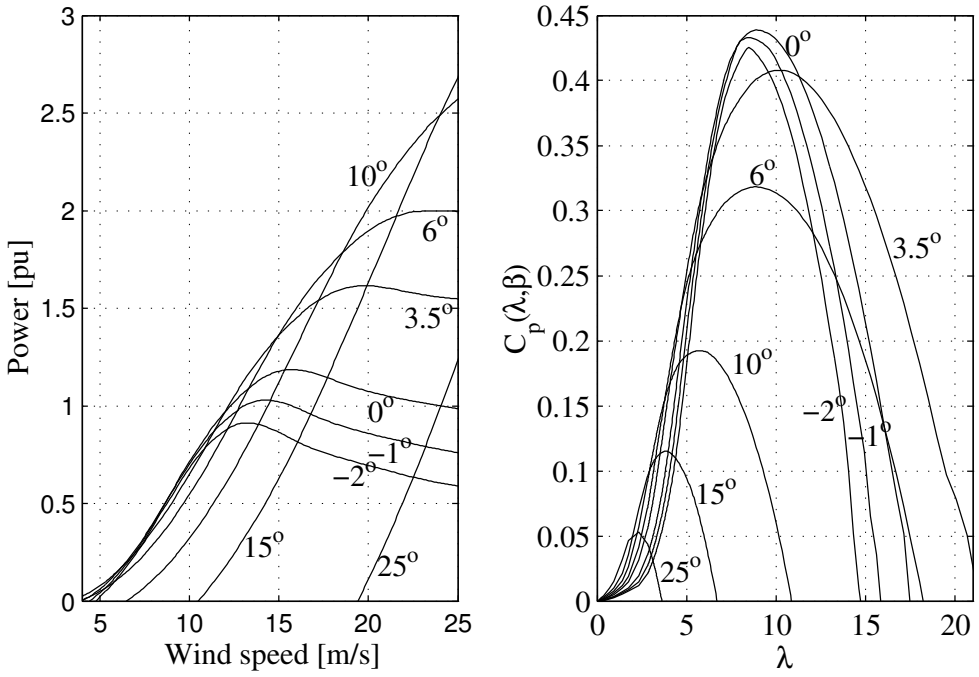

Figure 3.2: The mechanical power as function of wind speed and pitch angle for a fixed rotor speed,left plot, and the aerodynamic efficiency as function of λ and pitch angle, right plot.

3.2.2 Active stall control

If a pitching mechanism is available, a possibility is to slightly modify the pitch angle at high wind speeds also for turbines without a power electronic converter. When the wind speed is 15m/s a pitch angle of -1^o is used, but for 25m/s an angle of 0^o is used instead. In this way, the power level is kept at the rated value in the whole high wind speed region. In addition, the benefits of using a smaller brake and facilitated starting and emergency stopping is obtained.

3.2.3 Pitch control

Another way of obtaining a constant power level at high wind speeds is to turn the blades out of the wind, i.e. to increase the pitch angle. At 12 m/s a pitch angle of 0^o is used, at 17m/s 15^o and at 24 m/s and angle of 25^o is used, according to figure 3.2. The advantage of using pitch control instead of active stall control is that the thrust force (pressure on the turbine disc) is lower.

3.3 Dynamic aspects of aerodynamic power control

If fixed rotor speed is used there is a large drawback with using pitch control, there will be large power variations at high wind speeds. Let us consider the following case: The turbine is operating at 13 m/s with a pitch angle of 6^o. The power is now 1 pu. The wind speed increases rapidly to 15m/s and suddenly the power level is now 1.3 pu. The pitch controller has to increase the pitch angle to 10^o and the power error is eliminated.

However, if a new wind speed change occurs a new power pulsation is created. As can be noted from figure 3.2 this situation does not occur when using stall control. If we have a pitch angle of -1^o we can note that wind speed changes in the high wind speed area lead to very small power variations. This has led to that fixed-speed turbines are almost all stall-controlled, either passive or active.

However, if the rotor speed can be varied, pitch control becomes much more favorable. In this case the incoming power fluctuations can instead be taken up by changing the amount of energy stored in the rotor i.e. by adjusting the rotor speed. The wind turbine rotor thus acts as an active low-pass filter for power fluctuations. Variable rotor speed can of course also be used in combination with stall or active stall, but the advantage of using pitch control is, as mentioned, that the thrust force is lowered. This has led to that almost all variable-speed turbines are pitch regulated.

3.4 Variable speed wind turbines

As can be noted from figure 3.2, the right one, the maximum efficiency of the investigated turbine occurs at λ equal to 9. For the fixed-speed turbine λ is higher than 9 for lower wind speeds, and accordingly the efficiency of the fixed-speed rotor is lower than optimal at lower wind speeds. For the variable-speed turbine, it is possible to maximize the mechanical power by using a variable rotational speed of the wind turbine. This means that the pitch angle is kept constant at low wind speeds, zero in this case, and the rotational speed of the turbine is adjusted according to the actual wind speed so that λ always equals 9. This means that the turbine will work at the maximum efficiency which gives the maximum mechanical output power of the turbine, in the low wind speed region.

It should be kept in mind that the energy benefit is not the main reason for using variable speed, instead it is the reduced stresses on the turbine that is the main advantage. Also the fact that variable-speed turbines are capable of controlling the reactive power is an important reason for selecting a variable-speed turbine.

The upper rotational speed is limited by the mechanical stresses on the blades and the noise level, high speed results in large stresses on the blades and high noise levels [27]. In [41] it is stated that for a 1.5MW wind turbines the rotor diameter is approximately 64 to 66m and the rotational speed at rated wind speed is approximately 19 to 23.5rpm. Corresponding data for a 2MW wind turbine are: 80m rotor diameter and max rotor speed 19rpm. For the 2MW wind turbines in this work the rotor diameter is set to 80 m and the rotational speed at rated wind speed is set to 19rpm.

Today, two variable speed systems with different electrical generator systems are common: Full range variable speed or limited speed range system. Both systems have the same upper speed limit due to the noise level and mechanical stresses. It should be pointed out that, the upper rotor speed limit is an average limit. Shortly the speed is allowed to be above the average limit in order to reduce the mechanical stresses due to the power fluctuations originating from the wind speed variations. The full range variable speed system has no lower speed limit, the rotational speed is controlled so that λ equals 9 also at the lowest wind speeds. The purpose is, as mentioned, to have the highest efficiency of the wind turbine in the low wind speed region. In the limited speed range case there is a lower average speed limit apart from the upper one. Normally for the limited speed range systems the speed band is $\pm 30\%$ from synchronous speed [23].

Chapter 4

Energy efficiency comparison of wind turbine systems

In this chapter the different wind turbines used in this work are examined and the energy efficiency is compared in steady state. The energy conversion of the rotor is modelled using equation 3.5 and the rated (maximum) shaft power from the turbine is set equal for all wind turbine systems. This was made in order to make the comparison as comparable and relevant as possible. The losses of the other components in the wind turbine are modelled in appendix B. This means, that in this chapter only the results are presented, the loss calculations leading to the results are found in appendix B.

4.1 AC wind turbines

There exists several different types of wind turbines with an AC interface to the grid. In this work the most common wind turbine types that is produced today for high power applications (above 1MW) is taken under consideration.

4.1.1 Fix speed wind turbine

The fix speed wind turbine has been the most commonly used wind turbine type so far. This depends on that it has a very robust design with few components. The system is presented in figure 4.1. The weakest component is the gearbox which has to take

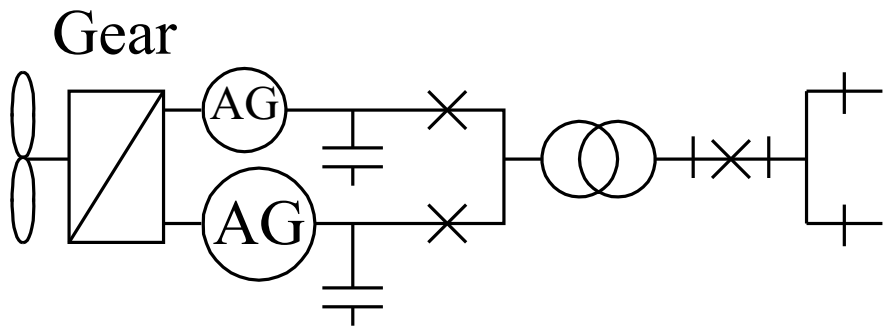

Figure 4.1: Principal scheme of the 2MW fix speed turbine, with two generators.

up a lot of torque pulsations. This is due to the fact that the turbine has an almost

fixed speed and can story very little energy from the incoming power pulsations. These pulsations are also seen in the output power from a fix speed wind turbine and they cause fast voltage fluctuations on the grid [3, 29, 37]. For a wind park, these caused voltage pulsations are not a problem from a grid point of view, since they are smothered out when several turbines are connected [28, 35, 48].

The efficiency of the fix speed turbine is increased by having two different generators, one larger and one smaller. The small generator has a lower rotational speed and is used at low wind speeds to increase the aerodynamical as well as the generator efficiency of the turbine (operation close to the ideal λ at low wind speeds and reduced iron losses). At higher wind speeds, the larger generator is used. In figure 4.2 the active and reactive powers for this system are shown, solid and dashed line, respectively. The switch over point between the generators in this work can be noticed in figure 4.2 as the knee of the solid line at 6.7m/s. The dotted line in figure 4.2 shows the output power from the wind turbine if the large generator had been used also for low wind speeds. By comparing the dotted line with the solid line for low wind speeds, the increase in efficiency by having two different generators is clearly seen. Due to this increase in efficiency the two generator system is the only one considered in this work.

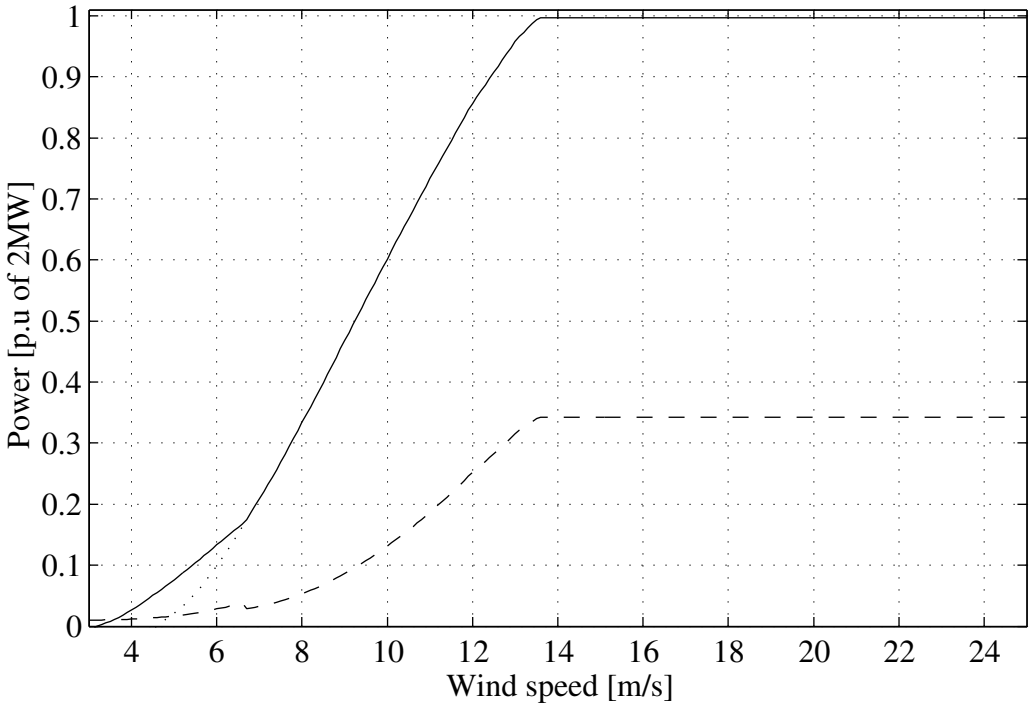

Figure 4.2: The produced active power to the grid is shown (solid) and the reactive power drawn from the grid (dashed) for the 2MW fix speed turbine. Dotted line shows the output power from the wind turbine if the large generator is used for low wind speed also.

A drawback of the fix speed wind turbine system is that the reactive power can not be controlled. The capacitors shown in figure 4.1 are only used to compensate for the no-load reactive power consumption of the generators. This means that the reactive power consumption of the wind turbine will increase when the power production

increase, as can be seen in figure 4.2 (dashed line). If the reactive power consumption is to be compensated for more, electronically switched capacitors or an SVC can be used. Due to the fact that if the generator is compensated more then for the no-load consumption of reactive power there is a risk that the generator will be self excited which leads to severe over-voltages.

As mention before, the generator used at low wind speeds has a lower rated power then the generator used for high wind speeds. Due to the lower rated power, the generator no-load losses of the system are lower, and accordingly the total generator losses can be reduced at low wind speeds. This can be noticed in figure 4.3 where the losses of the 2MW fix speed wind turbine is shown. The switch between the different generators can be noticed as the step at 6.7m/s in the losses for the generator (black dashed line). The dashed grey line shows the generator losses of the large generator, if it would have been used for low wind speeds also. By comparing the grey and the black dashed line for low wind speeds it is noticed that an improvement of the generator efficiency by approximately 0.9% at low wind speeds is obtained by having two different generators.

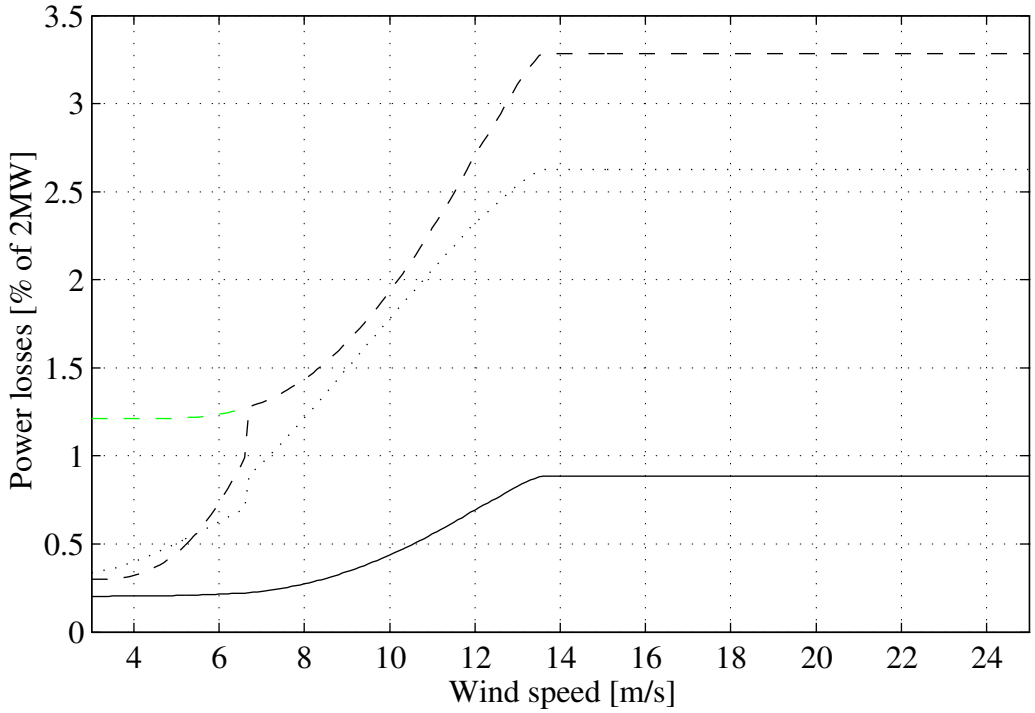

Figure 4.3: The losses for the turbine, solid transformer losses, black dashed generator losses and dotted gearbox losses. Grey dashed line shows the losses of the large generator if it would have been used at low wind speeds also.

4.1.2 Limited speed range wind turbine

There is a trend among the largest manufactures of wind turbines in the MW size towards the limited speed range wind turbine configuration [23]. The key component in this system is an asynchronous generator with a wound rotor and slip rings, also called Doubly-Feed Induction Generator (DFIG). The converter is connected to the rotor circuit via the slip rings and the stator circuit is connected directly to the transformer, as can be seen in figure 4.4. This system is discussed more in detail in appendix B.2.3.

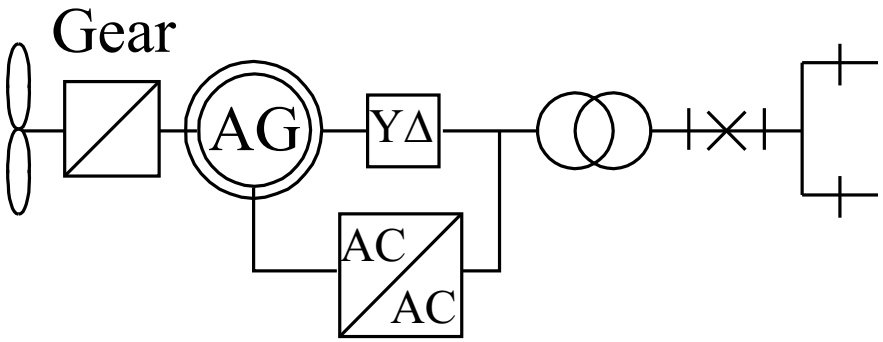

Figure 4.4: Principal scheme of the 2MW limited speed range wind turbine.

This system can be optimized to produce maximum energy by choosing the speed range and the stator to rotor winding ratio appropriately [36]. The speed range around synchronous speed is approximately equal to the power through the converter. A common speed range is ±30% from synchronous speed, see [23], which gives that the maximum power through the converter is 30% of the rated power, [36] and figure B.7. The fact that only a part of the power goes through the converter is the main advantage of this system, which gives a smaller converter (cheaper) and also lower losses.

In [36] it is shown that if the stator of the generator is connected in Y for low wind speeds and in Δ for high wind speeds the energy production can be increased by up to 1.2%. The $Y\Delta$ switch is shown in figure 4.4. This way of increasing the energy production of the DFIG system is used in this work as standard for the DFIG system.

In figure 4.5 the losses of the limited speed range wind turbine are shown. The switch from Y to Δ connection of the stator is seen at 8.7m/s as a step in the losses of the converter (grey line). If only the efficiency of the generator is studied it can be noticed that the losses of the DFIG is lower at rated power compared to the fix speed system in figure 4.3. This is mainly due to that the losses in the stator winding is lower, due to that 30% of the power is taken out through the rotor and therefore the stator current is approximately 30% lower.

The asynchronous generator can be magnetized through the rotor which gives that if it is desired, it is only the active power that is fed out from the stator. The converter side connected to the transformer, can also be used to generate or consume reactive power. This leads to that the semi variable wind turbine can produce power with a power factor equal to one in the whole wind speed region.

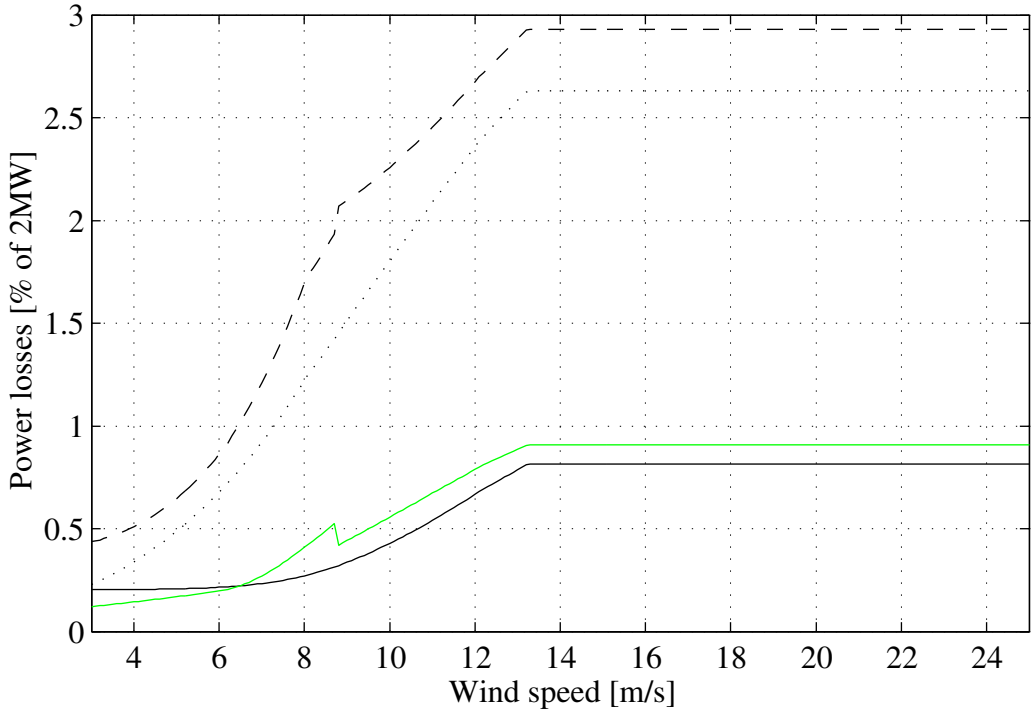

Figure 4.5: The losses of the 2MW limited speed range wind turbine. Solid transformer losses, dashed generator losses, dotted gearbox losses and grey converter losses.

4.1.3 Full range variable speed wind turbines

The "full range variable speed" wind turbines in this work uses a full power converter connected between the stator of the generator and the wind turbine transformer, as shown in figure 4.6. For the full range variable speed systems, the reactive power to the grid is fully controllable using the converter.

In this work two types of generators are used, an asynchronous generator and a low speed synchronous generator. Today the system with the low speed synchronous

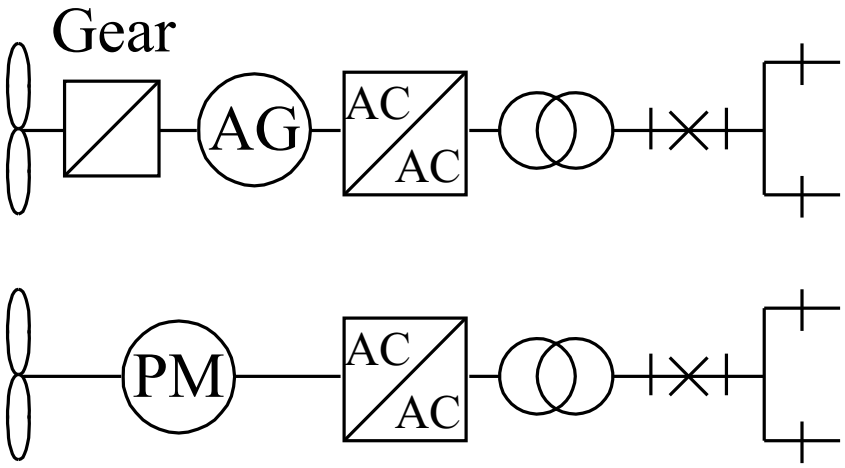

Figure 4.6: Principal schemes of the 2MW full range variable speed turbine, top with asynchronous generator and bottom with permanently magnetized generator.

generator is by far the most common one of the two. The reason for this is that this system does not need a gearbox, which is a quite sensitive component as mention before. If a permanently magnetized directly driven machine is used, a drawback is that this generator requires much more reactive power at rated power then the asynchronous generator requires. If an electrically magnetized generator is used, the reactive power is not a problem, since it can be produced internally using the field winding.

But if the generator is permanently magnetized the reactive power needed by the generator at high loads (high wind speeds) must be produced externally in order to have a good utilization of the generator, [21] and appendix B.3.3. This gives problems if a diode rectifier is connected to the generator. For this case some kind of reactive power compensation must be used, for example, capacitors on the AC side can be used. In this work it is assumed that the permanently and the electrically magnetized generator performs equally from an energy production point of view, so, only the permanently magnetized generator system is chosen to be investigated in this work.

In figure 4.7 the losses of the full range variable speed wind turbine with an asynchronous generator are shown. More details about this system is presented in appendix B.2.2. If figure 4.7 and figure 4.3 are compared it is noticed that the generator losses, at low wind speeds, is for the variable speed wind turbine almost the same as for the small generator used in the fix speed turbine. This is due to that in the full variable speed system the voltage and the frequency to the generator is fully controllable by the converter. At low wind speeds, field weakening of the generator is used in order to reduce the no-load losses. This is done by decreasing the voltage to the generator, se figure B.5.

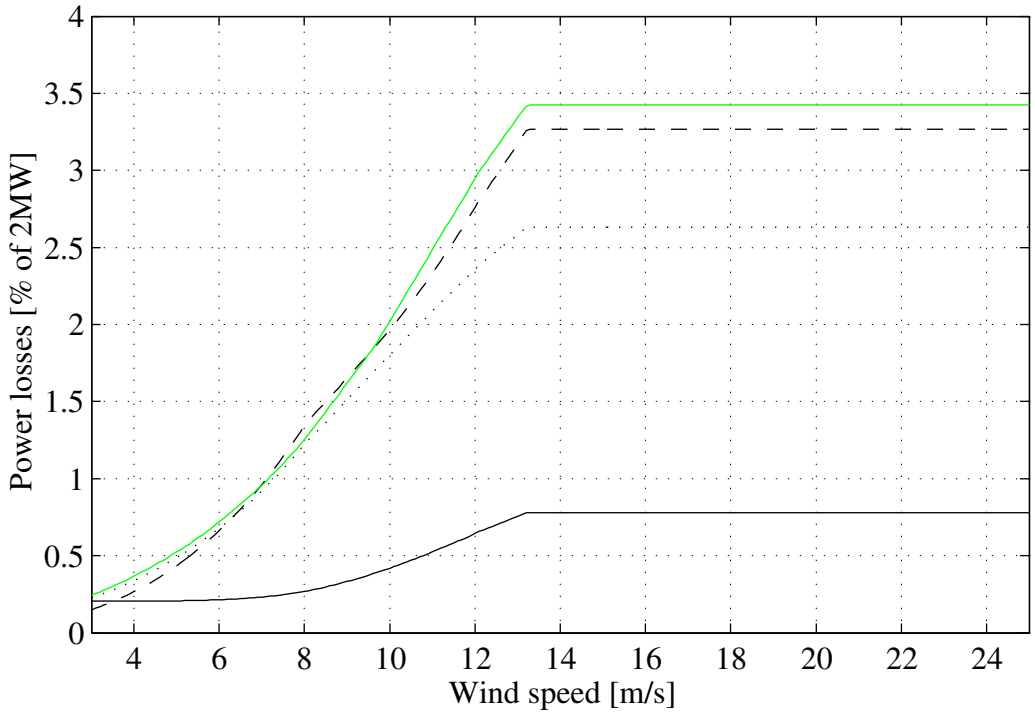

Figure 4.7: The losses of the 2MW full range variable speed turbine equipped with a asynchronous generator. Solid transformer losses, dashed generator losses, dotted gearbox losses and grey converter losses.

In figure 4.8 the losses of the full range variable speed wind turbine with a permanently magnetized generator and a back to back converter between the stator and the wind turbine transformer are shown. In appendix B.3.2 more information about this system is presented. From figure 4.8 it is noticed that the losses for the low speed generator is lower then the losses for the system with a gearbox and an asynchronous generator. It shall also be noticed that the converter losses for these two full variable speed systems are much higher then the converter losses in the semi variable system, se figure 4.5.

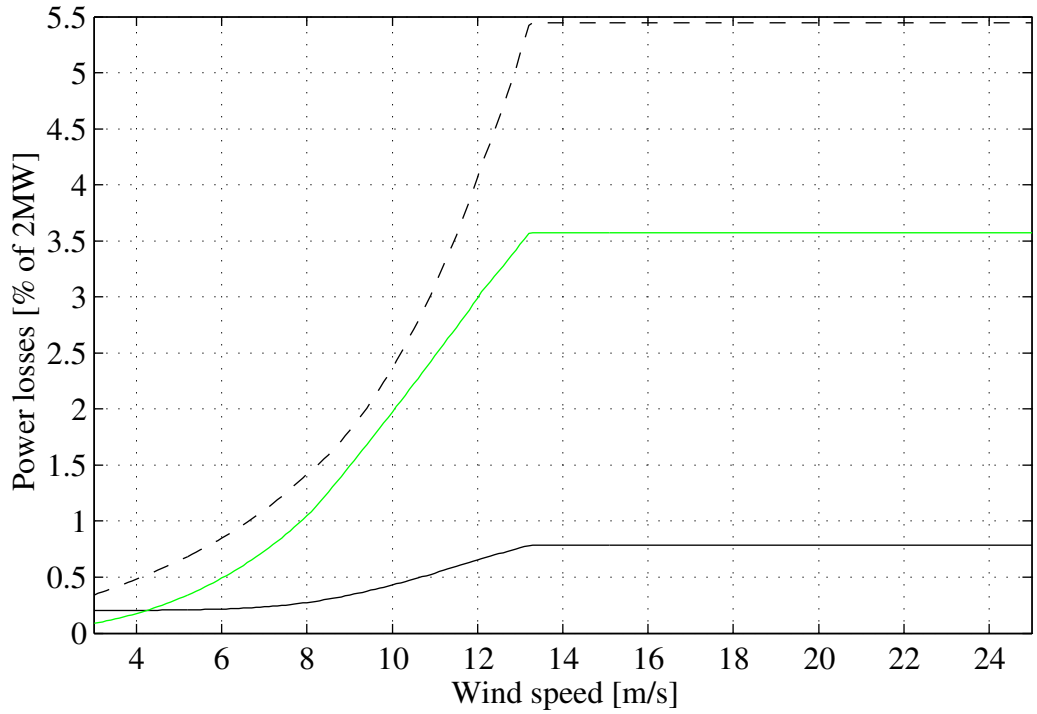

Figure 4.8: The losses of the 2MW full range variable speed turbine equipped with a permanent magnetized generator. Solid transformer losses, dashed generator losses and grey converter losses.

4.2 DC wind turbines

In this section some promising layouts of wind turbine units that produces a DC-voltage are examined. For all DC wind turbines, the generator is assumed to be a low speed permanently magnetized generator with a rated voltage of 690V and a rated power of 2MW. Note, that the notation DC wind turbines still means that we have an AC generator. In one case, a generator with 10kV rated voltage is used, and this generator is realized by using an ideal transformer connected to the 690V generator. In several of the DC systems, the generator is connected to a diode rectifier and the reactive power to the generator is supported by series capacitors, as discusses in [21] and appendix B.3.3. Of course, the capacitors and the main inductance of the generator will form a resonant circuit which must be investigated carefully in order to avoid any resonances which can cause high over-voltages. One DC system with an IGBT rectifier is also investigated. In this system the reactive power to the generator is controlled by the IGBT rectifier, as shown in appendix B.3.2.

The main philosophy of the DC-systems is that all wind turbines shall have a fix output voltage regardless of the wind speed in steady-state to simplify the DC-grid, as mention in chapter 2. The exception is in the series DC wind farm, where the sum of the output voltages of the wind turbines in one leg should be held constant.

In figure 4.9 the three DC/DC converter topologies selected in appendix A.3 to be used in this work are shown. To the left the boost converter, in the middle the full bridge converter and to the right the full bridge isolated boost converter are shown. For more information about the different topologies studied see appendix A.2 and in appendix B.6 the loss models of the three converters are shown.

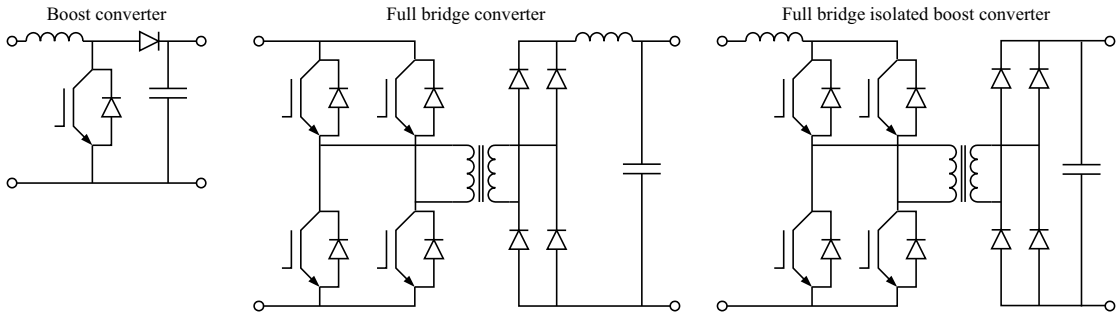

Figure 4.9: Principal scheme of the three most interesting DC/DC converter topologies.

4.2.1 DC-level locked speed wind turbine

In this concept the speed of the turbines are controlled by controlling the DC voltage. The main advantages of this system is that it has very few components and that all of them are passive, as can be seen in figure 4.10. This system is similar to the fix speed AC wind turbine system with the only difference that the speed is determined by the DC-voltage at the diode rectifier instead of the frequency of the AC voltage. This means that this systems has the same drawback of fluctuating power production as the fix speed AC wind turbine system. The slip of the conventional AC generator that is governed by the rotor resistance is now determined by the leakage inductance instead.

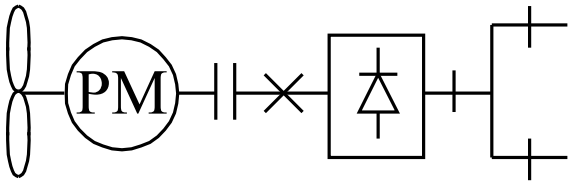

Figure 4.10: Principal scheme of the 2MW DC-level locked speed wind turbine.

Since this system in principle is a fixed-speed system with additional complications, it will not be taken into consideration in this report.

4.2.2 Variable speed DC wind turbines

In this sections some different layouts for variable speed DC wind turbines are presented and examined. The speed of the wind turbine is controlled by the DC/DC converter that is connected between the diode rectifier and the DC grid, as shown in figure 4.11. This means that the speed of the turbine is independent of the DC voltage on the grid.

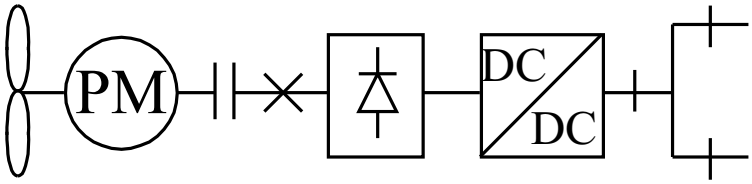

Figure 4.11: Principal scheme of the 2MW DC wind turbine with full variable speed and diode rectifier.

The drawback is that this system requires a DC/DC converter in the MW range, which does not exists today. Another drawback is of course, that the DC/DC converter will have losses.

In figure 4.12 the losses of the variable speed DC wind turbine with a boost converter as DC/DC converter are shown. In this configuration the generator has a rated voltage of 690V and the wind turbine with its DC/DC converter has an output voltage of 5kV. If instead a 10kV generator is used, which is quite possible, the output voltage can be increased to 40kV. The losses of this system are shown in figure 4.13.

In figure 4.14 the power production and the losses of the variable speed DC wind turbine with a full bridge converter as DC/DC converter are shown. In this configuration the generator has a rated voltage of 690V and the wind turbine has a output voltage of 40kV.

By comparing the three figures 4.12, 4.13 and 4.14 it is noticed that the losses for the generator are the same, the only difference is the losses for the diode rectifier and the DC/DC converter. The losses for the diode rectifier and the boost converter in the system with the 10kV generator is lower then for the other system, due to the fact that the current is lower.

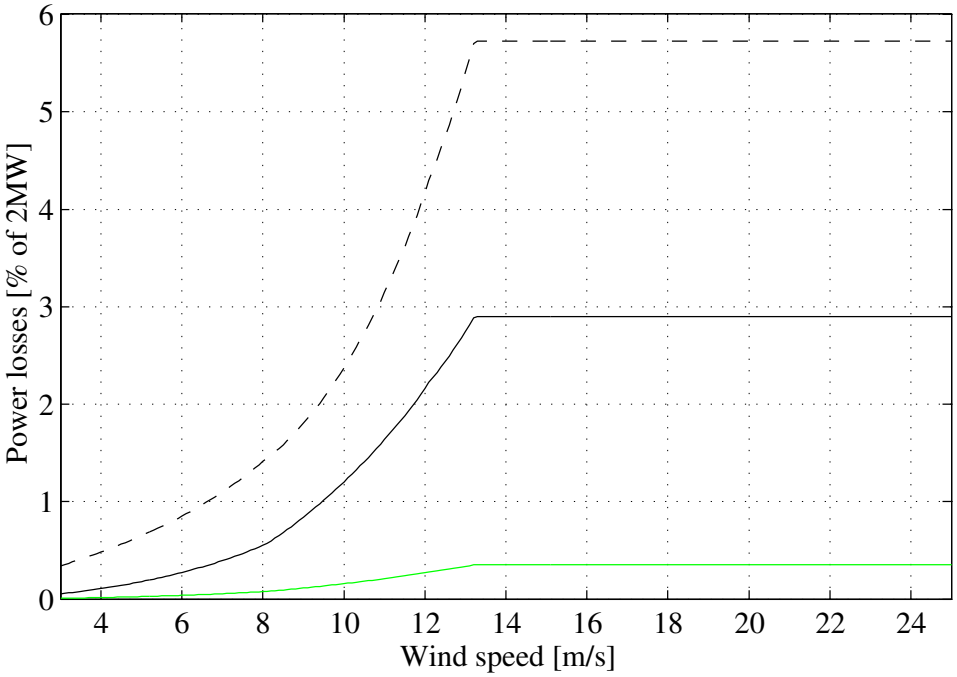

Figure 4.12: The losses of the 2MW wind turbine equipped with a permanent magnetized generator connected to a diode rectifier and a boost converter with 5kV output voltage. Dashed generator losses, solid DC/DC converter losses and grey diode rectifier losses.

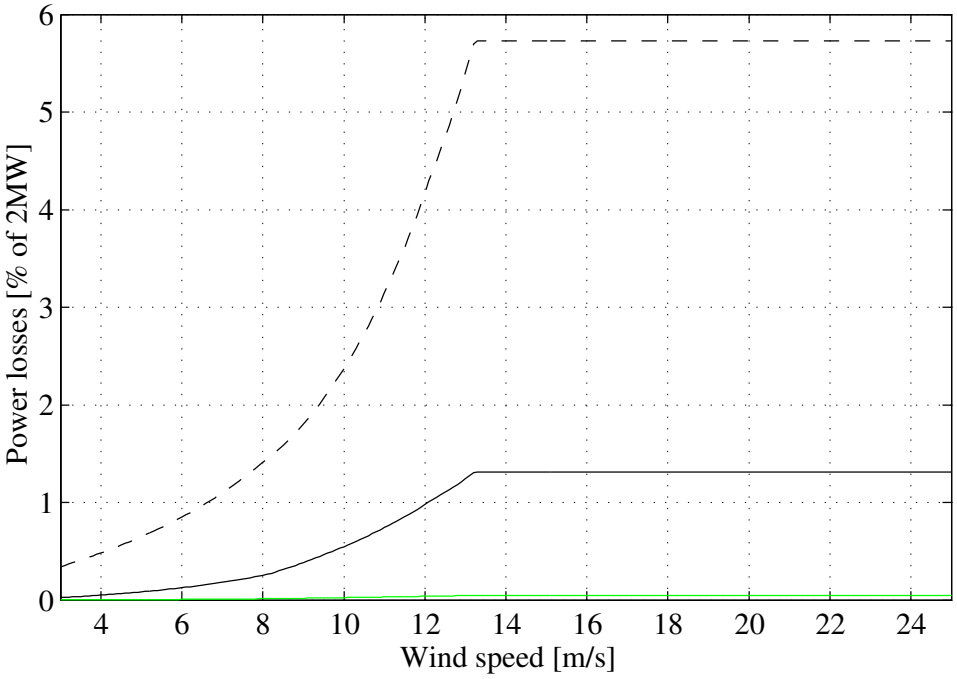

Figure 4.13: The losses of the 2MW turbine equipped with a permanent magnetized generator connected to a diode rectifier and a boost converter with 40kV output voltage. Dashed generator losses, solid DC/DC converter losses and grey diode rectifier losses.

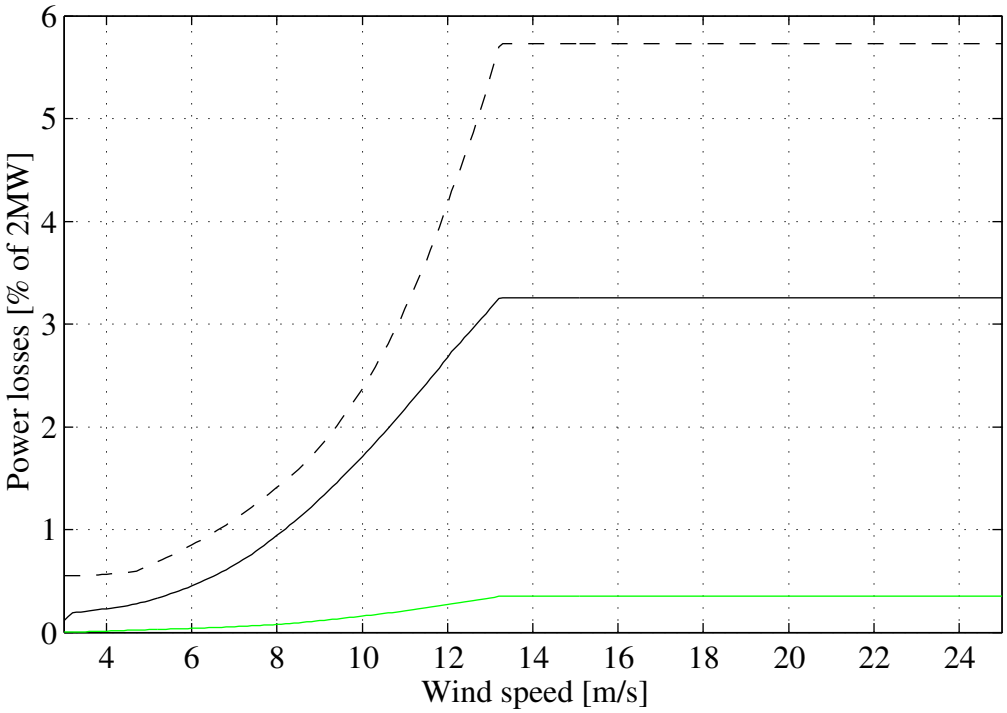

Figure 4.14: The losses of the 2MW turbine equipped with a permanent magnetized generator connected to a diode rectifier and a full bridge converter. Dashed generator losses, solid DC/DC converter losses and grey diode rectifier losses.

4.2.3 Variable speed DC wind turbine with IGBT rectifier

In this DC wind turbine, the diode rectifier and the series capacitors are replaced by an IGBT rectifier, as shown in figure 4.15. The benefit with the IGBT rectifier is that

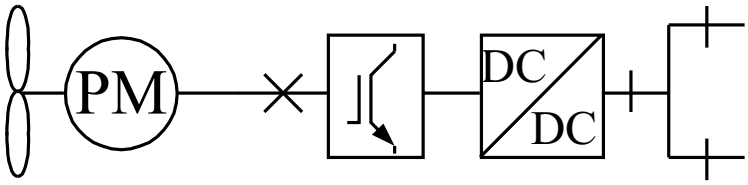

Figure 4.15: Principal scheme of the 2MW DC wind turbine with full variable speed and IGBT rectifier.

the torque of the generator and the reactive power to the generator is easily controlled. Due to the fact that the reactive power can be controlled, any type of generator can be used.

Another benefit of the IGBT rectifier is that it keeps the input voltage to the DC/DC converter constant. This leads to that the DC/DC converter works at a constant transformation ratio in normal operations. This means that the DC/DC converter can be better optimized, it will work as a constant ratio DC transformer.

In figure 4.16 the losses of the variable speed DC wind turbine with an IGBT rectifier and a full bridge converter as DC/DC converter are shown. In this configuration the generator has a rated voltage of 690V and the wind turbine has an output voltage of 40kV. In figure 4.16 it is noticed that the power loss in the generator is lower compared to the cases using a diode rectifier and series capacitors. This is due to the better control of the voltage and reactive power of the generator. It is also noticed that the losses for the full bridge converter is lower in this case compared to the case with a diode rectifier. This is due to that the converter is better utilized when it is operated with constant input and output voltage. The drawback is that the IGBT rectifier has much higher losses then the diode rectifier, which leads to that this wind turbine has a lower rated output power compared to the wind turbine with the 10kV generator, diode rectifier and the boost converter.

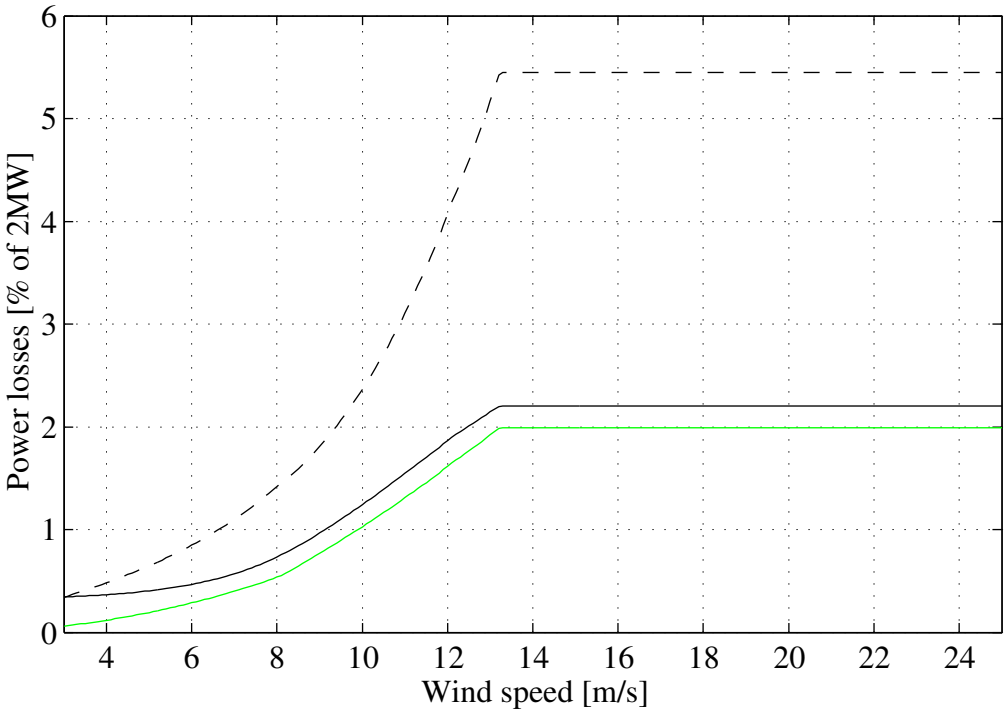

Figure 4.16: The losses of the 2MW wind turbine equipped with a permanent magnetized generator connected to a IGBT rectifier and a full bridge converter. Dashed generator losses, solid DC/DC converter losses and grey IGBT rectifier losses.

4.2.4 Series connected DC wind turbine unit

This type of wind turbine is designed to be connected in series with other wind turbines. The point is that it in this way is possible to get a sufficiently high voltage for transmission directly, without using large centralized DC-transformers. The series connected wind turbine does not differ so much from the variable speed DC wind turbines presented in chapter 4.2.2. The only difference is the type of DC/DC converter that is used, in this case the full bridge isolated boost converter. The series connection however implies that some components in the wind turbine must have a voltage insulation high enough to take up the whole transmission voltage to ground.

In this work, it is the transformer in the DC/DC converter that is the interface between the high transmission voltage and ground. In figure 4.17 the scheme of the series connected DC wind turbine is shown. From this figure it is noticed that the high voltage winding of the transformer in the DC/DC converter is isolated for the transmission voltage to ground. It is also seen that all components on the high voltage

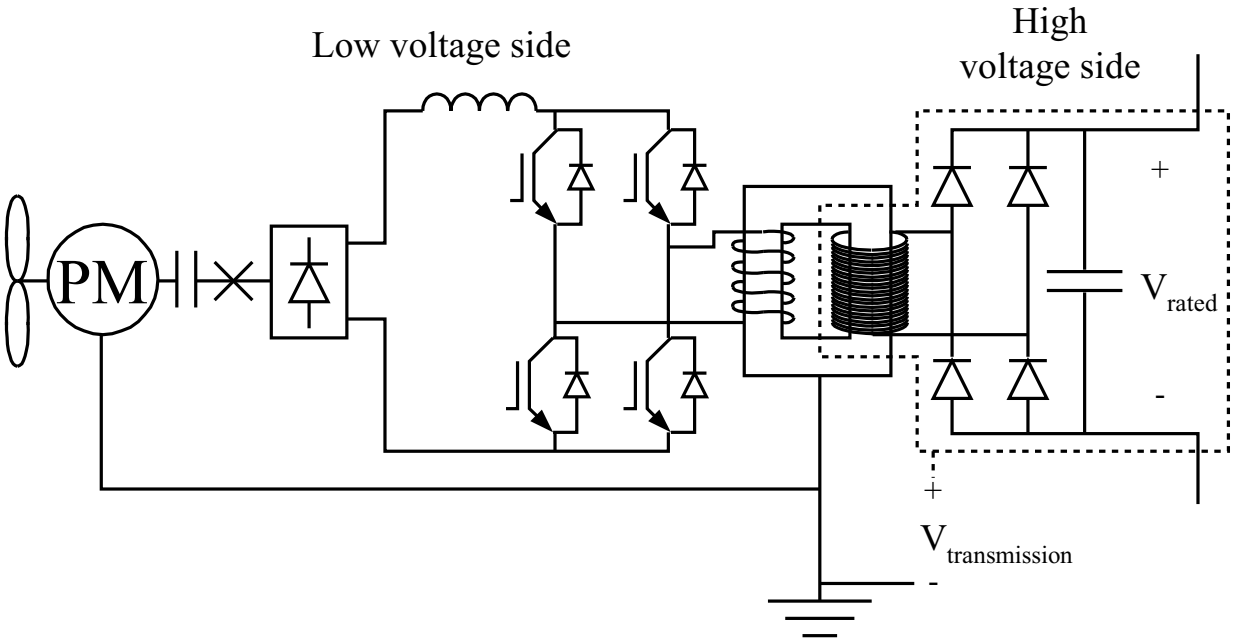

Figure 4.17: Principal scheme of the series connected DC wind turbine.

side in figure 4.17 must be isolated for the transmission voltage to ground. One benefit of the full bridge isolated boost converter is that it has a few numbers of components on the high voltage side of the transformer, the diode rectifier and the output capacitor. This means that it is a few components that must be placed or encapsuled so that they can withstand the transmission voltage to ground. As can be seen in figure 4.17 the voltage rating of the components on the high voltage side is determined by the output voltage rating of the converter and not by the transmission voltage. Another benefit of the full bridge isolated boost converter is that all components on the high voltage side are passive. This means that no control signals or drive circuits for active components is needed on the high voltage side.

In figure 4.18 the losses of the series connected wind turbine are shown. In this configuration the generator has a rated voltage of 690V and the wind turbine has an

output voltage of 20kV. As can be noticed from figure 4.18 the series connected wind

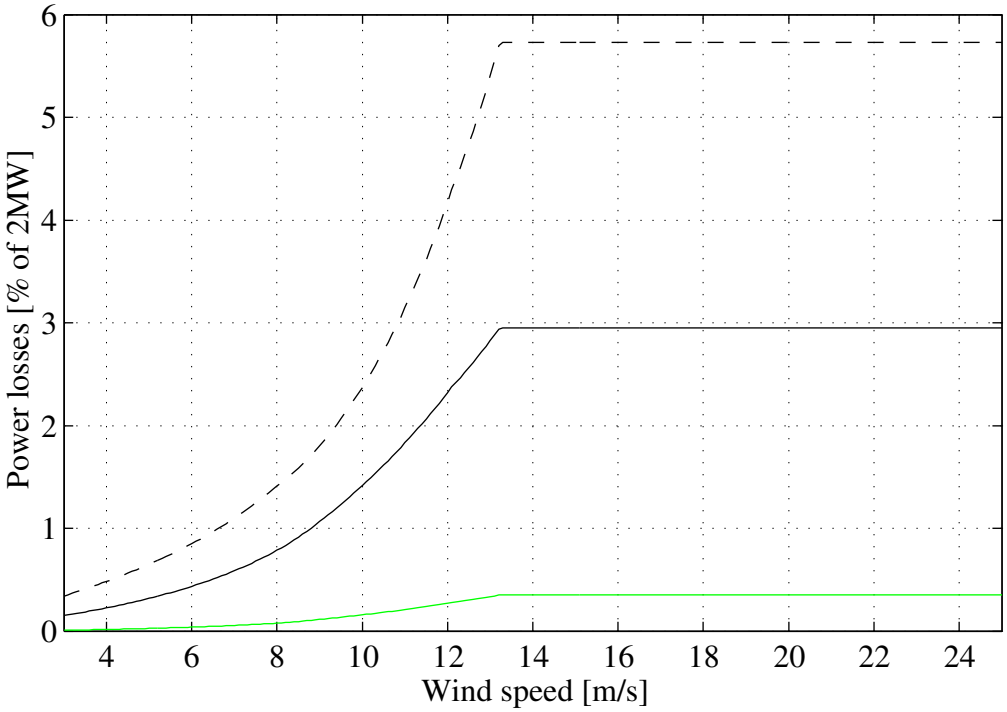

Figure 4.18: The losses of the 2MW series connected wind turbine. Dashed generator losses, solid DC/DC converter losses and grey diode rectifier losses.

turbine has the same generator and rectifier losses as the other DC wind turbines with a diode rectifier to the generator and a 690V generator. It can also be noticed that the DC/DC converter losses are lower for this wind turbine then for the variable speed wind turbine with a full bridge converter and a diode rectifier, se figure 4.14. This is due to that the full bridge isolated boost converter is better utilized in this voltage adjusting application then the full bridge converter.

4.3 Average power production comparison of different wind turbines

In this section the average power production of the wind turbines presented in this chapter will be determined. The average power production is calculated by using the wind speed distribution shown in chapter 3. The average power production is calculated in the same way as the mean wind speed, equation 3.2, ie. the output power is multiplied with the Rayleigh distribution and then integrated from cut in wind speed to cut out wind speed, as can be seen in equation 4.1. In this work the cut out wind speed is selected to 25m/s, this is a normal value for wind turbines. There is no point in using a higher cut out speed since the contribution to the average power production for wind speeds above 25m/s is very low, se figure 3.1 where the Rayleigh distribution has very low values over 25m/s. This means that a further mechanical over-dimension in order to allow operation at these high wind speeds does not pay back. The cut in wind speed is set to 3m/s. The contribution to the average power production from wind speeds lower then 3m/s is quite low due to that the power produced by the wind turbine is low, see figure 4.2, and due to that the distribution decrease rapidly for decreasing wind speeds below 3m/s. The average power production can thus be determined as:

$$P_{out,AVG} = \int_{cutin}^{cutout} P_{out}(w_s) f(w_s) \mathrm{d}w_s. \tag{4.1}$$

Where:

$P_{out,AVG}$	Average power production [kW]
$cutin$	Cut in wind speed =3 [m/s]
$cutout$	Cut out wind speed =25 [m/s]
$P_{out}(w_s)$	Output power of the wind turbine [kW]
$f(w_s)$	Rayleigh distribution

In table 4.1 the average power production of the different wind turbines are shown for some different average wind speeds and the power at cut in wind speed and at rated wind speed in per unit of 2MW. The four first are AC wind turbines and the five last are DC wind turbines. It shall be remembered that all wind turbines has the

Table 4.1: The output power in p.u. of 2MW for the different wind turbines at cut in wind speed and at rated wind speed and the mean output power in kW for the different wind turbines and for different mean wind speeds.

Type of wind turbine	Power at 3m/s	Rated power	5m/s	6m/s	8m/s	10m/s
AM Fix speed	0	0.997	271	434	769	1037
AM, Rotor converter	0.009	0.992	275	437	771	1038
AM, Stator converter	0.011	0.964	270	428	754	1012
PM, Stator converter	0.013	0.967	281	442	769	1027
PM, Diode, Boost 5kV	0.015	0.975	288	451	781	1040
PM, Diode, Boost 40kV	0.015	0.994	292	457	793	1058
PM, Diode, Full bridge	0.003	0.971	282	444	774	1033
PM, IGBT, Full bridge	0.012	0.968	281	442	770	1028
PM, Diode, FBiB	0.014	0.975	286	448	778	1038

same rated shaft power, so the differences in electric power production is only depending on the speed control of the turbine (fix speed, limited speed range or full range variable speed) and the losses in the drive train. From table 4.1 it can be seen that the differences in average power production between the different wind turbines for a given mean wind speed is not large, it is maximum 4-7%. Note, that a possibility is to increase the rotor diameter of the turbine at sites with low average wind speeds and in this way it is possible to adjust the turbine to the mean wind speed of the site. In this work the rotor diameter is the same for all average wind speeds, since the goal here is to compere the energy capture using various electrical systems, so the boundary conditions are set to be as equal as possible in this work.

From table 4.1 it can be noticed that almost all wind turbines with high power at cut in wind speed has the highest average production at low average wind speeds. It can also be noticed from table 4.1 that the wind turbines with high output power at rated wind speed has the highest average output power at high average wind speeds, as can be expected. This is due to the fact that at a low average wind speed the Rayleigh density function has the highest values for low wind speeds, as can be seen from figure 3.1. This gives that a high efficiency at part load gives a higher average output power. Accordingly, for a high average wind speed the Rayleigh density function has the highest values for higher wind speeds and this gives that high efficiency at rated load gives a higher average output power.

This is the explanation why the fix speed AC wind turbine has high average output power at high average wind speeds and low at low average wind speeds. The fix speed AC wind turbine has a lower efficiency at low wind speeds due to the fact that the speed is locked to two specific speeds and due to that the reduction of the no-load losses of the generators is limited (apart from the one archived by using two generators).

The wind turbine with the doubly fed asynchronous generator has a quite good performance for all average wind speeds. This is mainly due to the low losses in the converter and the $Y\Delta$ switch at low wind speeds. As mention before, the DFIG system can only work in a certain speed span and this system thus loose some energy at low wind speeds. But as can be observed from table 4.1, the rotor converter systems has almost the same output power at cut in wind speed as the stator converter system with the asynchronous generator, even though this system operate at full variable speed and can reduce the no-load losses of the generator to a maximum. But the stator converter has much higher losses then the rotor converter so the gain using the full variable speed operation and the reduction of the no-load losses is lost due to the high converter losses. The result is that the stator converter system with an asynchronous generator will not have the highest efficiency.

For the AC wind turbine with the stator converter system and a permanently magnetized generator it can be noticed that it performs well at low average wind speeds compared to the systems with a gearbox and an asynchronous generator. This is due to the fact that the permanently magnetized generator has lower losses at low wind speeds then the system with a gearbox and an asynchronous generator, as can be seen from figure 4.7 and 4.8. For high average wind speeds this system has a lower average output power then the fix speed system and rotor converter system due to the high losses in the converter at high wind speeds.

As it can be noted, the DC wind turbines all performs good for low average wind speeds due to the low losses in the permanently magnetized generator at low wind

speeds compared to the system with an asynchronous generator and a gearbox. But for higher average wind speeds they performs somewhat differently depending on the losses in the rectifier and in the DC/DC converter.

From table 4.1 it is found that the best wind turbine is the DC wind turbine with a 10kV generator and a boost converter with an output voltage of 40kV. This is due to that the 10kV generator is made from adding an ideal transformer to the stator of the 690V permanently magnetized generator used in the other wind turbines. This gives that the losses for the 10kV generator are identical to the losses of the 690V generator. But due to the higher voltage, the current is lower and therefore the conduction losses in the diode rectifier and the boost converter are much lower compared with the other DC wind turbines.

For the other DC wind turbines with a 690V generator and a diode rectifier it is noticed that the system with the boost DC/DC converter is the best and that the full bridge isolated boost system comes second and the least efficient is the full bridge system. This is only depending on the DC/DC converter losses, since that the generator is controlled in the same way in all three cases. By comparing the losses for the DC/DC converter in figure 4.12, 4.14 and 4.18 it is seen that the boost converter has the lowest losses.

For the DC wind turbine with an IGBT rectifier it is seen from table 4.1 that it produces the lowest average output power of the DC wind turbines. This is due to the much higher losses in the IGBT rectifier compared to the diode rectifier used in the other DC wind turbines. But it shall be noticed that this DC wind turbine performs quite equal to the AC wind turbine with a permanently magnetized generator and a stator-connected full power converter.

From this comparison of different wind turbine types, the fix speed AC wind turbine and the rotor converter AC wind turbine is chosen to be used in the evaluation of the wind parks with AC wind turbines. For the large DC wind park, the two wind turbine systems with the boost converter are used, the one with 5kV output voltage and the one with the 40kV output voltage. For the small DC wind park only the wind turbine system with the boost converter and 40kV output voltage is used. This due to that 5kV is a too low voltage for transmission over long distances. For the series connected DC wind park, the DC wind turbine with the full bridge isolated boost converter is chosen. This is due to that it has a higher average output power then the full bridge DC wind turbine and due to that the full bridge isolated boost converter has fewer components on the high voltage side of the transformer then what the full bridge converter has.

Chapter 5

Energy Production Cost of Different Wind Parks

In this chapter, the energy production cost for the six different wind park systems based on the wind turbine systems described in chapter 2 are compared with each other. All these six types are individually optimized to give the lowest energy production cost. In the first section the best configuration of these six types are compared with each other. And in the following sections the individual optimization is described for each of the configurations. The inputs, loss and cost models, for these calculations are taken from appendix B and appendix C.

The cost of the components are calculated with the functions presented in appendix C and the losses in the components are calculated with the functions presented in appendix B. The energy production cost is then calculated according to the equations in appendix C.1. The energy production cost for the six, in this chapter, investigated types of electrical system are normalized by the energy production cost obtained for the Horns Rev wind park. According to [4] Horns Rev has a yearly production of 600 000 000kWh, an average wind speed of 9.7m/s and a project cost of DKK 2 billion. This gives an energy production cost of approximately 0.28SEK/kWh, accordingly to the assumptions in this section.

5.1 Comparison of Energy Production Costs

In this section the best configuration of each of the six wind park types presented in chapter 2 are compared with each other, small AC, large AC, AC/DC, small DC, large DC and series DC. The comparison is made for the four different rated powers presented i chapter 2, 60MW, 100MW, 160MW and 300MW. The presented cases for an average wind speed of 10m/s are shown in figures 5.1 and 5.2.

In figure 5.1 the energy production cost is shown for the six wind park configurations, and as mention in the introduction of this chapter it is normalized by the production cost for Horns Rev. If the three wind parks with AC are compared, small AC (solid black), large AC (dashed) and AC/DC (dash-dotted) these results are as expected. The small AC wind park is the best solution for short distances, the AC/DC is best suitable for long distances and the large AC is best in between. The small AC wind park is the best for short distances due to that it does not require an offshore platform. So the additional cost for many low voltage transmission cables is less then

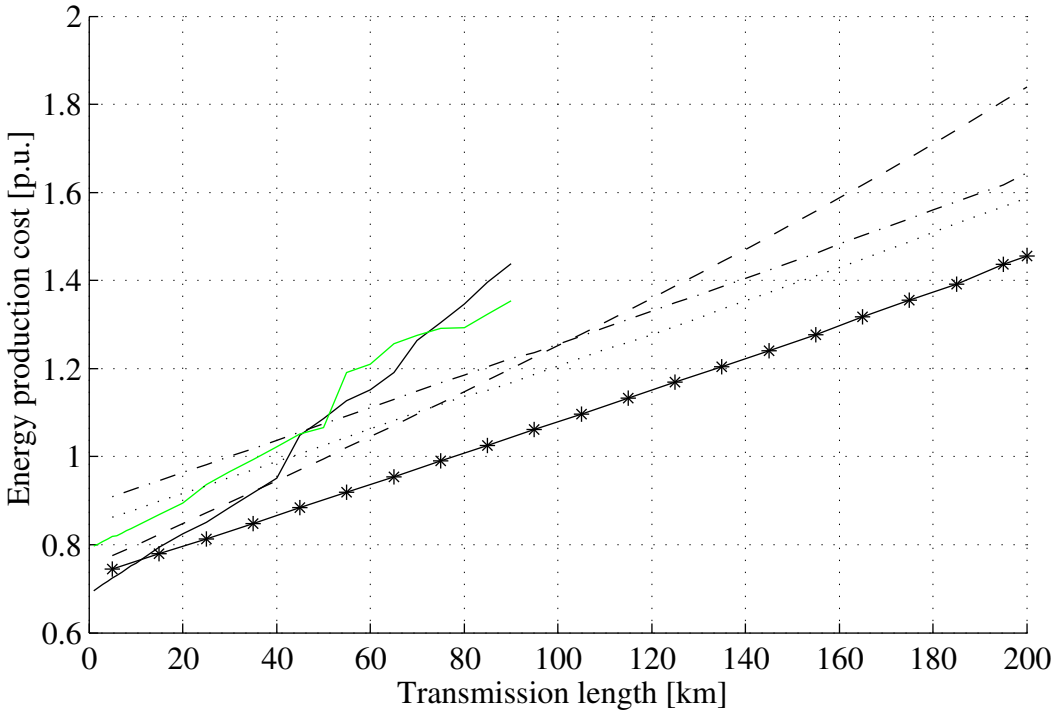

Figure 5.1: The normalized energy production cost of the different 60MW wind parks as function of the transmission distance for an average wind speed of 10m/s. Solid small AC, dashed large AC, dash-dotted AC/DC, grey small DC, dotted large DC and solid with stars series DC.

the cost for the platform and the high voltage transmission cable for short distances. The cost for the low voltage transmission increases rapidly when the transmission distance increases. The break even point between the small and large AC system is at a transmission distance of 37km. The AC/DC system has, due to the expensive converter stations, a high energy production cost for short distances. Due to the fact that the cost for the transmission cables are less for DC then for AC the AC/DC system gets better then the large AC system for transmission lengths over 100km, see appendix C.4.

The large DC system is better then the AC/DC system due to that the losses in the DC wind turbine is lower then in the AC wind turbine. Moreover, the cost for the local DC grid is less then the cost for the local AC grid and the losses in the DC transformer are less then the losses in the offshore converter station. These costs are independent of the transmission length, but since the two systems has the same transmission system (DC cables), the large DC wind farm will for any transmission length be better then the AC/DC wind farm (using the assumptions made in this work).

As could be expected, the small DC wind farm is no good solution. This is due to that it still requires a large DC transformer and a converter station. The gain of cheaper cables and somewhat lower losses is not enough to compensate for the expensive DC transformer and converter station. But compared to the large DC system it is better for short distances. The reason is that it does not require an offshore platform.

From figure 5.1 it can be seen that the best wind park solution for a transmission length over 11km is the series DC wind park. This is due to the fact that it does not require an offshore platform, it has a cheaper local wind turbine grid, DC transmission

(cheaper then AC) and this system has only one converter station. The uncertainty which is also a great challenge for research in the high voltage field, is how expensive it will be to have the high voltage insulation in each wind turbine.

In figure 5.2 the normalized energy production cost are shown for the six systems for a rated power of the wind park of 160MW. As can be noticed the cost found for the large AC park (The Horns Rev case, totaly 55km transmission length [15]) is 10% lower then the "real" case. However, since real price information is hard to obtain and the fact that Horns Rev was the first large offshore wind park the results are considered to be surprisingly good. It should be stressed that this work focuses on comparing systems rather then obtaining correct total costs, since this was considered to be out of reach without having access to really good cost data. It can be seen if the figures 5.1

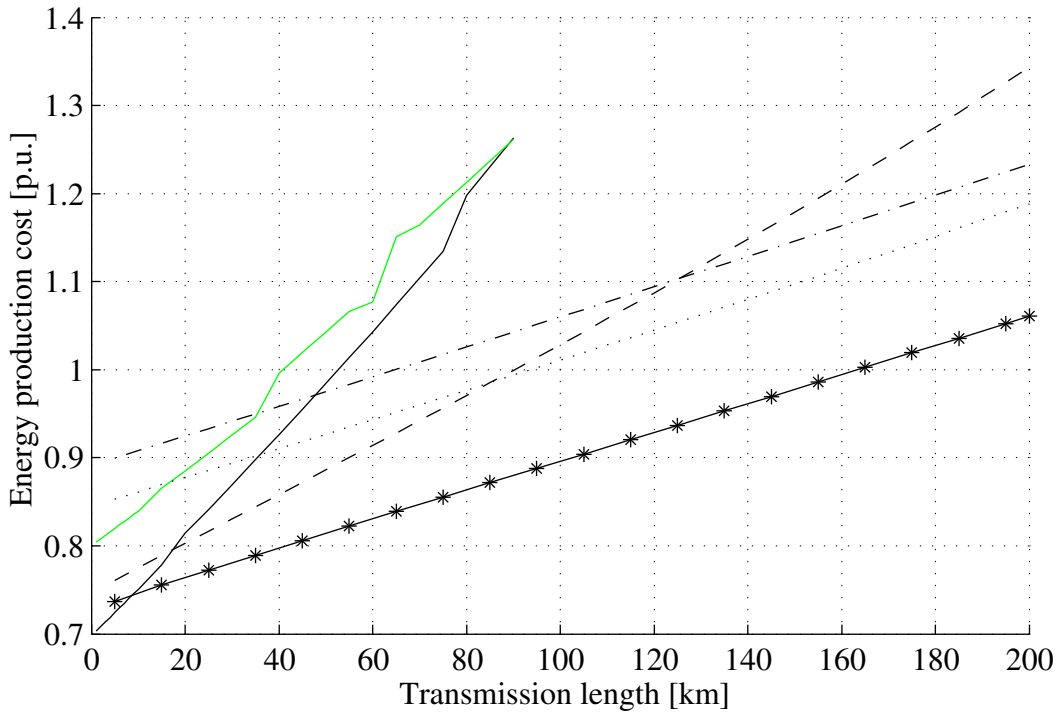

Figure 5.2: The normalized energy production cost of the different 160MW wind parks as function of the transmission distance and at a average wind speed of 10m/s. Solid small AC, dashed large AC, dash-dotted AC/DC, grey small DC, dotted large DC and solid with stars series DC.

and 5.2 are compared that the break even point between the small AC and large AC is decreasing when the wind park size is increased. This is caused by the fact that the contribution to the energy production cost from the transmission system decreases when the wind park size is increased. The decrease is larger for the large AC wind park then for the small AC wind park. Another observation that can be made is that the energy production cost decreases when the rated power of the wind park increases.

In figure 5.3 a curve of how the energy production cost varies with the average wind speed is presented. The curve is normalized by the costs at a average wind speed of 10m/s. As can be noticed from the figure 5.3 the cost increases rapidly if the average wind speed decreases. At a average wind speed of 6.5m/s the energy production cost is twice as high as at 10m/s.

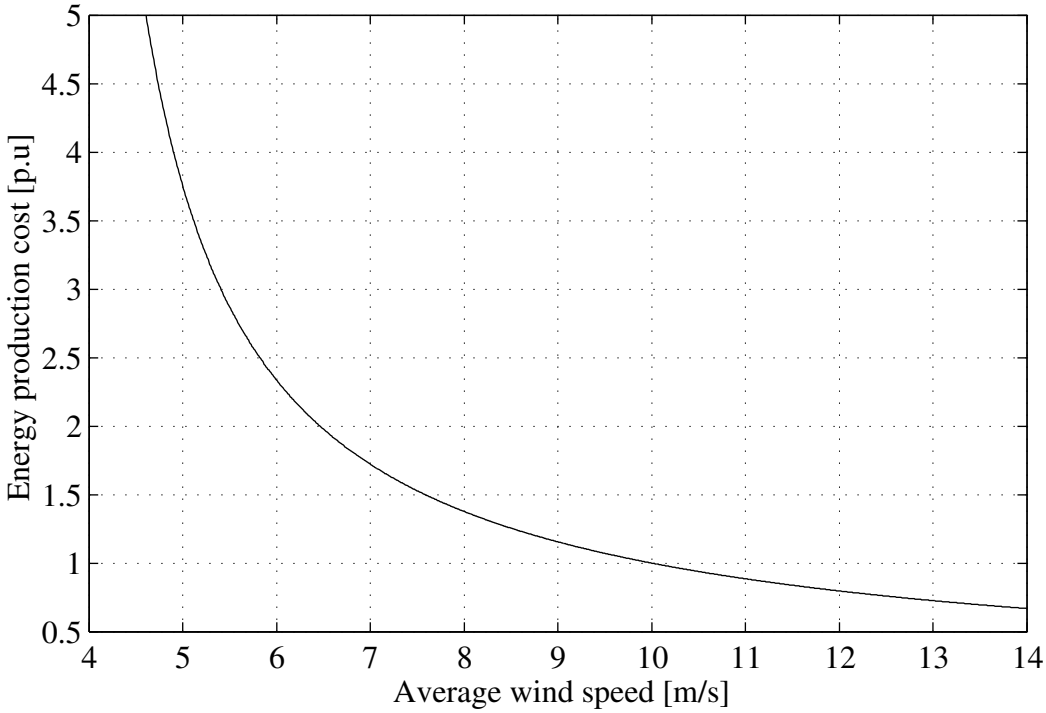

Figure 5.3: Energy production cost as function of the average wind speed, normalized with the cost at a average wind speed of 10m/s.

5.2 Small AC park, local grid for transmission

In this section, the small AC wind park is investigated in detail. First some selections are made to limit the number of cases and then the energy production cost is discussed for the different configurations of the small AC wind park.

5.2.1 Transformer size

The first selection to be made is the transformer size. The reason for investigating this is that it is possible to get lower losses and perhaps lower contribution to the energy production cost, if the transformer size is selected larger then the rating of the wind farm. The reason for this is that in these cases the cost of the losses in the transformer is reduced more then what the cost of the transformer increases. From appendix C.1 it is known that the contribution to the energy production cost from one component can be expressed as in equation 5.1.

$$E_{cost,c1} = E_{cost,invest,c1} + E_{cost,loss,c1} = K\frac{I_{c1}}{P_{in,AVG}} + K\frac{\text{Invest}}{P_{in,AVG}}\frac{P_{loss,c1,AVG}}{P_{out,AVG}} \tag{5.1}$$

Where:

$E_{cost,c1}$	Contribution to the energy production cost from component $c1$ [SEK/kWh]
$E_{cost,invest,c1}$	Contribution from the cost of component $c1$ [SEK/kWh]
$E_{cost,loss,c1}$	Contribution from the losses in component $c1$ [SEK/kWh]
K	Constant, defined in equation C.1
Invest	Investment [SEK]
I_{c1}	Cost of component $c1$ [SEK]
$P_{in,AVG}$	Average input power [kW]
$P_{out,AVG}$	Average output power [kW]
$P_{loss,c1,AVG}$	Average losses in the component $c1$ [kW]

Moreover, if it is assumed that the cost of the transformer is described by equation C.5 and that Invest $= B_I P_{n,wp} + \text{Cost}_{transformer}$, where $P_{n,wp}$ is the rated power of the wind park and B_I is the investment factor for the other components in the wind park. The input power to the wind farm as function of wind speed is described by equation 5.2 in per unit of $P_{n,wp}$.

$$\begin{aligned} P &= \frac{w_s^3}{w_{s,P}^3} \quad \text{for} \quad 0 \leq w_s \leq w_{s,P} \\ &= 1 \quad \text{for} \quad w_{s,P} \leq w_s \end{aligned} \tag{5.2}$$

Where:

P	Input power [p.u.]
w_s	Wind speed [m/s]
$w_{s,P}$	Wind speed for rated power =11.5m/s

The average input power is calculated with equation 4.1. The output power is calculated according to $P_{out,AVG} = P_{in,AVG} - P_{loss,transformer,AVG} - P_{loss,other,AVG}$. $P_{loss,other,AVG}$ is the average losses of the other components in the wind park and in this case (determination of transformer size) these are set equal to the relative losses of the 2MW wind turbine with the DFIG system. The losses of the transformer are assumed to be described by the approximation in equation B.75. The input power to the transformer

is also assumed to be described by equation 5.2 and the average losses are calculated by equation 4.1. Using these assumptions, the optimum transformer size that minimizes the contribution to the energy production cost, can be calculated. The key results from this calculation are presented in figure 5.4. The main conclusion from figure 5.4

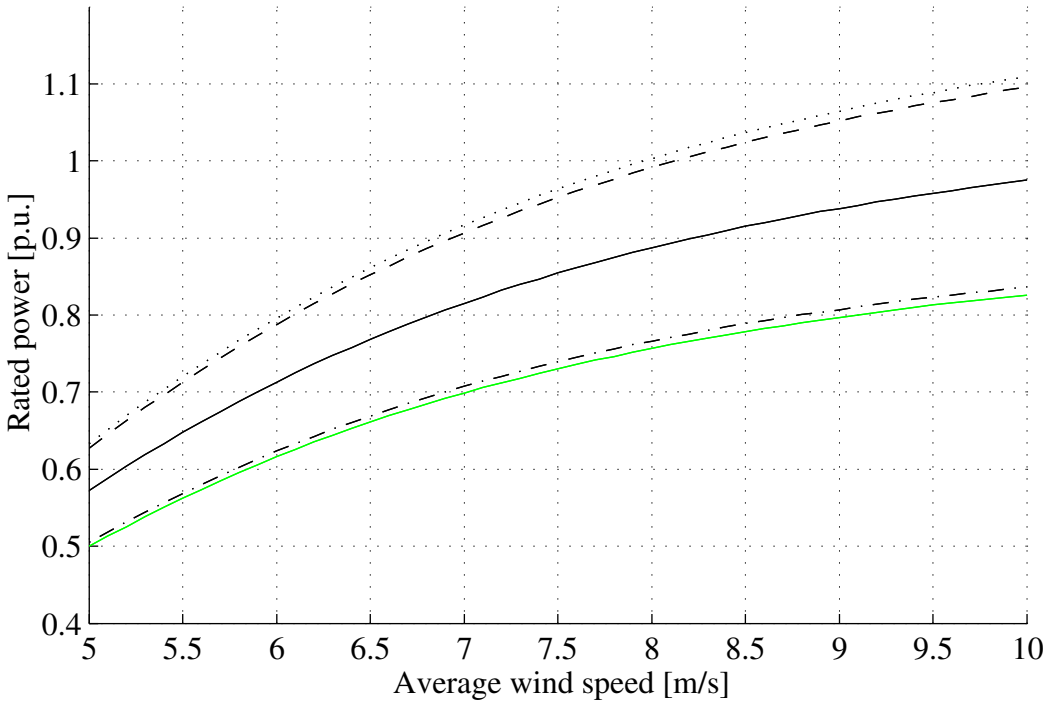

Figure 5.4: Rated power of the transformer in p.u. of the rated power of the wind park as function of the average wind speed for different rated powers of the wind park and different investment factors. Solid 150MW $B_I = 19$, dash-dotted 60MW $B_I = 19$, dotted 300MW $B_I = 19$, grey 150MW $B_I = 14$ and dashed 150MW $B_I = 24$.

is that it is for high rated powers of the wind park and for high average wind speeds that it is optimal to have a higher rating of the transformer. The fact that it is for high powers, depend on that the derivative of the cost for the transformer is lower for high power levels then it is for lower power levels as can be seen from figure C.2. In the same way as for electric machines, the load losses is of greater importance for high average wind speeds and the no-load losses for low average wind speeds. The result is that the smallest possible transformer shall almost always be selected. Only in the case of high rated power of the wind park and high average wind speeds, the transformer shall be slightly over-dimensioned. In this work the smallest transformer possible is accordingly always used.

5.2.2 Number of wind turbines per radial

With the same technique used to determine the rated power of the transformer, the ideal number of wind turbines per radial can be calculated. For this calculation the wind turbines, the cables between the wind turbines and the transmission cables are treated as the component to be optimized. The cable losses are calculated by equation B.83. Otherwise the procedure is similar to the one for the transformer above.

In figures 5.5 and 5.6 the results from these calculations are shown for different power levels. The two figures shows the results for the two transmission voltage levels, 22kV and 45kV. The small wind park is also investigated for a voltage level of 33kV, but since the results for this voltage level is in between the ones obtained for the 22kV and 45kV and, moreover, show the same pattern, they are not shown. The black curves in these two figures corresponds to the calculation of the number of wind turbines per radial that gives the lowest contribution to the energy production cost. But since the wind park should have a specific rating, the selection of the number of wind turbines per radial is not free to choice. Due to this fact, the number of wind turbines per radial multiplied by the number of radials multiplied with the rating of the wind turbine should be equal to the rating of the wind park. Therefore the grey curves in the two figures 5.5 and 5.6 shows the discrete number of wind turbines per radial that is used in this investigation. As can be noticed if the grey lines are studied in detail, the rated power of the wind park is allowed to vary somewhat around the desired rated power. This means that for some transmission distances the actual rated power of the wind park is somewhat higher or lower then the desired rated power (60, 100, 160 or 300MW).

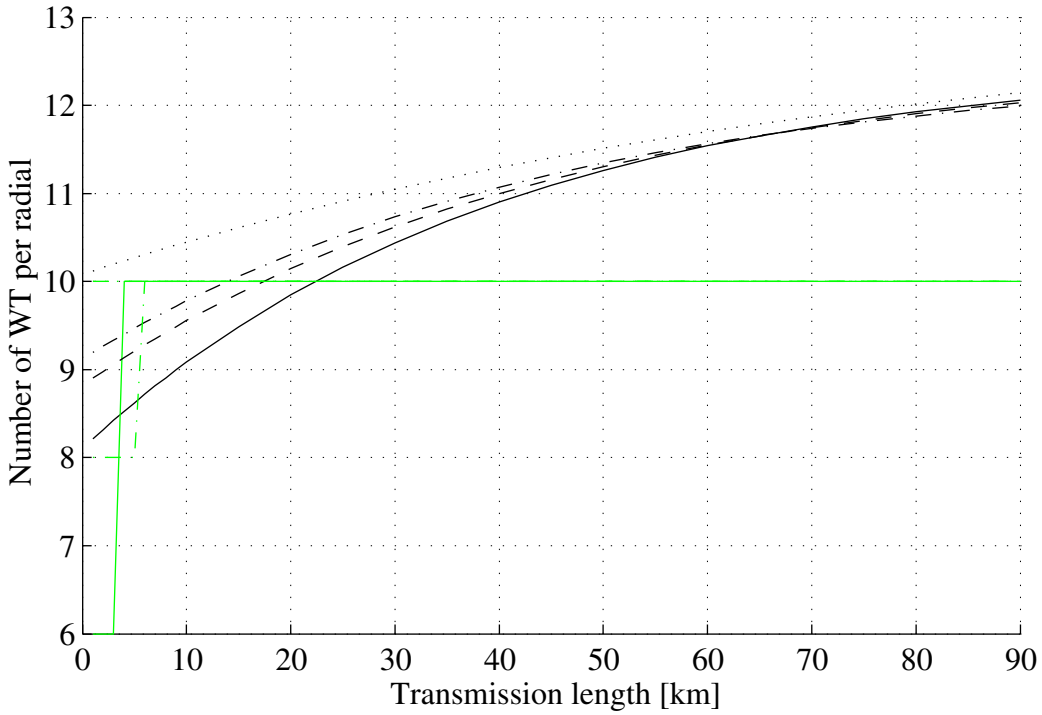

Figure 5.5: Number of wind turbines per radial for 22kV transmission voltage. Black theoretical curves and grey actual curves. Solid 60MW park, dashed 100MW, dash-dotted 160MW and dotted 300MW wind park.

In the calculation of the ideal number of wind turbines per radial, the ideal size of the transmission cables was also calculated. From this calculation it was indicated that the cables should be over-dimensioned if the transmission length is short, shorter then 10km. The desired over-dimension decreased when the transmission length increased. Since the focus in this work is mainly on somewhat longer distances, the smallest conductor area that can be used is chosen here.

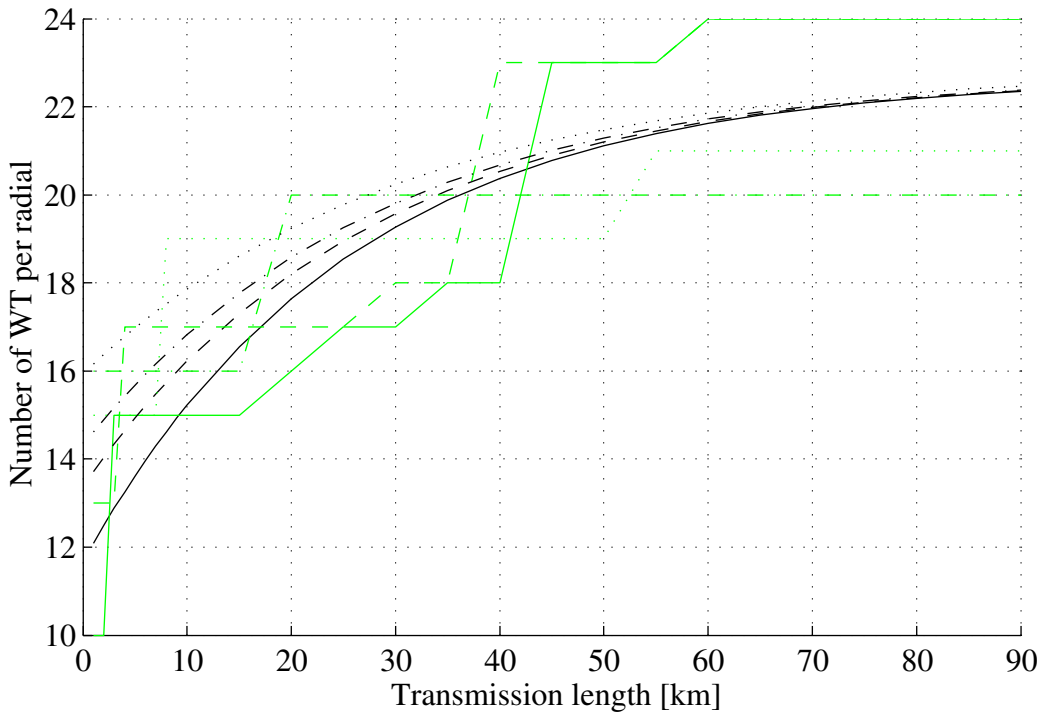

Figure 5.6: Number of wind turbines per radial for 45kV transmission voltage. Black theoretical curves and grey actual curves. Solid 60MW park, dashed 100MW, dash-dotted 160MW and dotted 300MW wind park.

5.2.3 Energy production cost for the different configurations of the small AC wind park

By using the above mentioned selections and the cost and loss functions from appendices C and B the energy production cost of the small AC wind farm can be calculated for different transmission lengths. In figure 5.7 the energy production cost of the 60MW small AC wind farm is shown for different voltage levels, wind turbine types and for an average wind speed of 10m/s. From figure 5.7 it is noticed that 45kV is the best

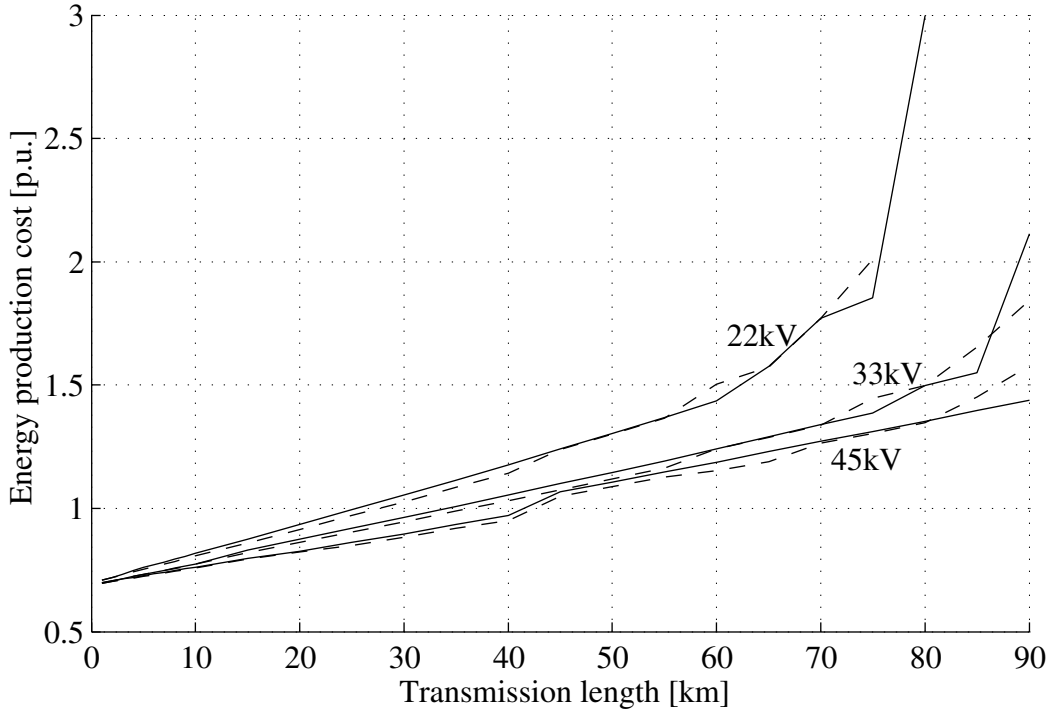

Figure 5.7: The normalized energy production cost for the different configurations of the small AC system. For a 60MW wind park, an average wind sped of 10m/s and for different transmissions lengths. Solid with fix speed wind turbines and dashed wind turbines with the DFIG system.

voltage level to use and up to approximate 80km the wind turbine with the DFIG system is to prefer. This result is similar for all the four investigated power levels of the wind park, and can thus be considered as general.

To make the discussion of the dependency of the energy production cost on different parameters more clear, one of the small AC wind park layouts has been selected as a reference and then one parameter at the time has been changed. Table 5.1 shows the selected reference wind park and the parameters that are varied.

In table 5.2 the different contributions to the energy production cost are shown for the different parameter variations from the reference case. The different contributions are presented in % of the total energy production cost of that configuration, i.e the sum of all contributions is always equal to 100%. The explanations of the abbreviations in table 5.2 are found in figure 5.8.

In figure 5.8 the components of the energy production cost are shown for the reference small AC wind park.

Table 5.1: Reference wind park and the variations.

Parameter	Reference			
Transmission length	40	2	40	80
Transmission voltage	45	22	33	45
Power level	60	60	100	160
Wind turbine type	DFIG	DFIG	Fix speed	
Average wind speed	10	5	6	10

Table 5.2: Reference wind park and the variations.

Case type	WT C	WT L	TM C	TM L	LG
Ref case	59.9	7.6	21.6	3.5	7.4
Length = 2	81	7.6	3.2	0.5	7.8
Length = 80	42.6	7.6	38.5	5	6.3
Voltage = 20	49.8	7.6	30.1	6.5	6
Voltage = 30	55.2	7.6	25.7	4.3	7.1
Power = 100	59.8	7.6	20.9	2.9	8.8
Power = 160	61.2	7.6	19.7	3.2	8.3
Fix speed	58.7	7.5	23.6	2.9	7.3
Wind speed = 5	59.2	10.3	21.3	2	7.2
Wind speed = 6	59.6	9.2	21.5	2.5	7.3

Influence of transmission length on the energy production cost

From figure 5.7 it can be noticed that the energy production cost increases when the transmission distance increases. This is, of course, due to the fact that the cost of the transmission system increases when the transmission length increases. This can also be seen in table 5.2 where the components of the energy production cost are shown for the reference wind park and for two different transmission lengths. From table 5.2 it is seen that both the investment cost and the cost of the losses for the transmission system increase when the transmission length increases.

Influence of transmission voltage

From figure 5.7 it can be seen that the energy production cost decreases with increasing transmission voltage. This is due to the fact that the cost of the transmission system is decreasing with an increasing transmission voltage as can be noticed in table 5.2. The decrease of the cost of the transmission system depends on that the number of needed radials decreases when the transmission voltage increases and therefore the number of parallel transmission cables decreases. The reason is that the number of wind turbines per radial increases when the transmission voltage increases, compere figures 5.5 and 5.6. From table 5.2 it can also be noticed that the cost of the local wind turbine grid increases when the transmission voltage increases. This is due to the fact that the VA rating of the cables increases when the voltage increases, due to that the number of wind turbines per radial increases with increasing voltage as noticed before.

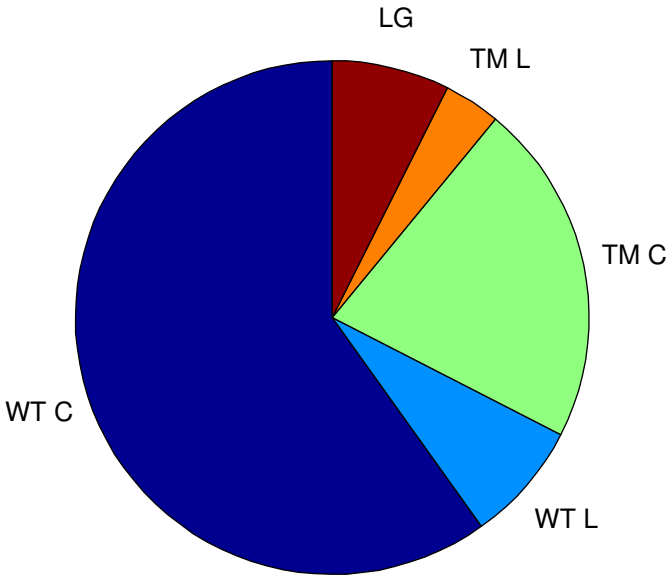

Figure 5.8: The energy production cost divided into components for the small AC wind farm for the reference case.

Where

WT C	Investment cost of the wind turbine
WT L	Cost of the losses in the wind turbine
TM C	Investment cost of the transmission system
TM L	Cost of the losses in the transmission system
LG	Investment and loss cost of the local wind turbine grid

Influence of rated power of the wind park

In table 5.2 the division of the energy production cost into components are also shown for three different power levels. A closer inspection reveals that the different contributions from the parts is almost equal for all power levels. But worth emphasizing again is that the energy production cost decreases when the power of the wind park increases.

Influence of the average wind speed

As was earlier presented, due to the increase in energy production, the energy production cost decreases when the average wind speed increases. From table 5.2 it can be noticed that the cost for the losses in the transmission system increases with an increasing average wind speed and the cost for the losses in the wind turbine decreases. This is mainly due to that the ratio between the load losses and the no-load losses for the transmission system is much larger then the same ratio for the wind turbine.

Influence of wind turbine type

As has been noticed from figure 5.7 the energy production cost for the wind park with wind turbines using the DFIG system is lower up to 80km. This is due to that the fix speed wind turbines require a transmission system that can support them with reactive power from the grid and therefore this system requires a larger conductor area. Therefore the cost of the transmission system is higher for the wind park with fix speed wind turbines, as can be observed in table 5.2.

5.3 Large AC park

In this section, the large AC wind park is investigated in detail.

5.3.1 Configuration selections

In the same way as for the small AC wind park some selections are made to limit the number of parameters. The transformer size is chosen in the same way as for the small AC wind park i.e. the rated power for the transformer is equal to the rated power of the wind park. The voltage for the local wind turbine grid is chosen to 33kV, the voltage level used at the Horns Rev offshore wind park. The number of wind turbines per radial can be calculated in the same way as for the small AC wind park and the result from this calculation can be approximated with the results from figures 5.5 and 5.6 if the transmission distance is put to zero. The selected number of wind turbines per radial and the number of radials are presented in table 5.10 for the different power levels.

Table 5.3: Number of wind turbines per radial and the numbers of radials for the large AC wind park.

Power level	WT/Rad	Rad
60MW	10	3
100MW	10	5
160MW	10	8
300MW	15	10

For the transmission cable it was shown that the cable should be over-dimensioned for short distances. The over-dimensioning decreases with increasing transmission distance and it also decreases with increasing power levels of the wind park. Since the smallest distances are not of such great interest and also to simplify the calculations, the cable with the smallest conductor area that can handle the current is used throughout this work.

5.3.2 Energy production cost for the different configurations of the large AC wind park

By using the above mentioned selections and the cost and loss functions from appendices C and B, the energy production cost of the large AC wind farm can be calculated for different transmission lengths. In figure 5.9 the energy production cost of the

100MW large AC wind farm is shown for different voltage levels, wind turbine types and for an average wind speed of 10m/s. From figure 5.9 it can be seen that the best

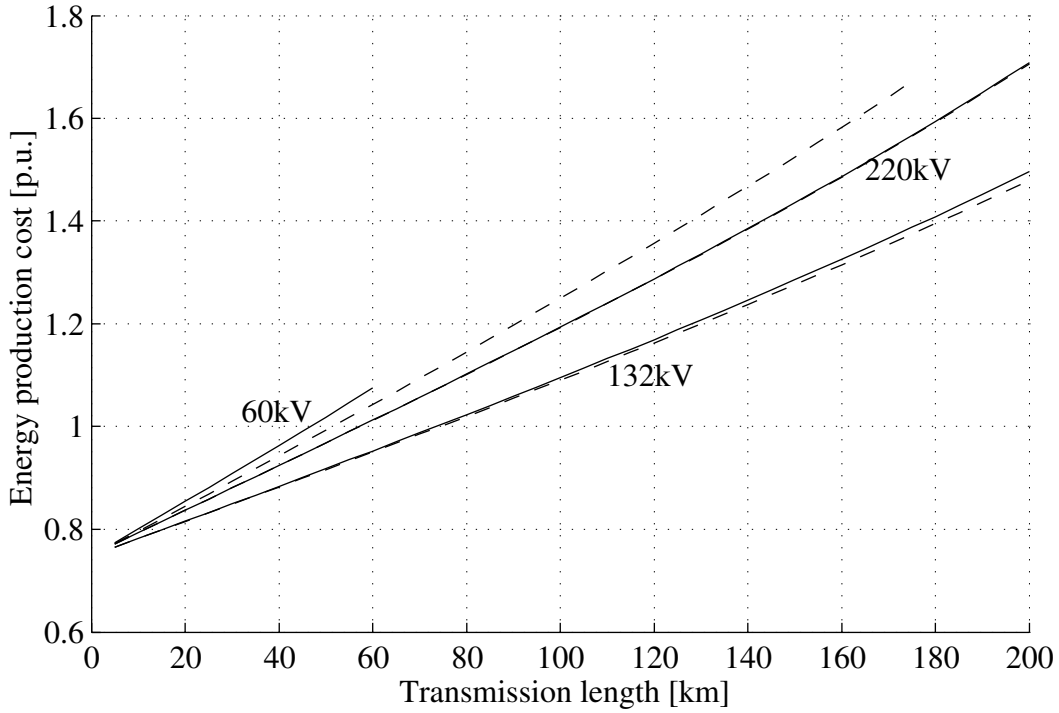

Figure 5.9: The normalized energy production cost for the different configurations of the large AC system. For a 100MW wind park, an average wind sped of 10m/s and for different transmissions lengths. Solid fix speed wind turbines and dashed wind turbines with the DFIG system.

wind park configuration of the 100MW large AC wind park is the one with a transmission voltage of 132kV and wind turbines with the DFIG system. For all investigated wind park sizes, the wind turbine with the DFIG system is the best. But the ideal transmission voltage is depending on the power level of the wind park. For the 60MW wind park the 132kV transmission system is the ideal. But for the 160MW and the 300MW wind park the 220kV transmission system is better. For the 160MW wind park the difference between the 220kV system and the 132kV system is small. But for the 300MW park the only system that works is the 220kV system.

To make the discussion of the dependency of the energy production cost on different parameters more clear, one of the large AC wind park layouts has been selected as a reference and then one parameter at the time has been changed. Table 5.4 shows the selected reference wind park and the parameters that are varied.

In table 5.5 the different contributions to the energy production cost are shown for the different parameter variations from the reference case. The different contributions are presented in % of the total energy production cost of that configuration, i.e the sum of all contributions is always equal to 100%. The explanations of the abbreviations in table 5.5 are found in figure 5.10. The cost of the other components, mark with O in table 5.5, the costs of the low and high voltage switch gear is included together with the cost of the cable compensating inductors and the transformer.

Table 5.4: Reference wind park and the variations.

Parameter	Reference			
Transmission length	100km	30	100	175
Transmission voltage	132kV	60	132	220
Power level	100MW	60	100	160
Wind turbine type	DFIG	DFIG	Fix speed	
Average wind speed	10m/s	5	6	10

Table 5.5: Reference wind park and the variations.

Case type	WT C	WT L	LG	TM L	TM C	O	PL
Ref case	51.3	7.6	7.5	3.1	25.1	1.4	4
Length = 30	65.9	7.6	9.5	0.9	9.7	1.2	5.2
Length = 175	40.7	7.6	6	6.1	34.9	1.5	3.2
Voltage = 60	44.7	7.6	6.6	4.3	32.2	1.1	3.5
Voltage = 220	46.9	7.6	6.9	1	31.8	2.1	3.7
Power = 60	44.7	7.6	6	3.2	32.9	1.6	4
Power = 160	53.7	7.6	8.2	2.1	23.4	1.2	3.9
Fix speed	51.1	7.5	7.5	3.5	25	1.4	4
Wind speed = 5	50.1	10.2	7.2	2.2	24.6	1.8	3.9
Wind speed = 6	50.7	9.2	7.3	2.4	24.8	1.6	4

In figure 5.10 the components of the energy production cost are shown for the reference large AC wind park.

Influence of transmission length on the energy production cost

From figure 5.9 it can be noticed, not surprisingly, that the energy production cost increases when the transmission distance increases. This can also be seen in table 5.5, where the components of the energy production cost is shown for the reference wind park and for two different transmission lengths. From table 5.5 it is seen that both the investment cost and the cost of the losses for the transmission system increases when the transmission length increases.

Influence of transmission voltage

From figure 5.9 it has been noticed that the ideal transmission voltage is 132kV for the 100MW large AC wind park. In table 5.5 it is noticed that the 132kV transmission system has the lowest investment contribution to the energy production cost. Another thing that can be noticed is that the cost of the losses in the transmission system decrease with increasing transmission voltage, due to that the current decreases. The contribution of the other components increases with the transmission voltage. This is due to that the cost of the high voltage protections increases with the voltage, se appendix C.6 and that the investment cost and the cost of the losses for the compensating inductance of the cable increase, see appendix C.4 and B.5.3. The fact that the cost of the compensating inductance increase is due to that the reactive power production of the cable increases with the voltage B.5.1.

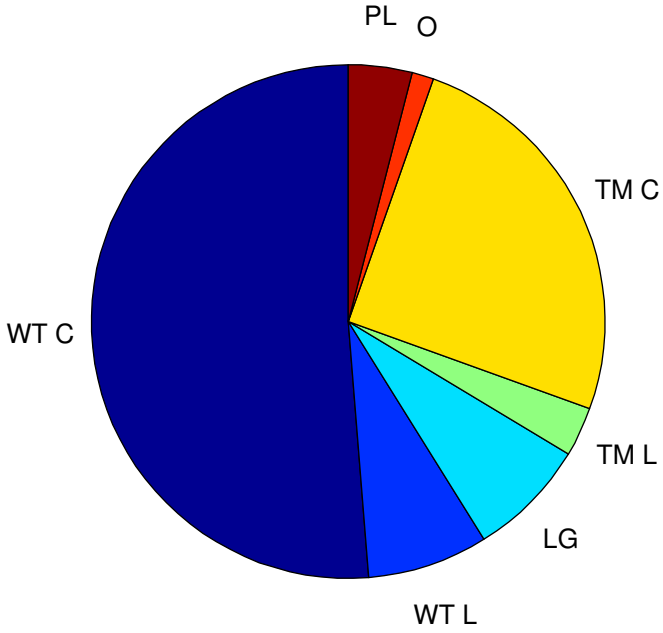

Figure 5.10: The energy production cost divided into components for the large AC wind farm for the reference case.

Where

WT C	Investment cost of the wind turbine
WT L	Cost of the losses in the wind turbine
TM C	Investment cost of the transmission system
TM L	Cost of the losses in the transmission system
LG	Investment and loss cost of the local wind turbine grid
PL	Investment cost of the offshore platform
O	Investment and loss cost of the other components

Influence of rated power of the wind park

The pattern is the same as before, the energy production cost decreases with an increased rated power of the wind park. This can be seen in table 5.5, where the components of the energy production cost is shown for different power levels. The energy production cost decreases due to that the contribution from the transmission system decreases.

Influence of wind turbine type

As can be noticed from figure 5.9 there is no large difference between the fix speed wind turbine and the DFIG wind turbine for the 132kV and 220kV transmission voltage. But for the 66kV transmission voltage there is a large difference, above 60km the fix speed system can not be used. This is due to the reactive power consumption of the fix speed wind turbine. As can be noticed from figure C.3 the cost of the 66kV increases rapidly when the rated power is increased over 100MVA. Due to the reactive power

consumption of the fix speed wind turbine, a transmission cable with an higher rating must be used in this case and due to the high derivative of the 66kV cable cost there is a large difference between the fix speed and the DFIG wind turbine for this transmission voltage and for 100MW rating of the wind park. As also can be noticed from figure C.3 the derivative of the cable cost for the 132kV and 220kV cable around 100MVA is low and therefore the increased rated power of the transmission cable for the fix speed wind turbine does not affect the energy production cost much. As can be seen from table 5.5 it is only the losses in the transmission system that is higher for the fix speed wind turbine compared with the DFIG wind turbine.

Influence of average wind speed

In the same way as for the small AC wind park there is a small variation in the cost of the wind turbine losses and the transmission losses for different average wind speeds. As has been noticed before, the cost for the losses in the transmission system increases with an increasing average wind speed and the cost for the losses in the wind turbine decreases. This is, as mentioned before, mainly due to that the ratio between the load losses and the no-load losses for the transmission system is much larger then the ratio for the wind turbine.

5.4 AC/DC Park

In this section, the AC/DC wind park is studied in detail. First some selections are made to limit the number of cases and then the energy production cost is discussed for the different configurations of the AC/DC wind park.

5.4.1 Configuration selections

With the same technique as for the transformer size for the small AC wind park, the ideal size of the converter stations can be calculated. The cost models and loss models of the converter stations are shown in appendix C.5 and B.6.2. In figure 5.11 the results from these calculation are shown. From figure 5.11 it is noticed that the station

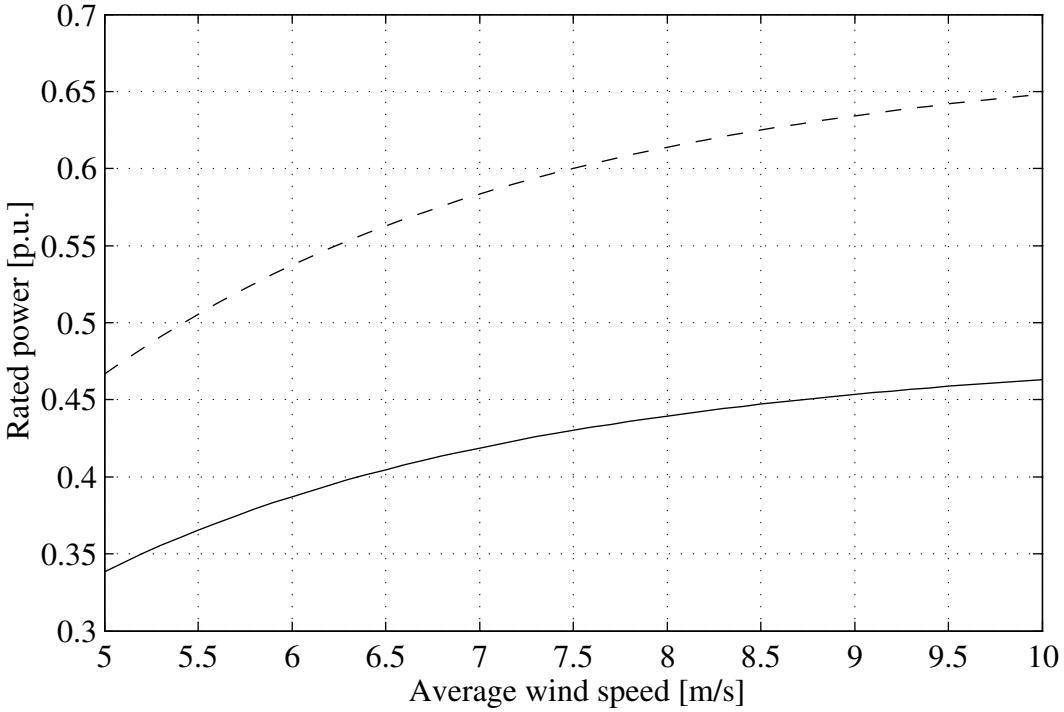

Figure 5.11: Rated power of the HVDC-station in p.u. of the rated power of the wind park as function of the average wind speed for different investment factors. Solid $B_I = 12$ and dashed $B_I = 24$.

should ideally have a rated power lower then the rated power of the wind park to be ideal. This is due to the fact that the reduction of cost for the losses is smaller then the increase of the investment cost when the rated power of the converter station is increased. Since this is not possible, the rated power of the converter station is selected equal to the rated power of the wind park.

For the DC cable is was found that it should be over-dimensioned to minimize the contribution to the energy production cost. The over-dimension increased with increasing transmission voltage, increasing transmission length, increasing average wind speed and with decreasing rated power of the wind park. However, since a discrete number of conductor areas are used, the cables will almost in all cases be over-dimensioned and due to the fact that it was found that the losses of the transmission cable has a minor

contribution to the energy production cost, the rating of the cable is set as close to the rating of the wind park as possible.

The local wind turbine grid for the large AC wind park is used for the AC/DC wind park also. Which means that the number of wind turbines per radial is presented in table 5.10 and the voltage level is 33kV.

5.4.2 Energy production cost for the different configurations of the AC/DC wind park

With these selections the energy production cost for the different configurations of the AC/DC wind park are calculated. In figure 5.12 the energy production cost of the 300MW AC/DC wind farm is shown for different voltage levels, wind turbine types and for an average wind speed of 10m/s. From figure 5.12 it is noticed that 150kV

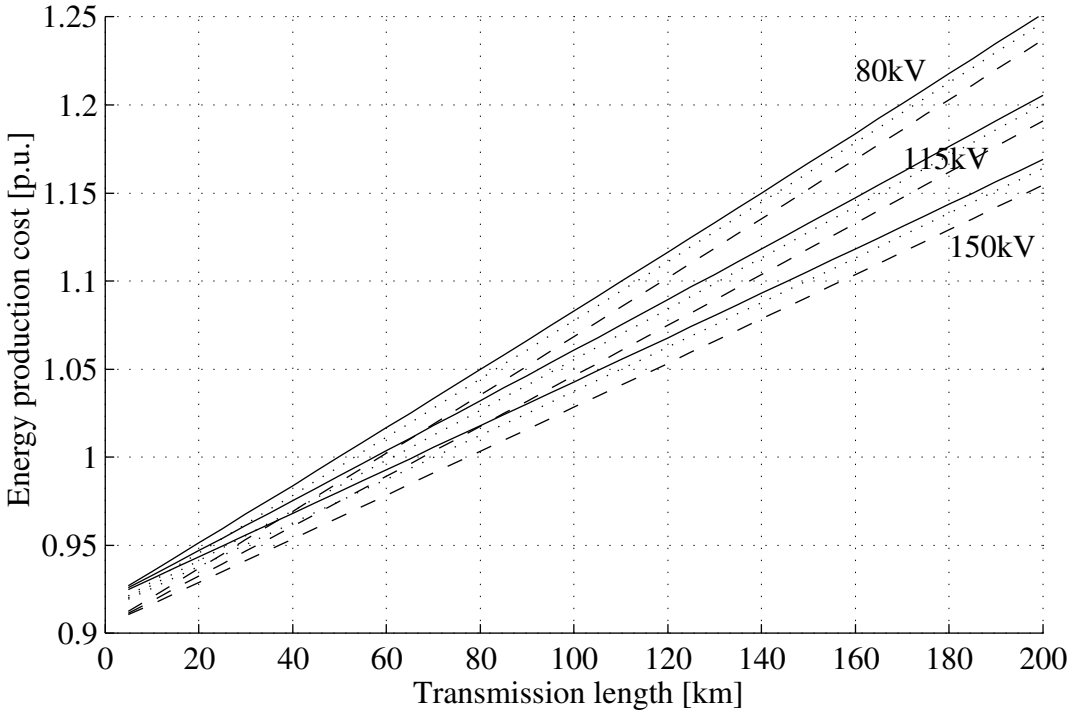

Figure 5.12: The normalized energy production cost for the different configurations of the AC/DC system. For a 300MW wind park, an average wind sped of 10m/s and for different transmissions lengths. Solid fix speed wind turbines, dashed wind turbines with the DFIG system and dotted fix speed wind turbines speed controlled with the offshore converter station.

is the best voltage level to use and the wind turbine using the DFIG system is to prefer. For all power levels, the wind turbine with the DFIG system is to prefer. The ideal voltage level for transmission is depending on the power level. For the 60MW wind park, the 115kV transmission voltage is to prefer and for the 100MW wind park 115kV is to prefer up to a transmission length of 150km. For the 100MW wind park for transmission lengths above 150km and for the 160MW and 300MW wind park the 150kV transmission voltage is to prefer.

To make the discussion of the dependency of the energy production cost on different parameters more clear, one of the AC/DC wind park layouts has been selected as a reference and then one parameter at the time has been changed. Table 5.6 shows the selected reference wind park and the parameters that are varied. The wind turbine

Table 5.6: Reference wind park and the variations.

Parameter	Reference			
Transmission length	100km	30	100	175
Transmission voltage	150kV	80	115	150
Power level	300MW	100	160	300
Wind turbine type	DFIG	DFIG	Fix speed	Fix variable
Average wind speed	10m/s	5	6	10

type Fix variable in table 5.6 is a fix speed wind turbine with only one large generator, with a rated power of 2MW. In this case all wind turbines in the wind park are speed controlled with the offshore converter station, the voltage is also controlled to reduce the iron losses in the generators, in the same way as for the wind turbine with induction generator and a full power converter in section 4.1.3. Using this system, collective variable speed and field weakening can be obtained, still the simple construction of the fix speed wind turbine is utilized [6, 45].

In figure 5.13 the components of the energy production cost are shown for the reference wind park. From figure 5.13 it can be noticed that the contribution to the energy production cost from the transmission system, TM C+TM L, is much lower compared to the large AC wind park. But it shall also be noticed that the converter stations have a significant contribution to the energy production cost. In table 5.7 the different contributions to the energy production cost are shown for the different parameter variations from the reference case. The different contributions are presented in % of the total energy production cost of that configuration, i.e the sum of all contributions is always equal to 100%. The explanations of the abbreviations in table 5.7 are found in figure 5.13.

Table 5.7: Reference wind park and the variations.

Case type	WT C	WT L	LG	TM C	TM L	ST C	ST L	PL
Ref case	54.5	7.6	9.7	9.5	1	9.5	4.6	3.6
Length = 30	59.5	7.6	10.6	3.1	0.3	10.3	4.6	4
Length = 175	49.9	7.6	9	15.3	1.7	8.7	4.6	3.3
Voltage = 80	52.4	7.6	9.4	11.7	1.7	9.1	4.6	3.5
Voltage = 115	53.5	7.6	9.6	10.7	1.1	9.3	4.6	3.6
Power = 100	49.4	7.6	7.2	16.5	2.2	8.6	4.6	3.9
Power = 160	52.9	7.6	8.1	12.1	1.7	9.2	4.6	3.8
Fix	53.7	7.5	10.3	9.4	1	9.9	4.6	3.6
Fix V	54	7.2	9.8	9.4	1	9.9	5	3.6
Wind speed = 5	53.6	10.3	9.3	9.4	0.5	9.3	4.1	3.6
Wind speed = 6	54	9.2	9.5	9.5	0.7	9.4	4.2	3.6

The variations in the contribution to total the energy production cost from the dif-

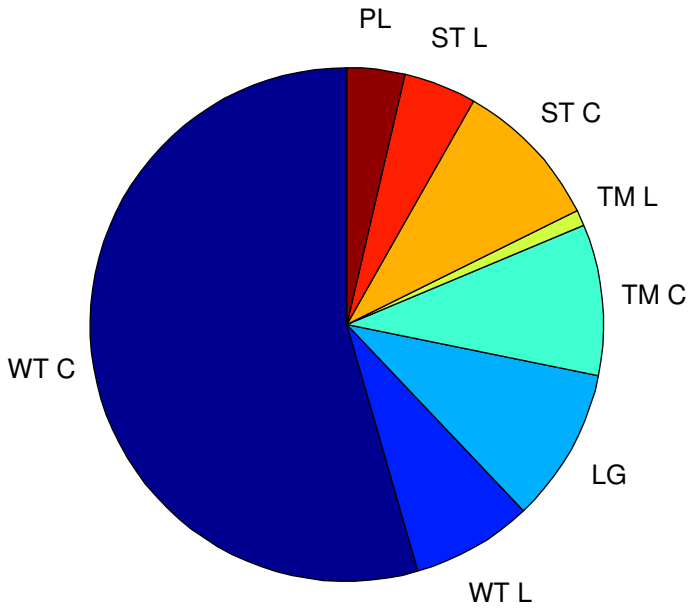

Figure 5.13: The energy production cost divided into components for the AC/DC wind farm for the reference case.

WT C	Investment cost of the wind turbine
WT L	Cost of the losses in the wind turbine
LG	Investment and loss cost of the local wind turbine grid
TM C	Investment cost of the transmission system
TM L	Cost of the losses in the transmission system
ST C	Investment cost of the two converter stations
ST L	Cost of the losses in the two converter stations
PL	Investment cost of the offshore platform

ferent components from variations in the transmission length, the transmission voltage, rated power of the wind park and the average wind speed can be explained in the same way as for the large AC wind park.

As has already been seen in figure 5.12 the wind turbine with the DFIG system is the best suitable. From table 5.7 it is seen that the configuration with the fix speed wind turbine, Fix, the wind turbine losses contributes less to the energy production cost then for the wind turbine with the DFIG system. But the local grid contributes with more for the fix speed system, which is due to the reactive power. For the configuration with the fix speed wind turbines controlled by the offshore station, Fix V, it can be seen that the contribution from the wind turbine losses is reduced compared with the case with wind turbine with the DFIG system. But the gain is lost in an increased contribution from the converter station losses. This is due to the fact that the control of the system is designed to reduce the losses in the wind turbine only. A better, but more complicated way is to use a control that reduces the losses in the whole local grid (wind turbines, cables and offshore converter station).

5.5 Small DC park, local grid for transmission

In this section the small DC wind park is studied in detail. First some selections are made to limit the number of cases and then the energy production cost is discussed for the different configurations of the small DC wind park.

5.5.1 Configuration selections

With the same technique as for the AC transformer size in the small AC wind park the size of the DC transformer can be calculated. The cost models and loss models of the DC transformer are shown in appendix C.5 and B.6.4. The ideal size of the DC transformer is shown in figure 5.14. From figure 5.14 it is noticed that the DC

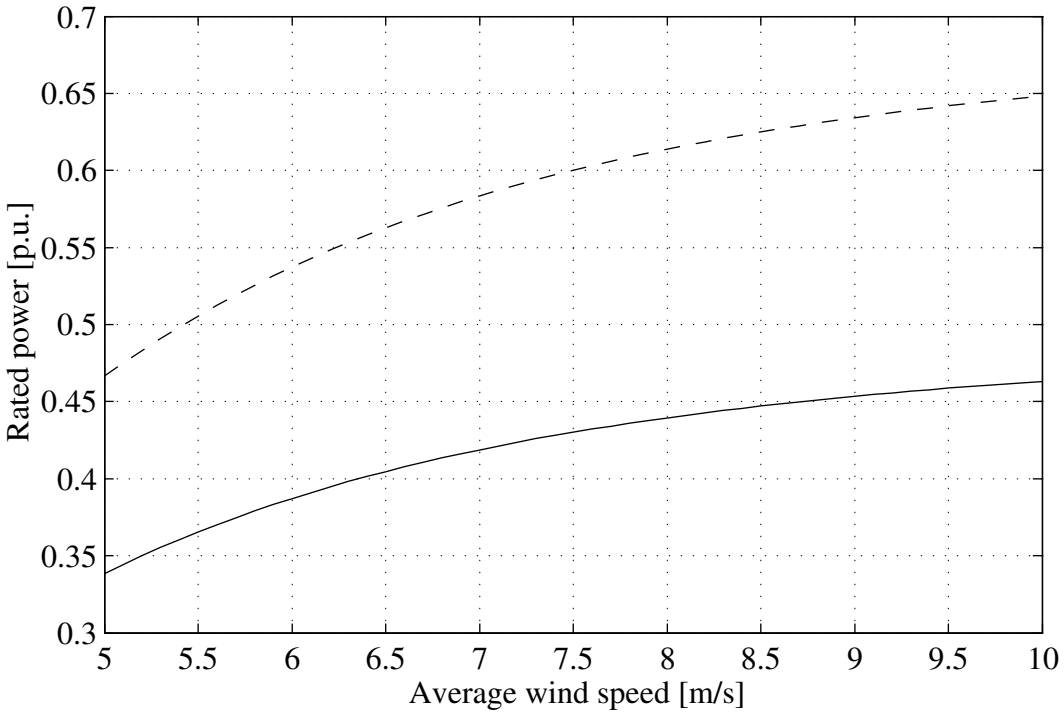

Figure 5.14: Rated power of the DC-transformer in p.u. of the rated power of the wind park as function of the average wind speed for different investment factors. Solid $B_I = 12$ and dashed $B_I = 24$.

transformer should ideally have a rated power lower then the rated power of the wind park to be ideal. Since this is not possible, the rated power of the DC transformer is selected equal to the rated power of the wind park. In the same way as for the AC/DC wind park the rated power of the converter station is selected equal to the rated power of the wind park.

In the same way as for the small AC wind park the ideal number of wind turbine per radial can be calculated. The results from this calculation is shown in figure 5.15 for a transmission voltage of 40kV, for different rated powers and for different transmission lengths. Due to the same reasons as for the small AC wind park, the number of wind turbines per radial is not a free choice. Therefore the grey curves in figure 5.15 describe the used number of wind turbines per radial. As can be noticed, the number of wind

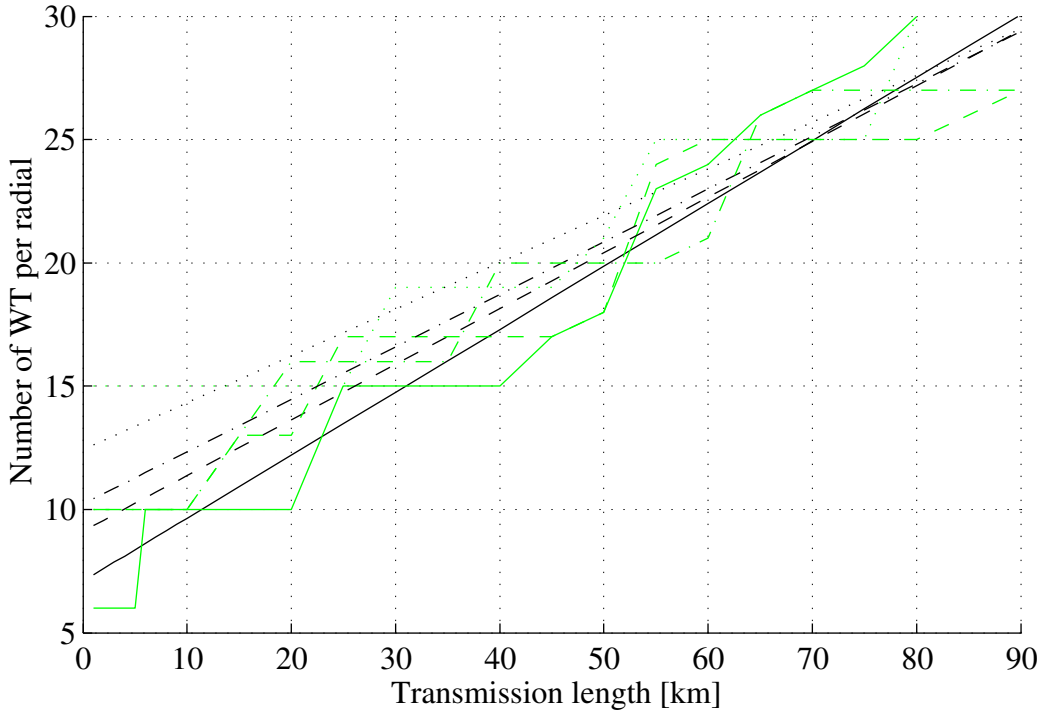

Figure 5.15: Number of wind turbines per radial for 40kV transmission voltage. Black theoretical curve and grey actual curve. Solid 60MW park, dashed 100MW, dash-dotted 160MW and dotted 300MW wind park.

turbines increases with the transmission length, in order to reduce the number of radials and thereby reduce the number of transmission cables. This is due to the fact that when the transmission length is long, it is expensive to put in an extra transmission cable. In the same way as for the small AC wind park the actual rated power of the wind park is allowed to vary somewhat around the desired rated power when the number of wind turbines per radial and the number of radials are selected.

Again it was found that the transmission cables should be over-dimensioned for short transmission distances in order to minimize the contribution to the energy production cost. But the over-dimensioning decreases with increasing transmission lengths. Therefore the rating of the transmission cables is set equal to the rated power of the radial, as before.

5.5.2 Energy production cost for the different configurations of the small DC wind park

With these selections, the energy production cost for the different configurations of the small DC wind park are calculated. In figures 5.1 and 5.2 the energy production cost of the 60MW and the 160MW small DC wind farm are shown (solid grey line) for an average wind speed of 10m/s.

As in the earlier sections, one of the small DC wind park layouts has been selected as a reference and then one parameter at the time has been changed. Table 5.8 shows the selected reference wind park and the parameters that are varied.

Table 5.8: Reference wind park and the variations.

Parameter	Reference			
Transmission length	40km	2	40	80
Transmission voltage	40kV			
Power level	60MW	60	100	160
Wind turbine type	Boost			
Average wind speed	10m/s	5	6	10

In figure 5.16 the components of the energy production cost are shown for the reference wind park. From figure 5.16 it can be noticed that the converter station and

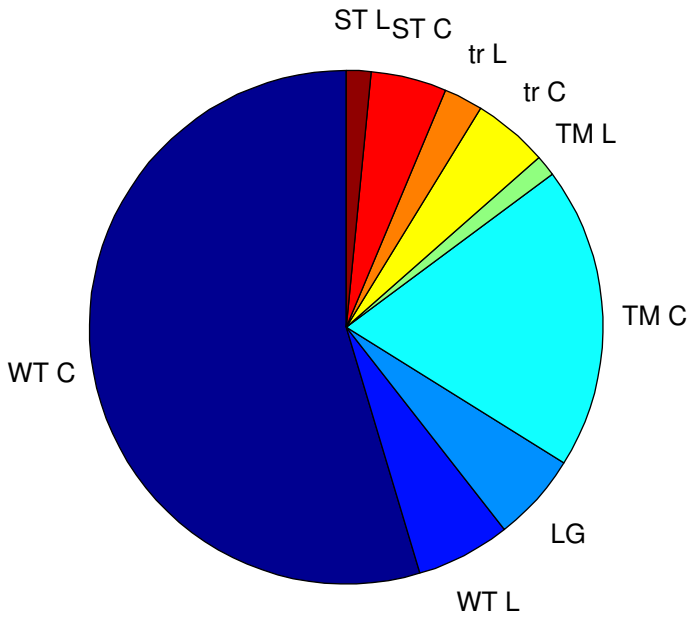

Figure 5.16: The energy production cost divided into components for the small DC wind farm for the reference case.

WT C	Investment cost of the wind turbine
WT L	Cost of the losses in the wind turbine
LG	Investment and loss cost of the local wind turbine grid
TM C	Investment cost of the transmission system
TM L	Cost of the losses in the transmission system
tr C	Investment cost of the DC transformer
tr L	Cost of the losses in the DC transformer
ST C	Investment cost of the converter station
ST L	Cost of the losses in the converter station

the DC transformer has a significant contribution to the energy production cost. In table 5.9 the different contributions to the energy production cost are shown for the different parameter variations from the reference case, see figure 5.16 for the abbreviations in the table. The different contributions are presented in % of the total energy

production cost of that configuration.

Table 5.9: Reference wind park and the variations.

Case type	WT C	WT L	LG	TM C	TM L	tr C	tr L	ST C	ST L
Ref case	54.6	5.9	5.6	19	1.3	4.8	2.4	4.8	1.6
Length = 2	69.6	5.9	4.6	3.4	0.2	6.1	2.5	6.1	1.6
Length = 80	43.2	5.9	6.7	30.6	2.1	3.8	2.4	3.8	1.5
Power = 100	55.8	5.9	6.2	17.2	1.2	4.9	2.4	4.9	1.6
Power = 160	56	5.9	7	16.3	1.1	4.9	2.4	4.9	1.6
Wind speed = 5	55.2	5.6	5.6	19.2	0.7	4.8	2.5	4.8	1.6
Wind speed = 6	55.2	5.5	5.6	19.2	0.9	4.8	2.4	4.8	1.6

From table 5.9 it is seen that the contribution from the local wind turbine grid, LG, increases when the transmission length increases, which was expected. This is due to the fact that the number of wind turbines per radial increases when the transmission length increases, see figure 5.15. The increase of number of wind turbines gives that the conductor area must increase and therefore the cost of the cables in the local wind turbine grid increases, appendix C.4.

In table 5.9 it is also seen that when the rated power of the wind park increases, the contribution from the local wind turbine grid increases. This is also due to the fact that the number of wind turbines per radial increases when the rated power of the wind park increases. The contribution from the transmission system decreases due to the decrease of the number of radials.

The variations in the energy production cost due to the average wind speed can be explained in the same way as for the small AC wind park.

5.6 Large DC Park

In this section the large DC wind park is studied in detail. As in the previous chapters, first some selections are made to limit the number of cases and then the energy production cost is discussed for the different configurations of the large DC wind park.

5.6.1 Configuration selections

In the same way as before some selections are made to limit the number of parameters. The DC transformer size and the converter station is chosen in the same way as for the small DC wind park i.e. the rated powers for the DC transformer and the converter station are equal to the rated power of the wind park. The number of wind turbines per radial for the large wind park with one DC transformer step can be calculated in the same way as for the small DC wind park and the result from this calculation can be approximated with the results from figure 5.15 if the transmission distance is put to zero. The selected number of wind turbines per radial and the number of radials for the large DC wind park with one DC transformer step is presented in table 5.10 for the different power levels. In table 5.10 the number of turbines per radial, the number of radials per cluster and the number of clusters in the large DC wind park with two DC transformer steps are also shown. The number of radials per cluster is the same as is used in [32] for this type of two step DC wind park.

Table 5.10: Number of wind turbines per radial (WT/Rad) and the numbers of radials (NRad) for the large DC wind park.

Power level	One step WT/Rad	NRad	Two steps WT/Rad	Rad/Cluster	Cluster
60MW	10	3	1	5	6
100MW	10	5	1	5	10
160MW	10	8	1	5	16
300MW	15	10	1	6	25

Due to the same reasons as for the AC/DC wind park, it was found that the transmission cable should be over-dimensioned. The over-dimension increased with increasing transmission voltage, increasing transmission length, increasing average wind speed and with decreasing rated power of the wind park. But as for the other types of wind parks the rating of the cable is set equal to the rating of the wind park.

5.6.2 Energy production cost for the different configurations of the large DC wind park

With these selections the energy production cost for the different configurations of the large DC wind park is calculated. In figure 5.17 the energy production cost of the 300MW large DC wind farm is shown for different voltage levels, wind turbine types and for an average wind speed of 10m/s. From figure 5.17 it is noticed that 150kV is the best voltage level to use and that the wind park configuration with only one DC transformer step is to prefer, for all power levels. The ideal voltage level for transmission is depending on the power level. For the 60MW wind park the 115kV is

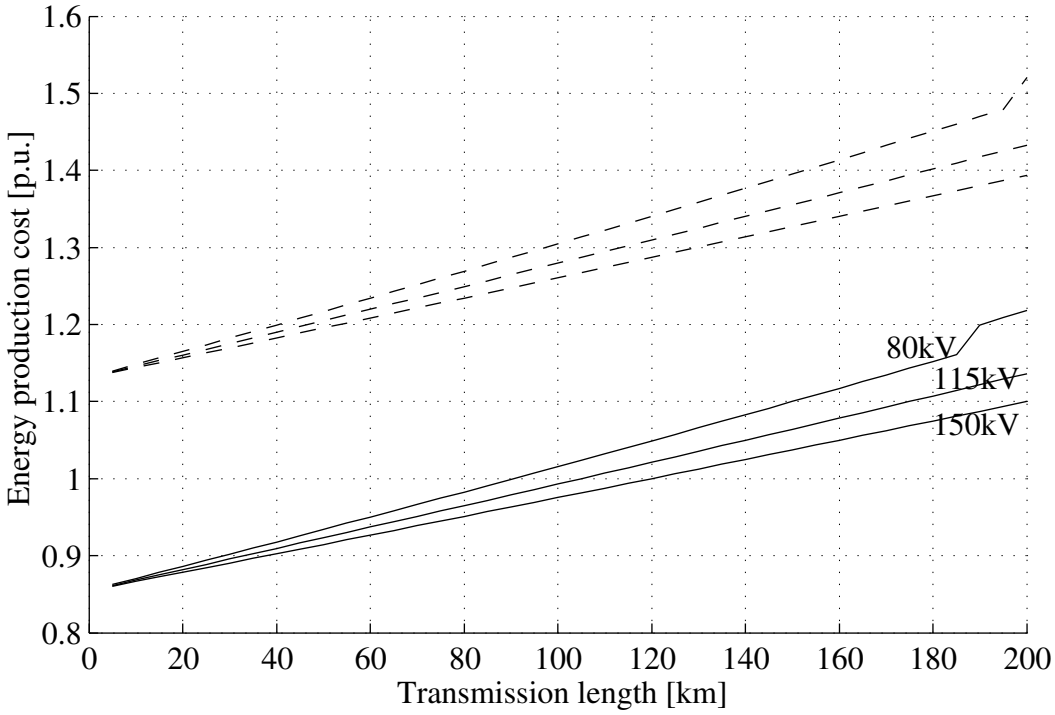

Figure 5.17: The normalized energy production cost for the different configurations of the large DC system, solid lines one DC transformer step and dashed lines two DC transformer steps. For a 300MW wind park, an average wind sped of 10m/s and for different transmissions lengths.

to prefer and for the 100MW wind park 115kV is to prefer up to a transmission length of 145km. For the 100MW wind park for transmission lengths above 145km and for the 160MW and 300MW wind park the 150kV transmission voltage is to prefer.

To make the discussion of the dependency of the energy production cost on different parameters more clear, one of the large DC wind park layouts has been selected as a reference and then one parameter at the time has been changed. Table 5.11 shows the selected reference wind park and the parameters that are varied.

Table 5.11: Reference wind park and the variations.

Parameter	Reference			
Transmission length	100km	30	100	175
Transmission voltage	150kV	80	115	150
Power level	300MW	100	160	300
Wind park type	One step	One step	Two step	
Average wind speed	10m/s	5	6	10

In figure 5.18 the components of the energy production cost are shown for the reference wind park. If this reference case is compared with the reference case for the large AC wind park, table 5.5, it can be noticed that the DC transmission system has a lower contribution to the energy production cost then the AC transmission system has. From figure 5.18 it can also be noticed that the converter station and the DC

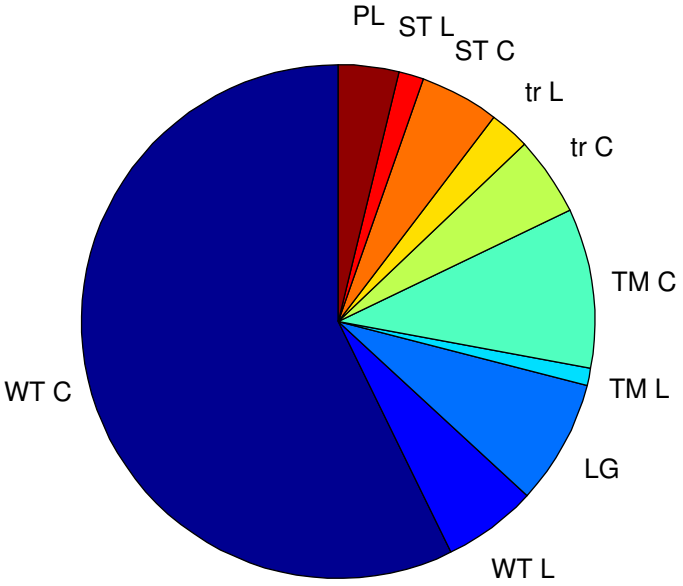

Figure 5.18: The energy production cost divided into components for the large DC wind farm for the reference case.

WT C	Investment cost of the wind turbine
WT L	Cost of the losses in the wind turbine
LG	Investment and loss cost of the local wind turbine grid
TM C	Investment cost of the transmission system
TM L	Cost of the losses in the transmission system
tr C	Investment cost of the DC transformer
tr L	Cost of the losses in the DC transformer
ST C	Investment cost of the converter station
ST L	Cost of the losses in the converter station
PL	Investment cost of the offshore platform

transformer has a significant contribution to the energy production cost. In table 5.12 the different contributions to the energy production cost are shown for the different parameter variations from the reference case, se figure 5.18 for explanations for the abbreviations in the table. The different contributions are presented in % of the total energy production cost of that configuration.

The variations in the energy production cost due to the variations in transmission voltage, rated power of the wind park and in the average wind speed can be explained in the same way as for the AC/DC wind park.

One observation that can be made from table 5.12 is that the increase in the contribution from the transmission system is less compared to the large AC wind park. The increase can be explained in the same way as for the AC/DC wind park.

As already has been noticed, the system with two steps of DC transformers has a much higher energy production cost then the system with only one step. This is due to the reason that the contribution from the offshore platforms and DC transformers

Table 5.12: Reference wind park and the variations.

Case type	WT C	WT L	LG	TM L	TM C	tr C	tr L	ST C	ST L	PL
Ref case	57.2	5.9	7.8	1.1	10	5	2.5	5	1.6	3.8
Length = 30	62.7	5.9	8.6	0.3	3.3	5.5	2.5	5.5	1.6	4.2
Length = 175	52.3	5.9	7.2	1.9	16.1	4.6	2.5	4.6	1.5	3.5
Voltage = 80	55	5.9	7.5	2	12.3	4.8	2.5	4.8	1.5	3.7
Voltage = 115	56.2	5.9	7.7	1.3	11.3	4.9	2.5	4.9	1.6	3.8
Power = 100	51.6	5.9	5.6	2.6	17.2	4.5	2.6	4.5	1.5	4
Power = 160	55.2	5.9	6.5	2	12.7	4.8	2.5	4.8	1.5	4
Two step	44.2	7.4	9.7	1	7.8	7.7	4.8	3.9	1.5	12.1
Wind speed = 5	57.8	5.5	7.8	0.6	10.1	5	2.6	5	1.6	3.9
Wind speed = 6	57.8	5.4	7.9	0.7	10.1	5	2.5	5	1.6	3.9

is higher for the two step, as could have been expected. The rest of the results shows the same pattern as presented in previous sections.

5.7 DC Park with series connected wind turbines

In this section the energy production cost of the DC park with series connected wind turbines is studied in detail.

5.7.1 Configuration selections

For the series DC wind park the onshore converter station and the DC transmission cable is selected in the same way as for the large DC wind park i.e the converter station and the DC transmission cable has a rated power equal to the rated power of the wind park.

The ideal number of wind turbines per leg can not be calculated in the same way as for the ideal number of wind turbines per radial. This is due to the fact that in this work there is no difference in the cost of the DC/DC converters when the output voltage is changed. Therefore the efficiency of the wind turbine DC/DC converter is only studied. The efficiency will be dependent on the maximum allowed failure ratio, maximum number of non producing wind turbines divided with the number of producing wind turbines per leg, of the wind turbines in one leg. This is due to the fact that the producing wind turbines in a leg must compensate for the zero output voltage of the non producing wind turbines by increasing their output voltage. This means that the DC/DC converters in the wind turbines must be overrated in the output voltage and this gives a lower efficiency. This can be seen in figure 5.19 where the average efficiency of the wind turbine DC/DC converter is shown for different average wind speeds. In this work a maximum failure ratio of 13 to 20% is used.

In general, the cost of the DC/DC converter in the wind turbine should increase with an increasing rated output voltage. This gives that the number of wind turbines per leg should be as high as possible and the failure ratio as low as possible to keep the output voltage as low as possible. In table 5.13 the used number of wind turbines per leg and the number of legs for the different power levels are shown.

Table 5.13: Number of wind turbines per leg and the numbers of legs for the series DC wind park.

Power level	WT/leg	leg
60MW	30	1
100MW	25	2
160MW	20	4
300MW	30	5

5.7.2 Energy production cost for the different configurations of the series DC wind park

With these selections the energy production cost for the different configurations of the series DC wind park are calculated. In figure 5.20 the energy production cost of the 300MW series DC wind farm is shown for different voltage levels, maximum allowed number of non-working wind turbines and for an average wind speed of 10m/s. From figure 5.20 it can be noticed that the three voltage levels crosses each other. This

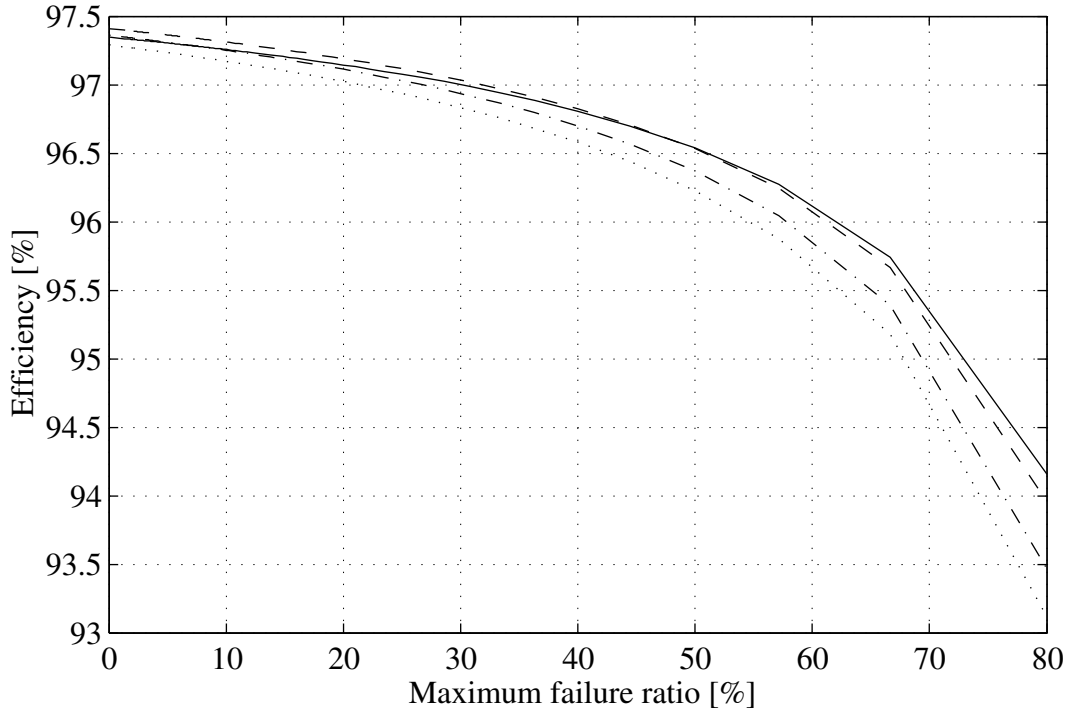

Figure 5.19: The efficiency of the wind turbine DC/DC converter as function of the maximum allowed failure ratio for different average wind speeds. Solid 5m/s, dashed 6m/s, dash-dotted 8m/s and dotted 10m/s.

means that the 80kV transmission is best for short transmission distances, the 150kV transmission voltage is best suitable for long transmission distances and the 115kV for distances in between. When the rated power of the wind park decrease, the crossover point increases. For example, for the 100MW wind park the 80kV is best up to 35km and the 150kV is best above 185km.

To make the discussion of the dependency of the energy production cost on different parameters more clear, one of the series DC wind park layouts has been selected as a reference and then one parameter at the time has been changed. Table 5.14 shows the selected reference wind park and the parameters that are varied.

Table 5.14: Reference series DC wind park and the variations.

Parameter	Reference			
Transmission length	100km	30	100	175
Transmission voltage	150kV	80	115	150
Power level	300MW	100	160	300
Max number of failed WT	4	4	8	
Average wind speed	10m/s	5	6	10

In figure 5.21 the components of the energy production cost are shown for the reference wind park. By comparing figure 5.21 and figure 5.18 it can be noticed that the series wind park has less components that contributes to the energy production cost then the large DC wind park has. Since the number of wind turbines is the same

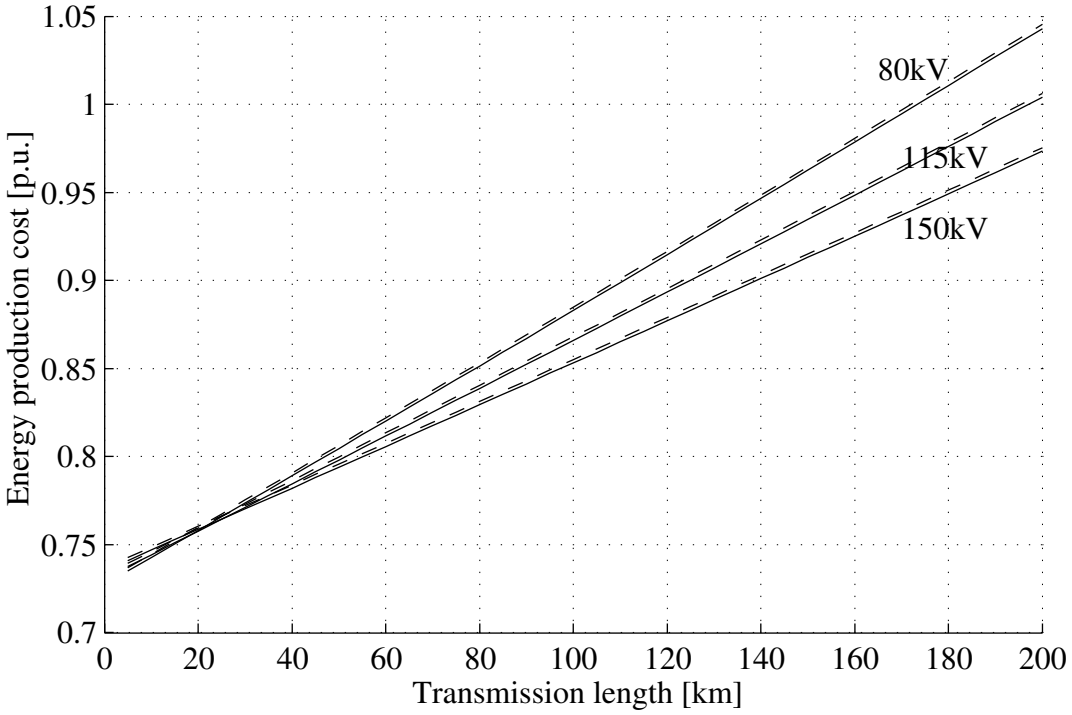

Figure 5.20: The normalized energy production cost for the different configurations of the series DC system. For a $300MW$ wind park, an average wind sped of $10m/s$ and for different transmissions lengths. Solid maximum 4 failed wind turbines per leg, dashed maximum 8 failed wind turbines per leg.

for both configurations and their cost is assumed to be the same, see appendix C.2, it can be noticed that the energy production cost for the series DC wind park must be lower. This is based on the fact that the wind turbines contributes more to the energy production cost in the series wind park compared to the large DC wind park.

In table 5.15 the different contributions to the energy production cost are shown for the different parameter variations from the reference case, se figure 5.21 for explanations for the abbreviations in the table. The different contributions are presented in % of the total energy production cost of that configuration.

The same pattern as for the large DC wind park can be noticed also for the variations in the energy production cost due to variations in transmission length, transmission voltage, rated power of the wind park and in the average wind speed.

For the failure ratio it can be noticed from figure 5.20 that an increasing failure ratio increases the energy production cost. This is due to the fact that the losses in the wind turbine increases, see table 5.15. This increase is caused by the decrease in efficiency in the DC/DC converter as mention before.

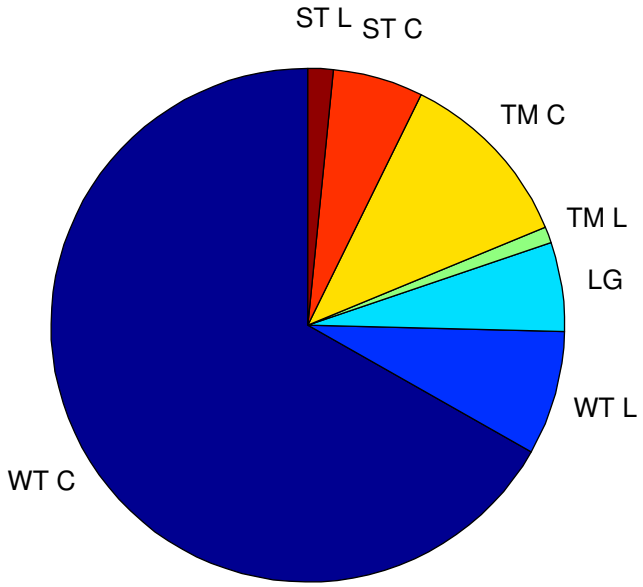

Figure 5.21: The energy production cost divided into components for the series DC wind farm for the reference case.

WT C	Investment cost of the wind turbine
WT L	Cost of the losses in the wind turbine
LG	Investment and loss cost of the local wind turbine grid
TM C	Investment cost of the transmission system
TM L	Cost of the losses in the transmission system
ST C	Investment cost of the converter station
ST L	Cost of the losses in the converter station

Table 5.15: Reference wind park and the variations.

Case type	WT C	WT L	LG	TM L	TM C	ST C	ST L
Ref case	66.8	7.8	5.6	1	11.5	5.7	1.6
Length = 30	74	7.8	6.2	0.3	3.8	6.3	1.6
Length = 175	60.4	7.8	5.1	1.8	18.2	5.2	1.6
Voltage = 80	63.8	7.8	5.4	1.8	14.1	5.5	1.6
Voltage = 115	65.4	7.8	5.5	1.2	12.9	5.6	1.6
Power = 100	59	7.8	4.9	2.3	19.3	5	1.5
Power = 160	63.6	7.9	5.3	1.9	14.3	5.4	1.6
Num fail = 8	66.6	8	5.6	1	11.5	5.7	1.6
Wind speed = 5	67.4	7.6	5.5	0.6	11.6	5.8	1.6
Wind speed = 6	67.4	7.4	5.6	0.7	11.6	5.8	1.6

Chapter 6

Conclusions

For the main components in a wind park, cost and loss models has been evaluated. The purpose has been to calculate the energy production cost of the different wind park configurations.

For the wind park configurations that utilizes DC at different levels, some sort of DC/DC converters are necessary. There are two main types of DC/DC converters that are needed, a voltage adjusting DC/DC converter and a DC transformer. The voltage adjusting converter should be able to handle a varying input voltage down to approximately 40% of the rated, while keeping the output voltage constant. The DC transformer works with a relatively fixed transformer ratio between the input and output voltage, the variations are less then 10%. To select the best DC/DC converter topology for these two types, a theoretical investigation of the utilization factor of the semiconductors was performed for various DC/DC converter topologies. From this investigation, the boost converter was selected for voltage adjusting operation, if the transformation ratio from rated input to rated output voltage is less then 5. If the transformation ratio is higher then this, or if galvanic isolation between the wind turbine and the DC grid is desired, the full bridge isolated boost converter is selected. This is due to that the full bridge isolated boost converter is better utilized in this voltage adjusting application then the full bridge converter. For the DC transformer the full bridge converter is chosen.

Some different configurations of the drive train for wind turbines were investigated for the energy capture of wind turbines. In this investigation it was found that the difference between the investigated systems was quite small. For the AC wind turbines, the fix speed system and the doubly feed induction generator system were selected. For the DC wind turbines, the system with a low speed permanently magnetized generator and a boost converter is used. In the series connected DC wind park, a system with a low speed permanently magnetized generator and a full bridge isolated boost converter is used. The result found was that given a specific rotor diameter, the energy capture is almost the same regardless of the system used. The selection of the system to be used thus depend on other factors.

Six different types of electrical configurations of wind parks has been investigated for the energy production cost. The investigate types are

Small AC	Where the local wind turbine grid is used for transmission
Large AC	Which has a low voltage grid between the wind turbines and has a central transformer on an offshore platform for increasing the voltage level to a level suitable for transmission to the PCC
AC/DC	Similar to the Large AC wind park but with the difference that the transmission is made using DC instead of AC
Small DC	Similar to the Small AC wind park but with the difference that the wind turbine has a DC voltage output
Large DC	Similar to the Large AC wind park but with the difference that the wind turbine has a DC voltage output
Series DC	Uses series connected wind turbines with a DC voltage output

The investigation is done for different rated wind park powers, different transmission lengths and different average wind speeds.

The results regarding the energy production cost for the AC wind parks was as expected. The small AC wind park was best for short transmission distances (up to approximately 20km) and the AC/DC wind park was best for long distances (above approximately 130km). The large AC wind park is best in between the small AC and the AC/DC wind park.

For the DC wind parks the results was somewhat surprising, except for the small DC wind park, where it was found that it is not a good solution, due to the high costs of the converter station and DC transformers. For the large DC wind park it was found that it is better then the AC/DC wind park. This is due to that the DC cables are cheaper then the AC cables. But the reduction in the energy production cost is not so large, which gives that the large AC wind park is still better for shorter transmission distances. The most surprising results was for the series DC wind park. This configuration shows very promising performance. The energy production cost for the series DC wind park was the lowest for all the six investigated wind park configurations for transmission lengths over 20km. For example, for a wind park with a rated power of 160MW, a transmission length of 80km and a average wind speed of 10m/s it was found that the series DC wind park has a energy production cost of 0.86p.u. The large AC has an energy production cost of 0.97p.u, the AC/DC 0.98p.u and the small AC and DC approximately 1.2p.u. The message can also be expressed as: An increased investment cost of 13% can be allowed for the series DC park before it gets a production cost equal to the large AC park, using the input data that was available in this work

As expected, the energy production cost was strongly dependent on the average wind speed. As an example, the energy production cost at an average wind speed of 6.5m/s was twice as high as the cost for an average wind speed of 10m/s. It was also found that the energy production cost decreases when the power of the wind park increases.

By comparing the contribution to the energy production cost from the fix speed wind turbine system with the wind turbine system using the DFIG system it was found that for the configuration with the fix speed wind turbines, the wind turbine losses contributes less to the energy production cost then for wind turbines using the DFIG system. But the local grid contributes with more for the fix speed system, due to the reactive power flow.

This work has presented necessary steps to determine the energy production cost.

It should be stressed that the cost results, of course, depend strongly on the cost input parameters. The aim here has been to present a determination strategy that can be of value for further wind park design and cost studies.

References

[1] F. Abrahamsen. *Energy Optimal Control of Induction Motor Drives*. Ph.D thesis, Aalborg University, Institute of Energy Technology, Aalborg, Denmark, February 2000.

[2] T. Ackermann. Transmission systems for offshore wind farms. *Power Engineering Review, IEEE*, 22(12):23–27, Dec. 2002.

[3] V. Akhmatov, H. Knudsen, and A.H. Nielsen. Advanced simulation of windmills in the electric power supply. *Electrical Power and Energy Systems*, 22(-):421–434, 2000.

[4] Elsam A/S. Horns Rev Offshore Wind Farm, The world´s largest offshore wind energy project. Information folder, www.elsam.com, ?

[5] R.J. Barthelmie and S. Pryor. A review of the economics of offshore wind farms. *Wind enginering*, 25(3):203–213, 2001.

[6] P. Bauer, S.W.H. de Haan, C.R. Meyl, and J.T.G. Pierik. Evaluation of electrical systems for offshore windfarms. In *Industry Applications Conference, 2000. Conference Record of the 2000 IEEE*, pages 1416 –1423 vol.3, -, 8-12 Oct. 2000.

[7] R. Bergen and Vijay Vittal. *Power system analysis, 2nd ed.* Prentice-Hall, 2000.

[8] F. Blaabjerg, U. Jaeger, and S. Munk-Nielsen. Power losses in pwm-vsi inverter using npt or pt igbt devices. *IEEE Transactions on Power Electronics*, 10(3):358–67, May 1995.

[9] F. Blaabjerg, J.K. Pedersen, S. Sigurjonsson, and A. Elkjaer. An extended model of power losses in hard-switched igbt-inverters. pages 1454–63 vol.3, 1996.

[10] K. Burges, E.J. van Zuylen, J. Morren, and S.W.H. de Haan. Dc transmission for offshore wind farms: Consepts and components. In *Second International Workshop on Transmission Networks for Offshore Wind Farms*, pages –, Stockholm, Sweden, 30-31 March, 2001.

[11] ABB High Voltage Cables and ABB Power Systems. HVDC Light for power transmission. Data sheet, ?

[12] ABB High Voltage Cables. Medium Voltage Power Cables 10(12)-30(36) kV. Data sheet, DECEMBER 1995.

[13] ABB High Voltage Cables. Power Cables for High and Extra-high Voltages. Data sheet, 1995.

[14] Jose M. del Castillo. The analytical expression of the efficiency of planetary gear trains. *Mechanism and Machine Theory*, 37:197–214, 2002.

[15] Eltra. Eltra's 150 kV-kabelanlaeg Blåvand-Karlgårde. Information folder, www.eltra.dk, ?

[16] Enercon. http://www.enercon.de. Home page, 2003.

[17] R.W. Erickson and D. Maksimovi´c. *Fundamentals of Power Electronics, Second Edition*. Kluwer Academic Publishers, 2001.

[18] eupec. Technical Information IGBT-Modules FZ1000R25KF1. Data sheet, ?

[19] eupec. Technical Information IGBT-Modules FZ1600R17KF6C B2. Data sheet, ?

[20] L. Ferraris, G. Griva, M. Lazzari, F. Profumo, and A. Tenconi. Iron losses analysis with different supply techniques in high poles number induction motors for automotive applications. pages 651–5 vol.2, 1999.

[21] A. Grauers and A. Lindskog. Pm generator with series compensated diode rectifier. In *2000 IEEE Nordic Workshop on Power and Industrial Electronics (NORpie/2000)*, pages 59–63, Aalborg, Denmark, 13-16 June, 2000.

[22] A. Grauers. *Design of Direct-Driven Permanent-Magnet Generators for Wind Turbines*. Ph.D thesis, Chalmers University of Technology, Department of Electric Power Enginering, Göteborg, Sweden, October 1996.

[23] L. H. Hansen, L. Helle, F. Blaabjerg, E. Ritchie, S. Munk-Nielsen, H. Bindner, P. Sørensen, and B. Bak-Jensen. Conceptual survey of generators and power electronics for wind turbines. Technical Report Risø-R-1205(EN), Risø National Laboratory, Roskilde, Denmark, December 2001. ISBN 87-550-2743-8.

[24] M. Häusler and F. Owman. Ac or dc for connecting offshore wind farms to the transmission grid? In *Third International Workshop on Transmission Networks for Offshore Wind Farms*, pages –, Stockholm, Sweden, 11-12 April, 2002.

[25] G.L. Johnson. *Wind Energy Systems*. Prentice-Hall, 1985.

[26] N.M. Kirby, Lie Xu, M. Luckett, and W. Siepmann. Hvdc transmission for large offshore wind farms. *Power Engineering Journal*, 16(3):135 –141, June 2003.

[27] H. Klug, T. Osten, and J. Gabriel. Noise from wind turbines or: How many megawatts can you get for a 100db(a)? In *European wind energy conference*, pages 124–127, Dublin Castle, Ireland, October 1997.

[28] S. Lundberg, T. Thiringer, and T. Petru. Electrical limiting factors for wind energy installations in weak grids. *International Journal of Renewable Energy Engineering*, 3(2):305–310, 2001.

[29] S. Lundberg. *Electrical limiting factors for wind energy installations*. Diploma thesis, Chalmers University of Technology, Department of Electric Power Enginering, Göteborg, Sweden, December 2000.

[30] K.J.P Macken, L.J. Driesen, and R.J.M. Belmans. A dc bus syetem for connecting offshore wind turbines with the utility system. In *European Wind Energy Conference 2001*, pages 1030 – 1035, Copenhagen, Denmark, 2-6 July 2001.

[31] O. Martander and J. Svensson. Connecting offshore wind farms using dc cables. In *Wind Power for the 21st Century*, pages –, Kassel, Germany, 25-27 September 2000.

[32] O. Martander. *DC Grids for Wind Farms*. Licentiate thesis, Chalmers University of Technology, Department of Electric Power Enginering, Göteborg, Sweden, June 2002.

[33] L.K. Mestha and P.D. Evans. Analysis of on-state losses in pwm inverters. *IEE Proceedings B (Electric Power Applications)*, 136(4):189–95, July 1989.

[34] NEG Micon. NM72/2000. Product brochure, 2003.

[35] E. Muljadi, C.P. Butterfield, and V. Gevorgian. The impact of the output power fluctuation of a wind farm on a power grid. In *Third International Workshop on Transmission Networks for Offshore Wind Farms*, pages –, Stockholm, Sweden, 11-12 April, 2002.

[36] A. Petersson and S. Lundberg. Energy efficiency comparison of electrical systems for wind turbines. In *Nordic Workshop on Power and Industrial Electronics (NORpie´2002)*, pages CD–ROM, Stockholm, Sweden, August 12-14, 2002.

[37] T. Petru. *Modeling of Wind Turbines for Power System Studies*. Ph.D thesis, Chalmers University of Technology, Department of Electric Power Enginering, Göteborg, Sweden, June 2003.

[38] S. Rehman, T.O. Halawani, and M. Mohandes. Wind power cost assessment at twenty locations in the kingdom of saudi arabia. *Renewable Energy*, 28(-):573–583, 2003.

[39] F. Santjer, L.-H. Sobeck, and G.J. Gerdes. Influence of the electrical design of offshore wind farms and of transmission lines on efficency. In *Second International Workshop on Transmission Networks for Offshore Wind Farms*, pages –, Stockholm, Sweden, 30-31 March, 2001.

[40] Mulukutla S. Sarma. *Electric machines: steady-state theory and dynamic performance*. International Thomson Publishing, 1994.

[41] M. Schubert and J.P. Molly. Megawatt wind turbines - lessons lerned. In *European wind energy conference*, pages 193–196, Dublin Castle, Ireland, October 1997.

[42] T. Schütte, M. Ström, and B. Gustavsson. The use of low frequency ac for offshore wind power. In *Second International Workshop on Transmission Networks for Offshore Wind Farms*, pages –, Stockholm, Sweden, 30-31 March, 2001.

[43] W. Siepmann. Ac transmission technology for offshore wind farms. In *Second International Workshop on Transmission Networks for Offshore Wind Farms*, pages –, Stockholm, Sweden, 30-31 March, 2001.

[44] C. Skaug and C. Stranne. *HVDC Wind Park Configuration Study.* Diploma thesis, Chalmers University of Technology, Department of Electric Power Enginering, Göteborg, Sweden, October 1999.

[45] A. Skytt, P. Holmberg, and L. Juhin. Hvdc light for connection of wind farms. In *Second International Workshop on Transmission Networks for Offshore Wind Farms*, pages –, Stockholm, Sweden, 30-31 March, 2001.

[46] Miroslaw ´Smieszek. Model of energy losses in a gearbox. *Modelling, Measurement & Control B*, v59(n1-3):p 1–5, 1995.

[47] K.J. Smith and G. Hagerman. The potential for offshore wind energy development in the united states. In *Second International Workshop on Transmission Networks for Offshore Wind Farms*, pages –, Stockholm, Sweden, 30-31 March, 2001.

[48] P. Sørensen, A. Hansen, L. Janosi, J. Bech, and B. Bak-Jensen. Simulation of interaction between wind farm and power system. Technical Report Risø-R-1281(EN), Risø National Laboratory, Roskilde, Denmark, September 2001. ISBN 87-550-2743-8.

[49] J. Svenson and F. Olsen. Cost optimising of large-scale offshore wind farms in the danish waters. In *1999 European Wind Energy Conference*, pages 294–299, Nice, France, 1-5 March, 1999.

[50] T. Thiringer and J. Linders. Control by variable rotor speed of a fixed-pitch wind turbine operating in a wide speed range. *IEEE Transactions on Energy Conversion*, 8(3):520–6, Sept. 1993.

[51] K. Thorborg. *Power Electronics – in Theory and Practice.* Studentlitteratur, 1993.

[52] Middelgrundens Vindmøllelaug. http://www.middelgrunden.dk/. Home page, 2000.

[53] L. Weimers. New markets need new technology. In *Power System Technology, 2000. Proceedings. PowerCon 2000. International Conference on , Volume: 2*, pages 873–877 vol.2, –, 4-7 Dec. 2000.

[54] L. Weixing and O. Boon-Teck. Optimal acquisition and aggregation of offshore wind power by multiterminal voltage-source hvdc. *Power Delivery, IEEE Transactions on*, 18(1):201 –206, Jan 2003.

[55] P.J. Wolfs. A current-sourced dc-dc converter derived via the duality principle from the half-bridge converter. *Industrial Electronics, IEEE Transactions on*, 40(1):139–144, Feb. 1993.

[56] E.X. Yang, Y. Jiang, G. Hua, and F.C. Lee. Isolated boost circuit for power factor correction. In *Applied Power Electronics Conference and Exposition*, pages 196 –203, –, 7-11 March 1993.

Appendix A

DC/DC Converters

There are many different DC/DC converter topologies. In this appendix some topologies will be presented and analyzed generally. The analysis is made with inspiration from [17] and [32]. From this analysis the most interesting topologies will be chosen for a more detail loss evaluation in appendix B.

A.1 Tasks for the DC/DC converters

There are three main functions for the DC/DC converter:
Voltage adjuster
DC-transformer
Series Converter

The voltage adjusting DC/DC converter is used in a wind turbine equipped with a PM generator connected to a diode rectifier. The output voltage from the diode rectifier will vary with the rotational speed of the generator, se appendix B.3.3. The DC/DC converter is used to adjust (increase) this voltage to a fixed output voltage. In figure A.1 the input voltage to the voltage adjusting converter is shown, solid line. As can be noticed, the voltage increases linearly with the wind speed up to approximately 8m/s and then it drops to a constant level for higher wind speeds. But for the coming analysis, in this appendix, of the different DC/DC converter topologies the input voltage is approximated, somewhat crudely, by equation A.1, which is also shown in figure A.1 as dashed line.

$$\begin{aligned} V &= \frac{w_s}{w_{s,V}} \quad for \quad 0 \leq w_s \leq w_{s,V} \\ &= 1 \quad for \quad w_{s,V} \leq w_s \end{aligned} \tag{A.1}$$

Where:

V	Input voltage [p.u.]
w_s	Wind speed [m/s]
$w_{s,V}$	Wind speed for rated voltage =8 [m/s]

In figure A.2 the input power to the voltage adjusting converter is shown, solid line. As can be noticed, the power increases with the wind speed up to approximately 11.5m/s and for higher wind speeds it is constant. For the coming analysis of the different DC/DC converter topologies the input power is approximated by the following equa-

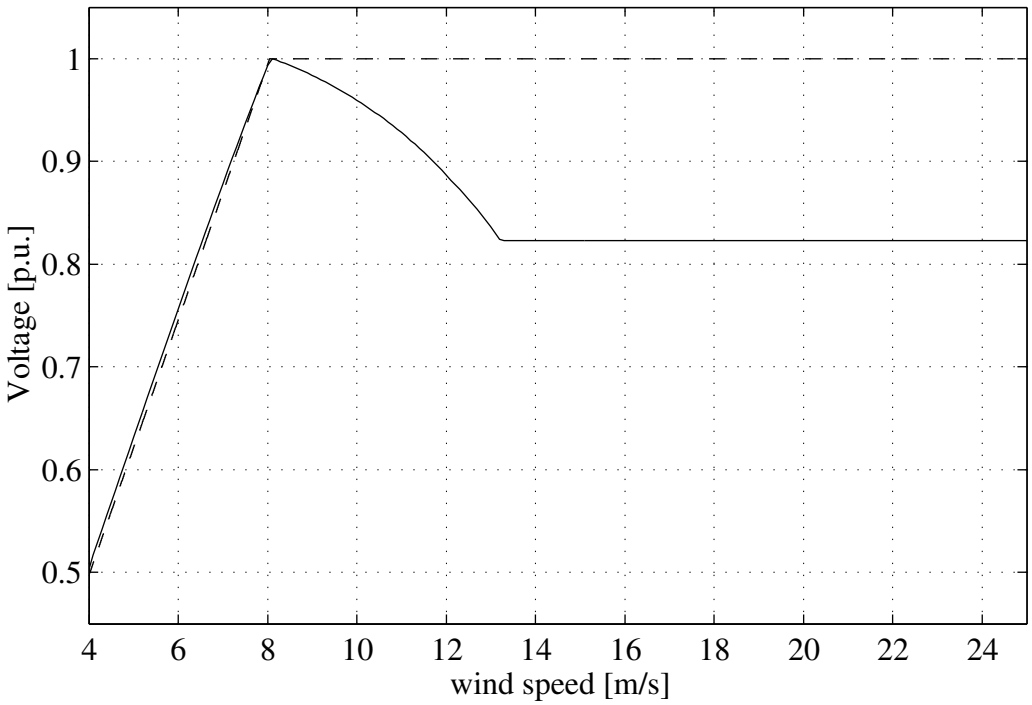

Figure A.1: Input voltage to the voltage adjusting converter. Solid the real voltage, dashed the approximation in equation A.1.

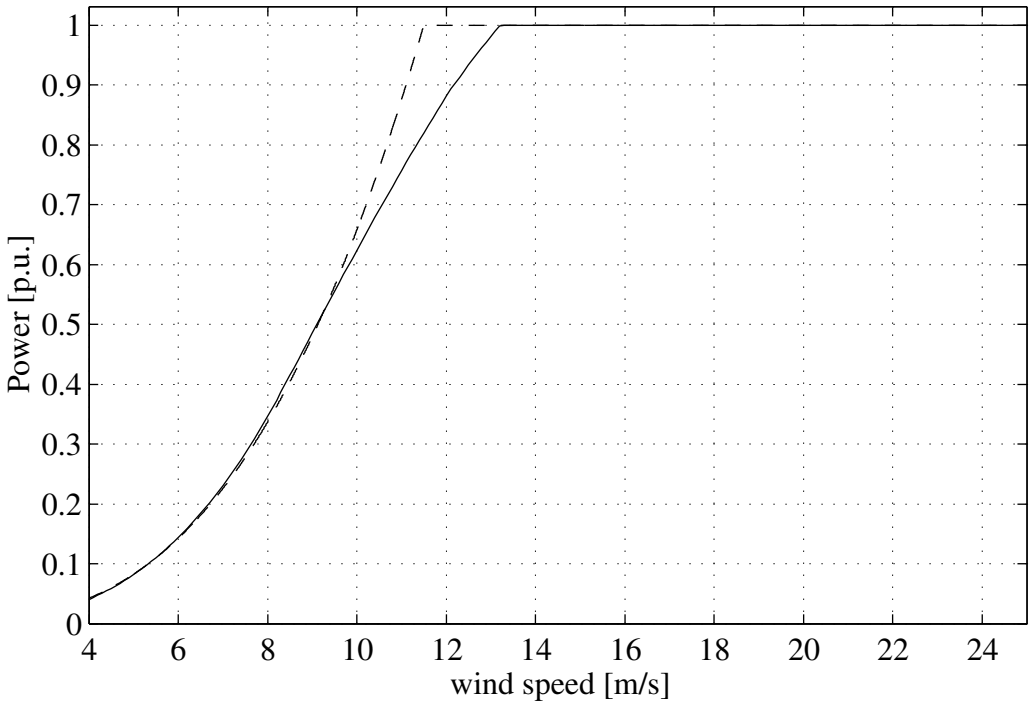

Figure A.2: Input power to the voltage adjusting converter. Solid the real voltage, dashed the approximation in equation A.2.

tion, which is also shown in figure A.2 as dashed line.

$$\begin{aligned} P &= \frac{w_s^3}{w_{s,R}^3} \quad for \quad 0 \leq w_s \leq w_{s,R} \\ &= 1 \quad for \quad w_{s,R} \leq w_s \end{aligned} \tag{A.2}$$

Where:

P	Input power [p.u.]
w_s	Wind speed [m/s]
$w_{s,R}$	Wind speed for rated power =11.5 [m/s]

The DC-transformer is used to increase a fix DC-voltage to another fix DC-voltage. The input power to the DC-transformer will be approximately as the solid line in figure A.2 and will therefore be modulated with equation A.2.

The series converter is used if the wind turbines are connected in series in order to obtain a voltage that is suitable for transmission directly without further transformation steps. The series converter will always work as a voltage adjusting converter. This is due to the fact that the output voltage is directly related to the output power. The reason is that the current through all wind turbines in one leg is the same. But for the analysis in this appendix the voltage division between the wind turbines are assumed to be ideal and therefore the output voltage is fix. Using this approximation, two types of the series DC/DC converter can be identified, the voltage adjusting or the DC transformer, depending on the interface between the generator and the converter. If the interface is a diode rectifier it will work as a voltage adjuster and the input voltage and power will be approximated with equation A.1 and A.2. If the interface is a IGBT rectifier the series converter will work as a DC-transformer with a fix input and output voltage and the input power will be approximated with equation A.2.

A.2 DC/DC Converter Topologies

In this section some hard switching topologies will be investigated, especially currents and voltages in the converters are evaluated. Some advantages and drawbacks of the topologies will also be presented. The utilization of the switches will also be calculated. The utilization factor can be defined as in equation A.3.

$$U = \frac{P_{Rated}}{\sum_{allswitches} \hat{V}_{max} I_{RMS,max}} \tag{A.3}$$

Where:

U	Utilization
P_{Rated}	Rated power of the converter [W]
$\hat{V}_{max}$	Maximum peak voltage over the device [V]
$I_{RMS,max}$	Maximum RMS current through the device [A]

From the equation A.3 it is seen that the utilization factor is a quantity that shall be maximized in order to give the smallest rated power of the switch.

A.2.1 Boost Converter

The boost or step-up converter is common when no galvanic insulation is needed and for moderate input/output voltage ratios. The converter is simple with few components, as

can be seen in figure A.3. But the converter can only be used when the output voltage V_{out} is higher then the input voltage V_{in}. The boost converter operates by repeatedly

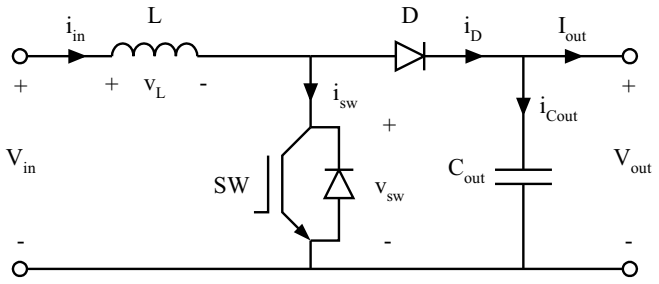

Figure A.3: Boost converter circuit.

storing energy in the inductor, L, during a period of time and during the other period transfer it to the output. Energy is stored in the inductor when the switch, SW, is on (conducting) and the energy is then transferred to the output when the switch is off (blocking). During the time the switch is on, the output is supplied with energy from the capacitor C_{out}. When energy is stored in the inductor, the current through it increases and when energy is taken from it the current decreases. If the current is always greater then zero then the converter is operated in the continuous current mode (CCM) and if the current reaches zero the converter is operating in the discontinuous current mode (DCM). If the ripple in the current through the inductor and in the voltage over the capacitor are neglected, the current and voltage in the boost converter can be drawn for CCM as in figure A.4, solid lines. In figure A.4 the ripple in the

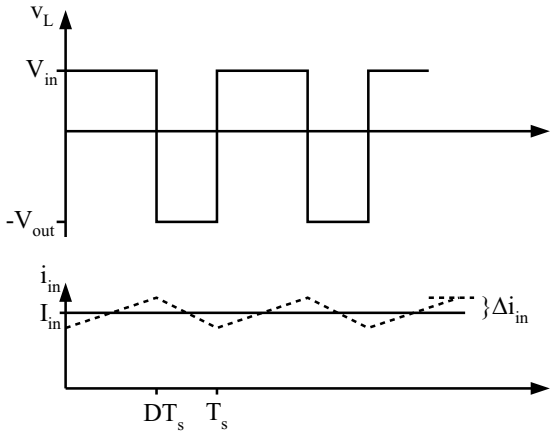

Figure A.4: Idealized voltages and current wave forms of the boost converter.

inductor current is also shown, dashed lines. In steady state, the mean value of the voltage over the inductor and the mean value of the current through the capacitor must be zero. Otherwise, energy is stored or drawn from the component, which means no steady state operation. From figure A.4 the mean values of the inductor voltage, v_L,

and capacitor current, $i_{C_{out}}$ can be formulated as

$$\begin{aligned} 0 &= mean(v_L) = V_L = V_{in}D - (V_{in} - V_{out})D' \\ 0 &= mean(i_{C_{out}}) = I_{C_{out}} = -I_{out}D + (I_{in} - I_{out})D' \\ D &= \frac{t_{on}}{T_s} \\ 1 &= D + D'. \end{aligned} \tag{A.4}$$

Where:

D	Duty ratio
t_{on}	time the switch is conducting [s]
T_s	Period time of the switching frequency

From these equations the input/output voltage and current relations can be formulated as

$$V_{out} = \frac{1}{1-D}V_{in} \tag{A.5}$$

$$I_{out} = (1-D)I_{in}. \tag{A.6}$$

From equation A.5 it can be noticed that the voltage goes to infinity when the duty ratio goes to one. Of course this does not happen in a real converter. The voltage ratio between the input and output voltage is limited by the parasitic resistances in the inductor, the switch and in the diode and by the output current. This limit the maximum duty ratio to between 0.8 and 0.9 in a normal case.

For calculating the ripple in the current through the inductor, shown in figure A.4, and in the voltage over the capacitor a linear approximation is used. This means that the voltage over the inductor is assumed to be constant over the period when the current increases or decreases. And the current through the capacitor is constant during the period the voltage increases or decreases. This approximation gives that

$$V_L = L\frac{\Delta i_L}{\Delta t} \Rightarrow \Delta i_{in} = \frac{V_{in}}{2L}DT_s \tag{A.7}$$

$$I_C = C\frac{\Delta v_C}{\Delta t} \Rightarrow \Delta v_{out} = \frac{I_{out}}{2C_{out}}DT_s. \tag{A.8}$$

It is clearly seen from the equations that the ripple gets smaller with a larger inductor and a larger capacitor. But with a larger inductor the control speed of the current gets slower, so the size of the inductor is a balance between the size of the ripple in the current and the regulator speed of the current.

The semiconductor stresses, peak voltage and RMS current, can be evaluated from figure A.4 if all transients from the switching are neglected. The peak voltages and

RMS current can be expressed as

$$\begin{aligned} \hat{v}_{SW} &= \hat{v}_D = V_{out} + \Delta v_{out} && \text{(A.9)} \\ I_{SW,RMS} &= \sqrt{\frac{1}{T_s}\int_0^{DT_s} [I_{in} + \Delta i_{in}(2\frac{t}{DT_s} - 1)]^2 \mathrm{d}t} \\ &= \sqrt{D[I_{in}^2 + \frac{\Delta i_{in}^2}{3}]} = \sqrt{D[(\frac{I_{out}}{1-D})^2 + \frac{\Delta i_{in}^2}{3}]} && \text{(A.10)} \\ I_{D,RMS} &= \sqrt{\frac{1}{T_s}\int_0^{D'T_s} [I_{in} + \Delta i_{in}(2\frac{t}{D'T_s} - 1)]^2 \mathrm{d}t} \\ &= \sqrt{D'[I_{in}^2 + \frac{\Delta i_{in}^2}{3}]} = \sqrt{(1-D)[(\frac{I_{out}}{1-D})^2 + \frac{\Delta i_{in}^2}{3}]}. && \text{(A.11)} \end{aligned}$$

From these equations and by assuming that the ripple components are so small that they can be neglected, the utilization factor for the transistor and diode can be calculated. In this evaluation the converter is assumed to operate at normal conditions as a voltage adjusting converter or a DC-transformer. This means for the instance that the maximum peak voltage over the transistor and diode are equal to the rated output voltage, $V_{out,R}$. The RMS current for the voltage adjusting converter type can be found by approximate the output power with equation A.2 and by calculating the duty ratio with equation A.5. For the duty ratio the input voltage is assumed to be described with equation A.1 and that $V_{out,R} = V_{in,R}N$, ie. N is the voltage ratio between the rated output voltage and the rated input voltage. With these equations the RMS current through the switch can be expressed as

$$I_{SW,RMS} = \sqrt{D}\frac{I_{out}}{1-D}$$

$$= \begin{cases} \sqrt{1 - \frac{w_s}{w_{s,V}N}\frac{\frac{w_s^3}{w_{s,R}^3}\frac{P_{out,R}}{V_{out,R}}}{\frac{w_s}{w_{s,V}N}}} = \frac{w_{s,V}N}{w_{s,R}^3}\sqrt{1 - \frac{w_s}{w_{s,V}N}}w_s^2\frac{P_{out,R}}{V_{out,R}} & 0 < w_s \leq w_{s,V} \\ \sqrt{1 - \frac{1}{N}\frac{\frac{w_s^3}{w_{s,R}^3}\frac{P_{out,R}}{V_{out,R}}}{\frac{1}{N}}} = \frac{N}{w,s,R^3}\sqrt{1 - \frac{1}{N}}w_s^3\frac{P_{out,R}}{V_{out,R}} & w_{s,V} < w_s \leq w_{s,R} \\ \sqrt{1 - \frac{1}{N}\frac{\frac{P_{out,R}}{V_{out,R}}}{\frac{1}{N}}} = N\sqrt{1 - \frac{1}{N}}\frac{P_{out,R}}{V_{out,R}} & w_{s,R} < w_s. \end{cases} \quad \text{(A.12)}$$

By analyzing this current it is seen that the maximum current is reached at wind speeds, w_s, over the rated one, $w_{s,R}$, if the voltage ratio between the rated input and output voltage, N, is greater then 1.2. In this work it is assumed that the ratio is greater then 1.2, which gives that the maximum RMS current through the switch can be expressed as

$$I_{SW,RMS,max} = N\sqrt{1 - \frac{1}{N}}\frac{P_{out,R}}{V_{out,R}}. \quad \text{(A.13)}$$

and in a similar way the maximum RMS current through the diode can be delivered as

$$I_{D,RMS,max} = \sqrt{N}\frac{P_{out,R}}{V_{out,R}}. \quad \text{(A.14)}$$

It shall be noticed that these equations for the maximum RMS current through the switch and the diode also holds for the DC-transformer. This is due to that the maximum value was reached at the point where the input-output voltage ratio was constant, i.e. the same operation as for the DC-transformer. By using the equations for the maximum peak voltage and RMS current, the utilization of the semiconductors can be calculated using equation A.3 which gives

$$U_{SW} = \frac{P_{out,R}}{V_{out,R} N \sqrt{1 - \frac{1}{N}\frac{P_{out,R}}{V_{out,R}}}} = \frac{1}{\sqrt{N(N-1)}} \tag{A.15}$$

$$U_D = \frac{1}{\sqrt{N}} \tag{A.16}$$

$$U_{SW+D} = \frac{1}{\sqrt{N(N-1)} + \sqrt{N}}. \tag{A.17}$$

From these equations it is noticed that the components are best utilized when the voltage ratio, $N > 1.2$, is as small as possible. It shall be remembered that the utilization factors holds both for the voltage adjusting converter and the DC-transformer.

The main advantages and drawbacks for the boost converter are:

+ The converter is simple with a low number of components
+ Low input current ripple in CCM
− Limited maximum duty cycle to approximated 0.8-0.9 due to parasitic resistances and this limits the boost ratio to approximate 10
− Large switch current when the duty cycle is high
− Poor transient response due to that the stored energy in the inductor must be transferred to the output even if the load is disconected
− Regulator loop hard to stabilize since the gain is load dependent
− No current limiting of output short circuits
− The power can only flow in one direction due to the diode

Prototypes have been build up to about 100kW with efficiency up to approximately 95%.

A.2.2 ´Cuk Converter

The ´cuk converter is used when a small current ripple is needed and for moderate voltage changes. The output is inverted and the converter can be used when the input voltage is higher and lower then the output voltage. In figure A.5 the scheme of the ´cuk converter is shown. The ´cuk converter operates by repeatedly shifting energy between the inductors L_1 and L_2, the capacitor C_1 and the load. The energy transfer from the input to the output is dependent on the capacitor C_1. If we compere it to the boost converter, the energy transfere was depending on the inductor. Energy is stored in the inductor L_1 when the switch, SW, is on (conducting) and inductor L_2 is storing energy from the capacitor C_1 during the same time. When the switch is off, L_1 charges C_1 and L_2 is transferring energy to the output. During the time the switch is on, the output is supplied from the capacitor C_{out} and L_2.

If the ripple in the currents through the inductors and in the voltages over the capacitors are neglected, the currents and voltages in the ´cuk converter can be drawn for CCM as in figure A.6. In figure A.6 the ripple in the currents through inductors

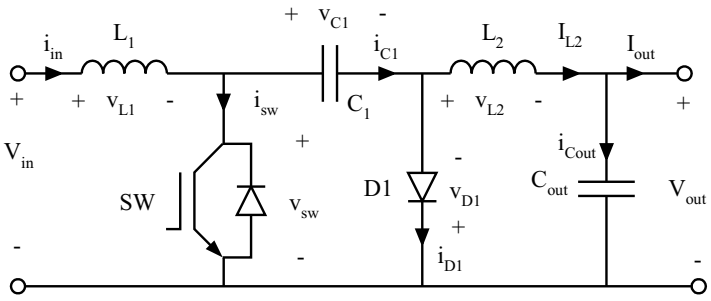

Figure A.5: ´Cuk converter circuit.

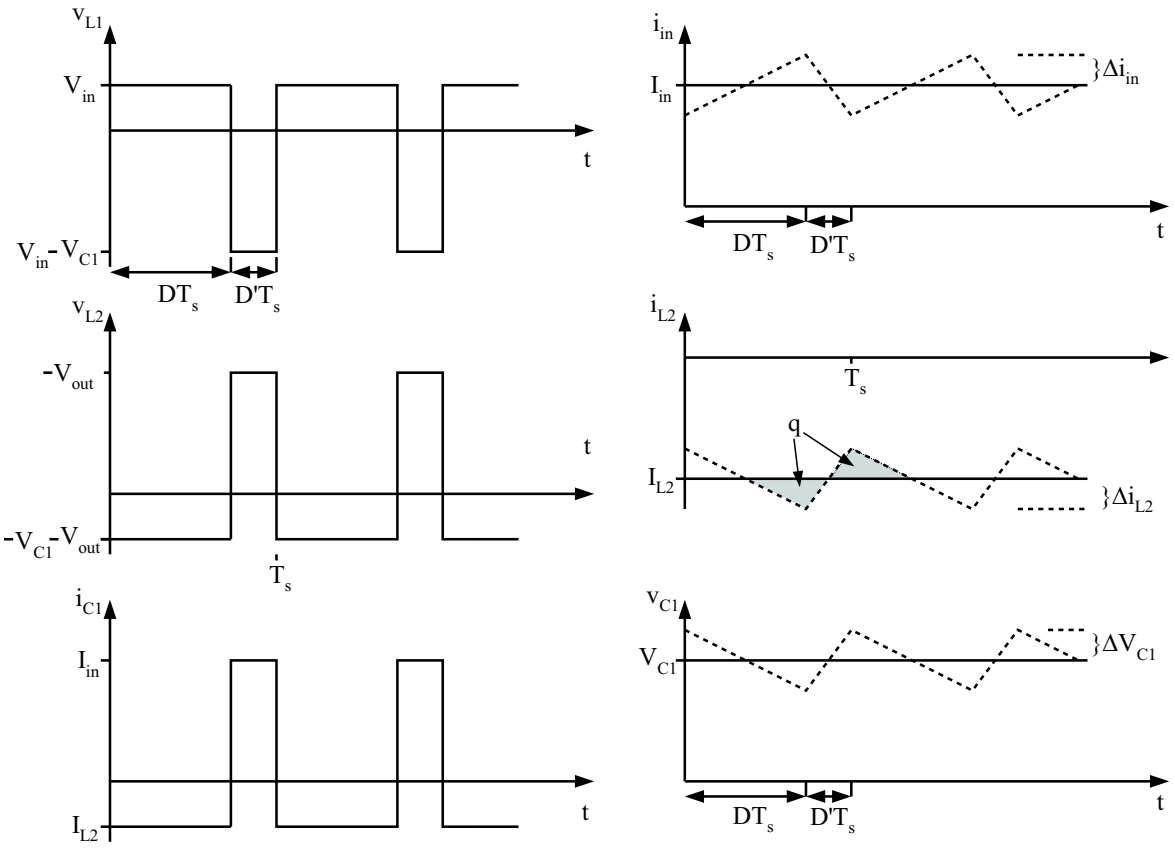

Figure A.6: Idealized voltages and current wave forms of the ´cuk converter, solid lines. Dashed lines current and voltage ripple.

L_1 and L_2 and in the voltage over C_1 are also shown, dashed lines. If capacitor charge balance and inductor volt-second balance are applied on the currents and voltages shown in figure A.6 the voltages and currents in the converter can be calculated for

steady state operation. The currents and voltages becomes

$$V_{out} = \frac{D}{1-D}V_{in} \tag{A.18}$$

$$I_{out} = \frac{1-D}{D}I_{in} \tag{A.19}$$

$$V_{C_1} = \frac{V_{in}}{1-D} \tag{A.20}$$

$$D = \frac{t_{on}}{T_s}. \tag{A.21}$$

From the equations it is clearly seen that the output voltage can be both smaller and greater then the input voltage depending on the duty ratio D.

The ripple components in the voltage over C_1 and the currents through L_1 and L_2 can be calculated in the same way as for the boost converter, this gives

$$\Delta i_{in} = \frac{V_{in}}{2L_1}DT_s \tag{A.22}$$

$$\Delta i_{L_2} = \frac{V_{in}}{2L_2}DT_s \tag{A.23}$$

$$\Delta v_{C_1} = -\frac{I_{out}}{2C_1}DT_s. \tag{A.24}$$

But the output voltage ripple can not be calculated with this approach. Instead, it is assumed that the output capacitor takes care of all the current ripple in the current through L_2, and then the output voltage ripple can be calculated by

$$q = C_{out}2\Delta v_{out} \tag{A.25}$$

$$q = \frac{1}{2}\Delta i_{L_2}\frac{T_s}{2} \Rightarrow \tag{A.26}$$

$$\Delta v_{out} = \frac{\Delta i_{L_2}}{8C_{out}}T_s. \tag{A.27}$$

As expected, it is seen that the ripple in the voltages and currents can be low by using sufficient large inductors and capacitors.

The semiconductor stresses in the ´cuk converter becomes

$$\hat{v}_{SW} = \hat{v}_D = V_{in} - V_{out} + \Delta v_{C_1} = -\frac{V_{out}}{D} + \Delta v_{C_1} \tag{A.28}$$

$$I_{SW,RMS} = \sqrt{D[(\frac{I_{out}}{1-D})^2 + \frac{1}{3}(\Delta i_{in} + \Delta i_{L_2})^2]} \tag{A.29}$$

$$I_{D,RMS} = \sqrt{(1-D)[(\frac{I_{out}}{1-D})^2 + \frac{1}{3}(\Delta i_{in} + \Delta i_{L_2})^2]}. \tag{A.30}$$

In the same way as for the boost converter, the utilization of the components can be calculated by neglecting the ripple components of the voltages and currents. First the maximum peak voltages and RMS currents for both the voltage adjuster and the

DC-transformer can be expressed as

$$\hat{v}_{SW,max} = \hat{v}_{D,max} = (1 + \frac{1}{N})V_{out,R} \tag{A.31}$$

$$I_{SW,RMS,max} = \sqrt{N(N+1)}\frac{P_{out,R}}{V_{out,R}} \tag{A.32}$$

$$I_{D,RMS,max} = \sqrt{N+1}\frac{P_{out,R}}{V_{out,R}}. \tag{A.33}$$

From these equations the utilization factor for the semiconductors can be calculated to

$$U_{SW} = \frac{\sqrt{N}}{(N+1)\sqrt{N+1}} \rightarrow \max \text{ at } N = \frac{1}{2} \tag{A.34}$$

$$U_D = \frac{N}{(N+1)\sqrt{N+1}} \rightarrow \max \text{ at } N = 2 \tag{A.35}$$

$$U_{SW+D} = \frac{N}{(N+1)\sqrt{N+1}(\sqrt{N}+1)} \rightarrow \max \text{ at } N = 1. \tag{A.36}$$

It can be noticed from the equations that the components are best utilized at a certain transformation ratio N. A deviation from this optimum gives that a component with a higher rating must be used for the same rated output power.

The main advantages and drawbacks of the ´cuk converter are:

+ Only two active components, SW and D
+ Low input and output current ripple in CCM
− The ripple current in the capacitor C_1 is equal to half the sum of the input and output current
− The switch must handle the sum of the input and output current
− The power can only flow in one direction

The converter has so far only been used for low power applications with efficiency up to approximately 94 %.

A.2.3 Sepic Converter

The sepic converter works similar to the ´cuk converter but has positive output voltage, as shown in figure A.7. The input current ripple is small and the converter is used for moderate voltage changes when the output voltage is smaller or greater then the input voltage. The sepic converter operates by repeatedly shifting energy between the inductors L_1 and L_2, the capacitor C_1 and the load. Energy is stored in the inductor L_1 when the switch, SW, is on and inductor L_2 is storing energy from the capacitor C_1 during the same time. When the switch is off, L_1 charges C_1 and together with L_2 also supplies energy to the output. During the time when the switch is on, the output is supplied from the capacitor C_{out}.

If the ripple in the currents through the inductors and in the voltages over the capacitors are neglected, the currents and voltages in the sepic converter can be drawn for CCM as in figure A.8. In figure A.8 the ripple in the currents through the inductors L_1 and L_2 and in the voltage over the capacitor C_1 are shown as before, dashed lines. If energy balance is used on the currents and voltages shown in figure A.8 the voltages

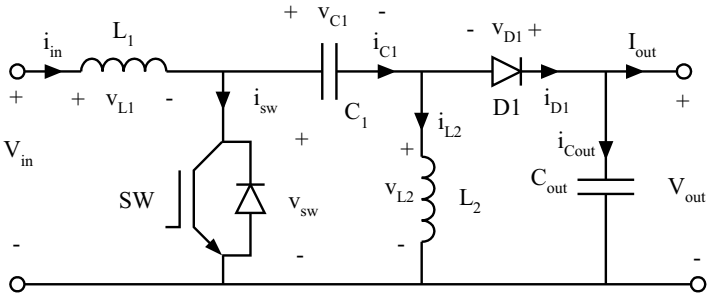

Figure A.7: Sepic converter circuit.

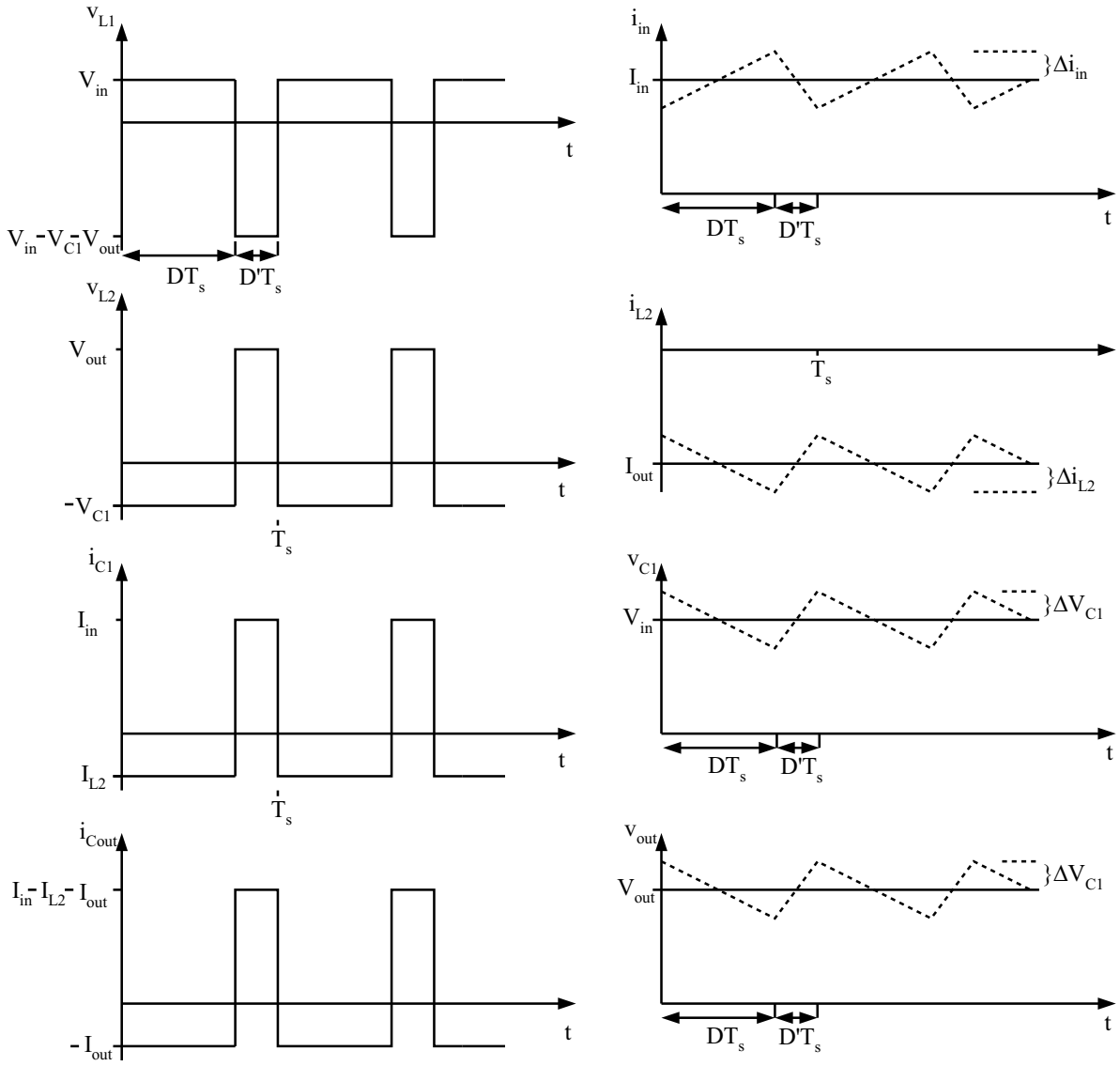

Figure A.8: Idealized voltages and current wave forms of the sepic converter, solid lines. Dashed lines ripple in the currents and voltage

and currents in the converter can be calculated for steady state operation. The currents

and voltages becomes

$$V_{out} = \frac{D}{1-D}V_{in} \quad (A.37)$$

$$I_{out} = \frac{1-D}{D}I_{in} \quad (A.38)$$

$$V_{C_1} = V_{in} \quad (A.39)$$

$$I_{L_2} = -I_{out}. \quad (A.40)$$

From the equations it is clearly seen that the output voltage can be both smaller and greater then the input voltage depending on the duty ratio D.

The ripple components in the voltage over C_1 and C_{out} and in the currents through L_1 and L_2, shown in figure A.8, can be calculated in the same way as for the boost converter, this gives

$$\Delta i_{in} = \frac{V_{in}}{2L_1}DT_s \quad (A.41)$$

$$\Delta i_{L_2} = \frac{V_{in}}{2L_2}DT_s \quad (A.42)$$

$$\Delta v_{C_1} = \frac{I_{out}}{2C_1}DT_s \quad (A.43)$$

$$\Delta v_{out} = \frac{I_{out}}{2C_{out}}DT_s. \quad (A.44)$$

As expected, it is seen that the ripple in the voltages and currents can be low by using sufficient large inductors and capacitors.

The semiconductor stresses in the sepic converter becomes

$$\hat{v}_{SW} = \hat{v}_D = V_{in} + V_{out} + \Delta v_{C_1} + \Delta v_{C_{out}} = \frac{V_{out}}{D} + \Delta v_{C_1} + \Delta v_{C_{out}} \quad (A.45)$$

$$I_{SW,RMS} = \sqrt{D[(\frac{I_{out}}{1-D})^2 + \frac{1}{3}(\Delta i_{in} + \Delta i_{L_2})^2]} \quad (A.46)$$

$$I_{D,RMS} = \sqrt{(1-D)[(\frac{I_{out}}{1-D})^2 + \frac{1}{3}(\Delta i_{in} + \Delta i_{L_2})^2]}. \quad (A.47)$$

In the same way as for the boost converter, the utilization of the components can be calculated. By neglecting the ripple component in voltages and currents, the maximum peak voltage and RMS current for both the voltage adjuster and the DC-transformer can be expressed as

$$\hat{v}_{SW,max} = \hat{v}_{D,max} = (1 + \frac{1}{N})V_{out,R} \quad (A.48)$$

$$I_{SW,RMS,max} = \sqrt{N(N+1)}\frac{P_{out,R}}{V_{out,R}} \quad (A.49)$$

$$I_{D,RMS,max} = \sqrt{N+1}\frac{P_{out,R}}{V_{out,R}}. \quad (A.50)$$

From these equations the utilization factor for the semiconductors can be calculated to

$$U_{SW} = \frac{\sqrt{N}}{(N+1)\sqrt{N+1}} \rightarrow \max \text{ at } N = \frac{1}{2} \quad \text{(A.51)}$$

$$U_D = \frac{N}{(N+1)\sqrt{N+1}} \rightarrow \max \text{ at } N = 2 \quad \text{(A.52)}$$

$$U_{SW+D} = \frac{N}{(N+1)\sqrt{N+1}(\sqrt{N}+1)} \rightarrow \max \text{ at } N = 1. \quad \text{(A.53)}$$

It shall be noticed that this is the same utilization factors as for the ´cuk converter.

The main advantages and drawbacks of the sepic converter are:

+ Only two active components, SW and D
+ Low input current ripple in CCM
− The ripple current in the capacitor C_1 is equal to half the sum of the input and output current
− The switch and the diode must handel the sum of the input and output voltage and the sum of the input and output current
− Large output voltage ripple
− The power can only flow in one direction

The converter has so far only been used for low power applications with efficiency up to approximately 94%.

A.2.4 Zeta Converter

The zeta converter, sometimes called the inverted sepic converter, works similar to the ´cuk converter but has a positive output, as shown in figure A.9. The output current ripple is small and the converter is used for moderate voltage changes when the output voltage is smaller or greater then the input voltage. The zeta converter operates by

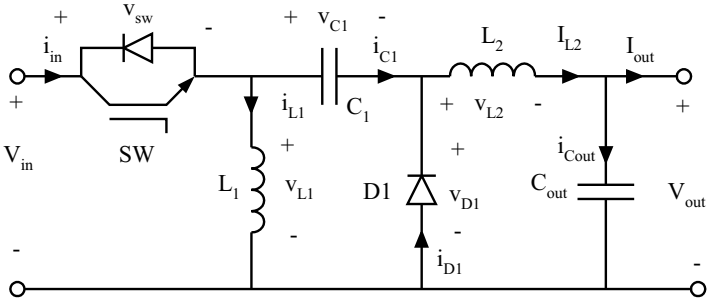

Figure A.9: Zeta converter circuit.

repeatedly shifting energy between the inductors L_1 and L_2, the capacitor C_1 and the load. Energy is stored in the inductor L_1 when the switch, SW, is on and inductor L_2 is storing energy from the capacitor C_1 and from the input during the same time. When the switch is off L_1 charges C_1 and L_2 supplies energy to the output. During the time the switch is on the output is supplied from the input and capacitor C_1.

If the ripple in the currents through the inductors and in the voltages over the capacitors are neglected, the currents and voltages in the zeta converter can be drawn

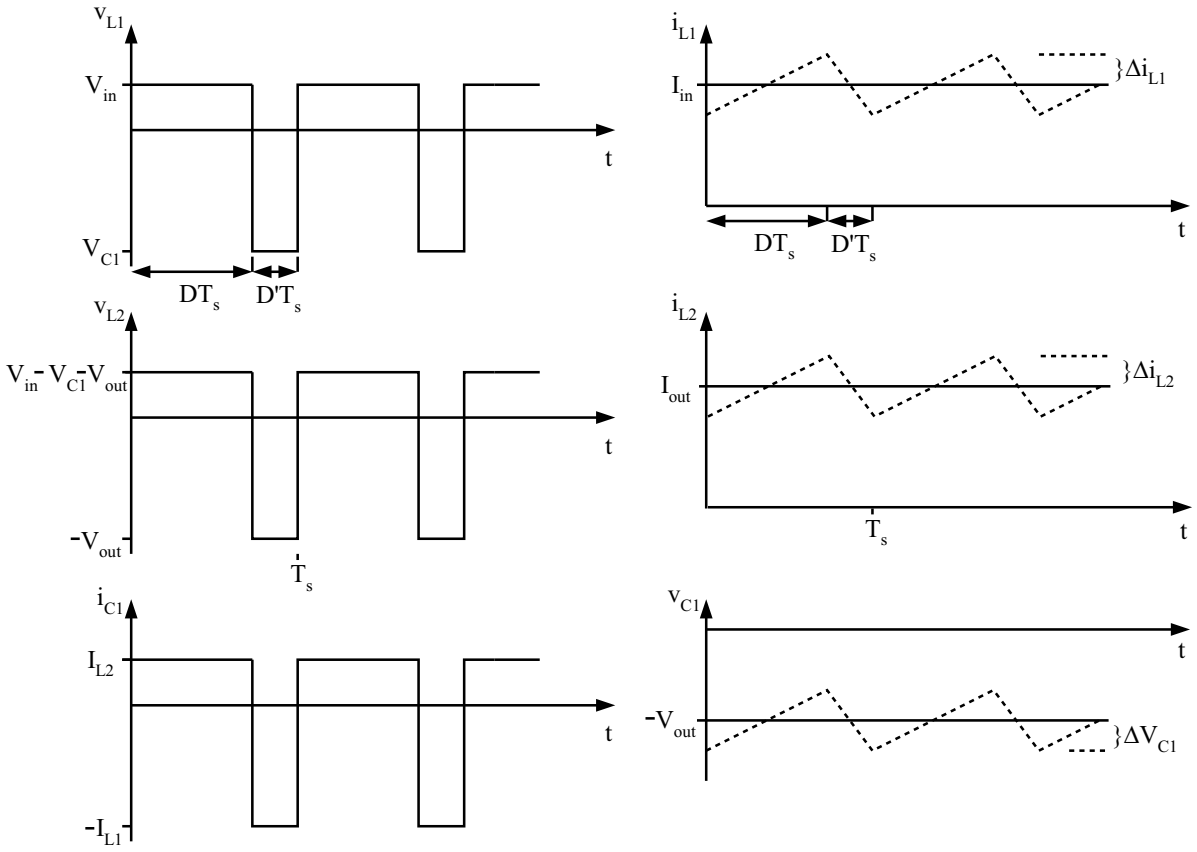

Figure A.10: Idealized voltages and current wave forms of the zeta converter, solid lines. Dashed lines ripple in the currents and voltage

for CCM as in figure A.8. In the same way as for the other converters the currents and voltages can be calculated in steady state as

$$V_{out} = \frac{D}{1-D} V_{in} \tag{A.54}$$

$$I_{out} = \frac{1-D}{D} I_{in} \tag{A.55}$$

$$V_{C_1} = -V_{out} \tag{A.56}$$

$$I_{L_1} = I_{in} \tag{A.57}$$

$$I_{L_2} = I_{out}. \tag{A.58}$$

From the equations it is clearly seen that the output voltage can be both smaller and greater then the input voltage depending on the duty ratio D.

The ripple components in the voltage over C_1 and C_{out} and in the currents through

L_1 and L_2 can be calculated in the same way as for the ´cuk converter, this gives

$$\Delta i_{L_1} = \frac{V_{in}}{2L_1} DT_s \tag{A.59}$$

$$\Delta i_{L_2} = \frac{V_{in}}{2L_2} DT_s \tag{A.60}$$

$$\Delta v_{C_1} = \frac{I_{out}}{2C_1} DT_s \tag{A.61}$$

$$\Delta v_{out} = \frac{\Delta i_{L_2}}{8C_{out}} T_s. \tag{A.62}$$

As expected it is seen that the ripple in the voltages and currents can be small by using sufficient large inductors and capacitors.

The semiconductor stresses in the zeta converter becomes

$$\hat{v}_{SW} = \hat{v}_D = V_{in} + V_{out} + \Delta v_{C_1} = \frac{V_{out}}{D} + \Delta v_{C_1} \tag{A.63}$$

$$I_{SW,RMS} = \sqrt{D[(\frac{I_{out}}{1-D})^2 + \frac{1}{3}(\Delta i_{L_1} + \Delta i_{L_2})^2]} \tag{A.64}$$

$$I_{D,RMS} = \sqrt{(1-D)[(\frac{I_{out}}{1-D})^2 + \frac{1}{3}(\Delta i_{L_1} + \Delta i_{L_2})^2]}. \tag{A.65}$$

In the same way as for the boost converter, the utilization of the components can be calculated. By neglecting ripple in voltages and currents the maximum peak voltage and RMS current within the normal operational interval for both the voltage adjuster and the DC-transformer can be expressed as

$$\hat{v}_{SW,max} = \hat{v}_{D,max} = (1 + \frac{1}{N}) V_{out,R} \tag{A.66}$$

$$I_{SW,RMS,max} = \sqrt{N(N+1)} \frac{P_{out,R}}{V_{out,R}} \tag{A.67}$$

$$I_{D,RMS,max} = \sqrt{N+1} \frac{P_{out,R}}{V_{out,R}}. \tag{A.68}$$

From these equations the utilization factor for the semiconductors can be calculated to

$$U_{SW} = \frac{\sqrt{N}}{(N+1)\sqrt{N+1}} \rightarrow \max \text{ at } N = \frac{1}{2} \tag{A.69}$$

$$U_D = \frac{N}{(N+1)\sqrt{N+1}} \rightarrow \max \text{ at } N = 2 \tag{A.70}$$

$$U_{SW+D} = \frac{N}{(N+1)\sqrt{N+1}(\sqrt{N}+1)} \rightarrow \max \text{ at } N = 1. \tag{A.71}$$

It shall be noticed that this is the same utilization factors as for the ´cuk and sepic converter.

The main advantages and drawbacks of the zeta converter are:

+ Only two active components, SW and D
+ Low output current ripple
− The ripple current in the capacitor C_1 is equal to half the sum of the input and output current
− The switch and the diode must handel the sum of the input and output voltage and the sum of the input and output current
− Large input current ripple
− The power can only flow in one direction

A.2.5 Flyback Converter

The flyback converter is common when galvanic insulation is needed for low power applications, typically below 100W. The converter has few components as shown in figure A.11. The most complicated part of the converter is the transformer which has a high magnetizing inductance. The flyback converter operates by repeatedly shifting

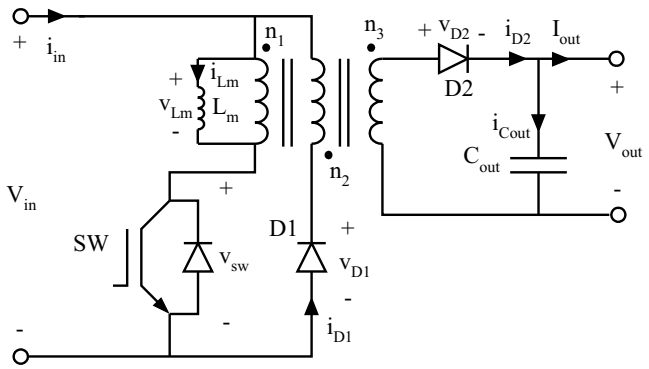

Figure A.11: Flyback converter circuit.

energy between the transformer and the load. Energy is stored in the transformer magnetizing inductance L_m when the switch, SW, is on and the output capacitor C_{out} supplies the load. When the switch is off L_m discharges via the winding n_3 and the diode D_2 and supplies the load and C_{out}. The winding n_2 is only used in no-load operation to discharge the magnetizing inductance back to the input.

If the ripple components in the current through the magnetizing inductance and in the voltage over the output capacitor are neglected, the currents and voltages in the flyback converter can be drawn for CCM as in figure A.12. CCM or DCM is in this case referred to the current through the magnetizing inductance, if it is continuous or discontinuous. In figure A.12 the ripple in the current through the magnetizing inductance is also shown, dashed lines. In the same way as before, if the mean values

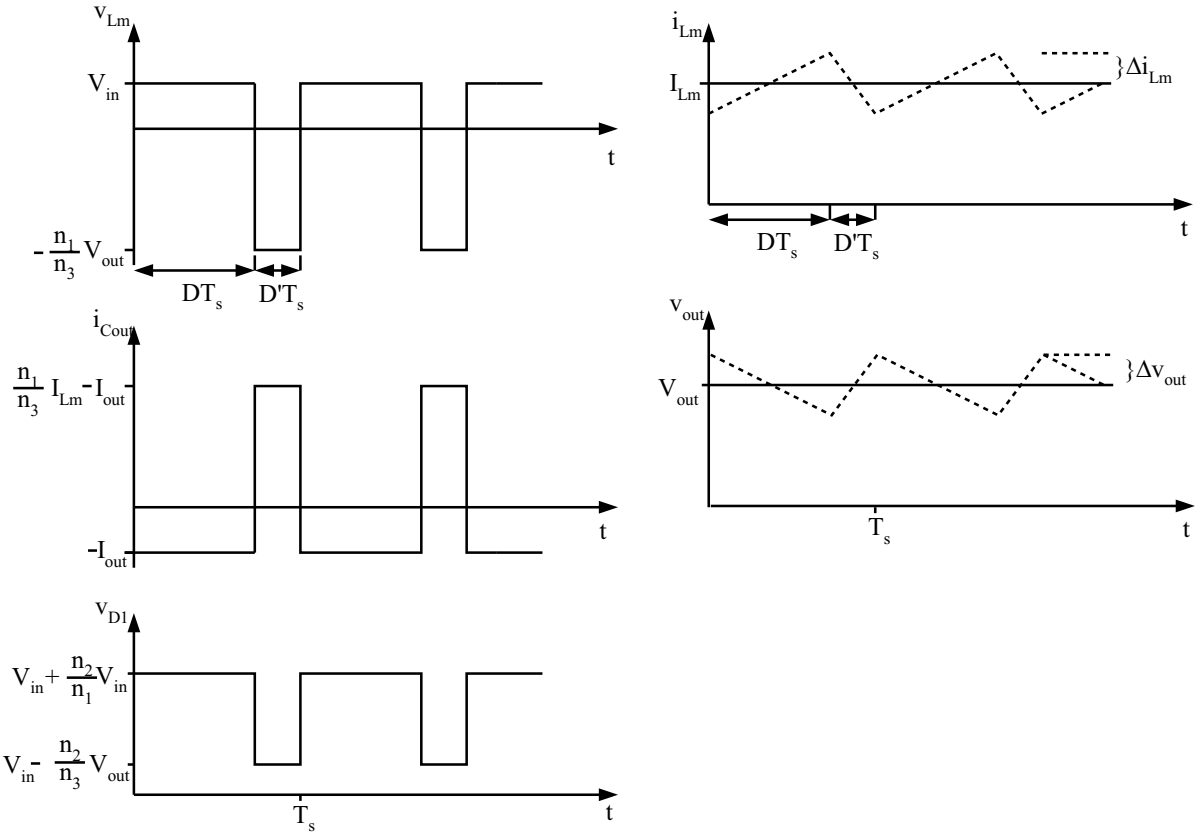

Figure A.12: Idealized voltages and current wave forms of the flyback converter.

are used the currents and voltages can be calculated in steady state as

$$V_{out} = \frac{n_3}{n_1}\frac{D}{1-D}V_{in} \quad \text{(A.72)}$$

$$V_{out,max} = \frac{n_3}{n_2}V_{in} \quad \text{(A.73)}$$

$$I_{out} = \frac{n_1}{n_3}\frac{1-D}{D}I_{in} \quad \text{(A.74)}$$

$$I_{L_m} = \frac{I_{in}}{D}. \quad \text{(A.75)}$$

From the equations, it is clearly seen that the output voltage can be both smaller and greater then the input voltage depending on the duty ratio D. It is also noticed that the transformation ratio between the output and input voltage is limited to a maximum value, set by the winding n_2.

The ripple components in the voltage over C_{out} and in the current through L_m can be calculated in the same way as for the boost converter, this gives

$$\Delta i_{L_m} = \frac{V_{in}}{2L_m}DT_s \quad \text{(A.76)}$$

$$\Delta v_{out} = \frac{I_{out}}{2C_{out}}DT_s. \quad \text{(A.77)}$$

As expected it is seen that the ripple in the voltage and current can be low if a sufficient large magnetizing inductor and output capacitor is used.

The semiconductor stresses in the flyback converter becomes

$$\hat{v}_{SW} = V_{in} + \frac{n_1}{n_3}(V_{out} + \Delta v_{C_{out}}) = \frac{n_1}{n_3}(\frac{V_{out}}{D} + \Delta v_{C_{out}}) \quad (A.78)$$

$$\hat{v}_{D_1} = \frac{n_1 + n_2}{n_1} V_{in} \quad (A.79)$$

$$\hat{v}_{D_2} = \frac{V_{out}}{D} + \Delta v_{C_{out}} \quad (A.80)$$

$$I_{SW,RMS} = \sqrt{D[(\frac{n_3}{n_1}\frac{I_{out}}{1-D})^2 + \frac{\Delta i_{L_m}^2}{3}]} \quad (A.81)$$

$$I_{D_2,RMS} = \sqrt{(1-D)[(\frac{I_{out}}{1-D})^2 + \frac{\Delta i_{L_m}^2}{3}]}. \quad (A.82)$$

In the same way as for the other converters, the utilization of the components can be calculated. By neglecting ripple in voltages and currents, the maximum peak voltage and RMS current within the normal operational interval for both the voltage adjuster and the DC-transformer can be expressed as

$$\hat{v}_{SW,max} = \frac{n_1}{n_3}(N + \frac{n_3}{n_1})\frac{V_{out,R}}{N} \quad (A.83)$$

$$\hat{v}_{D_2,max} = (N + \frac{n_3}{n_1})\frac{V_{out,R}}{N} \quad (A.84)$$

$$I_{SW,RMS,max} = \sqrt{N(N + \frac{n_3}{n_1})}\frac{P_{out,R}}{V_{out,R}} \quad (A.85)$$

$$I_{D_2,RMS,max} = \sqrt{\frac{n_3}{n_1}N + 1}\frac{P_{out,R}}{V_{out,R}}. \quad (A.86)$$

From these equations the utilization factor for the semiconductors can be calculated to

$$U_{SW} = \frac{1}{\frac{n_1}{n_3}\frac{\sqrt{N}}{N}(N + \frac{n_3}{n_1})\sqrt{N + \frac{n_3}{n_1}}} = \frac{n\sqrt{N}}{(N+n)^{\frac{3}{2}}} \quad (A.87)$$

$$U_{D_2} = \frac{N\sqrt{n}}{(N+n)^{\frac{3}{2}}} \quad (A.88)$$

$$U_{SW+D_2} = \frac{nN}{(N+n)^{\frac{3}{2}}(\sqrt{N} + \sqrt{n})} \quad (A.89)$$

$$n = \frac{n_3}{n_1}. \quad (A.90)$$

From the equations it is seen that the utilization factors are depending on the desired input output voltage ratio N and the winding ratio of the transformer n. By choosing the winding ratio of the transformer cleverly the utilization factor of the components can be maximized, which gives

$$U_{SW,max} = \frac{2}{3\sqrt{3}} \text{ for } n = 2N \quad (A.91)$$

$$U_{D_2,max} = \frac{2}{3\sqrt{3}} \text{ for } n = \frac{N}{2} \quad (A.92)$$

$$U_{SW+D_2,max} = \frac{1}{4\sqrt{2}} \text{ for } n = N. \quad (A.93)$$

As can be seen, the maximum utilization factor for the different components do not occur for the same winding ratio. This means that one can maximize the utilization for one component or use a compromise. One compromise is to use the utilization factor for the switch and the diode, $U_{SW+D_2,max}$, where the rating of the switch and the rating of the diode are added, according to equation A.3. Another way to add the ratings of the devices, is to first multiply them with a weight factor that can be depending on size, losses and/or cost. In this way, for example, the most expensive component can be utilized more, in order to reduce the cost. It can also be noticed that the maximum utilization factor is independent of the voltage ratio N compared to the transformer less converters discussed before.

The main advantages and drawbacks of the flyback converter are:

+ The flyback converter is, from a circuit perspective, the simplest of the low-power isolated converters and uses only three components besides the transformer (if the no-load capability is omitted)
+ The utilization factor can be maximized due to the transformer
− Critical transformer design and the high energy, which must be stored in the transformer windings in the form of a DC current, requires a high magnetizing inductance, a high current primary, which in turn requires larger cores than would be needed with pure AC
− Poor transformer utilization since the core is only magnetized in one direction
− Large output voltage ripple and input current ripple
− A snubber circuit is needed for the leakage inductance of the transformer
− The power can only flow in one direction

A.2.6 Forward Converter

The forward converter is very common when galvanic insulation is needed and for applications above the power range of the flyback converter. The converter is simple and has few components, as shown in figure A.13. The most complicated part of the converter is the transformer with three windings. The forward converter operates by

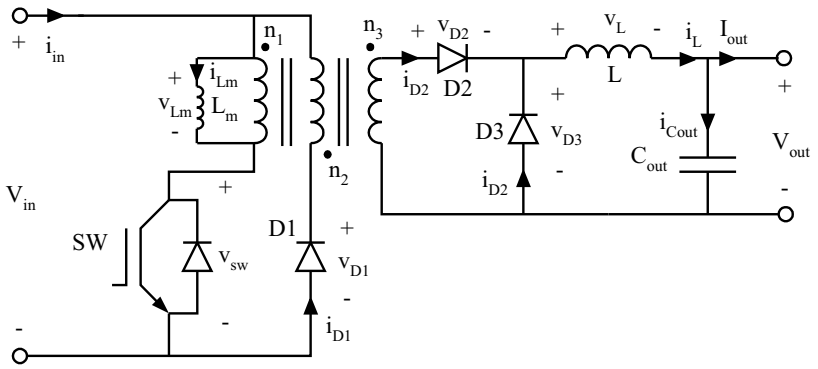

Figure A.13: Forward converter circuit.

repeatedly transferring energy between the input and the load through the transformer. Energy is transferred when the switch, SW, is on. When the switch is off L_m discharges

via the winding n_2 to the supply and the inductor L and the capacitor C_{out} supplies the load.

If the ripple in the currents through the inductances and in the voltage over the output capacitor are neglected, the currents and voltages in the forward converter can be drawn for CCM as in figure A.14. The currents and voltages for the forward

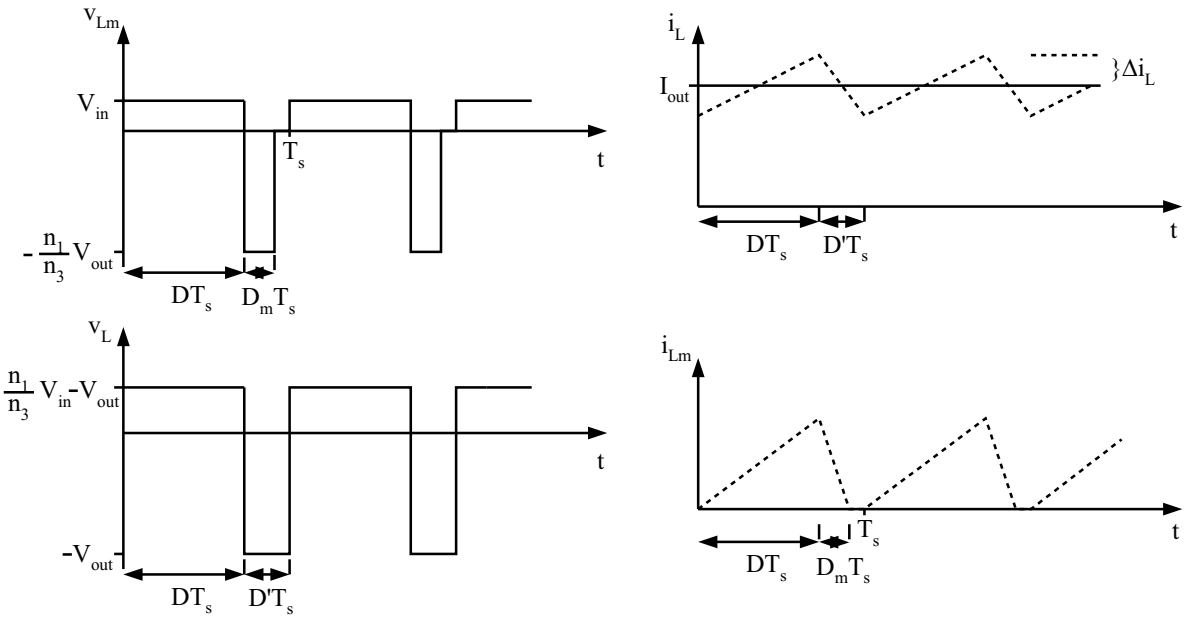

Figure A.14: Idealized voltages and current wave forms of the forward converter, solid lines. Dashed lines ripple.

converter using the same reasoning as for the previous converters become

$$V_{out} = \frac{n_3}{n_1} D V_{in} \tag{A.94}$$

$$I_{out} = \frac{n_1}{n_3} \frac{1}{D} I_{in} \tag{A.95}$$

$$D_{max} = \frac{1}{1 + \frac{n_2}{n_1}}. \tag{A.96}$$

From the equations and figure A.14 it is seen that the maximum duty cycle is limited. If the duty cycle exceeds it's maximum value, the magnetizing inductance will not be discharged completely and after a time the transformer will be saturated.

The ripple components in the voltage over C_{out} and in the currents through L_m and L can be calculated in the same way as for the ´cuk converter, this gives

$$\Delta i_{L_m} = \frac{V_{in}}{2L_m} D T_s \tag{A.97}$$

$$\Delta i_L = \frac{n_3}{n_1} \frac{V_{in}}{2L} (1 - D) D T_s \tag{A.98}$$

$$\Delta v_{out} = \frac{\Delta i_L}{8 C_{out}} T_s. \tag{A.99}$$

As expected, it is seen that the ripple in the voltage and current can be low by having a sufficient large inductor and output capacitor. Due to the fact that the magnetizing

current is not used in the energy transfer, it is desired to be small. This gives that the magnetization inductance of the transformer has to be large.

The semiconductor stresses in the forward converter become

$$\hat{v}_{SW} = \hat{v}_{D_1} = V_{in} + \frac{n_1}{n_2}V_{in} = \frac{n_1+n_2}{n_2}V_{in} \quad (A.100)$$

$$\hat{v}_{D_2} = \frac{n_3}{n_2}V_{in} \quad (A.101)$$

$$\hat{v}_{D_3} = \frac{n_3}{n_1}V_{in} = \frac{V_{out}}{D} \quad (A.102)$$

$$I_{SW,RMS} = \sqrt{D[(\frac{n_3}{n_1}I_{out} + \Delta i_{L_m})^2 + \frac{1}{3}\Delta i_{L_m}^2]} \quad (A.103)$$

$$I_{D_1,RMS} = 2\Delta i_{L_m}\sqrt{\frac{1}{3}\frac{n_2}{n_1}D} \quad (A.104)$$

$$I_{D_2,RMS} = \sqrt{D[(I_{out}^2 + \frac{1}{3}\Delta i_L^2]} \quad (A.105)$$

$$I_{D_3,RMS} = \sqrt{(1-D)[(I_{out}^2 + \frac{1}{3}\Delta i_L^2]}. \quad (A.106)$$

In the same way as for the other converters the utilization of the components can be calculated. By neglecting ripple in voltages and currents the maximum peak voltage and RMS current within the normal operational interval for both the voltage adjuster and the DC-transformer can be expressed as

$$\hat{v}_{SW,max} = \hat{v}_{D_1,max} = \frac{1}{1-D_{max}}\frac{V_{out,R}}{N} \quad (A.107)$$

$$\hat{v}_{D_2,max} = \frac{D_{max}}{1-D_{max}}\frac{n_3}{n_1}\frac{V_{out,R}}{N} \quad (A.108)$$

$$\hat{v}_{D_3,max} = \frac{n_3}{n_1}\frac{V_{out,R}}{N} \quad (A.109)$$

$$I_{SW,RMS,max} = \sqrt{N\frac{n_3}{n_1}\frac{P_{out,R}}{V_{out,R}}} \quad (A.110)$$

$$I_{D_1,RMS} \simeq 0 \quad (A.111)$$

$$I_{D_2,RMS,max} = \sqrt{N\frac{n_1}{n_3}\frac{P_{out,R}}{V_{out,R}}} \quad (A.112)$$

$$I_{D_3,RMS,max} = \sqrt{1-\frac{n_1}{n_3}N\frac{P_{out,R}}{V_{out,R}}}. \quad (A.113)$$

From these equations, the utilization factor for the semiconductors can be calculated

to

$$U_{SW} = (1 - D_{max})\sqrt{\frac{n_1}{n_3}N} = (1 - D_{max})\sqrt{\frac{N}{n}} \quad \text{(A.114)}$$

$$U_{D_2} = \frac{1 - D_{max}}{D_{max}}\sqrt{\frac{N}{n}} \quad \text{(A.115)}$$

$$U_{D_3} = \frac{\frac{N}{n}}{\sqrt{1 - \frac{N}{n}}} \quad \text{(A.116)}$$

$$n = \frac{n_3}{n_1}. \quad \text{(A.117)}$$

From the equations it is seen that the utilization factors are depending on the desired input output voltage ratio N, the winding ratio of the transformer n and by the maximum duty cycle D_{max}. For the utilization factor for the switch it is seen that it is maximized if the winding ratio of the transformer n and the maximum duty cycle D_{max} is as low as possible. But for the voltage adjusting converter these parameters are limited by the following equation

$$\frac{N}{n_{min}} = D_{max} vmin. \quad \text{(A.118)}$$

Where $vmin$ is the smallest input voltage in p.u., this means that V_{in} in p.u. is limited to $vmin \leq \leq 1$. If this is used the maximum utilization factors for the semiconductors can be calculated to

$$U_{SW,max} = \frac{2\sqrt{vmin}}{3\sqrt{3}} \text{ for } n = \frac{3N}{vmin} \text{ and } D_{max} = \frac{1}{3} \quad \text{(A.119)}$$

$$U_{D_2,max} \rightarrow \infty \text{ when } n \rightarrow \infty \quad \text{(A.120)}$$

$$U_{D_3,max} = \frac{vmin}{1 - vmin} \text{ when } D_{max} = 1 \text{ and } n = \frac{N}{vmin}. \quad \text{(A.121)}$$

As seen, the utilization maximum for the different components do not occur for the same winding ratio and the maximum points for the diodes occur at unrealistic points. It can be noticed that the maximum utilization factors are independent of the voltage ratio N compared to the converters without transformer as was discussed previously. It shall also be noticed that these maximum points also are valid for the DC-transformer if $vmin = 1$.

The main advantages and drawbacks of the forward converter are:

+ The forward converter is simple but compared with the flyback converter has one more diode and a additional output filter inductor
+ The utilization factor can be maximized due to the transformer
+ The output current ripple is small due to the extra inductor L
− Poor transformer utilization since the core is only magnetized in one direction
− Large input current ripple
− The transformer design is critical to minimize the magnetizing current and, thus, the losses in the diode D_1
− A snubber circuit is needed for the leakage inductance of the transformer
− The power can only flow in one direction

Converters have been built up to 15kW at 100kHz and with an efficiency of up to 97%.

A.2.7 Two-Transistor Forward Converter

The two-transistor forward converter can replace the forward converter when the blocking voltages for the switches or the transformer design is critical. The converter has two transistors, as shown in figure A.15. The converter has the advantage that the switch voltage is clamped to the input voltage and no demagnetizing winding is needed on the transformer. The two-transistor forward converter operates in the same way as

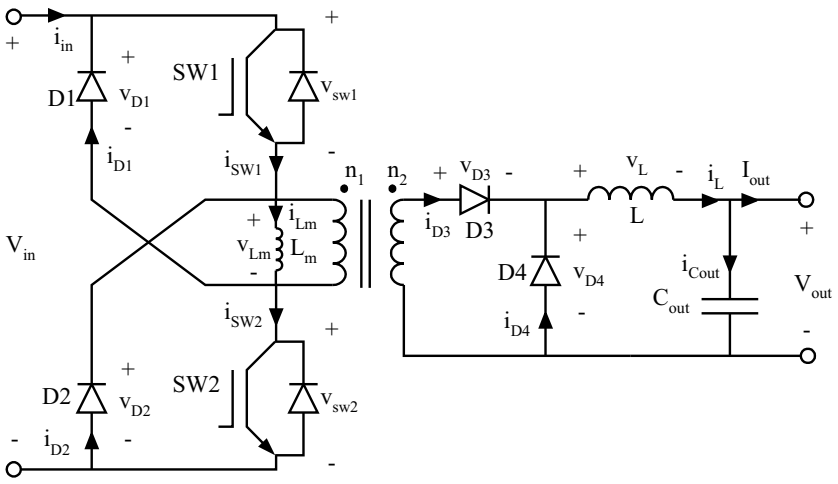

Figure A.15: Tow-Transistor forward converter circuit.

the forward converter. This means that energy is transferred through the transformer when the switch, SW, is on. When the switch is off, L_m discharges via the two diodes D_1 and D_2 to the supply and the inductor L and the capacitor C_{out} supplies the load.

If the ripple in the currents through the inductances and in the voltage over the output capacitor are neglected the currents and voltages in the two-transistor forward converter can be drawn for CCM as in figure A.16. In the same way as for the previous

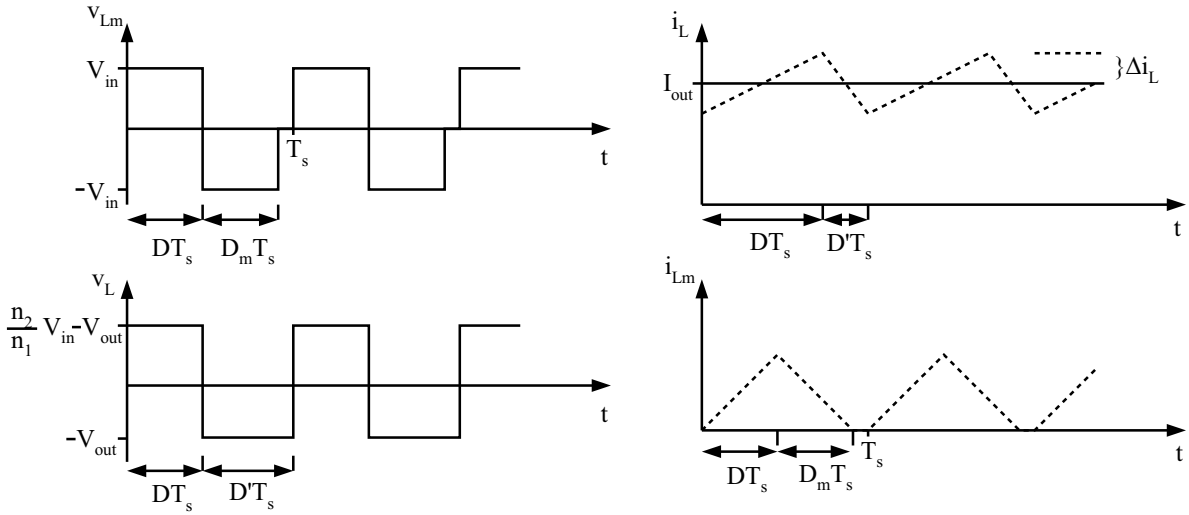

Figure A.16: Idealized voltages and current wave forms of the tow-transistor forward converter.

converters the currents and voltages can be calculated for steady state as

$$V_{out} = \frac{n_2}{n_1} D V_{in} \tag{A.122}$$

$$I_{out} = \frac{n_1}{n_2} \frac{1}{D} I_{in} \tag{A.123}$$

$$D_{max} = \frac{1}{2}. \tag{A.124}$$

From the equations and figure A.16 it is seen that the maximum duty cycle is limited. If the duty cycle exceeds it's maximum value the magnetizing inductance will not be discharged completely and after a time the transformer will be saturated.

The ripple components in the voltage over C_{out} and in the current through L_m and L can be calculated in the same way as for the forward converter, the following expressions are found.

$$\Delta i_{L_m} = \frac{V_{in}}{2L_m} D T_s \tag{A.125}$$

$$\Delta i_L = \frac{n_2}{n_1} \frac{V_{in}}{2L} (1 - D) D T_s \tag{A.126}$$

$$\Delta v_{out} = \frac{\Delta i_L}{8 C_{out}} T_s. \tag{A.127}$$

As expected, it is seen that the ripple in the voltage and current can be low by having a sufficiently large inductor and output capacitor. Due to the fact that the magnetizing current is not used in the energy transfer, it is desired to be small. This gives that the magnetization inductance of the transformer has to be large.

The semiconductor stresses in the two-transistor forward converter become

$$\hat{v}_{SW_1} = \hat{v}_{SW_2} = \hat{v}_{D_1} = \hat{v}_{D_2} = V_{in} \tag{A.128}$$

$$\hat{v_{D_3}} = \hat{v_{D_4}} = \frac{V_{out}}{D} \tag{A.129}$$

$$I_{SW_1,RMS} = I_{SW_2,RMS} = \sqrt{D[(\frac{n_2}{n_1} I_{out} + \Delta i_{L_m})^2 + \frac{1}{3} \Delta i_{L_m}^2]} \tag{A.130}$$

$$I_{D_1,RMS} = I_{D_2,RMS} = 2 \Delta i_{L_m} \sqrt{\frac{D}{3}} \tag{A.131}$$

$$I_{D_3,RMS} = \sqrt{D[(I_{out}^2 + \frac{1}{3} \Delta i_L^2]} \tag{A.132}$$

$$I_{D_4,RMS} = \sqrt{(1 - D)[(I_{out}^2 + \frac{1}{3} \Delta i_L^2]}. \tag{A.133}$$

In the same way as for the other converters, the utilization of the components can be calculated. By neglecting the ripple in voltages and currents the maximum peak voltage and RMS current within the normal operational interval for both the voltage

adjuster and the DC-transformer can be expressed as

$$\hat{v}_{SW_1,max} = \hat{v}_{SW_2,max} = \hat{v}_{D_1,max} = \hat{v}_{D_2,max} = \frac{V_{out,R}}{N} \tag{A.134}$$

$$\hat{v}_{D_3,max} = \hat{v}_{D_4,max} = \frac{n_2}{n_1}\frac{V_{out,R}}{N} \tag{A.135}$$

$$I_{SW_1,RMS,max} = I_{SW_2,RMS,max} = \sqrt{N\frac{n_2}{n_1}}\frac{P_{out,R}}{V_{out,R}} \tag{A.136}$$

$$I_{D_1,RMS} = I_{D_2,RMS} \simeq 0 \tag{A.137}$$

$$I_{D_3,RMS,max} = \sqrt{\frac{n_1}{n_2}N}\frac{P_{out,R}}{V_{out,R}} \tag{A.138}$$

$$I_{D_4,RMS,max} = \sqrt{1-\frac{n_1}{n_2}N}\frac{P_{out,R}}{V_{out,R}}. \tag{A.139}$$

From these equations the utilization factor for the semiconductors can be calculated to

$$U_{SW} = \frac{1}{2}\sqrt{\frac{n_1}{n_2}N} = \frac{1}{2}\sqrt{\frac{N}{n}} \tag{A.140}$$

$$U_{D_3} = \sqrt{\frac{N}{n}} \tag{A.141}$$

$$U_{D_4} = \frac{\frac{N}{n}}{\sqrt{1-\frac{N}{n}}} \tag{A.142}$$

$$U_{SW+D} = \frac{1}{\frac{n}{N}\sqrt{\frac{N}{n}} + \frac{n}{N}\sqrt{1-\frac{N}{n}} + \frac{2}{N}\sqrt{\frac{N}{n}}} \tag{A.143}$$

$$n = \frac{n_2}{n_1}. \tag{A.144}$$

From the equations it is seen that the utilization factors are depending on the desired input output voltage ratio N and the winding ratio of the transformer n. It is seen that all utilization factors are maximized if the winding ratio of the transformer n is as low as possible. But for the voltage adjusting converter the winding ratio is limited by the following equation

$$n_{min} = \frac{2N}{vmin}. \tag{A.145}$$

Where $vmin$ is the smallest input voltage in p.u., this means that V_{in} in p.u. is limited to $vmin \leq \leq 1$. If this is used, the maximum utilization factors for the semiconductors can be calculated to

$$U_{SW,max} = \frac{\sqrt{vmin}}{2\sqrt{2}} \tag{A.146}$$

$$U_{D_3,max} = \sqrt{\frac{vmin}{2}} \tag{A.147}$$

$$U_{D_4,max} = \frac{vmin}{\sqrt{2}\sqrt{2-vmin}} \tag{A.148}$$

$$U_{SW+D,max} = \frac{vmin}{3\sqrt{2vmin} + \sqrt{4-2vmin}}. \tag{A.149}$$

As noticed before, the maximum utilization for the different components occurs for the same winding ratio. This means that the converter can be optimized to utilize all components to the maximum. It shall also be noticed that these maximum points also are valid for the DC-transformer if $vmin = 1$.

The main advantages and drawbacks of the two transistor forward converter are:

+ The switch voltage is clamped by the diodes D_1 and D_2 to the input voltage
+ A smaller snubber circuit is needed compared to the forward converter, due to the current path trough the diodes D_1 and D_2 for the current in the leakage inductance
+ The utilization factor can be maximized due to the transformer
+ The output current ripple is small
+ The transformer only needs two windings
− Poor transformer utilization since the core is only magnetized in one direction
− The transformer design is critical to minimize the magnetizing current and, thus, the losses in the diode D_1 and D_2
− Large input current ripple
− The power can only flow in one direction

A.2.8 Push-Pull Converter

The push-pull converter has two transistors and two primary windings, as seen in figure A.17. The push-pull converter operates by alternatively turning on and off

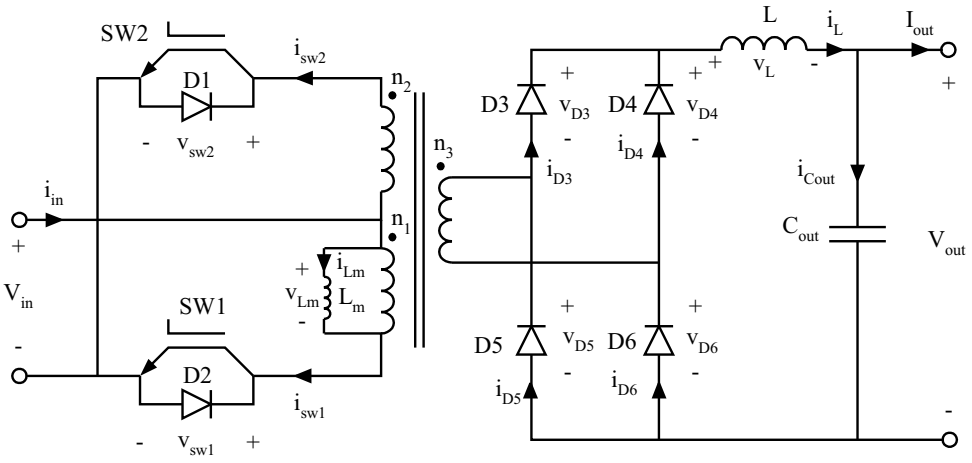

Figure A.17: Push-Pull converter circuit.

the switches, when SW_1 is on SW_2 is off and vice versa. When SW_1 is on, energy is transferred from the input via windings n_1 and n_3 to the output and a positive magnetization is build up in the transformer. When SW_2 is on, energy is transferred from the input via windings n_2 and n_3 to the output and a negative magnetization is build up in the transformer. When both switches are off, the inductor L and the output capacitor supplies the load. The diodes D_1 and D_2 are only used under no-load operation.

If the ripple in the currents through the inductances and in the voltage over the output capacitor is neglected, and it is assumed that $n_1 = n_2$, the currents and voltages in the push-pull converter can be drawn for CCM as in figure A.18. The currents and

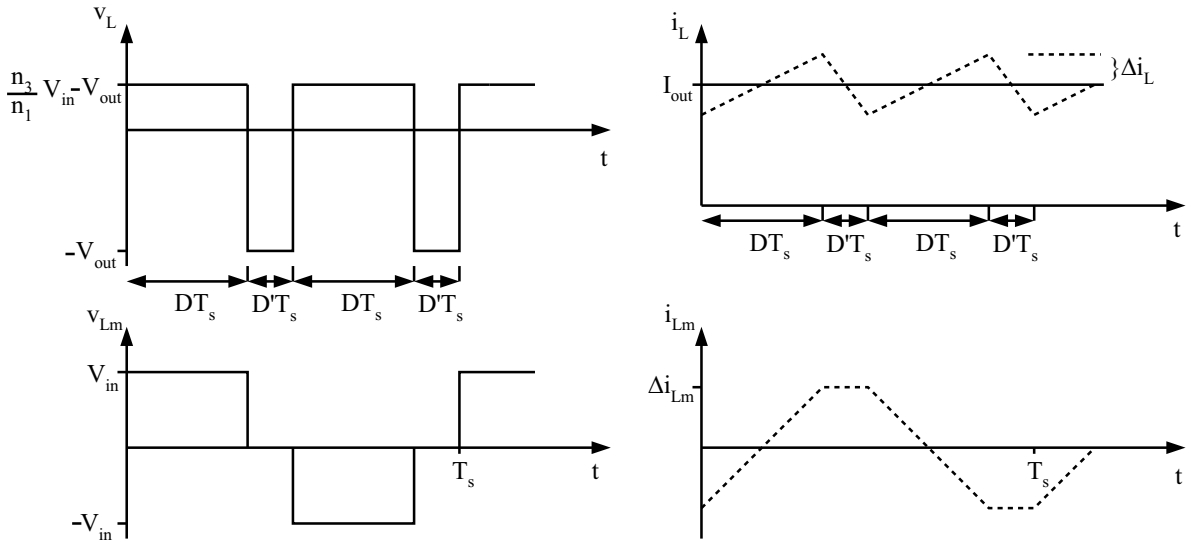

Figure A.18: Idealized voltages and current wave forms of the push-pull converter, solid lines. Dashed lines ripple.

voltages become for steady state

$$V_{out} = 2\frac{n_3}{n_1}DV_{in} \tag{A.150}$$

$$I_{out} = \frac{1}{2}\frac{n_1}{n_3}\frac{1}{D}I_{in} \tag{A.151}$$

$$D_{max} = \frac{1}{2}. \tag{A.152}$$

From the equations and figure A.18 it is seen that the maximum duty cycle is limited. It is also seen that if there is no volt-second balance between the voltages applied to windings n_1 and n_2, the magnetizing will increase and after a time the transformer will be saturated. This imbalance can be eliminated by means of current-mode control of the converter [17].

The ripple components in the voltage over C_{out} and in the current through L_m and L can be calculated in the same way as for the forward converter, which gives

$$\Delta i_{L_m} = \frac{V_{in}}{2 * L_m}DT_s \tag{A.153}$$

$$\Delta i_L = \frac{n_3}{n_1}\frac{V_{in}}{2 * L}(1-2D)DT_s \tag{A.154}$$

$$\Delta v_{out} = \frac{\Delta i_L}{16 * C_{out}}T_s. \tag{A.155}$$

As expected, it is seen that the ripple in the voltages and currents can be low by having a sufficiently large inductors and output capacitor.

The semiconductor stresses in the push-pull converter becomes

$$\hat{v}_{SW_1} = \hat{v}_{SW_2} = \hat{v}_{D_1} = \hat{v}_{D_2} = 2V_{in} \tag{A.156}$$

$$\hat{v}_{D_3} = \hat{v}_{D_4} = \hat{v}_{D_5} = \hat{v}_{D_6} = \frac{V_{out}}{2D} \tag{A.157}$$

$$I_{SW_1,RMS} = I_{SW_2,RMS} = \sqrt{D[(\frac{n_3}{n_1}I_{out})^2 + \frac{1}{3}(\frac{n_3}{n_1}\Delta i_L + \Delta i_{L_m})^2]} \tag{A.158}$$

$$\begin{aligned} I_{D_3,RMS} &= I_{D_4,RMS} = I_{D_5,RMS} = I_{D_6,RMS} \\ &= \sqrt{(1+2D)[(\frac{I_{out}}{2})^2 + \frac{1}{3}(\frac{\Delta i_L}{2})^2] + (1-2D)\frac{n_1}{n_3}\Delta i_{L_m}^2}. \end{aligned} \tag{A.159}$$

In the same way as for the other converters, the utilization of the components can be calculated. By neglecting ripple in voltages and currents, the maximum peak voltage and RMS current within the normal operational interval for both the voltage adjuster and the DC-transformer can be expressed as

$$\hat{v}_{SW_1,max} = \hat{v}_{SW_2,max} = \hat{v}_{D_1,max} = \hat{v}_{D_2,max} = 2\frac{V_{out,R}}{N} \tag{A.160}$$

$$\hat{v}_{D_3,max} = \hat{v}_{D_4,max} = \hat{v}_{D_5,max} = \hat{v}_{D_6,max} = \frac{n_3}{n_1}\frac{V_{out,R}}{N} \tag{A.161}$$

$$I_{SW_1,RMS,max} = I_{SW_2,RMS,max} = \sqrt{\frac{N}{2}\frac{n_3}{n_1}}\frac{P_{out,R}}{V_{out,R}} \tag{A.162}$$

$$I_{D_1,RMS} = I_{D_2,RMS} \simeq 0 \tag{A.163}$$

$$\begin{aligned} I_{D_3,RMS,max} &= I_{D_4,RMS,max} = I_{D_5,RMS,max} = I_{D_6,RMS,max} \\ &= \frac{1}{\sqrt{2}}\sqrt{\frac{1}{2} + \frac{1}{2}\frac{n_1}{n_3}N}\frac{P_{out,R}}{V_{out,R}}. \end{aligned} \tag{A.164}$$

From these equations the utilization factor for the semiconductors can be calculated to

$$U_{SW_1+SW_2} = U_{SW} = \frac{1}{2}\sqrt{\frac{n_1}{n_3}\frac{N}{2}} = \frac{1}{2}\sqrt{\frac{N}{2n}} \tag{A.165}$$

$$U_{D_3+D_4+D_5+D_6} = U_D = \frac{\frac{N}{n}}{2\sqrt{1+\frac{N}{n}}} \tag{A.166}$$

$$U_{SW+D} = \frac{1}{2\sqrt{\frac{2n}{N}} + 2\frac{n}{N}\sqrt{1+\frac{N}{n}}} \tag{A.167}$$

$$n = \frac{n_3}{n_1}. \tag{A.168}$$

From the equations it is seen that the utilization factors are depending on the wanted input output voltage ratio N and the winding ratio of the transformer n. It is seen that all utilization factors are maximized if the winding ratio of the transformer n is as low as possible. But for the voltage adjusting converter the winding ratio is limited by the following equation

$$n_{min} = \frac{N}{vmin}. \tag{A.169}$$

Where $vmin$ is the smallest input voltage in p.u., this means that V_{in} in p.u. is limited to $vmin \leq \leq 1$. If this is used the maximum utilization factors for the semiconductors can be calculated to

$$U_{SW,max} = \frac{\sqrt{vmin}}{2\sqrt{2}} \tag{A.170}$$

$$U_{D_3,max} = \sqrt{\frac{vmin}{2}} \tag{A.171}$$

$$U_{D,max} = \frac{vmin}{2\sqrt{1+vmin}} \tag{A.172}$$

$$U_{SW+D,max} = \frac{vmin}{2\sqrt{2vmin}+2\sqrt{1+vmin}}. \tag{A.173}$$

As noticed before the maximum utilization for the different components occurs for the same winding ratio. This means that the converter can be optimized to utilize all components to the maximum. It shall also be noticed that these maximum points are also valid for the DC-transformer if $vmin = 1$.

The main advantages and drawbacks of the push-pull converter are:

+ The switch voltage is clamped by the diodes D_1 and D_2 to the double input voltage
+ A smaller snubber circuit is needed compared to the forward converter, due to that diodes D_1 and D_2 forms a path for the leakage inductance current
+ The utilization factor can be maximized due to the transformer
+ The output current ripple is small
+ Good utilization of the transformer while operating with both positive and negative flux
+ Double frequency in the output reduces the requirements for the output filter
− The transformer needs two primary windings
− The transformer design is critical to minimize the magnetizing current.
− The primary of the transformer needs a volt-second balance to prevent the transformer core from saturation
− Large input current ripple
− The power can only flow in one direction

A.2.9 Half Bridge Converter

The half bridge converter has two transistors working together with two capacitors, as shown in figure A.19. As seen from the figure the transformer is quite simple with only two windings. The half bridge converter operates by alternative turning on and off the switches, when SW_1 is on SW_2 is off and vice versa. When SW_1 is on, energy is transferred from the input via the transformer and the diode bridge to the output and a positive magnetization is build up in the transformer. When SW_2 is on, energy is transferred from the input via the transformer and the diode bridge to the output and a negative magnetization is build up in the transformer. When both switches are off the inductor L and the output capacitor supplies the load.

If the ripple in the currents through the inductances and in the voltage over the output capacitor is neglected the currents and voltages in the half bridge converter can be drawn for CCM as in figure A.20. As before the currents and voltages becomes

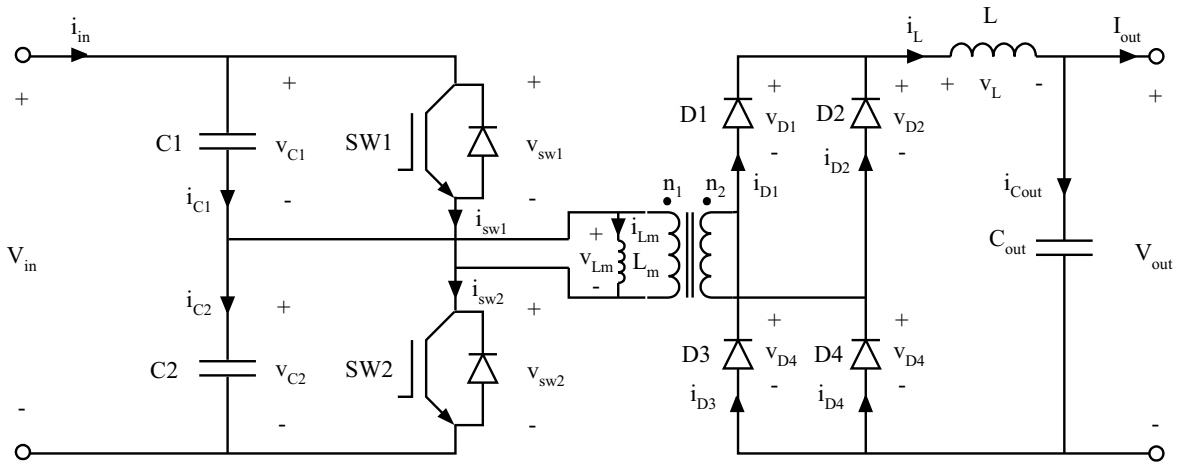

Figure A.19: Half bridge converter circuit.

Figure A.20: Idealized voltages and current wave forms of the half bridge converter, solid lines. Dashed lines ripple.

$$V_{out} = \frac{n_2}{n_1} D V_{in} \tag{A.174}$$

$$I_{out} = \frac{n_1}{n_2} \frac{1}{D} I_{in} \tag{A.175}$$

$$D_{max} = \frac{1}{2}. \tag{A.176}$$

From the equations and figure A.20 it is seen that the maximum duty cycle is limited. It is also seen that if there is no volt-second balance on the primary the magnetizing will increase and after a time the transformer will be saturated. This can, as mention before, be eliminated by means of current-mode control of the converter [17].

The ripple components in the voltage over C_{out} and in the current through L_m and

L can be calculated in the same way as for the forward converter, this gives

$$\Delta i_{L_m} = \frac{V_{in}}{4L_m} DT_s \tag{A.177}$$

$$\Delta i_L = \frac{n_2}{n_1}\frac{V_{in}}{4L}(1-2D)DT_s \tag{A.178}$$

$$\Delta v_{out} = \frac{\Delta i_L}{16C_{out}} T_s. \tag{A.179}$$

The semiconductor stresses in the half-bridge converter becomes

$$\hat{v}_{SW_1} = \hat{v}_{SW_2} = V_{in} \tag{A.180}$$

$$\hat{v}_{D_1} = \hat{v}_{D_2} = \hat{v}_{D_3} = \hat{v}_{D_4} = \frac{V_{out}}{D} \tag{A.181}$$

$$I_{SW_1,RMS} = I_{SW_2,RMS} = \sqrt{D[(\frac{n_2}{n_1} I_{out})^2 + \frac{1}{3}(\frac{n_2}{n_1}\Delta i_L + \Delta i_{L_m})^2]} \tag{A.182}$$

$$\begin{aligned} I_{D_1,RMS} &= I_{D_2,RMS} = I_{D_3,RMS} = I_{D_4,RMS} \\ &= \sqrt{(1+2D)[(\frac{I_{out}}{2})^2 + \frac{1}{3}(\frac{\Delta i_L}{2})^2] + (1-2D)\frac{n_1}{n_2}\Delta i_{L_m}^2}. \end{aligned} \tag{A.183}$$

In the same way as for the other converters, the utilization of the components can be calculated. By neglecting ripple in voltages and currents the maximum peak voltage and RMS current for both the voltage adjuster and the DC-transformer can be expressed as

$$\hat{v}_{SW_1,max} = \hat{v}_{SW_2,max} = \frac{V_{out,R}}{N} \tag{A.184}$$

$$\hat{v}_{D_1,max} = \hat{v}_{D_2,max} = \hat{v}_{D_3,max} = \hat{v}_{D_4,max} = \frac{n_2}{n_1}\frac{V_{out,R}}{N} \tag{A.185}$$

$$I_{SW_1,RMS,max} = I_{SW_2,RMS,max} = \sqrt{N\frac{n_2}{n_1}\frac{P_{out,R}}{V_{out,R}}} \tag{A.186}$$

$$\begin{aligned} I_{D_1,RMS,max} &= I_{D_2,RMS,max} = I_{D_3,RMS,max} = I_{D_4,RMS,max} \\ &= \frac{1}{\sqrt{2}}\sqrt{\frac{1}{2} + \frac{n_1}{n_2}N}\frac{P_{out,R}}{V_{out,R}}. \end{aligned} \tag{A.187}$$

From these equations the utilization factor for the semiconductors can be calculated to

$$U_{SW_1+SW_2} = U_{SW} = \frac{1}{2}\sqrt{\frac{n_1}{n_2}N} = \frac{1}{2}\sqrt{\frac{N}{n}} \tag{A.188}$$

$$U_{D_1+D_2+D_3+D_4} = U_D = \frac{\frac{N}{n}}{2\sqrt{1+2\frac{N}{n}}} \tag{A.189}$$

$$U_{SW+D} = \frac{1}{2\sqrt{\frac{n}{N}} + 2\frac{n}{N}\sqrt{1+2\frac{N}{n}}} \tag{A.190}$$

$$n = \frac{n_2}{n_1}. \tag{A.191}$$

From the equations it is seen that the utilization factors are depending on the wanted input output voltage ratio N and the winding ratio of the transformer n. It is seen

that all utilization factors are maximized if the winding ratio of the transformer n is as low as possible. But for the voltage adjusting converter, the winding ratio is limited by the following equation

$$n_{min} = \frac{2N}{vmin}. \tag{A.192}$$

Where $vmin$ is the smallest input voltage in p.u., this means that V_{in} in p.u. is limited to $vmin \leq \leq 1$. If this is used the maximum utilization factors for the semiconductors can be calculated to

$$U_{SW,max} = \frac{\sqrt{vmin}}{2\sqrt{2}} \tag{A.193}$$

$$U_{D,max} = \frac{vmin}{4\sqrt{1+vmin}} \tag{A.194}$$

$$U_{SW+D,max} = \frac{vmin}{2\sqrt{2vmin}+4\sqrt{1+vmin}}. \tag{A.195}$$

As noticed before the maximum utilization for the different components occurs for the same winding ratio. This means that the converter can be optimized to utilize all components to the maximum. It shall also be noticed that these maximum points are also valid for the DC-transformer if $vmin = 1$.

The main advantages and drawbacks of the half bridge converter are:

+ The switch voltage is clamped by the diodes anti parallel to the transistors to the input voltage
+ A smaller snubber circuit is needed compared to the forward converter, due to that the anti parallel diodes forms a path for the leakage inductance current
+ The utilization factor can be maximized due to the transformer
+ The output current ripple is small
+ Good utilization of the transformer while operating with both positive and negative flux
+ Double frequency in the output reduces the requirements for the output filter
− The transformer design is critical to minimize the magnetizing current.
− The primary of the transformer needs a volt-second balance to prevent the transformer core from saturation
− The power can only flow in one direction

A.2.10 Full Bridge Converter

The full bridge converter has four transistors working together, as shown in figure A.21. It is also seen that the transformer is simple with only two windings. The full bridge converter operates by alternative turning on and off the switches, when SW_1 and SW_4 is on SW_2 and SW_3 is off and vice versa. When SW_1 and SW_4 is on, energy is transferred from the input via the transformer and the diode bridge to the output and a positive magnetization is build up in the transformer. When SW_2 and SW_3 is on, energy is transferred from the input via the transformer and the diode bridge to the output and a negative magnetization is build up in the transformer. When both switches are off the inductor L and the output capacitor supplies the load.

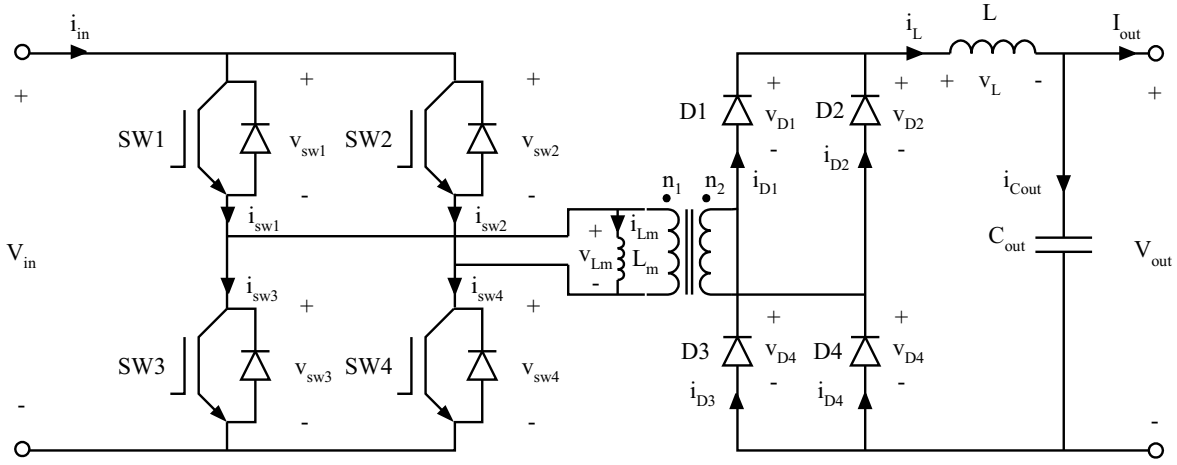

Figure A.21: Full bridge converter circuit.

If the ripple in the currents through the inductances and in the voltage over the output capacitor are neglected the currents and voltages in the full bridge converter can be drawn for CCM as in figure A.22. As before the currents and voltages become

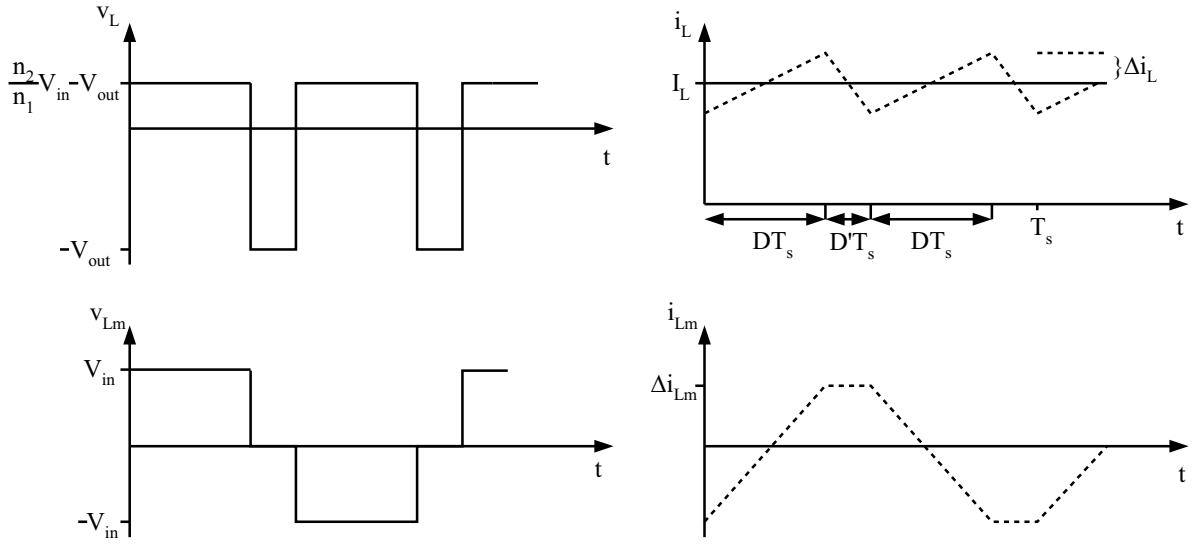

Figure A.22: Idealized voltages and current wave forms of the full bridge converter, solid lines. Dashed lines ripple.

$$V_{out} = 2\frac{n_2}{n_1}DV_{in} \tag{A.196}$$

$$I_{out} = \frac{1}{2}\frac{n_1}{n_2}\frac{1}{D}I_{in} \tag{A.197}$$

$$D_{max} = \frac{1}{2}. \tag{A.198}$$

From the equations and figure A.22 it is seen that the maximum duty cycle is limited. It is also seen that if there is no volt-second balance on the primary the magnetizing

will increase and after a time the transformer will be saturated. This can as mention before, be eliminated by means of current-mode control of the converter [17].

The ripple components in the voltage over C_{out} and in the current through L_m and L can be calculated in the same way as for the forward converter, this gives

$$\Delta i_{L_m} = \frac{V_{in}}{2L_m} DT_s \tag{A.199}$$

$$\Delta i_L = \frac{n_2}{n_1}\frac{V_{in}}{2L}(1-2D)DT_s \tag{A.200}$$

$$\Delta v_{out} = \frac{\Delta i_L}{16C_{out}} T_s. \tag{A.201}$$

The semiconductor stresses in the full bridge converter become

$$\hat{v}_{SW_1} = \hat{v}_{SW_2} = \hat{v}_{SW_3} = \hat{v}_{SW_4} = V_{in} \tag{A.202}$$

$$\hat{v}_{D_1} = \hat{v}_{D_2} = \hat{v}_{D_3} = \hat{v}_{D_4} = \frac{V_{out}}{2D} \tag{A.203}$$

$$\begin{aligned} I_{SW_1,RMS} &= I_{SW_2,RMS} = I_{SW_3,RMS} = I_{SW_4,RMS} \\ &= \sqrt{D[(\frac{n_2}{n_1}I_{out})^2 + \frac{1}{3}(\frac{n_2}{n_1}\Delta i_L + \Delta i_{L_m})^2]} \end{aligned} \tag{A.204}$$

$$\begin{aligned} I_{D_1,RMS} &= I_{D_2,RMS} = I_{D_3,RMS} = I_{D_4,RMS} \\ &= \sqrt{(1+2D)[(\frac{I_{out}}{2})^2 + \frac{1}{3}(\frac{\Delta i_L}{2})^2] + (1-2D)\frac{n_1}{n_2}\Delta i_{L_m}^2}. \end{aligned} \tag{A.205}$$

In the same way as for the other converters the utilization of the components can be calculated. By neglecting ripple in voltages and currents the maximum peak voltage and RMS current for both the voltage adjuster and the DC-transformer can be expressed as

$$\hat{v}_{SW_1,max} = \hat{v}_{SW_2,max} = \hat{v}_{SW_3,max} = \hat{v}_{SW_4,max} = \frac{V_{out,R}}{N} \tag{A.206}$$

$$\hat{v}_{D_1,max} = \hat{v}_{D_2,max} = \hat{v}_{D_3,max} = \hat{v}_{D_4,max} = \frac{n_2}{n_1}\frac{V_{out,R}}{N} \tag{A.207}$$

$$\begin{aligned} I_{SW_1,RMS,max} &= I_{SW_2,RMS,max} = I_{SW_3,RMS,max} = I_{SW_4,RMS,max} \\ &= \sqrt{\frac{N}{2}\frac{n_2}{n_1}\frac{P_{out,R}}{V_{out,R}}} \end{aligned} \tag{A.208}$$

$$\begin{aligned} I_{D_1,RMS,max} &= I_{D_2,RMS,max} = I_{D_3,RMS,max} = I_{D_4,RMS,max} \\ &= \frac{1}{2}\sqrt{1+\frac{n_1}{n_2}N\frac{P_{out,R}}{V_{out,R}}}. \end{aligned} \tag{A.209}$$

From these equations the utilization factor for the semiconductors can be calculated to

$$U_{SW_1+SW_2+SW_3+SW_4} = U_{SW} = \frac{1}{2}\sqrt{\frac{n_1}{n_2}\frac{N}{2}} = \frac{1}{2}\sqrt{\frac{N}{2n}} \tag{A.210}$$

$$U_{D_1+D_2+D_3+D_4} = U_D = \frac{\frac{N}{n}}{2\sqrt{1+\frac{N}{n}}} \tag{A.211}$$

$$U_{SW+D} = \frac{1}{2\sqrt{\frac{2n}{N}} + 2\frac{n}{N}\sqrt{1+\frac{N}{n}}} \tag{A.212}$$

$$n = \frac{n_2}{n_1}. \tag{A.213}$$

From the equations it is seen that the utilization factors are depending on the wanted input output voltage ratio N and the winding ratio of the transformer n. It is seen that all utilization factors are maximized if the winding ratio of the transformer n is as low as possible. But for the voltage adjusting converter the winding ratio is limited by the following equation

$$n_{min} = \frac{N}{vmin}. \tag{A.214}$$

Where $vmin$ is the smallest input voltage in p.u., this means that V_{in} in p.u. is limited to $vmin \leq \ \leq 1$. If this is used the maximum utilization factors for the semiconductors can be calculated to

$$U_{SW,max} = \frac{\sqrt{vmin}}{2\sqrt{2}} \tag{A.215}$$

$$U_{D,max} = \frac{vmin}{2\sqrt{1+vmin}} \tag{A.216}$$

$$U_{SW+D,max} = \frac{vmin}{2\sqrt{2vmin} + 2\sqrt{1+vmin}}. \tag{A.217}$$

In the same way as earlier, the maximum utilization for the different components occurs for the same winding ratio. This means that the converter can be optimized to utilize all components to the maximum. It shall also be noticed that these maximum points are also valid for the DC-transformer if $vmin = 1$.

The main advantages and drawbacks of the full bridge converter are:

+ The switch voltage is clamped by the diodes anti parallel to the transistors to the input voltage
+ A smaller snubber circuit is needed compared to the forward converter, due to that the anti parallel diodes forms a path for the leakage inductance current
+ The utilization factor can be maximized due to the transformer
+ The output current ripple is small
+ Good utilization of the transformer while operating with both positive and negative flux
+ Double frequency in the output reduces the requirements for the output filter
− The transformer design is critical to minimize the magnetizing current.
− The primary of the transformer needs a volt-second balance to prevent the transformer core from saturation
− Large input current ripple
− The power can only flow in one direction

Efficiency at different loads is up to 97%

A.2.11 Isolated SEPIC Converter

The isolated sepic converter is obtained by substituting the inductance L_2 in the sepic converter, se figure A.7, to a transformer. The transformer in the isolated sepic converter has only two windings as can be seen in figure A.23. The isolated sepic converter

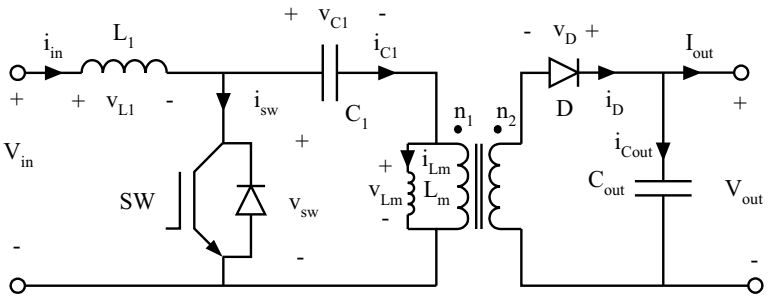

Figure A.23: Isolated sepic converter circuit.

operates by repeatedly shifting energy between the inductor L_1, the transformer, the capacitor C_1 and the load. Energy is stored in the inductor L_1 when the switch, SW, is on and the transformer is storing energy from the capacitor C_1 during the same time. When the switch is off, L_1 charges C_1 and together with the transformer also supplies energy to the output. During the time the switch is on, the output is supplied from the capacitor C_{out}.

If the ripple in the currents through the inductors and in the voltages over the capacitors are neglected the currents and voltages in the isolated sepic converter can be drawn for CCM as in figure A.24. The currents and voltages in steady state become

$$V_{out} = \frac{n_2}{n_1}\frac{D}{1-D}V_{in} \tag{A.218}$$

$$I_{out} = \frac{n_1}{n_2}\frac{1-D}{D}I_{in} \tag{A.219}$$

$$V_{C_1} = V_{in} \tag{A.220}$$

$$I_{L_m} = -\frac{n_1}{n_2}I_{out}. \tag{A.221}$$

From the equations it is clearly seen that the output voltage can be both lower or higher then the input voltage depending on the duty ratio D.

The ripple components in the voltage over C_1 and C_{out} and in the currents through L_1 and L_m can be calculated in the same way as for the boost converter, this gives

$$\Delta i_{in} = \frac{V_{in}}{2L_1}DT_s \tag{A.222}$$

$$\Delta i_{L_m} = \frac{V_{in}}{2L_m}DT_s \tag{A.223}$$

$$\Delta v_{C_1} = \frac{n_2}{n_1}\frac{I_{out}}{2C_1}DT_s \tag{A.224}$$

$$\Delta v_{out} = \frac{I_{out}}{2C_{out}}DT_s. \tag{A.225}$$

As expected, it is seen that the ripple in the voltages and currents can be low by having sufficiently large inductors and capacitors.

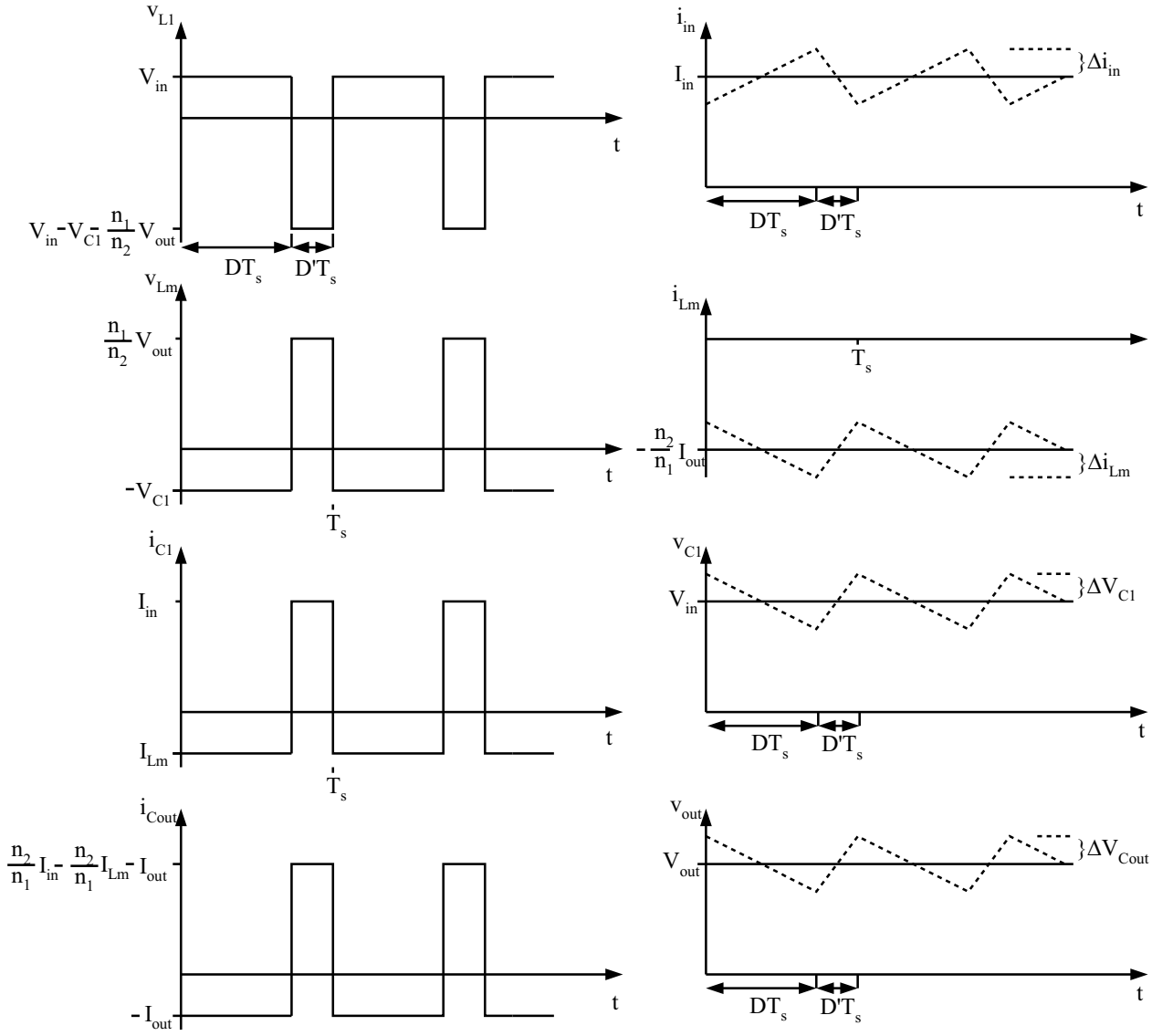

Figure A.24: Idealized voltages and current wave forms of the isolated sepic converter, solid lines. Dashed lines ripple.

The semiconductor stresses in the isolated sepic converter become

$$\hat{v_{SW}} = = \frac{n_1}{n_2}(\frac{V_{out}}{D} + \Delta v_{C_{out}}) + \Delta v_{C_1} \quad \text{(A.226)}$$

$$\hat{v_D} = \frac{V_{out}}{D} + \Delta v_{C_{out}} + \frac{n_2}{n_1}\Delta v_{C_1} \quad \text{(A.227)}$$

$$I_{SW,RMS} = \sqrt{D[(\frac{n_2}{n_1}\frac{I_{out}}{1-D})^2 + \frac{1}{3}(\Delta i_{in} + \Delta i_{L_m})^2]} \quad \text{(A.228)}$$

$$I_{D,RMS} = \sqrt{(1-D)[(\frac{I_{out}}{1-D})^2 + \frac{1}{3}(\frac{n_1}{n_2}\Delta i_{in} + \frac{n_1}{n_2}\Delta i_{L_m})^2]}. \quad \text{(A.229)}$$

In the same way as for the other converters, the utilization of the components can be calculated. By neglecting the ripple in voltages and currents the maximum peak voltage and RMS current for both the voltage adjuster and the DC-transformer can be

expressed as

$$\hat{v}_{SW,max} = \frac{n_1}{n_2}(N + \frac{n_2}{n_1})\frac{V_{out,R}}{N} = \frac{N+n}{Nn}V_{out,R} \quad (A.230)$$

$$\hat{v}_{D,max} = (1 + \frac{n}{N})V_{out,R} \quad (A.231)$$

$$I_{SW,RMS,max} = \sqrt{N(N+n)}\frac{P_{out,R}}{V_{out,R}} \quad (A.232)$$

$$I_{D,RMS,max} = \sqrt{\frac{N}{n} + 1}\frac{P_{out,R}}{V_{out,R}} \quad (A.233)$$

$$n = \frac{n_2}{n_1}. \quad (A.234)$$

From these equations the utilization factor for the semiconductors can be calculated to, compere with the equations for the flyback converter,

$$U_{SW} = \frac{n\sqrt{N}}{(N+n)^{\frac{3}{2}}} \quad (A.235)$$

$$U_{D_2} = \frac{N\sqrt{n}}{(N+n)^{\frac{3}{2}}} \quad (A.236)$$

$$U_{SW+D_2} = \frac{nN}{(N+n)(\sqrt{N}+\sqrt{n}}. \quad (A.237)$$

From the equations it is seen that the utilization factors are depending on the wished input output voltage ratio N and the winding ratio of the transformer n. By choosing the winding ratio of the transformer cleverly the utilization factor of the components can be maximized, which gives

$$U_{SW,max} = \frac{2}{3\sqrt{3}} \text{ for } n = 2N \quad (A.238)$$

$$U_{D_2,max} = \frac{2}{3\sqrt{3}} \text{ for } n = \frac{N}{2} \quad (A.239)$$

$$U_{SW+D_2,max} = \frac{1}{4\sqrt{2}} \text{ for } n = N. \quad (A.240)$$

As can be seen, the maximum utilization factor for the different components do not occur for the same winding ratio. This means that one can maximize the utilization for one component or use a compromise. One compromise is to use the utilization factor for the switch and the diode, $U_{SW+D_2,max}$, where the rating of the switch and the rating of the diode are added, according to equation A.3. Another way to add the ratings of the devices, is to first multiply them with a weight factor that can be depending on size, losses and/or cost. In this way, for example, the most expensive component can be utilized more, in order to reduce the cost.

The main advantages and drawbacks of the isolated sepic converter are:

+ Only two active components, SW and D
+ Low input current ripple in CCM
+ The utilization factor can be maximized due to the transformer
− Critical transformer design and the high energy, which must be stored in the transformer windings in the form of a DC current, requires a high magnetizing inductance, a high current primary, which in turn requires larger cores than would be needed with pure AC
− Poor transformer utilization since the core is only magnetized in one direction
− The large current ripple in the capacitor C_1
− Large output voltage ripple
− The power can only flow in one direction

A.2.12 Isolated ´Cuk Converter

The isolated ´cuk converter is obtained by splitting the capacitor C_1 in the ´cuk converter, see figure A.5, into two capacitors C_1 and C_2 and place the transformer between them, this is shown in figure A.25. As seen from the figure the transformer is simple with only two windings. The isolated ´cuk converter operates by repeatedly shifting

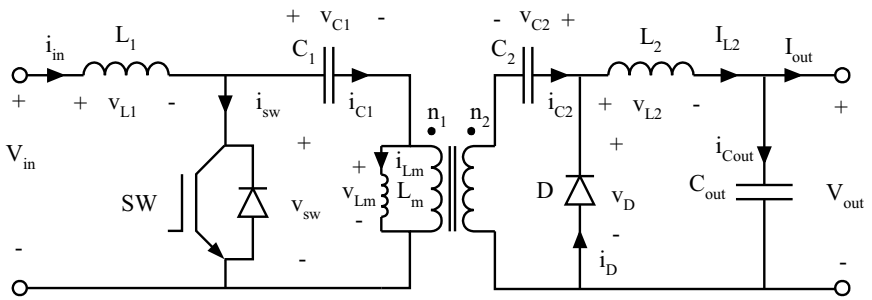

Figure A.25: Isolated ´cuk converter circuit.

energy between the inductors L_1 and L_2, the capacitors C_1 and C_2 and the load. Energy is stored in the inductor L_1 when the switch, SW, is on (conducting) and inductor L_2 and the output capacitor C_{out} are storing energy from the capacitors C_1 and C_2 during the same time. When the switch is off, L_1 charges C_1 and C_2 and L_2 is transferring energy to the output. During the time the switch is on, the output is supplied from the capacitor C_{out} and L_2. The transformer is only used to transfer energy from the primary side to the secondary side, almost no energy is stored in the transformer.

If the ripple in the current through the inductor and in the voltage over the capacitor are neglected the currents and voltages in the isolated ´cuk converter can be drawn for CCM as in figure A.26. As for the previous converters the currents and voltages for

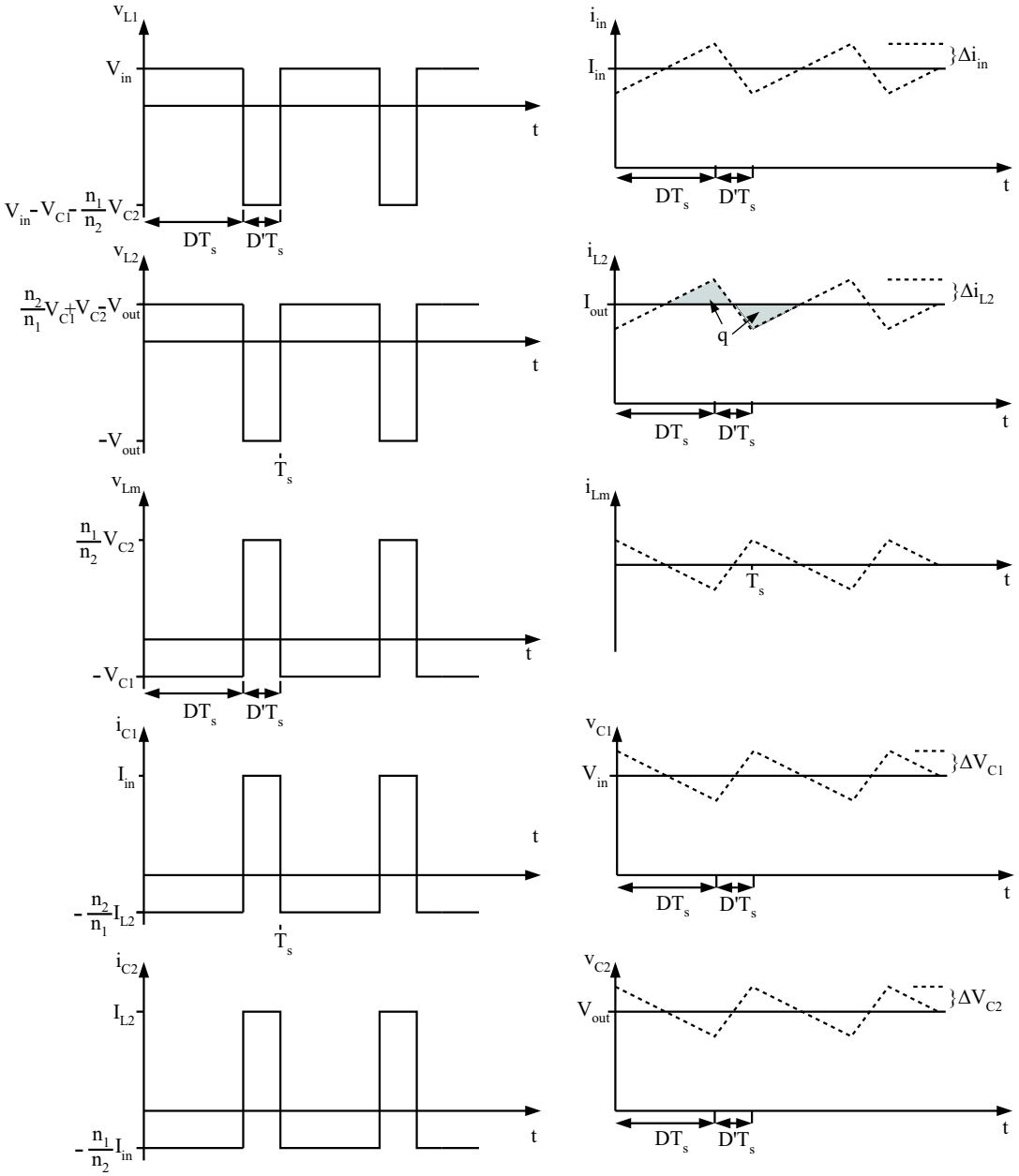

Figure A.26: Idealized voltages and current wave forms of the isolated ´cuk converter, solid lines. Dashed lines ripple.

steady state becomes

$$V_{out} = \frac{n_2}{n_1}\frac{D}{1-D}V_{in} \quad \text{(A.241)}$$

$$I_{out} = \frac{n_1}{n_2}\frac{1-D}{D}I_{in} \quad \text{(A.242)}$$

$$V_{C_1} = V_{in} \quad \text{(A.243)}$$

$$V_{C_2} = V_{out} \quad \text{(A.244)}$$

$$D = \frac{t_{on}}{T_s}. \quad \text{(A.245)}$$

From the equations it is clearly seen that the output voltage can be regulated both up and down depending on the duty ratio D.

The ripple components in the voltage over C_1, C_2 and C_{out} and the currents through L_1, L_2 and L_m can be calculated in the same way as for the other converter, which gives

$$\Delta i_{in} = \frac{V_{in}}{2L_1}DT_s \tag{A.246}$$

$$\Delta i_{L_2} = \frac{n_2}{n_1}\frac{V_{in}}{2L_2}DT_s \tag{A.247}$$

$$\Delta i_{L_m} = \frac{V_{in}}{2L_m}DT_s \tag{A.248}$$

$$\Delta v_{C_1} = \frac{n_2}{n_1}\frac{I_{out}}{2C_1}DT_s \tag{A.249}$$

$$\Delta v_{C_2} = \frac{I_{out}}{2C_2}DT_s \tag{A.250}$$

$$\Delta v_{out} = \frac{\Delta i_{L_2}}{8C_{out}}T_s. \tag{A.251}$$

As expected, it is seen that the ripple in the voltages and currents can be low by using sufficiently large inductors and capacitors.

The semiconductor stresses in the isolated ´cuk converter become

$$\hat{v}_{SW} = \frac{n_1}{n_2}\frac{V_{out}}{D} + \Delta v_{C_1} + \frac{n_1}{n_2}\Delta v_{C_2} \tag{A.252}$$

$$\hat{v}_D = \frac{V_{out}}{D} + \frac{n_2}{n_1}\Delta v_{C_1} + \Delta v_{C_2} \tag{A.253}$$

$$I_{SW,RMS} = \sqrt{D[(\frac{n_2}{n_1}\frac{I_{out}}{1-D})^2 + \frac{1}{3}(\Delta i_{in} + \frac{n_2}{n_1}\Delta i_{L_2} + \Delta i_{L_m})^2]} \tag{A.254}$$

$$I_{D,RMS} = \sqrt{(1-D)[(\frac{I_{out}}{1-D})^2 + \frac{1}{3}(\frac{n_1}{n_2}\Delta i_{in} + \Delta i_{L_2} + \frac{n_1}{n_2}\Delta i_{L_m})^2]}. \tag{A.255}$$

In the same way as for the other converters, the utilization of the components can be calculated. By neglecting ripple in voltages and currents the maximum peak voltage and RMS current for both the voltage adjuster and the DC-transformer can be expressed as

$$\hat{v}_{SW,max} = \frac{n_1}{n_2}(N + \frac{n_2}{n_1})\frac{V_{out,R}}{N} = \frac{N+n}{Nn}V_{out,R} \tag{A.256}$$

$$\hat{v}_{D,max} = (1 + \frac{n}{N})V_{out,R} \tag{A.257}$$

$$I_{SW,RMS,max} = \sqrt{N(N+n)}\frac{P_{out,R}}{V_{out,R}} \tag{A.258}$$

$$I_{D,RMS,max} = \sqrt{\frac{N}{n} + 1}\frac{P_{out,R}}{V_{out,R}} \tag{A.259}$$

$$n = \frac{n_2}{n_1}. \tag{A.260}$$

From these equations the utilization factor for the semiconductors can be calculated to,

compere with the equations for the flyback converter and the isolated sepic converter.

$$U_{SW} = \frac{n\sqrt{N}}{(N+n)^{\frac{3}{2}}} \tag{A.261}$$

$$U_{D_2} = \frac{N\sqrt{n}}{(N+n)^{\frac{3}{2}}} \tag{A.262}$$

$$U_{SW+D_2} = \frac{nN}{(N+n)(\sqrt{N}+\sqrt{n}}. \tag{A.263}$$

From the equations it is seen that the utilization factors are depending on the wanted input output voltage ratio N and the winding ratio of the transformer n. By choosing the winding ratio of the transformer in a clever way, the utilization factor of the components can be maximized, which gives

$$U_{SW,max} = \frac{2}{3\sqrt{3}} \text{ for } n = 2N \tag{A.264}$$

$$U_{D_2,max} = \frac{2}{3\sqrt{3}} \text{ for } n = \frac{N}{2} \tag{A.265}$$

$$U_{SW+D_2,max} = \frac{1}{4\sqrt{2}} \text{ for } n = N. \tag{A.266}$$

As can be noticed, the maximum utilization factor for the different components do not occur for the same winding ratio. This means that one can maximize the utilization for one component or use a compromise. One compromise is to use the utilization factor for the switch and the diode, $U_{SW+D_2,max}$, where the rating of the switch and the rating of the diode are added, according to equation A.3. Another way to add the ratings of the devices, is to first multiply them with a weight factor that can be depending on size, losses and/or cost. In this way, for example, the most expensive component can be utilized more, in order to reduce the cost. It can also be noticed that the maximum utilization factor is independent of the voltage ratio N compared to the transformer less converters discussed before.

The main advantages and drawbacks of the isolated ´cuk converter are:

+ Only two active components, SW and D
+ Low input and output current ripple in CCM
+ The utilization factor can be maximized due to the transformer
+ Good utilization of the transformer while operating with both positive and negative flux
+ No saturation of the transformer is possible due to the capacitors C_1 and C_2
− High number of components
− High current ripple in the capacitors C_1 and C_2
− The power can only flow in one direction

A.2.13 Full Bridge Isolated Boost Converter

The full bridge isolated boost converter is obtained by moving the output filter inductor from the output to the input of the full bridge converter and changing the switching pattern of the switches. In figure A.27 the full bridge isolated boost converter is shown. The full bridge isolated boost converter operates by repeatedly shifting energy between the inductor L_1 and the output capacitor and the load. First, energy is stored in the

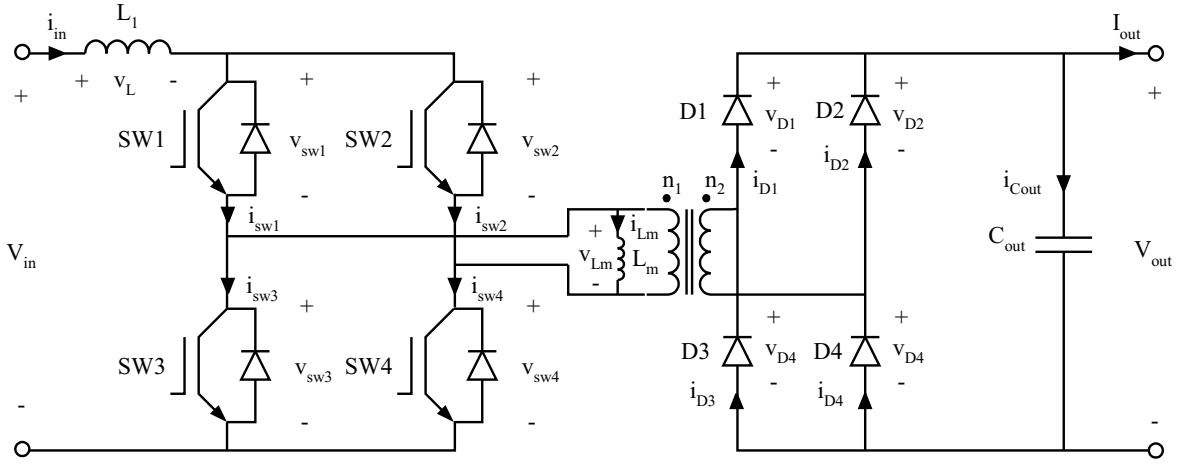

Figure A.27: Full bridge isolated boost converter circuit.

input inductor L_1 by turning all switches on. The stored energy in the inductance is transferred through the transformer to the output by turning switch SW_2 and SW_3 off. This builds up a positive flux in the transformer. Next the inductance is charged again by turning all switches on. The energy is transferred to the output by turning SW_1 and SW_4 off. This builds up a negative flux in the transformer. During the time the input inductor is charged the output capacitor supplies the load.

If the ripple in the currents through the inductances and in the voltage over the output capacitor are neglected the currents and voltages in the full bridge isolated boost converter can be drawn for CCM as in figure A.28. It shall be noticed from the figure A.28 that if the output voltage is low (zero) the inductor L_1 can not be discharged which will mean that the inductor will be saturated. This can occur at start up or at overloading of the converter. A solution for this problem is shown in [56], [55].

As for the previous converters, the currents and voltages for steady state becomes

$$V_{out} = \frac{n_2}{n_1}\frac{1}{1-2D}V_{in} \tag{A.267}$$

$$I_{out} = \frac{n_1}{n_2}(1-2D)I_{in} \tag{A.268}$$

$$D_{max} = \frac{1}{2}. \tag{A.269}$$

From the equations and figure A.28 it is seen that the maximum duty cycle is limited. It is also seen that if there is no volt-second balance on the primary the magnetizing will increase and after a time the transformer will be saturated. This can as mention before, be eliminated by means of current-mode control of the converter [17].

The ripple components in the voltage over C_{out} and in the current through L_m and L_1 can be calculated in the same way as for the other converters, which gives

$$\Delta i_{L_1} = \frac{V_{in}}{2 * L_1}DT_s \tag{A.270}$$

$$\Delta i_{L_m} = \frac{V_{in}}{4 * L_m}T_s \tag{A.271}$$

$$\Delta v_{out} = \frac{I_{out}}{2 * C_{out}}DT_s. \tag{A.272}$$

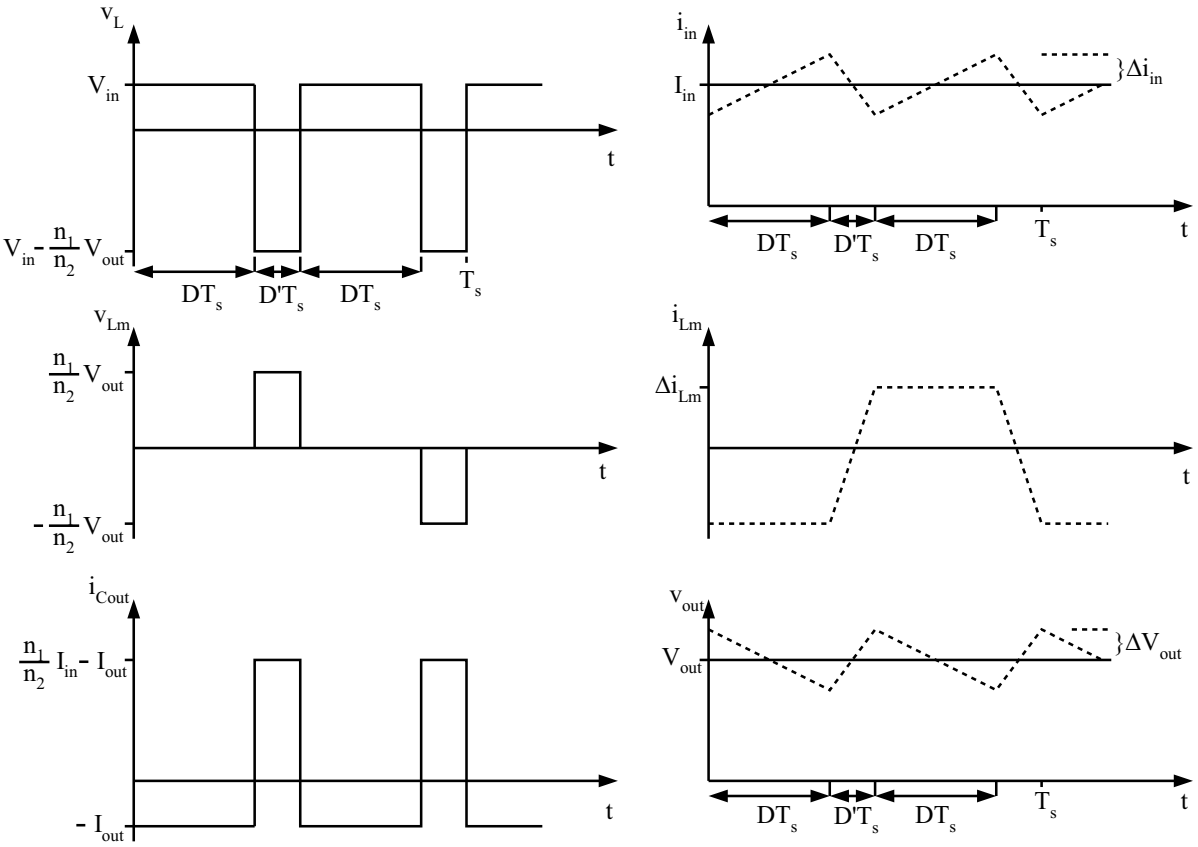

Figure A.28: Idealized voltages and current wave forms of the full bridge isolated boost converter, solid lines. Dashed lines ripple.

The semiconductor stresses in the full bridge isolated boost converter becomes

$$\hat{v}_{SW_1} = \hat{v}_{SW_2} = \hat{v}_{SW_3} = \hat{v}_{SW_4} = \frac{n_1}{n_2}(V_{out} + \Delta v_{out}) \quad \text{(A.273)}$$

$$\hat{v}_{D_1} = \hat{v}_{D_2} = \hat{v}_{D_3} = \hat{v}_{D_4} = V_{out} + \Delta v_{out} \quad \text{(A.274)}$$

$$I_{SW_1,RMS} = I_{SW_2,RMS} = I_{SW_3,RMS} = I_{SW_4,RMS}$$

$$= \sqrt{\frac{1-D}{2}[(\frac{n_2}{n_1}\frac{I_{out}}{1-2D})^2 + \frac{\Delta i_{L_1}^2}{6}] + \frac{D}{2}\Delta i_{L_m})^2} \quad \text{(A.275)}$$

$$I_{D_1,RMS} = I_{D_2,RMS} = I_{D_3,RMS} = I_{D_4,RMS}$$

$$= \sqrt{(\frac{1}{2} - D)[(\frac{I_{out}}{2(\frac{1}{2} - D)})^2 + \frac{1}{3}(\frac{n_1}{n_2})^2(\Delta i_{L_1} + \Delta i_{L_m})^2]}. \quad \text{(A.276)}$$

In the same way as for the other converters, the utilization of the components can be calculated. By neglecting the ripple in voltages and currents, the maximum peak voltage and RMS current for both the voltage adjuster and the DC-transformer can be

expressed as

$$\begin{aligned}
\hat{v}_{SW_1,max} &= \hat{v}_{SW_2,max} = \hat{v}_{SW_3,max} = \hat{v}_{SW_4,max} = \frac{n_1}{n_2} V_{out,R} && \text{(A.277)}\\
\hat{v}_{D_1,max} &= \hat{v}_{D_2,max} = \hat{v}_{D_3,max} = \hat{v}_{D_4,max} = V_{out,R} && \text{(A.278)}\\
I_{SW_1,RMS,max} &= I_{SW_2,RMS,max} = I_{SW_3,RMS,max} = I_{SW_4,RMS,max} \\
&= \frac{N}{2}\sqrt{1+\frac{1}{N}\frac{n_2}{n_1}}\frac{P_{out,R}}{V_{out,R}} && \text{(A.279)}\\
I_{D_1,RMS,max} &= I_{D_2,RMS,max} = I_{D_3,RMS,max} = I_{D_4,RMS,max} \\
&= \frac{1}{\sqrt{2}}\sqrt{\frac{n_1}{n_2}N}\frac{P_{out,R}}{V_{out,R}}. && \text{(A.280)}
\end{aligned}$$

From these equations the utilization factor for the semiconductors can be calculated to be

$$\begin{aligned}
U_{SW_1+SW_2+SW_3+SW_4} &= U_{SW} = \frac{n}{2\sqrt{N}\sqrt{N+n}} && \text{(A.281)}\\
U_{D_1+D_2+D_3+D_4} &= U_D = \frac{1}{2\sqrt{2}}\sqrt{\frac{n}{N}} && \text{(A.282)}\\
U_{SW+D} &= \frac{1}{2\frac{\sqrt{N}}{n}\sqrt{N+n}+2\sqrt{2}\sqrt{\frac{N}{n}}} && \text{(A.283)}\\
n &= \frac{n_2}{n_1}. && \text{(A.284)}
\end{aligned}$$

From the equations it is seen that the utilization factors are depending on the desired input output voltage ratio N and the winding ratio of the transformer n. It is seen that all utilization factors are maximized if the winding ratio of the transformer n is as large as possible. But the winding ratio is limited by the following equation

$$V_{out} \geq \frac{n_2}{n_1} V_{in} = n V_{in} \rightarrow n_{max} = N. \qquad \text{(A.285)}$$

If this is used, the maximum utilization factors for the semiconductors can be calculated to

$$\begin{aligned}
U_{SW,max} &= \frac{1}{2\sqrt{2}} && \text{(A.286)}\\
U_{D,max} &= \frac{1}{2\sqrt{2}} && \text{(A.287)}\\
U_{SW+D,max} &= \frac{1}{4\sqrt{2}}. && \text{(A.288)}
\end{aligned}$$

As noticed before, the maximum utilization for the different components occurs for the same winding ratio. This means that the converter can be optimized to utilize all components to the maximum.

The main advantages and drawbacks of the full bridge isolated boost converter are:

+ The utilization factor can be maximized due to the transformer
+ The input current ripple is small
+ Good utilization of the transformer while operating with both positive and negative flux
+ Double frequency in the output reduces the requirements for the output filter
− A snubber circuit is needed to take care of the inductor current as the current is built up in the leakage inductance of the transformer
− The transformer design is critical to minimize the magnetizing current and the leakage inductance
− The primary of the transformer needs a volt-second balance to prevent the transformer core from saturation
− Risk for inductor saturation if the output voltage is to low
− The power can only flow in one direction

A.2.14 Push-Pull Isolated Boost Converter

The push-pull isolated boost converter is also obtained by moving the output filter inductor from the output to the input of the push-pull converter and changing the switching pattern of the switches. In figure A.29 the push-pull isolated boost converter is shown. The push-pull isolated boost converter operates by repeatedly shifting energy

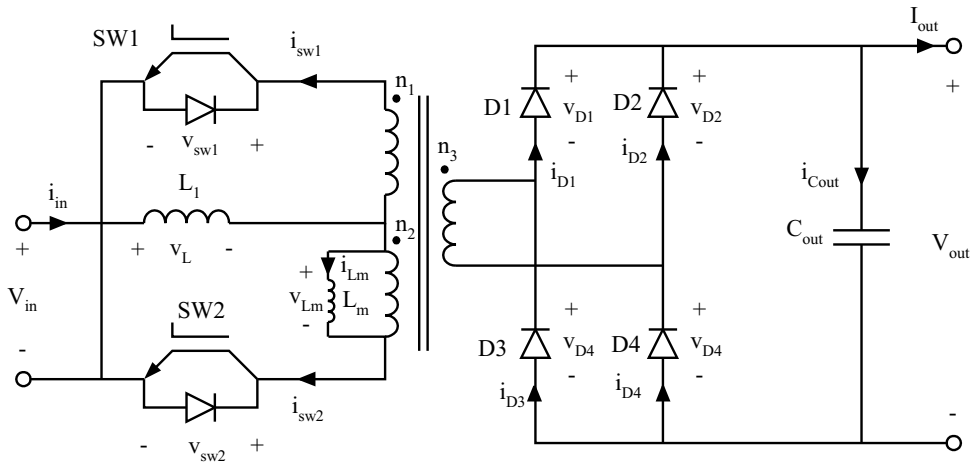

Figure A.29: Push-pull isolated boost converter circuit.

between the inductor L_1 and the output capacitor and the load. First energy is stored in the input inductor L_1 by turning all switches on. The stored energy in the inductance is transferred through the transformer to the output by turning switch SW_2 off. This builds up a negative flux in the transformer. Next, the inductance is charged again by turning all switches on. The energy is transferred to the output by turning SW_1 off. This builds up a positive flux in the transformer. During the time when the input inductor is charged, the output capacitor supplies the load.

If the ripple in the currents through the inductances and in the voltage over the output capacitor are neglected and it is assumed that $n_1 = n_2$ the currents and voltages in the push-pull isolated boost converter can be drawn for CCM as in figure A.30. It shall be noticed from the figure A.30 that if the output voltage is low (zero) the inductor L_1 can not be discharged which will mean that the inductor will be saturated. This

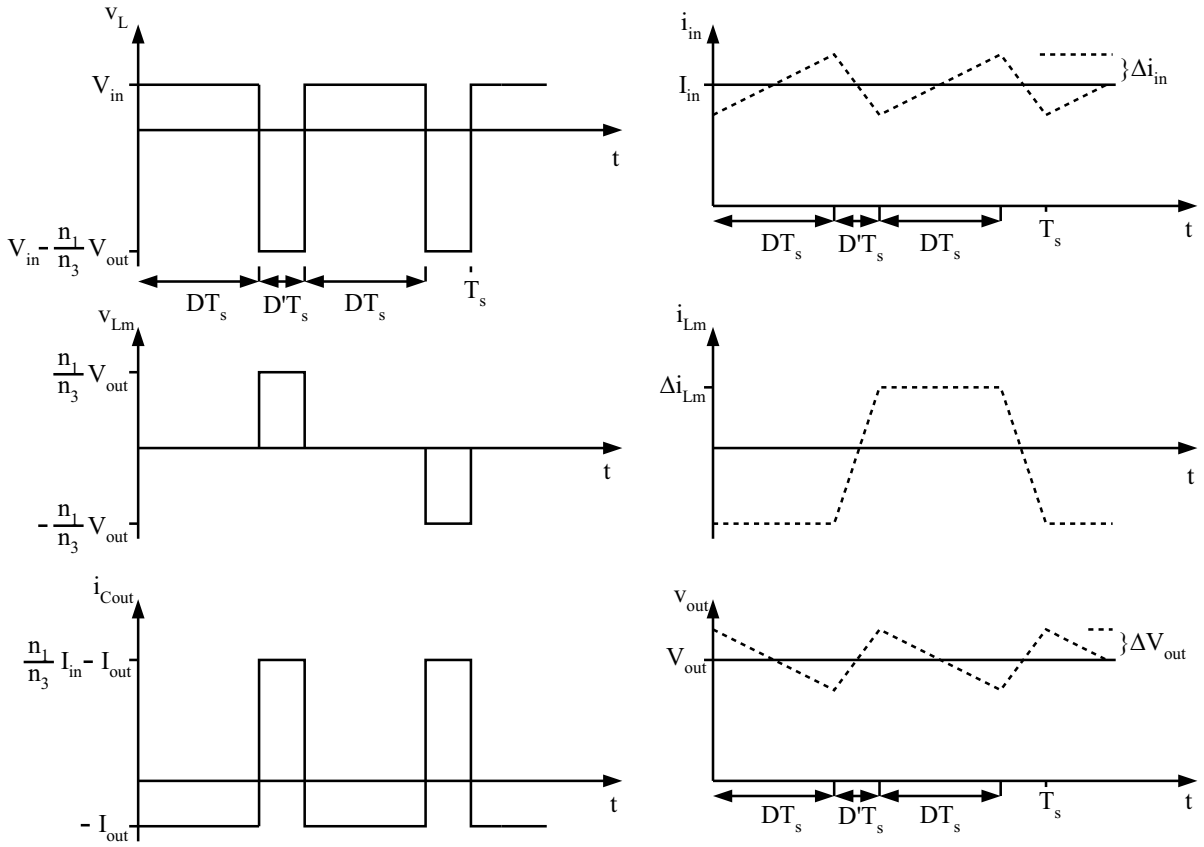

Figure A.30: Idealized voltages and current wave forms of the push-pull isolated boost converter.

can occur at start up or at overloading of the converter. A solution for this problem is shown in [56], [55].

The currents and voltages for steady state becomes, as before,

$$V_{out} = \frac{n_3}{n_1}\frac{1}{1-2D}V_{in} \tag{A.289}$$

$$I_{out} = \frac{n_1}{n_3}(1-2D)I_{in} \tag{A.290}$$

$$D_{max} = \frac{1}{2}. \tag{A.291}$$

From the equations and figure A.30 it is seen that the maximum duty cycle is limited. It is also seen that if there is no volt-second balance on the primary the magnetizing will increase and after a time the transformer will be saturated. As previously mentioned, this can be eliminated by means of current-mode control of the converter [17].

The ripple components in the voltage over C_{out} and in the current through L_m and

L_1 can be calculated in the same way as for the other converters, this gives

$$\Delta i_{L_1} = \frac{V_{in}}{2 * L_1} D T_s \tag{A.292}$$

$$\Delta i_{L_m} = \frac{V_{in}}{4 * L_m} T_s \tag{A.293}$$

$$\Delta v_{out} = \frac{I_{out}}{2 * C_{out}} D T_s. \tag{A.294}$$

The semiconductor stresses in the push-pull isolated boost converter become

$$\hat{v}_{SW_1} = \hat{v}_{SW_2} = 2\frac{n_1}{n_3}(V_{out} + \Delta v_{out}) \tag{A.295}$$

$$\hat{v}_{D_1} = \hat{v}_{D_2} = \hat{v}_{D_3} = \hat{v}_{D_4} = V_{out} + \Delta v_{out} \tag{A.296}$$

$$I_{SW_1,RMS} = I_{SW_2,RMS} = \sqrt{\frac{1-D}{2}[(\frac{n_3}{n_1}\frac{I_{out}}{1-2D})^2 + \frac{\Delta i_{L_1}^2}{6}] + \frac{D}{2}\Delta i_{L_m})^2} \tag{A.297}$$

$$\begin{aligned} I_{D_1,RMS} &= I_{D_2,RMS} = I_{D_3,RMS} = I_{D_4,RMS} \\ &= \sqrt{(\frac{1}{2} - D)[(\frac{I_{out}}{2(\frac{1}{2} - D)})^2 + \frac{1}{3}(\frac{n_1}{n_3})^2(\Delta i_{L_1} + \Delta i_{L_m})^2]}. \end{aligned} \tag{A.298}$$

In the same way as for the other converters, the utilization of the components can be calculated. By neglecting ripple in voltages and currents the maximum peak voltage and RMS current for both the voltage adjuster and the DC-transformer can be expressed as

$$\hat{v}_{SW_1,max} = \hat{v}_{SW_2,max} = 2\frac{n_1}{n_3} V_{out,R} \tag{A.299}$$

$$\hat{v}_{D_1,max} = \hat{v}_{D_2,max} = \hat{v}_{D_3,max} = \hat{v}_{D_4,max} = V_{out,R} \tag{A.300}$$

$$I_{SW_1,RMS,max} = I_{SW_2,RMS,max} = \frac{N}{2}\sqrt{1 + \frac{1}{N}\frac{n_3}{n_1}}\frac{P_{out,R}}{V_{out,R}} \tag{A.301}$$

$$\begin{aligned} I_{D_1,RMS,max} &= I_{D_2,RMS,max} = I_{D_3,RMS,max} = I_{D_4,RMS,max} \\ &= \frac{1}{\sqrt{2}}\sqrt{\frac{n_1}{n_3}N}\frac{P_{out,R}}{V_{out,R}}. \end{aligned} \tag{A.302}$$

From these equations the utilization factor for the semiconductors can be calculated to

$$U_{SW_1+SW_2} = U_{SW} = \frac{n}{2\sqrt{N}\sqrt{N+n}} \tag{A.303}$$

$$U_{D_1+D_2+D_3+D_4} = U_D = \frac{1}{2\sqrt{2}}\sqrt{\frac{n}{N}} \tag{A.304}$$

$$U_{SW+D} = \frac{1}{2\frac{\sqrt{N}}{n}\sqrt{N+n} + 2\sqrt{2}\sqrt{\frac{N}{n}}} \tag{A.305}$$

$$n = \frac{n_3}{n_1}. \tag{A.306}$$

From the equations it is seen that the utilization factors are depending on the wanted input output voltage ratio N and the winding ratio of the transformer n. It is seen

that all utilization factors are maximized if the winding ratio of the transformer n is as large as possible. But the winding ratio is limited by the following equation

$$V_{out} \geq \frac{n_3}{n_1} V_{in} = nV_{in} \rightarrow n_{max} = N. \tag{A.307}$$

If this is used the maximum utilization factors for the semiconductors can be calculated to

$$U_{SW,max} = \frac{1}{2\sqrt{2}} \tag{A.308}$$

$$U_{D,max} = \frac{1}{2\sqrt{2}} \tag{A.309}$$

$$U_{SW+D,max} = \frac{1}{4\sqrt{2}}. \tag{A.310}$$

As noticed before, the maximum utilization for the different components occurs for the same winding ratio. This means that the converter can be optimized to utilize all components to the maximum.

The main advantages and drawbacks of the push-pull isolated boost converter are:

+ The utilization factor can be maximized due to the transformer
+ The input current ripple is small
+ Good utilization of the transformer while operating with both positive and negative flux
+ Double frequency in the output reduces the requirements for the output filter
− A snubber circuit is needed to take care of the inductor current as the current is built up in the leakage inductance of the transformer
− The transformer must have three windings
− The transformer design is critical to minimize the magnetizing current and the leakage inductance
− The primary of the transformer needs a volt-second balance to prevent the transformer core from saturation
− Risk for inductor saturation if the output voltage is to low
− The power can only flow in one direction

A.2.15 Half Bridge Isolated Boost Converter

The half bridge isolated boost converter or two inductor boost converter is shown in figure A.31. The half bridge isolated boost converter operates by repeatedly shifting energy between the inductors L_1 and L_2 and the output capacitor and the load. First energy is stored in the inductors L_1 and L_2 by turning all switches on. The stored energy in the inductance L_2 is transferred through the transformer to the output by turning switch SW_2 off, mean while L_1 is still storing energy. This builds up a negative flux in the transformer. Next, the inductances is charged again by turning switch SW_2 on again. The energy in inductance L_1 is transferred to the output by turning SW_1 off, meanwhile L_2 is still storing energy. This builds up a positive flux in the transformer. During the time the inductors are charged the output capacitor supplies the load.

If the ripple in the currents through the inductances and in the voltage over the output capacitor is neglected and it is assumed that $L_1 = L_2 = L$, the currents and voltages in the half bridge isolated boost converter can be drawn for CCM as in

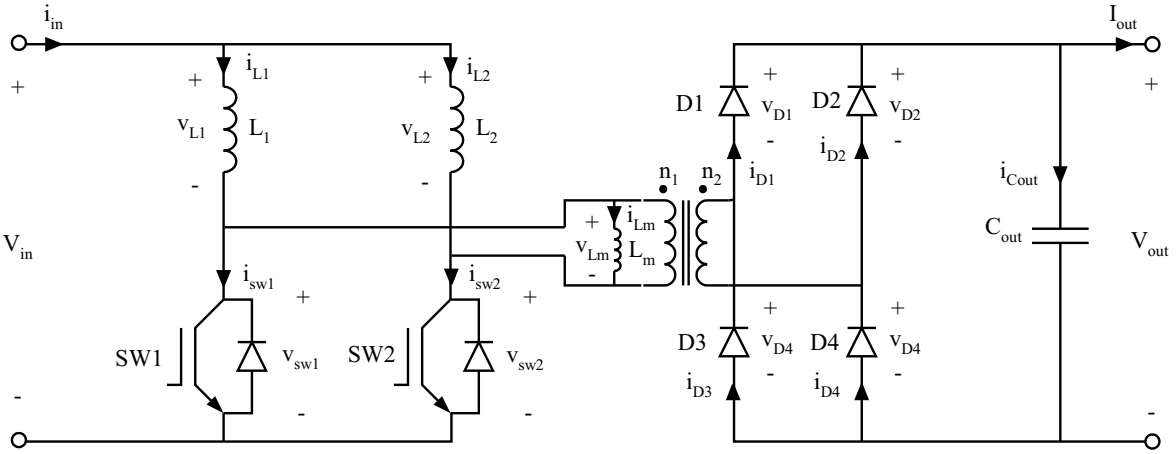

Figure A.31: Half Bridge Isolated Boost Converter circuit.

figure A.32. We have the same pattern as before, if the output voltage is low (zero), the inductors L_1 and L_2 can not be discharged which will mean that the inductors will be saturated. This can occur at start up or at overloading of the converter [56], [55].

If capacitor charge balance and inductor volt-second balance are applied on the currents and voltages shown in figure A.32 the voltages and currents in the converter can be calculated for steady state operation and CCM. The currents and voltages become

$$V_{out} = \frac{n_2}{n_1}\frac{1}{1-D}V_{in} \quad \text{(A.311)}$$

$$I_{out} = \frac{n_1}{n_2}(1-D)I_{in} \quad \text{(A.312)}$$

$$\frac{1}{2} \leq D \leq 1. \quad \text{(A.313)}$$

From the equations and figure A.30 it is seen that the duty cycle is limited. It is also seen that if there is no volt-second balance on the primary side the magnetizing will increase and after a while the transformer will be saturated. As previously stated, this can be eliminated by means of current-mode control of the converter [17].

The ripple components in the voltage over C_{out} and in the current through L_m, L_1 and L_2 can be calculated in the same way as for the other converters, this gives

$$\Delta i_{L_1} = \Delta i_{L_2} = \Delta i_L = \frac{V_{in}}{2*L}DT_s \quad \text{(A.314)}$$

$$\Delta i_{in} = \frac{V_{in}}{2*L}(2D-1)T_s \quad \text{(A.315)}$$

$$\Delta i_{L_m} = \frac{V_{in}}{2*L_m}T_s \quad \text{(A.316)}$$

$$\Delta v_{out} = \frac{I_{out}}{4*C_{out}}(2D-1)T_s. \quad \text{(A.317)}$$

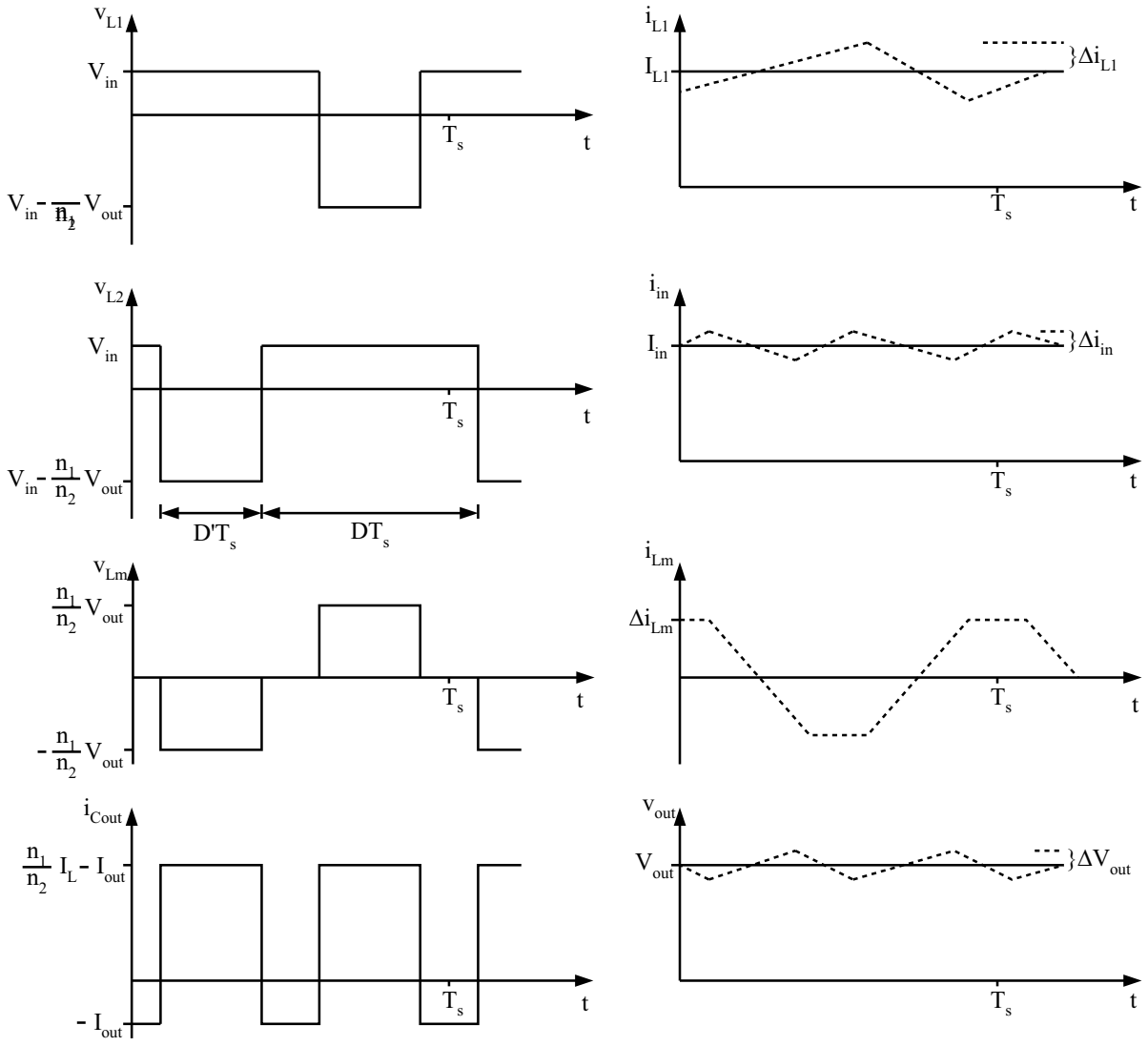

Figure A.32: Idealized voltages and current wave forms of the half bridge isolated boost converter.

The semiconductor stresses in the half bridge isolated boost converter become

$$\hat{v}_{SW_1} = \hat{v}_{SW_2} = \frac{n_1}{n_2}(V_{out} + \Delta v_{out}) \tag{A.318}$$

$$\hat{v}_{D_1} = \hat{v}_{D_2} = \hat{v}_{D_3} = \hat{v}_{D_4} = V_{out} + \Delta v_{out} \tag{A.319}$$

$$\begin{aligned} I_{SW_1,RMS} &= I_{SW_2,RMS} \\ &= \sqrt{\frac{3-2D}{4}[\frac{n_2}{n_1}\frac{I_{out}}{1-D}]^2 + (1-D)\frac{\Delta i_{in}^2}{3} + (2D-1)[\Delta i_{L_m} + \frac{\Delta i_{in}}{2(2D-1)}]^2} \end{aligned} \tag{A.320}$$

$$\begin{aligned} I_{D_1,RMS} &= I_{D_2,RMS} = I_{D_3,RMS} = I_{D_4,RMS} \\ &= \sqrt{(1-D)[(\frac{I_{out}}{2(1-D)})^2 + \frac{1}{3}(\frac{n_1}{n_2})^2(\Delta i_L + \Delta i_{L_m})^2]}. \end{aligned} \tag{A.321}$$

In the same way as for the other converters, the utilization of the components can

be calculated. By neglecting ripple in voltages and currents, the maximum peak voltage and RMS current for both the voltage adjuster and the DC-transformer, can be expressed as

$$\hat{v}_{SW_1,max} = \hat{v}_{SW_2,max} = \frac{n_1}{n_2} V_{out,R} \tag{A.322}$$

$$\hat{v}_{D_1,max} = \hat{v}_{D_2,max} = \hat{v}_{D_3,max} = \hat{v}_{D_4,max} = V_{out,R} \tag{A.323}$$

$$I_{SW_1,RMS,max} = I_{SW_2,RMS,max} = \frac{N}{2}\sqrt{1 + \frac{2}{N}\frac{n_2}{n_1}}\frac{P_{out,R}}{V_{out,R}} \tag{A.324}$$

$$\begin{aligned} I_{D_1,RMS,max} &= I_{D_2,RMS,max} = I_{D_3,RMS,max} = I_{D_4,RMS,max} \\ &= \frac{1}{2}\sqrt{\frac{n_1}{n_2}N}\frac{P_{out,R}}{V_{out,R}}. \end{aligned} \tag{A.325}$$

From these equations the utilization factor for the semiconductors can be calculated to

$$U_{SW_1+SW_2} = U_{SW} = \frac{n}{\sqrt{N}\sqrt{N+2n}} \tag{A.326}$$

$$U_{D_1+D_2+D_3+D_4} = U_D = \frac{1}{2}\sqrt{\frac{n}{N}} \tag{A.327}$$

$$U_{SW+D} = \frac{1}{\frac{\sqrt{N}}{n}\sqrt{N+2n} + 2\sqrt{\frac{N}{n}}} \tag{A.328}$$

$$n = \frac{n_2}{n_1}. \tag{A.329}$$

From the equations it is seen that the utilization factors are depending on the desired input output voltage ratio N and the winding ratio of the transformer n. It is seen that all utilization factors are maximized if the winding ratio of the transformer n is as large as possible. But the winding ratio is limited by the following equation

$$V_{out} \geq 2\frac{n_2}{n_1}V_{in} = 2nV_{in} \rightarrow n_{max} = \frac{N}{2}. \tag{A.330}$$

If this is used, the maximum utilization factors for the semiconductors can be calculated to

$$U_{SW,max} = \frac{1}{2\sqrt{2}} \tag{A.331}$$

$$U_{D,max} = \frac{1}{2\sqrt{2}} \tag{A.332}$$

$$U_{SW+D,max} = \frac{1}{4\sqrt{2}}. \tag{A.333}$$

As noticed before, the maximum utilization for the different components occurs for the same winding ratio. This means that the converter can be optimized to utilize all components to the maximum.

The main advantages and drawbacks of the half bridge isolated boost converter are:

+ The utilization factor can be maximized due to the transformer
+ The input current ripple is small
+ Good utilization of the transformer while operating with both positive and negative flux
+ Double frequency in the output reduces the requirements for the output filter
− A snubber circuit is needed to take care of the inductor current, mean while the current is build up in the leakage inductance of the ransformer
− The transformer design is critical to minimize the magnetizing current and the leakage inductance
− The primary of the transformer needs a volt-second balance to prevent the transformer core from saturation
− Risk for inductor saturation if the output voltage is to low
− The power can only flow in one direction

A.3 Choosing DC/DC Converter Topologies

From the utilization factor for the switch and from the main advantages/drawbacks of the different DC/DC-topologies presented in appendix A.2, the best topology for the different converter types (DC-transformer and voltage adjusting converter) will be chosen. In table A.1 all converter topologies are presented. In figure A.33 the maximum utilization factor for the switch for the different converter topologies are shown for different transformations ratios N and for three values of the smallest input voltage to the converter, $vmin = 1, 0.5$ and 0.25 in p.u. From the figure A.33 it is seen

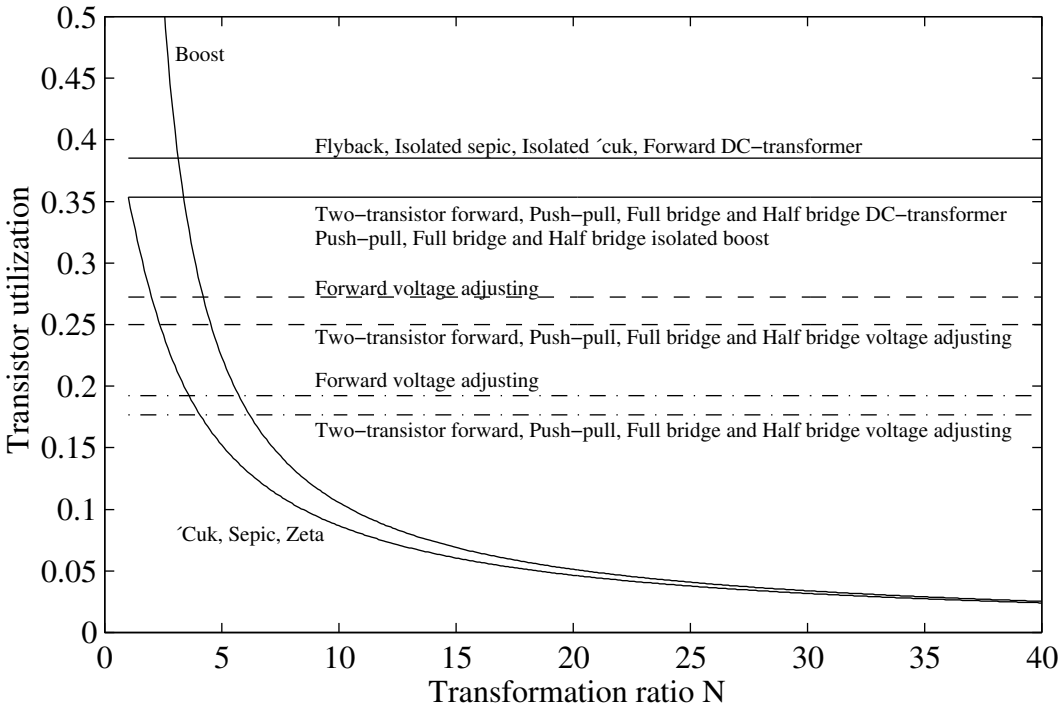

Figure A.33: Maximum utilization factors of the switch for the different DC/DC converter topologies for different N and $vmin$, dashed line $vmin = 0.5$ and dash-dotted line $vmin = 0.25$.

Table A.1: The different DC/DC converter topologies. For definitions of the variables see the previous sections.

Type	$\frac{V_{out}}{V_{in}}$	Duty cycle D	$U_{SW,max}$	U_D	Core	n_1	n_2	n_3
Boost	$\frac{1}{1-D}$	$0 \leq \ \leq 1$	$\frac{1}{\sqrt{N(N-1)}}$	Same	-	-	-	-
´Cuk	$-\frac{D}{1-D}$	$0 \leq \ \leq 1$	$\frac{\sqrt{N}}{(N+1)\sqrt{N+1}}$	Same	-	-	-	-
Sepic, Zeta	$\frac{D}{1-D}$	$0 \leq \ \leq 1$	$\frac{\sqrt{N}}{(N+1)\sqrt{N+1}}$	Same	-	-	-	-
Flyback	$\frac{n_3}{n_1}\frac{D}{1-D}$	$0 \leq \ \leq 1$	$\frac{2}{3\sqrt{3}}$	Not same	$\frac{1}{2}$	1	$\simeq 0$	1
Forward	$\frac{n_3}{n_1}D$	$0 \leq \ \leq \frac{1}{1+\frac{n_2}{n_1}}$	$\frac{2\sqrt{vmin}}{3\sqrt{3}}$	Not same	$\frac{1}{2}$	1 $(\frac{1}{3})$	1	1 $(\frac{1}{3})$
T-T forward	$\frac{n_2}{n_1}D$	$0 \leq \ \leq \frac{1}{2}$	$\frac{\sqrt{vmin}}{2\sqrt{2}}$	Same	$\frac{1}{2}$	1	$\frac{1}{2}$	-
Push-Pull	$2\frac{n_3}{n_1}D$	$0 \leq \ \leq \frac{1}{2}$	$\frac{\sqrt{vmin}}{2\sqrt{2}}$	Same	1	$\frac{1}{2}$	$\frac{1}{2}$	1
Half bridge	$\frac{n_2}{n_1}D$	$0 \leq \ \leq \frac{1}{2}$	$\frac{\sqrt{vmin}}{2\sqrt{2}}$	Same	1	1	1	-
Full bridge	$2\frac{n_2}{n_1}D$	$0 \leq \ \leq \frac{1}{2}$	$\frac{\sqrt{vmin}}{2\sqrt{2}}$	Same	1	1	1	-
Isol. ´cuk	$\frac{n_2}{n_1}\frac{D}{1-D}$	$0 \leq \ \leq 1$	$\frac{2}{3\sqrt{3}}$	Not same	1	1	1	-
Isol. sepic	$\frac{n_2}{n_1}\frac{D}{1-D}$	$0 \leq \ \leq 1$	$\frac{2}{3\sqrt{3}}$	Not same	$\frac{1}{2}$	1	1	-
F B I boost	$\frac{n_2}{n_1}\frac{1}{1-2D}$	$0 \leq \ \leq \frac{1}{2}$	$\frac{1}{2\sqrt{2}}$	Same	1	1	1	-
P-P I boost	$\frac{n_3}{n_1}\frac{1}{1-2D}$	$0 \leq \ \leq \frac{1}{2}$	$\frac{1}{2\sqrt{2}}$	Same	1	$\frac{1}{2}$	$\frac{1}{2}$	1
H B I boost	$\frac{n_2}{n_1}\frac{1}{1-D}$	$\frac{1}{2} \leq \ \leq 1$	$\frac{1}{2\sqrt{2}}$	Same	1	1	1	-

U_D	Indicates if the maximum utilization of the diodes occurs for the same choice of winding ratio n as for the maximum utilization of the switches. If it is the same point then the converter can can be optimized to utilize all components to the maximum
Core	Indicates how good the core of the transformer is utilized, one means magnetized on both directions and a half means only in one direction
n_1, n_2, n_3	Indicated how good the windings are utilized, "1" means that it can be used up to the hole switching period, "$\frac{1}{2}$" up to half the period and "-" does not exist

that for the converter topologies without transformer, the utilization factor decreases with a increasing transformation ratio N. This gives that if a high transformation ratio is desired it is best to use a converter with a transformer. As noticed before, the transformation ratio for the boost converter is limited by parasitical resistances to about 10 and therefore it is necessarily to use a converter with a transformer, if the transformation ratio is high.

To get a clearer overview of the different topologies working as a voltage adjusting converter the advantages and drawbacks of them has been put together in table A.2. In the table the different factors are marked with only + and − to make it clearer. In the table U_{SW} is the utilization of the switch and U_D is positive if the utilization of the diode/diodes occurs at the same point as for the switch. U_{core} and U_{wind} is how good the core and all the windings are utilized respectively. Δin and Δout is positive if the ripple on the input and on the output is small. Snub is positive if the converter topology only needs a small snubber circuit and finally SC is positive if the converter can handle a short circuit on the output. With handle means that the converter shall be able to stop the power flow from the input to the output if a short circuit occurs and it shall withstand temporarily overloads.

Table A.2: The different DC/DC converter topologies. For definitions of the variables see the previous sections.

Type	U_{SW}	U_D	U_{core}	U_{wind}	Δin	Δout	Snub	SC	Other
Flyback	+	-	-	-	-	-	-	+	
Isolated sepic	+	-	-	+	+	-	+	+	-large Δi_C
Isolated ´cuk	+	-	+	+	+	+	+	+	-large Δi_C -large num of comp.
P-P I boost	+	+	+	-	+	-	-	-	-start prob.
H B I boost	+	+	+	+	+	-	-	-	-start prob.
F B I boost	+	+	+	+	+	-	-	-	-start prob.
Boost	+/-	+	+	+	+	-	+	-	-limited N
´Cuk	-	+	+	+	+	+	+	+	-large Δi_C
Sepic	-	+	+	+	+	-	+	+	-large Δi_C
Zeta	-	+	+	+	-	+	+	+	-large Δi_C
Forward	-	-	-	-	-	+	-	+	
T T forward	-	+	-	+	-	+	+	+	
Push-Pull	-	+	+	-	-	+	+	+	
Half bridge	-	+	+	+	-	+	+	+	-large Δi_C
Full bridge	-	+	+	+	-	+	+	+	

From the table A.2 it is seen that the flyback and forward converter has a lot of minus and therefore they are excluded. The ´cuk, sepic and zeta converter is approximate the same as the boost converter, but they have a lower utilization of the switch. Therefore, they are excluded and the boost converter is used to represent these converters without a transformer. From table A.2 it is also noticed that the two-transistor forward converters have almost the same drawbacks as the push-pull, half bridge and full bridge converter, it has the additional drawback of not utilizing the transformer core. Therefore, the two-transistor forward converter is excluded. All three isolated boost converters has problems at start up, they do not work when the output voltage is zero without additional components. And due to that all converters only can deliver power in one direction the output capacitor of these can not be charged to the rated voltage by the converter connected to their outputs. Therefore, these converter topologies are excluded. The isolated sepic converter is also excluded due to the complicated transformer, the poor utilization of the transformer core and the high current ripple trough the capacitor C_1.

If the push-pull and half bridge converter are compared with the full bridge converter it is noticed that the voltage over the switch in the push-pull converter is twice the voltage over the switch in the full bridge converter. The current trough the switch in the half bridge converter is twice the current trough the switch in the full bridge. For the 2MW voltage adjusting converter often used in this work, the input ratings are approximate $U_{in,R} = 1$kV and $I_{in,R} = 2.2$kA. With this rating, IGBT:s for the full bridge converter are available today or almost available depending on the input voltage range. But there is today (2003) no one available for the double voltage or current. This means that in the push-pull or half bridge converter, two transistors must be series connected or parallel connected, at each transistor position in the converter. But for the full bridge converter one transistor can be used at each transistor position, there

is no need for parallel or series connections. Therefore the full bridge converter is to prefer of these three topologies.

This means that there is three candidates left of the topologies in table A.2 for the voltage adjusting converter.

Boost
Full bridge
Isolated ´cuk

As mention before, the boost converter is to prefer if the transformation ratio is low $N < 5$. The drawback of using the full bridge converter is the poor utilization of the switches and diodes when the input voltage range is large compared with the isolated ´cuk converter. This means that the switches and diodes must totaly have a higher power rating then the ´cuk converter. For example, if the input voltage is allowed to vary between 0.25 and 1p.u. the total rating of the switches in the full bridge must be approximately 2.2 times higher then for the isolated ´cuk converter and the total rating of the diodes must be approximately 4.4 times higher. The drawbacks of using the isolated ´cuk converter is that it needs some extra components C_1, C_2 and L_1 compared with the full bridge converter. The ripple in the current trough the capacitors C_1 and C_2 are also high in the isolated ´cuk converter which is a drawback. Due to this, the full bridge converter is used when a high transformation ratio is wanted for the voltage adjusting converter.

For the series converter the same discussion as for the voltage adjusting converter can be used with two additional requirements. One is that the converter topology must have a transformer that can take up the high voltage difference between the low voltage side and the high voltage side. The other is, that it is an advantage if the high voltage side has a low number of components and that the components are small in physical size. This is due to that these components must be isolated for a very high voltage between the component and ground.

The transformer requirement makes the boost, ´cuk, sepic and the zeta converter unusable. The flyback, forward, two transistor forward, isolated sepic, push-pull and half bridge converter are excluded with the same arguments as for the voltage adjusting converter. The start up problem with the isolated boost converters does not occur in this configuration due to that the output capacitor is charged to the rated voltage by the DC to AC converter on shore. This makes the three isolated boost converters, push-pull, half bridge and full bridge, interesting for the series converter. The same reasoning can be applied to these three isolated boost converter topologies as was made for the push-pull, half bridge and the full bridge converter for the voltage adjusting converter previous. But in these cases, the voltage over the switch is twice the voltage over the switch in the full bridge isolated boost for both the push-pull and the half bridge isolated boost converter. But the outcome is still the same, the full bridge isolated boost converter is to prefer.

This means that there is three candidates left of the topologies in table A.2 for the series converter.

Full bridge isolated Boost
Full bridge
Isolated ´cuk

The drawback of using the full bridge isolated boost converter is that it requires a large snubber compared to the other two topologies. The drawbacks of the full bridge and the isolated ´cuk is the same as for the voltage adjusting converter with one additional for both topologies. Both the full bridge and the isolated ´cuk converter has a inductor on the output, which is large in size. Due to this the full bridge isolated boost converter is used as the series converter.

A similar table to table A.2 can be put up to get a clearer overview of the different topologies working as a DC-transformer. This is not done due to that the only difference between these tables would be that the switch utilization for the forward, two transistor forward, push-pull, half bridge and the full bridge converter is positive instead of negative as in table A.2.

This gives that much of the discussions of choosing the right topology for the voltage adjusting converter are valid even for choosing topology for the DC-transformer. The only thing that does not have to be valid is the discussion about the push-pull, half bridge and full bridge converter. This is due to that the input voltage and current for the DC-transformer usually is much greater then 1kV and 2.2kA and therefore series and parallel connections must be used in all three converter topologies. But due to that the push-pull converter requires a transformer with three windings and the half bridge converter has high ripple currents trough the capacitors C_1 and C_2, the full bridge converter is still chosen of these three. Due to that the utilization of the switches and diodes are not a problem for the full bridge converter working as a DC-transformer this topology is to prefer of all topologies in table A.2 when a high transformation ratio is needed. Otherwise the boost converter is to prefer.

Appendix B

Loss modelling of components

In this appendix loss models of the components that are used in his work are derived and described. All models are derived in steady state.

B.1 Gearbox

Gearboxes in wind turbines are used to adapt the low-speed rotation of the blades to the high-speed rotation of the generator. The rotational speed of the generator is typically around 1000-1500rpm and for a 2MW wind turbine the rotational speed of the rotor is approximately 19rpm at rated wind speeds, as mention in Chapter 3.4.

The typical maximum increase of speed per step in a normal gearbox is 6:1. This gives that for a 2MW wind turbine 3 steps are needed to increase the low speed of the rotor to the generator speed. The number of steps influences the cost and efficiency of the gearbox. In wind turbine gearboxes, the first step is usually a planetary gear because it can be made smaller and with a higher gear ratio. The disadvantage with the planetary gear is that the losses are higher.

The losses in a gearbox comes from different types of frictions, the four main losses are [46] [14]:

- Gear teeth losses. They result from the friction at the tangent surfaces between cog wheels.
- Bearing losses. In case of ball bearings it is due to strain hysteresis, friction in oil slide, slide and micro slide due to the strain. For slide bearings the main cause of losses is friction on oil slide.
- Seal losses. They result from the friction at the constant areas of the elastic component of the ring and the shaft.
- Lubricant losses are due to the oil resistance, squeezing the oil out of inner tooth space and splashing.

These four losses can be divided into two different parts, one that depends on the rotation speed and one that depends on the input power. Gear teeth losses and some of the bearing losses are dependent on the input power. This is due to that when the input power increases, the pressure between the meshed teeth is higher and thereby the friction losses increases and the stresses on the bearing increases when the input power

increases which leads to higher losses. Normally these losses are modelled as a fixed percentage of the input power and independent of the shaft speed. Bearing friction, seal and lubricant losses are losses that comes from movement of shafts, cogwheels and bearings and can therefore be modelled as dependent on the shaft speed only. This leads to that the losses for a gearbox can be modulated as

$$P_{loss} = K_P P_{in} + K_\omega P_n \frac{\omega_{in}}{\omega_n}. \tag{B.1}$$

Where:

P_{in}	input power [W]
P_n	rated power [W]
ω_{in}	input speed [rad/s]
ω_n	rated speed [rad/s]
K_P	Constant for the power dependent losses =0.02
K_ω	Constant for the speed dependent losses =0.005

For a 0.5MW wind turbine gearbox the efficiency at rated load is approximately 97% and for a 3MW wind turbine gearbox approximately 97.7% at rated load [22]. In figure B.1 the gearbox losses that will be used in this work is shown for a 2 MW gearbox. From the figure B.1 it can be noticed that the gearbox model has an efficiency of 97.5%

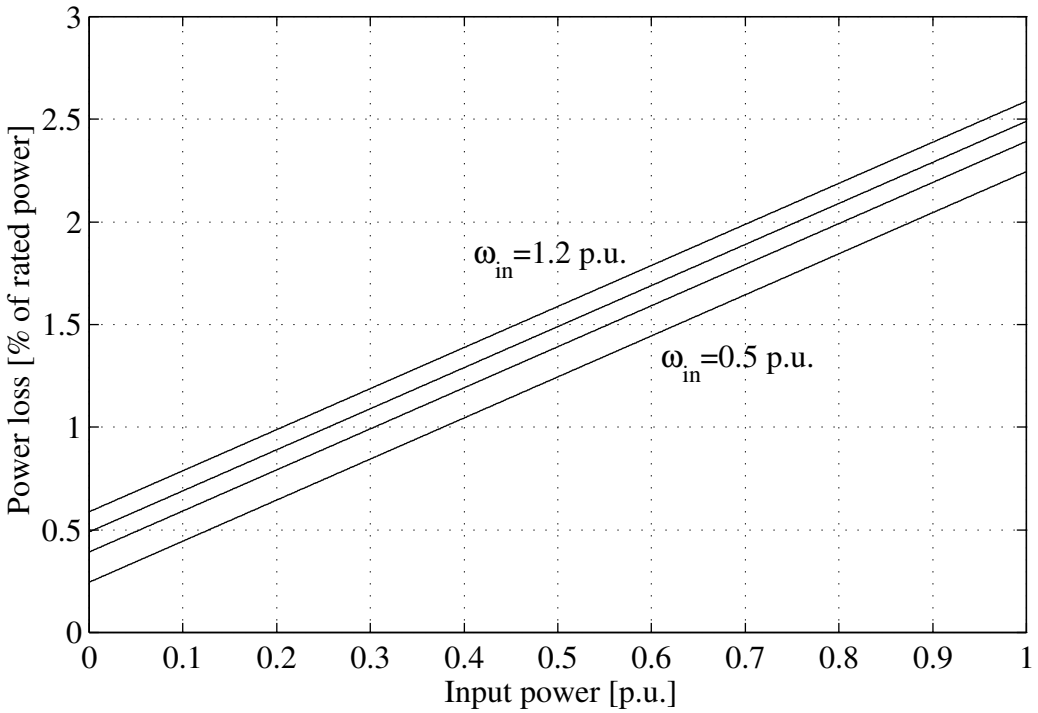

Figure B.1: Power loss for the gearbox in per unit of the rated power and for different rotational speeds (0.5 0.8 1 1.2 p.u.).

at rated power and speed, which is a normal value as mention before.

B.2 Induction generator

In this section a general model for the induction generator and the control strategy for the different induction generator systems mentioned in section 4.1 are developed. The control strategy for minimizing the losses in the generator is also discussed. As noticed in section 4.1 the induction generator has been and still is commonly used in wind turbines, this due to the simple and robust design.

B.2.1 Model of the induction generator

The general model of the induction generator can be derived by first consider the stator circuit. If a voltage space vector $\vec{v_s^s}$ is applied to the stator circuit, equation B.2 must be valid. The space vector is given in the standstill stationary stator coordinate system, denoted by $(^s)$. For the rotor circuit the same equation becomes equation B.3 by applying the rotor state space voltage vector $\vec{v_r^r}$, given in the rotating rotor coordinate system, denoted by $(^r)$. The rotor coordinate system is rotating with the electrical rotating speed of the rotor.

$$\vec{v_s^s} - R_s\vec{i_s^s} - N_s\frac{\mathrm{d}\vec{\Phi_s^s}}{\mathrm{d}t} = 0 \tag{B.2}$$

$$\vec{v_r^r} - R_r\vec{i_r^r} - N_r\frac{\mathrm{d}\vec{\Phi_r^r}}{\mathrm{d}t} = 0 \tag{B.3}$$

Where:

$\vec{v_s^s}$	stator voltage space vector [V]
$\vec{v_r^r}$	rotor voltage space vector [V]
$\vec{i_s^s}$	stator current space vector [A]
$\vec{i_r^r}$	rotor current space vector [A]
$\vec{\Phi_s^s}$	stator flux space vector [Wb]
$\vec{\Phi_r^r}$	rotor flux space vector [Wb]
N_s	number of turns in the stator [-]
N_r	number of turns in the rotor [-]
R_s	stator winding resistance [Ω]
R_r	rotor winding resistance [Ω]

By using equation B.4 the rotor equation B.3 can be transformed from rotor coordinates system to stator coordinates.

$$\vec{v_r^s} = e^{j\theta_r}\vec{v_r^r}, \quad \vec{i_r^s} = e^{j\theta_r}\vec{i_r^r}, \quad \vec{\Phi_r^s} = e^{j\theta_r}\vec{\Phi_r^r}, \quad \theta_r = \int \omega_r dt \tag{B.4}$$

Where:

ω_r	electrical speed of the rotor $= p\omega_{mec}$ [rad/s]
p	pole pair number [-]
ω_{mec}	mechanical speed of the rotor [rad/s]

The rotor equation in stator coordinates becomes

$$\vec{v_r^s} - R_r\vec{i_r^s} + jN_r\omega_r\vec{\Phi_r^s} - N_r\frac{\mathrm{d}\vec{\Phi_r^s}}{\mathrm{d}t} = 0. \tag{B.5}$$

Now the stator and rotor equations can be transformed to a coordinate system rotating with the angular speed of the grid ω_s, equation B.2 and B.5 becomes

$$N_s\frac{\mathrm{d}\vec{\Phi_s}}{\mathrm{d}t} = \vec{v_s} - R_s\vec{i_s} - jN_s\omega_s\vec{\Phi_s} \quad \text{(B.6)}$$

$$N_r\frac{\mathrm{d}\vec{\Phi_r}}{\mathrm{d}t} = \vec{v_r} - R_r\vec{i_r} + jN_r\omega_r\vec{\Phi_r} - jN_r\omega_s\vec{\Phi_r}. \quad \text{(B.7)}$$

In steady state the derivatives are equal to zero and the equations becomes

$$\vec{v_s} - R_s\vec{i_s} - jN_s\omega_s\vec{\Phi_s} = 0 \quad \text{(B.8)}$$

$$\vec{v_r} - R_r\vec{i_r} + jN_r\omega_r\vec{\Phi_r} - jN_r\omega_s\vec{\Phi_r} = 0. \quad \text{(B.9)}$$

By assuming linear magnetic relations the following equations are valid

$$\Phi_s = \Phi_{sl} + \Phi_{rs} + \Phi_{sr} = \frac{L_{sl}}{N_s}i_s + \frac{L_{rs}}{N_r}i_s + \frac{L_{sr}}{N_s}i_r \quad \text{(B.10)}$$

$$\Phi_r = \Phi_{rl} + \Phi_{sr} + \Phi_{rs} = \frac{L_{rl}}{N_r}i_r + \frac{L_{sr}}{N_s}i_r + \frac{L_{rs}}{N_r}i_s. \quad \text{(B.11)}$$

Where:

L_{sl}	stator leakage inductance [H]
L_{rl}	rotor leakage inductance [H]
L_{rs}	mutual inductance between stator and rotor [H]
L_{sr}	mutual inductance between rotor and stator [H]

By implementing this relations in equations B.8 and B.9 these equations becomes

$$v_s - R_si_s - j\omega_sL_{sl}i_s - j\omega_s\frac{N_s}{N_r}L_{rs}i_s - j\omega_sL_{sr}i_r = 0 \quad \text{(B.12)}$$

$$v_r - R_ri_r + jN_r\omega_r\Phi_r - j\omega_sL_{rl}i_r - j\omega_s\frac{N_r}{N_s}L_{sr}i_r - j\omega_sL_{rs}i_s = 0. \quad \text{(B.13)}$$

For homogenous materials with constant permeability the following relation holds $L_{sr} = L_{rs}$. With this relation and with the substitutions in equations B.14 the rotor and stator equations B.13 and B.12 can be rewritten as equations B.16 and B.15

$$i_r = \frac{N_s}{N_r}i_r^{'}, v_r = \frac{N_r}{N_s}v_r^{'}, R_r^{'} = (\frac{N_s}{N_r})^2R_r, L_{rl}^{'} = (\frac{N_s}{N_r})^2L_{rl}, L_m = \frac{N_s}{N_r}L_{rs} = \frac{N_s}{N_r}L_{sr} \quad \text{(B.14)}$$

$$v_s - R_si_s - j\omega_sL_{sl}i_s - j\omega_sL_mi_s - j\omega_sL_mi_r^{'} = 0 \quad \text{(B.15)}$$

$$v_r^{'} - R_r^{'}i_r^{'} + j\omega_r\Phi_r^{'} - j\omega_sL_{rl}^{'}i_r^{'} - j\omega_sL_mi_r^{'} - j\omega_sL_mi_s = 0 \quad \text{(B.16)}$$

$$\Phi_r^{'} = N_s\Phi_r = L_{lr}\frac{N_s}{N_r}\frac{N_s}{N_r}i_r^{'} + L_{sr}\frac{N_s}{N_r}i_r^{'} + L_{rs}\frac{N_s}{N_r}i_s = L_{rl}^{'}i_r^{'} + L_mi_r^{'} + L_mi_s. \quad \text{(B.17)}$$

It shall be noticed that the substitutions in equation B.14 are the same as for a transformer. The equivalent circuit for the generator can be drawn as in figure B.2. For the electro-mechanical power that is consumed by the generator the following equation can be formulated

$$P_e = 3Re(j\omega_r\Phi_r^{'}\bar{i}_r^{'}) = -3Re(j\omega_rN_s\Phi_s\bar{i}_s) = 3\frac{L_m}{L_s}Re(j\omega_r\Phi_s\bar{i}_r^{'}) = -3\frac{L_m}{L_r}Re(j\omega_r\Phi_r^{'}\bar{i}_s)$$

$$= -3L_mRe(j\omega_ri_r^{'}\bar{i}_s) = -3\frac{L_m}{L_sL_r - L_m^2}Re(j\omega_r\Phi_r^{'}N_s\bar{\Phi}_s). \quad \text{(B.18)}$$

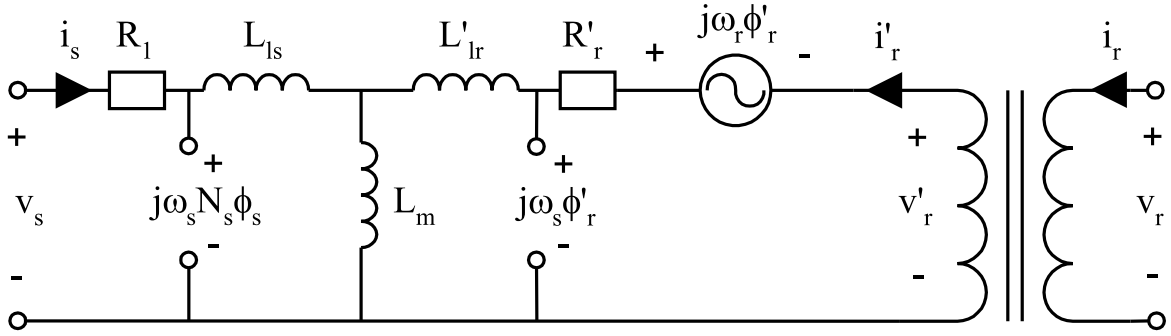

Figure B.2: Equivalent circuit for the induction generator.

Where:

$L_s = L_{sl} + L_m$	stator inductance [H]
$L_r = L_{rl} + L_m$	rotor inductance [H]
$P_e > 0$	Generator
$P_e < 0$	Motor

The model in equations B.15 and B.16 or in figure B.2 only take into account the losses in the windings and not the losses in the iron and the friction losses. The iron losses can be expressed with equation B.19 [40] [20].

$$P_{FE} = K_e \omega^2 \Phi^2 + K_h \omega \Phi^n \tag{B.19}$$

Where:

K_e	constant for eddy current losses
K_h	constant for hysteresis losses
Φ	magnitude of the flux [Wb]
ω	angular frequency of the flux [rad/s]
n	constant, normally between 1,7 to 2,3

If the constant n is set to 2, the losses are directly proportional to the magnitude of the flux in square. To easily modulate the iron losses in the stator and rotor, the losses will be represented by two resistances. Due to that the iron losses are proportional to the magnitude of the flux in square these two resistances will be put in parallel with the stator inductance, L_s, and the rotor inductance, L_r, respective. Because the voltage over these inductances are proportional to the magnitude of the fluxes and therefore the power consumed of these two resistances will be proportional to the magnitude of the flux in square, see figure B.2. The iron loss resistances for the stator and rotor becomes

$$R_{FEs} = \frac{N_s^2 \omega_s^2}{K_{es} \omega_s^2 + K_{hs} \omega_s} \tag{B.20}$$

$$R'_{FEr} = \frac{\omega_s^2}{K_{er} |\omega_s - \omega_r|^2 + K_{hr} |\omega_s - \omega_r|}. \tag{B.21}$$

Where:

R_{FEs}	iron loss resistances for the stator
R'_{FEr}	iron loss resistances for the rotor

As noticed from equation B.21 the iron loss resistance for the rotor is much higher then the resistance for the stator due to that the frequency of the flux is much smaller. The iron losses in the rotor is thus insignificant compared with the iron losses in the stator in normal operation of the induction generator and are usually not specified. Accordingly, the iron losses are in this report assumed to be equal to the losses in the stator when the rotor stand still, which gives the same frequency in the rotor as in the stator. This assumption is based on the fact that the saturation is higher in the rotor, but there is a smaller amount of iron in the rotor then in the stator. This gives that $K_{es} = K_{er}$ and $K_{hs} = K_{hr}$.

For the mechanical losses in the generator they can be modulated with one term that is proportional to the rotational speed and one term that is proportional to the speed in cubic

$$P_{loss,mec} = T_0|\omega_r| + T_k|\omega_r|^3 \quad \text{(B.22)}$$

$$P_{mec} = P_e + P_{loss,mec}. \quad \text{(B.23)}$$

Where:

$P_{loss,mec}$	mechanical losses in the generator
T_0	constant friction torque
T_k	constant for the friction torque proportional to the square of the speed
P_{mec}	mechanical input power to the generator

If the iron losses and the friction losses are added to the model in figure B.2 the equivalent circuit becomes as in figure B.3 and the equations becomes equations B.24 - B.37.

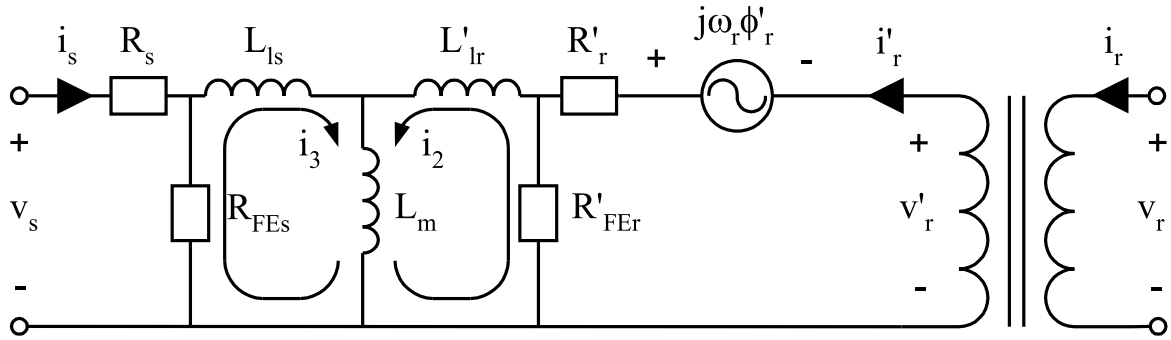

Figure B.3: Equivalent circuit for the induction generator with iron losses.

$$
\begin{aligned}
R_{FEs} &= \frac{N_s^2\omega_s^2}{K_{es}\omega_s^2 + K_{hs}\omega_s} && \text{(B.24)}\\
R_{FEr}^{'} &= \frac{\omega_s^2}{K_{er}|\omega_s - \omega_r|^2 + K_{hr}|\omega_s - \omega_r|} && \text{(B.25)}\\
v_r' &= \frac{N_s}{N_r} v_r && \text{(B.26)}\\
i_r &= \frac{N_s}{N_r} i_r' && \text{(B.27)}\\
\Psi_s &= N_s\Phi_s = L_{sl}i_3 + L_m i_3 + L_m i_2 && \text{(B.28)}\\
\Psi_r &= \Phi_r' = N_s\Phi_r = L_{rl}' i_2 + L_m i_2 + L_m i_3 && \text{(B.29)}\\
v_r' &= (R_r' + R_{FEr}')i_r' - (R_{FEr}' - j\omega_r(L_{rl}' + L_m))i_2 - j\omega_r L_m i_3 && \text{(B.30)}\\
0 &= -R_{FEr}' i_r' + (R_{FEr}' + j\omega_s(L_{rl}' + L_m))i_2 + j\omega_s L_m i_3 && \text{(B.31)}\\
0 &= j\omega_s L_m i_2 + (R_{FEs} + j\omega_s(L_{sl} + L_m))i_3 - R_{FEs} i_s && \text{(B.32)}\\
v_s &= -R_{FEs} i_3 + (R_s + R_{FEs})i_s && \text{(B.33)}\\
P_e &= 3Re(j\omega_r \Phi_r^{'} \vec{i}_r^{'}) && \text{(B.34)}\\
P_{lossel} &= 3(R_{FEs}|i_s - i_3|^2 + R_{FEr}'|i_r' - i_2|^2 + R_s|i_s|^2 + R_r'|i_r'|^2) && \text{(B.35)}\\
P_{lossmec} &= T_0|\omega_r| + T_k|\omega_r|^3 && \text{(B.36)}\\
P_{mec} &= P_e + P_{lossmec} && \text{(B.37)}
\end{aligned}
$$

In figure B.4 the power flow and references of the induction generator is shown

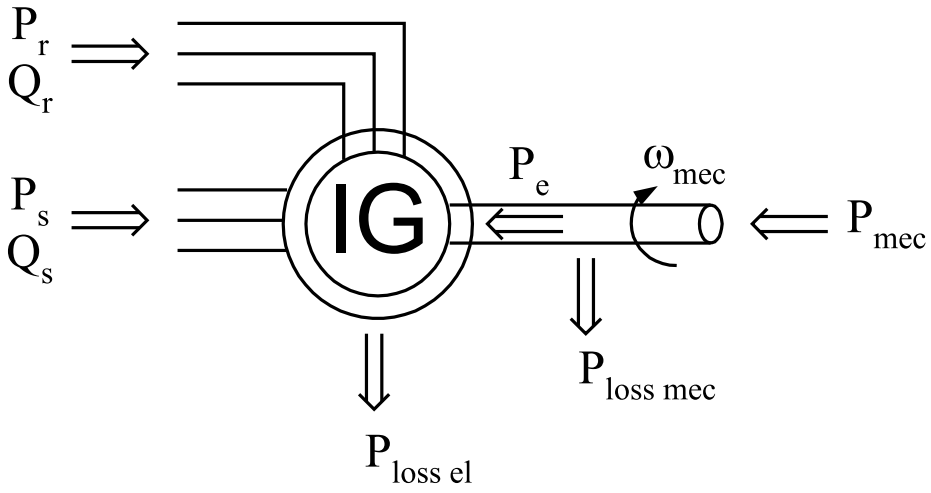

Figure B.4: Power flow in the induction generator.

B.2.2 Variable speed of the induction generator with a full power converter

For a drive with full variable speed with an induction generator, a squirrel-cage induction generator is usually used. This gives that the rotor voltage v_r is equal to zero. The full power converter is connected between the stator of the generator and the grid. In case of a wind turbine this would mean that the power electronic converter is connected between the generator and the wind turbine transformer, as shown in figure 4.6.

The advantages, as mention before, by having variable speed on a wind turbine are that the mechanical loads can be lowered, the output power variations to the grid can be reduced compared to a fixed-speed turbine and the reactive power can be controlled.

The energy capture can be increased by controlling the speed so that the turbine always is operating at the highest efficiency, this means the maximum value of $C_p(\lambda)$. From figure 3.2 it is seen that the λ value should be around 9 to give the highest efficiency of the turbine. Holding λ constant means that the ratio between the rotating speed of the turbine and the wind speed is constant. This gives that a higher wind speed gives a higher rotating speed but as mention before the upper rotating speed of the turbine is limited by the mechanical structure of the blades and by the noise emission of the turbine. As mention in section 3.4, the rotational speed limit of the blades is set to 19rpm.

Another thing that can be done to increase the efficiency of the wind turbine at low wind speeds is to lower the magnetization of the induction generator. From equation B.19 it is seen that if the flux decrease the iron losses drops. In equation B.18 it is also seen that if the flux decreases, the current must increase to keep the power constant. This gives that when the flux is lowered to decrease the iron losses, the losses in the stator and rotor winding increases, unless the machine is lightly loaded. This gives an optimal flux for a given mechanic input power and rotational speed that minimizes the losses in the generator. With some approximations the optimal voltage magnitude can be derived from equations B.24 - B.37. By assuming that $\Psi_s = \Psi_{sd} + j0$ and that ω_r and ω_s are known the following can be derived

$$\begin{aligned} i_s &= i_{sd} + j i_{sq} = i_{sd} + j\frac{-P_e}{3\omega_r \Psi_s} \\ i'_r &= i'_{rd} + j i'_{rq} = \frac{\Psi_s}{L_m} - \frac{L_s}{L_m} i_{sd} + j\frac{L_s}{L_m}\frac{P_e}{3\omega_r \Psi_s}. \end{aligned}$$

Now assume that $i'_r = 0$ and $R_s = 0$ which gives that

$$\begin{aligned} \Psi_s &= L_s i_s \Rightarrow i_{sd} = \frac{\Psi_s}{L_s} \Rightarrow i_{rd} = 0 \\ v_s &= j\omega_s \Psi_s \Rightarrow U = |v_s| = \omega_s \Psi_{sd}. \end{aligned}$$

From this the, electrical losses of the induction generator can be calculated as function of the voltage amplitude, U. From this an approximative equation that gives a minimum of the electrical losses in the induction machine can be calculated as in equation B.38.

$$U = \omega_s \sqrt[4]{\frac{L_s^2}{L_m^2}\frac{R_s L_m^2 + R'_r L_s^2 + (K_e|\omega_s - p\omega_r|^2 + K_h|\omega_s - p\omega_r|)(L_m^2 - L_s L'_r)^2}{R_s + \omega_s^2 L_s^2 K_e + \omega_s L_s^2 K_h + L_m^2(K_e|\omega_s - p\omega_r|^2 + K_h|\omega_s - p\omega_r|)}(\frac{-P_e}{3\omega_r})^2} \quad \text{(B.38)}$$

In figure B.5 the approximate voltage in equation B.38 and the stator frequency is shown for a 2MW wind turbine as function of wind speed. From the left plot in figure B.5 it is seen that the rotational speed of the turbine increases linearly with the wind speed up to the maximal value and then it is held constant. This is done in order to have the maximum efficiency of the turbine as discussed previously. In the right plot in figure B.5 it can be noticed that the approximative voltage value is rather good

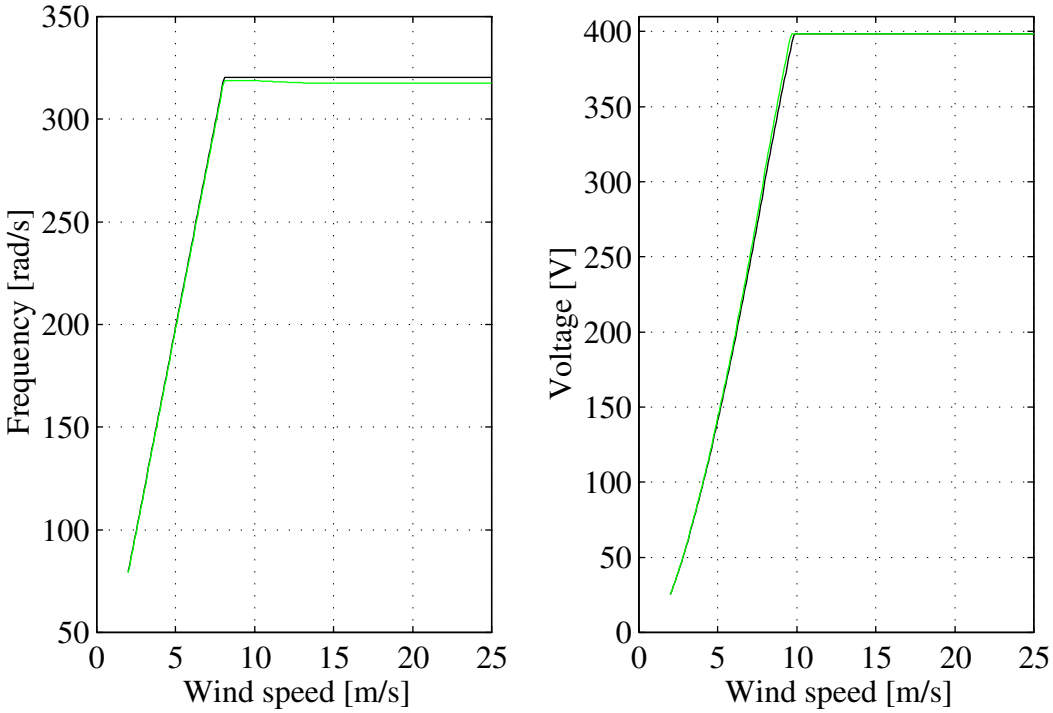

Figure B.5: In the left plot the black curve is the electrical rotational speed ω_r of the generator and the grey is the stator frequency ω_s. In the right plot the voltage that minimizes the losses for the IG is shown, black curve is from equation B.38 and the grey the exact voltage.

compared with the exact value that minimizes the losses. All wind turbine with full power converters and induction generators in this study has this type of control of the rotational speed and amplitude of the voltage.

In addition, the reactive power is fully controllable with the converter. This gives the benefit that the wind turbine can produce power with a power factor of one.

B.2.3 Variable speed of the induction generator with a rotor converter

For the variable speed system of the induction generator with a rotor converter, an induction generator with a wound rotor and slip rings is used. The stator of the generator is connected to the wind turbine transformer and between the rotor and the wind turbine transformer a converter is connected, as can be seen in figure 4.4.

Since the stator is connected to the wind turbine transformer, the stator voltage and frequency is almost fix. This means that the amplitude of the flux is almost constant and therefore it is not possible to affect the iron losses in the same way as with the stator-connected converter. However, it is possible to reduce the iron loses at low load. In [36] two ways are presented: The stator can be short-circuited and the generator can then be driven as a full variable speed system with the supply from the rotor, or use a Δ/Y connector between the stator and the wind turbine transformer can be used, as shown in figure 4.4. In this work and in [36] the Δ/Y connector is chosen. This means

that at low wind speeds, the generator is Y-connected and Δ-connected at high wind speeds. This gives that the stator voltage is $\sqrt{3}$ times lower at low wind speeds and thereby the iron losses are approximately 3 times lower.

The speed regulation strategy for this system is the same as for the system with a full power converter connected to the stator, it is to keep the λ value constant. From figure B.3 and equations B.24 - B.37 it is noticed that the rotational speed of the generator can be controlled by changing the frequency in the rotor, $\omega_{rotor} = \omega_s - \omega_r$. But it is also noticed that the rotor voltage must increase as the rotational speed changes from the synchronous speed. Otherwise the current will be too large, the voltage of the voltage source in the rotor, $j\omega_r\Psi'_r$, plus the rotor voltage, v'_r, must be in the same range as the stator voltage. This means that if the generator stands still, the rotor voltage, v'_r, must be in the same range as the stator voltage, v_s, in order to keep the current within the rated one. Since the rotor current, i'_r, is of the same magnitude as the stator current, i_s, the rated power of the converter needed to drive the machine also at zero speed is the same as for the full power converter in section B.2.2. However, if the rotor converter systems has a limited speed range around synchronous speed, it is possible to utilize a converter with a lower rated power. This is done in order to decrease the losses and the cost of the converter. The speed domain is typically $\pm 30\%$ of the synchronous speed which gives a rotor voltage v'_r of approximately $\pm 30\%$ of the stator voltage. But in order to have a small rotor current and to have a converter with standard valves, the winding ratio between the stator and rotor often is set so that the rotor has a higher number of turns, for example the rotor voltage can be 690V line to line, at the maximum speed derivation from synchronous speed.

Another quantity that can be controlled by the rotor voltage is the reactive power that the generator consumes from the grid. By controlling the rotor voltage the generator can consume or produce reactive power. But often it is wanted that the generator shall neither consume or produce reactive power. By controlling the frequency, amplitude and phase angle of the rotor voltage space vector, the rotational speed, electrodynamic torque and reactive power consumption of the induction generator can be controlled. By making some approximations and assumptions the rotor voltage vector can be derived from equations B.24 - B.37. Assume that $v_s, \omega_s, \omega_r, P_e$ are known and that the reactive power to the stator Q_s shall be equal to Q_{sRef} and that $v_s = 0 + jU$. Approximate $R_s = R'_r = 0$ and $R_{FEs} = R'_{FEr} = \infty$ then the following holds

$$P_e = 3Re\{\frac{\omega_r}{\omega_s - \omega_r} v'_r \bar{i'_r}\} \tag{B.39}$$

$$Q_s = 3Im\{v_s \bar{i_s}\}. \tag{B.40}$$

If now i'_r and i_s are expressed in v'_r and v_s the following can be derived

$$\begin{aligned} v'_r = & -\frac{\omega_s - \omega_r}{\omega_r} \frac{\omega_s(L_{sl}L_r + L_m L_{lr})}{L_m U} \frac{P_e}{3} + \\ & j \frac{\omega_s - \omega_r}{\omega_s} \frac{(L_{rl} + L_m)U^2 - \omega_s(L_s L_{rl} + L_m L_{sl})\frac{Q_{sRef}}{3}}{L_m U}. \end{aligned} \tag{B.41}$$

In figure B.6 the rotor voltage and rotational speed for the 2MW wind turbine that is used in this report are shown as function of the wind speed. From the left plot in figure B.6 it is seen that the rotational speed is limited upwards to 410 rad/s, that the electrical drive system can give as low speeds as is desired. This is due to the

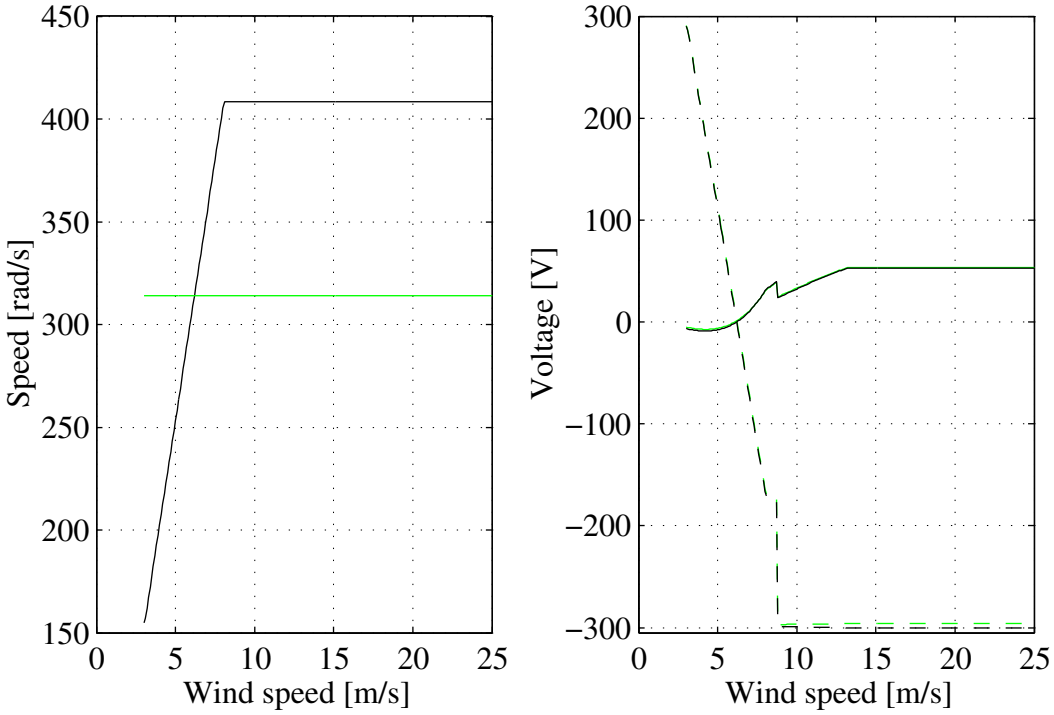

Figure B.6: In the left plot the black curve is the electrical rotational speed ω_r of the generator and the grey is the stator frequency ω_s. In the right plot the rotor voltage v_r is shown, black curve is from equation B.41 and the grey the exact voltage, solid is the real part and dashed imaginary part.

Δ/Y connector used in the stator circuit, at low wind speeds the stator voltage is $\sqrt{3}$ times lower and this also means that the rotor voltage is $\sqrt{3}$ times lower. By this it is possible to run the generator at a lower rotational speed with the same voltage rating of the converter. From the right plot in figure B.6 it is noticed that the approximate equation B.41 gives a very good result compared with the exactly calculated voltage. (The grey curve cannot be distinguish from the black one)

In figure B.7 the power flow in the rotor converter system is shown. From figure B.7 it can be noticed that the power into the rotor is a third of the rated power of the generator which means that a smaller and cheaper converter can be used compared to the case with the full power converter system in section B.2.2. It is also noticed that when the generator is operating below synchronous speed, active power is feed into the rotor circuit and when it is operating above synchronous speed active power is taken out from the rotor. From the figure it can also be seen that the reactive power to the stator is zero, black dashed line.

B.3 Synchronous generator

In this section, a general model for the synchronous generator with a round rotor and the control strategy for the three different synchronous generator systems mentioned in chapter 4 are developed. As noticed in section 4.1.3 the by far most commonly used type of synchronous generator in wind turbines is the directly driven generator, this

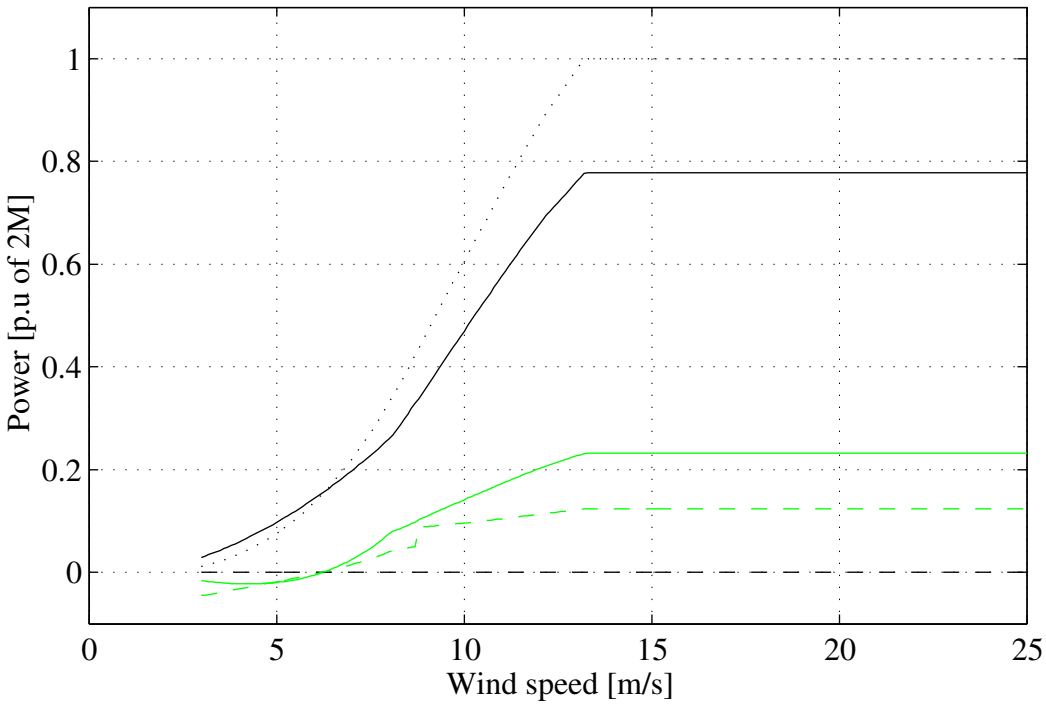

Figure B.7: Power flow in the rotor converter system. Black curve is the power from the stator, grey power from the rotor, solid lines active power and dashed lines reactive power. Dotted line total active power to the wind turbine transformer.

due to that the gearbox can be removed with this type of generator.

B.3.1 Model of the generator

The model for the synchronous generator can be derived in the same way as for the induction generator. The stator circuit of the synchronous generator is similar to the stator circuit of the induction generator, therefore the stator equation B.2 for the induction generator must hold for the synchronous generator

$$\vec{v_s^s} - R_s\vec{i_s^s} - \frac{\mathrm{d}\vec{\Psi}_s^s}{\mathrm{d}t} = 0.$$

In this case the stator flux linkage becomes

$$\vec{\Psi}_s^s = L_s\vec{i_s^s} + \vec{\Psi}_r^s. \tag{B.42}$$

In equation B.42 $\vec{\Psi}_r^s$ is the rotor flux linkage that is formed by the permanent magnets or from the magnetizing coil in the rotor. In a synchronous generator which is electrically magnetized, the rotor flux instead comes from a field winding. The rotor flux linkage is displaced by an angle θ, the rotor position, compared to the rotating stator coordinate system and can therefore be expressed as

$$\vec{\Psi}_r^s = \Psi_m \mathrm{e}^{j\theta} \tag{B.43}$$

$$\vec{\Psi}_r^s = K_{mag} I_f \mathrm{e}^{j\theta}. \tag{B.44}$$

Where:

Ψ_m	Magnetization flux linkage from the permanent magnets
K_{mag}	Magnetization constant
I_f	Field current [A]
θ	Angle between the rotor flux linkage and the rotating stator coordinate system

Where equation B.43 shall be used if the generator is permanently magnetized and equation B.44 if the generator is electrically magnetized. In the following only the permanently magnetized generator is considered and equation B.43 is used to describe the connection between the stator and rotor. If an electrically magnetized generator is desired instead of the permanently magnetized, it is just to substitute Ψ_m against $K_{mag}I_f$ in the following equations. By inserting equation B.43 into equation B.42 the following equation is obtain, with $\omega_r = \frac{\mathrm{d}\theta}{\mathrm{d}t}$

$$L_s \frac{\mathrm{d}\vec{i_s^s}}{\mathrm{d}t} = \vec{v_s^s} - R_s \vec{i_s^s} - j\omega_r \Psi_m \mathrm{e}^{j\theta}. \tag{B.45}$$

Now, by transforming equation B.45 to stator coordinates by the angle θ_s and assuming steady state operation as in section B.2.1 the equation becomes

$$v_s = R_s i_s + j\omega_s L_s + E_p \tag{B.46}$$

$$E_p = j\omega_s \Psi_m \mathrm{e}^{j(\theta-\theta_s)} = j\omega_s \Psi_m \mathrm{e}^{j\tilde{\theta}}. \tag{B.47}$$

Where:

$\omega_s = \frac{\mathrm{d}\theta_s}{\mathrm{d}t}$	Angular frequency of the grid, in steady state $= \omega_r$
E_P	Back-emf of the synchronous generator
$\tilde{\theta}$	torque angle

If the iron losses of the generator is introduced in the same way as in section B.2.1 the equivalent circuit for the synchronous generator in steady state operation becomes as in figure B.8. The equations that describes the permanently magnetized synchronous

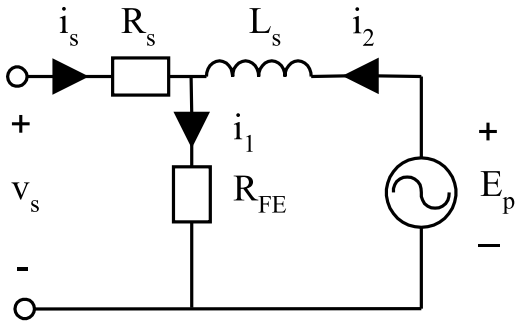

Figure B.8: Equivalent circuit of the synchronous generator.

generator can be formulated as

$$
\begin{aligned}
R_{FEs} &= \frac{\omega_s^2}{K_{es}\omega_s^2 + K_{hs}\omega_s} && \text{(B.48)}\\
v_s &= (R_s + R_{FE})i_s + R_{FE}i_2 && \text{(B.49)}\\
E_p &= R_{FE}i_s + (R_{FE} + j\omega_s L_s)i_2 && \text{(B.50)}\\
E_p &= j\omega_s \Psi_m \mathrm{e}^{j\tilde{\theta}} && \text{(B.51)}\\
\Psi_s &= L_s i_s + \frac{E_p}{j\omega_s} && \text{(B.52)}\\
P_e &= 3Re(E_p \bar{i}_2) && \text{(B.53)}\\
P_{lossel} &= 3(R_{FE}|i_s + i_2|^2 + R_s|i_s|^2) && \text{(B.54)}\\
P_{lossmec} &= T_0|\omega_r| + T_k|\omega_r|^3 && \text{(B.55)}\\
P_{mec} &= P_e + P_{lossmec}. && \text{(B.56)}
\end{aligned}
$$

If the generator is electrically magnetized two of the equations above shall be changed to

$$
\begin{aligned}
E_p &= j\omega_s K_{mag} I_f \mathrm{e}^{j\tilde{\theta}} && \text{(B.57)}\\
P_{lossel} &= 3(R_{FE}|i_s + i_2|^2 + R_s|i_s|^2 + R_{field}I_f^2). && \text{(B.58)}
\end{aligned}
$$

Where:

R_{field} Resistance of the field winding

In figure B.9 the reference directions of the power flows in the synchronous generator are shown.

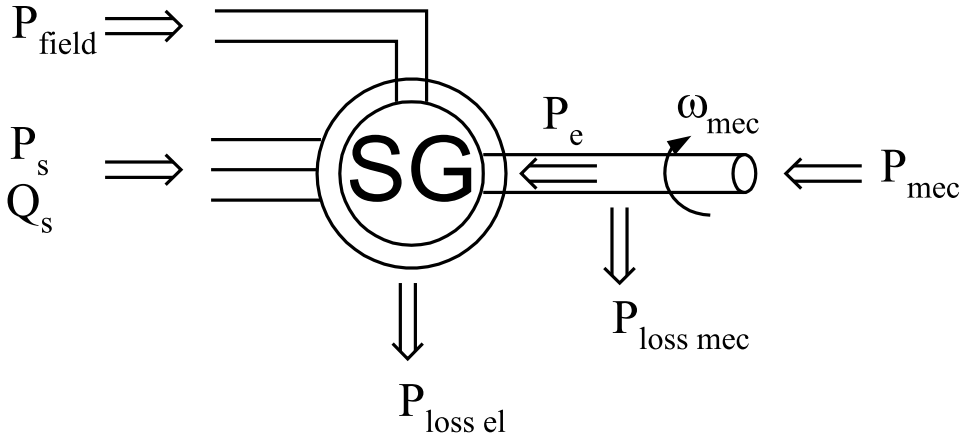

Figure B.9: Power references of the synchronous generator.

B.3.2 Variable speed with full power converter

The control of the synchronous generator by a self commutating converter can be done in several ways. The rotational speed of the generator is controlled so that the turbine is operating at its maximum efficiency, same as for the induction generator system in

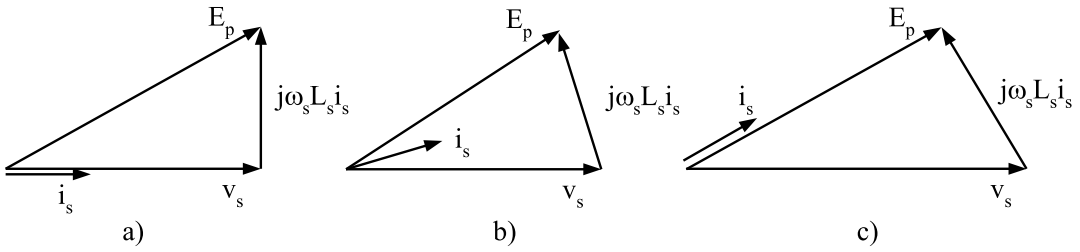

Figure B.10: Different control methods for the stator voltage.

section B.2.2. The stator voltage can be controlled in at least three different ways according to [22], in figure B.10 these ways are presented. In figure B.10 the stator and iron loss resistance are neglected. In case a) the stator voltage is controlled so that the reactive power in to the generator is zero. This gives that the stator voltage at rated load is lower then the internal emf. In this case the converter must be rated for the no-load emf which is higher, then the stator voltage at rated voltage. This gives that the converter must have a higher kVA rating. In case b) the amplitude of the stator voltage is kept equal to the amplitude of the internal emf. In this case, the reactive power to the inductance is provided equally from the converter and from the internal emf. This control method maximizes the active power from a generator and inverter with the same kVA rating. In case c) the stator voltage is controlled so that the stator current is in phase with the internal emf of the generator. With this control method the internal emf of the generator is lower then the stator voltage at rated load. This also means that the kVA rating of the generator and converter must be higher. Based on the properties of these three methods, control method b) will be selected due to the fact that it utilizes the generator and converter best. By assuming $E_p = j\omega_s\Psi_m$ and $|v_s| = |E_p| = \omega_s\Psi_m$ the following holds

$$\begin{aligned} P_e &= 3Re\{E_p\bar{i_2}\} = 3\omega_s\Psi_m i_{2q} \rightarrow \\ i_{2q} &= \frac{P_e}{3\omega_s\Psi_m}. \end{aligned} \tag{B.59}$$

and the stator voltage can be expressed as

$$\begin{aligned} v_s &= v_{sd} + jv_{sq} = \omega_s L_s(1 + \frac{R_s}{R_{FE}})i_{2q} - R_s i_{2d} \\ &+ j\{\omega_s(1 + \frac{R_s}{R_{FE}})\Psi_m - R_s i_{2q} - \omega_s L_s(1 + \frac{R_s}{R_{FE}})i_{2d}\}. \end{aligned} \tag{B.60}$$

Using equation B.59 and B.60 and the assumption that the amplitude of the stator voltage and the amplitude of the internal emf are equal, the current component i_{2d} can be calculated by solving the second order equation. From the current components i_{2d} and i_{2q} the stator voltage can be calculated from equation B.60. In figure B.11, the stator voltage, internal emf and the rotational speed for a 2 MW wind turbine with a directly driven permanently magnetized generator are shown. From the right plot in figure B.11 it is noticed that the speed follows the wind speed up to the nominal speed and after this it is held constant. This is done in order to maximize the efficiency of the blades as mention before. From the left plot it is observed that the magnitude of the stator voltage is equal to the magnitude of the internal emf.

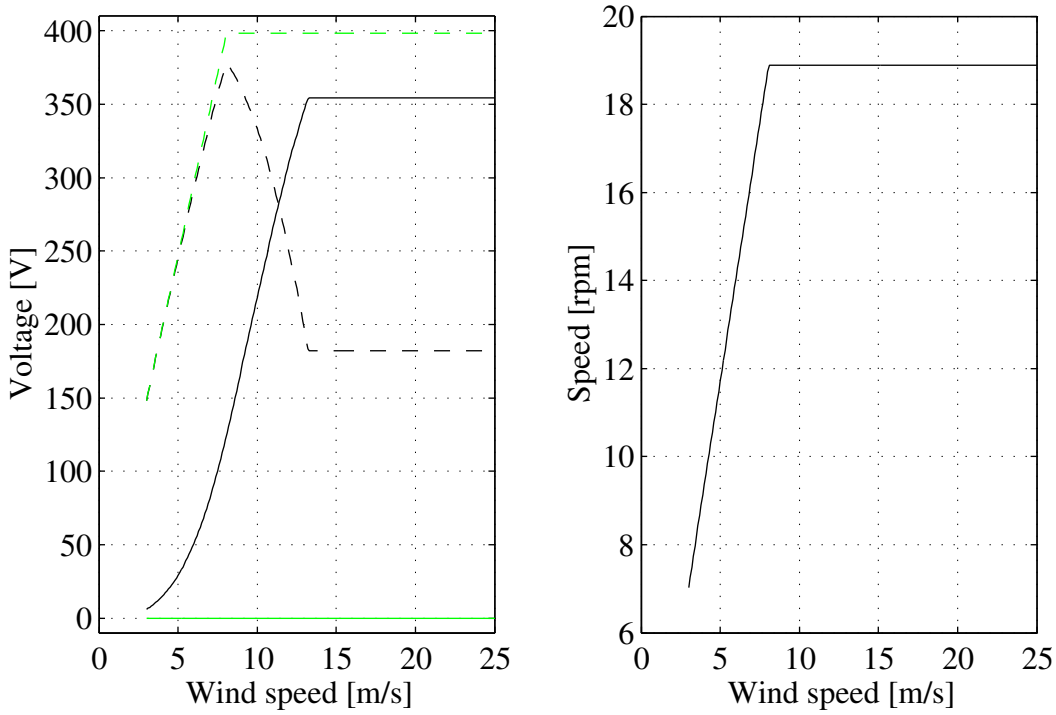

Figure B.11: Left plot the stator voltage, black, and internal emf grey. Solid real part and dashed imaginary part. Right plot rotational speed of the generator.

B.3.3 Variable speed system with diode rectifier

When connecting the permanently magnetized generator to a diode rectifier, some form of reactive power compensation must be used in order to utilize the generator fully. In [21] it is shown that the best way of doing this is to connect capacitors in series between the stator and the diode rectifier, as shown in figure B.12. From [21] it

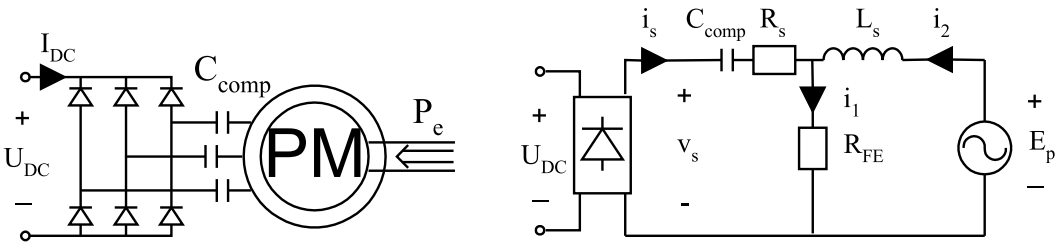

Figure B.12: Permanent magnetized generator connected to a three phase diode rectifier with series compensation of reactive power.

was concluded that if no compensation is used, the maximum produced power of the generator is strongly limited. This is due to the fact that the voltage drop over the internal impedance of the generator is too large, so that the stator voltage decrease. This leads to that the output power of the generator decreases and at sufficiently high currents, the stator voltage equals zero. By supporting the generator with reactive power this effect can be reduced. In figure B.13 the maximum mechanical input power

to the PM generator is shown for rated speed and as function of the stator current and the degree of reactive power compensation. From figure B.13 it is seen that if the

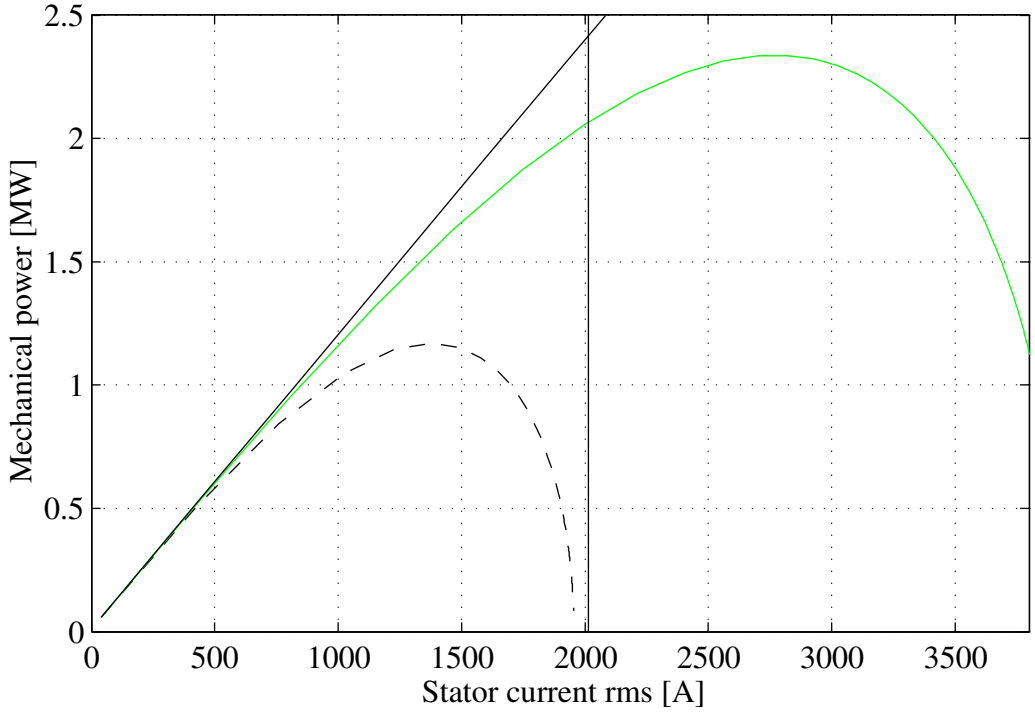

Figure B.13: The maximum mechanical input power to the PM generator for different degrees of compensation, solid black full compensation, solid grey half compensation and dashed no compensation at rated speed.

compensation does not fully compensate for the machine inductance and the system will still have a limited input power. This means that some caution must be taken when designing the wind turbine and the electrical system if a reduced compensation is used. The reason for this is, if the input power to the generator exceeds the maximum for some reasons, large gust etc, the speed will accelerate quickly. In [21] it was shown that the case with half compensation is sufficient for wind turbine applications and therefore half compensation is used in this work.

Normally there will be a voltage drop in the diode rectifier due to the fact that the commutation of the current from one valve to another is not instantaneous. The reason for this is the inductances in the commutation circuit, se [51]. In the case using series compensation, the commutation circuit is more complicate. The commutation is faster due to the capacitors that helps under the commutation interval, therefore the introduced error is less compared to the case without the capacitors. Therefore the voltage drop due to commutation is neglected.

Another approximation that is done is that the stator current i_s is assumed to be sinusoidal. From [21] it can be observed that this gives a good agrement with a more exact model for currents up to rated current.

By controlling the DC-voltage to the diode rectifier, the speed of the generator can be controlled $|E_p| = \omega_s \Psi_m \simeq |v_s| \sim U_{DC}$. This means that there exist two ways of controlling the wind turbines, to connect them to a common DC-buss (fix DC-voltage

→ fix speed system) or by connect them via a DC/DC-converter (variable DC-voltage → variable speed system). For both these systems the following assumptions can be made to calculate the working point of the wind turbine

$$\begin{aligned} v_s &= v_{sd} + jv_{sq} = jU = j\frac{\pi}{3\sqrt{6}}U_{DC} \\ i_s &= i_{sd} + ji_{sq} = jI \\ P_e &= 3Re\{E_p\bar{i_2}\} = 3\{E_{pd}i_{2d} + E_{pq}i_{2q}\}. \end{aligned}$$

From these equations and the equivalent circuit in figure B.12 the stator current and voltage can be calculated as

$$\begin{aligned} i_s &= \frac{E_{pd}}{R_{FE}} - i_{2d} + \frac{\omega_s L_s}{R_{FE}}i_{2q} + j[\frac{E_{pq}}{R_{FE}} - i_{2q} - \frac{\omega_s L_s}{R_{FE}}i_{2d}] = jI \rightarrow \\ i_{2d} &= \frac{E_{pd}}{R_{FE}} + \frac{\omega_s L_s}{R_{FE}}i_{2q} \qquad \text{(B.61)} \\ v_s &= \frac{E_{pq}}{\omega_s C comp R_{FE}} + (1 - \frac{\omega_s L_s}{\omega_s C comp R_{FE}^2})E_{pq} + (\omega_s L_s - \frac{1}{\omega_s C comp} - \frac{\omega_s^2 L_s^2}{\omega_s C comp R_{FE}^2})i_{2q} \\ &+ j[(\frac{R_s}{R_{FE}} + 1)E_{pq} - \frac{\omega_s L_s R_s}{R_{FE}^2}E_{pd} - (R_s + \frac{\omega_s^2 L_s^2 R_s}{R_{FE}^2})i_{2q} - \omega_s L_s i_{2d}] \\ &= jU \rightarrow \\ i_{2q} &= -\frac{R_{FE}E_{pq} + (\omega_s C_{comp} R_{FE}^2 - \omega_s L_s)E_{pd}}{\omega_s^2 L_s C_{comp} R_{FE}^2 - R_{FE}^2 - \omega_s^2 L_s^2}. \qquad \text{(B.62)} \end{aligned}$$

From equations B.61 and B.62 the stator voltage and the electric power taken from the shaft can be written as

$$\begin{aligned} v_s &= j[1 + \frac{R_s}{R_{FE}} + (R_s + \frac{\omega_s^2 L_s^2 R_s}{R_{FE}^2} + \frac{\omega_s^2 L_s^2}{R_{FE}})\frac{R_{FE}}{\omega_s^2 L_s C_{comp} R_{FE}^2 - R_{FE}^2 - \omega_s^2 L_s^2}]E_{pq} \\ &- j[\frac{\omega_s L_s R_s}{R_{FE}^2} + \frac{\omega_s L_s}{R_{FE}} \\ &- (R_s + \frac{\omega_s^2 L_s^2 R_s}{R_{FE}^2} + \frac{\omega_s^2 L_s^2}{R_{FE}})\frac{\omega_s C_{comp} R_{FE}^2 - \omega_s L_s}{\omega_s^2 L_s C_{comp} R_{FE}^2 - R_{FE}^2 - \omega_s^2 L_s^2}]E_{pd} \qquad \text{(B.63)} \\ P_e &= 3(\frac{1}{R_{FE}} - \frac{\omega_s L_s}{R_{FE}}\frac{\omega_s C_{comp} R_{FE}^2 - \omega_s L_s}{\omega_s^2 L_s C_{comp} R_{FE}^2 - R_{FE}^2 - \omega_s^2 L_s^2})E_{pd}^2 \\ &- 3\frac{R_{FE}}{\omega_s^2 L_s C_{comp} R_{FE}^2 - R_{FE}^2 - \omega_s^2 L_s^2}E_{pq}^2 \\ &- 3\frac{\omega_s C_{comp} R_{FE}^2}{\omega_s^2 L_s C_{comp} R_{FE}^2 - R_{FE}^2 - \omega_s^2 L_s^2}E_{pd}E_{pq}. \qquad \text{(B.64)} \end{aligned}$$

For the fix speed system, i.e. a fix DC-voltage, the working point of the wind turbine can be calculated by an iterative process. First equation B.63 is solved for E_{pd} and the solution is inserted into equation B.64. From this equation, the voltage E_{pq} can now be expressed as function of the frequency ω_s and the electrodynamic power P_e. Now the frequency of the stator voltage is determined approximately using the relation $|v_s| = |E_p| = \omega_s \Psi_m$. The electrodynamic power is calculated from equation B.56 and this power is used to calculate the voltages E_{pd} and E_{pq}. The new frequency is

calculated by $\omega_s = \frac{\sqrt{E_{pd}^2+E_{pq}^2}}{\Psi_m}$. This process is repeated until sufficient accuracy is reached.

For the variable speed system, variable DC-voltage, the rotational speed of the turbine is known and accordingly also the frequency and the power from the turbine. Therefore, the voltage E_p can be solved directly from equation B.64 with the additional restriction that $E_{pd}^2 + E_{pq}^2 = \omega_s^2 \Psi_m^2$.

In figure B.14 the stator voltage, internal emf and the rotational speed of the two systems are shown.

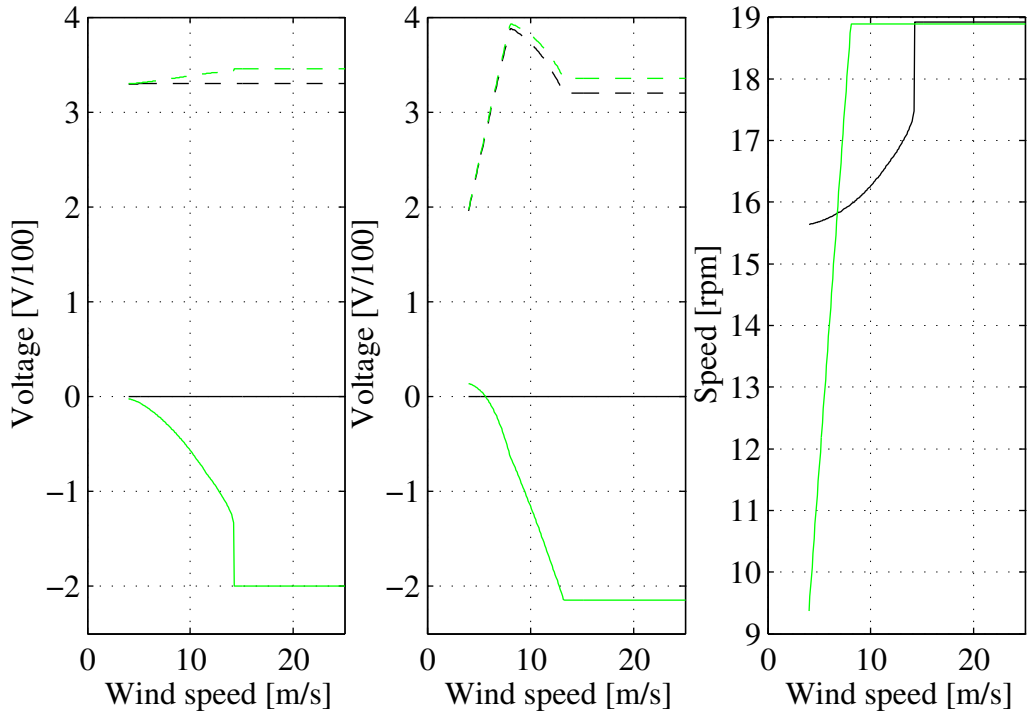

Figure B.14: In the left plot the stator voltage (black) and the internal emf (grey) are shown for the fix speed system, solid real part and dashed imaginary part. In the center plot the stator voltage (black) and the internal emf (grey) are shown for the variable speed system, solid real part and dashed imaginary part. In the right plot the rotational speed of the two systems are shown, black fix speed and grey variable speed.

B.4 Transformer

The loss model for the transformer can be derived in the same way as for the induction generator. The only difference is that the rotational term for the rotor circuit is, of course, not needed and thus removed. This gives that the equivalent circuit becomes as in figure B.15. From the circuit in figure B.15 the following equations can be

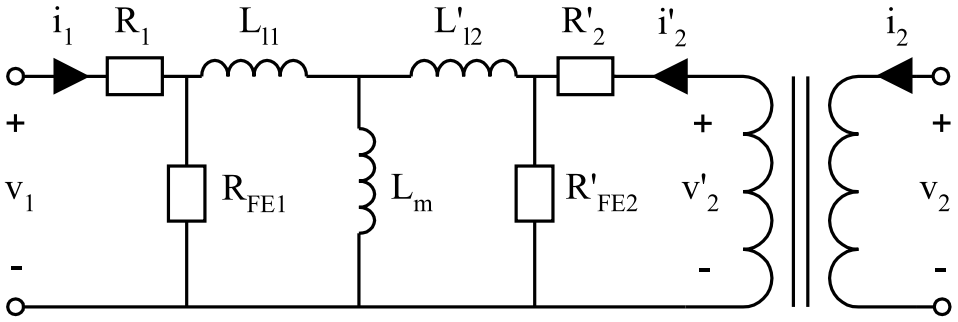

Figure B.15: Equivalent circuit of the transformer.

formulated, which describes the steady state performance of the transformer

$$R_{FE1} = \frac{\omega_s^2}{K_{e1}\omega_s^2 + K_{h1}\omega_s} \quad \text{(B.65)}$$

$$R_{FE2}^{'} = R_{FE1} \quad \text{(B.66)}$$

$$v_2' = \frac{N_1}{N_2} v_2 \quad \text{(B.67)}$$

$$i_2 = \frac{N_1}{N_2} i_2' \quad \text{(B.68)}$$

$$Z' = (\frac{N_1}{N_2})^2 Z \quad \text{(B.69)}$$

$$v_2' = (R_2' + R_{FE2}')i_2' - R_{FE2}' i_3 \quad \text{(B.70)}$$

$$0 = -R_{FE2}' i_2' + (R_{FE2}' + j\omega_s(L_{l2}' + L_m))i_3 + j\omega_s L_m i_4 \quad \text{(B.71)}$$

$$0 = j\omega_s L_m i_3 + (R_{FE1} + j\omega_s(L_{l1} + L_m))i_4 - R_{FE1} i_1 \quad \text{(B.72)}$$

$$v_s = -R_{FE1} i_4 + (R_1 + R_{FE1})i_1 \quad \text{(B.73)}$$

$$P_{loss} = 3(R_{FE1}|i_1 - i_4|^2 + R_{FE2}'|i_2' - i_3|^2 + R_1|i_1|^2 + R_2'|i_2'|^2). \quad \text{(B.74)}$$

Where:

R_1 and R_2	Winding resistance [Ω]
L_1 and L_2	Leakage inductances [H]
R_{FE1} and R_{FE2}	Iron loss resistances [Ω]
L_m	Magnetization inductance [H]
N_1 and N_2	Number of turns for the windings
Z	Arbitrary impedanse

To modulate transformers with more than two windings per phase it is only to add circuits in parallel with the second one, denoted 2. This means for example that if a three winding transformer is modulated, R_3, L_3, R_{FE3} are added and an ideal transformer with transformer ratio $N1 : N3$ is connected in parallel over the magnetization inductance.

As an approximation, the losses in the transformer can be described by equation B.75. This approximation is obtained by assuming that, for the no-load losses, the voltages over the iron loss resistances are constant, and for the load losses that the

voltages v_1 and v_2 in figure B.15 are constant.

$$P_{loss} = S_n P_0 + \frac{P_k}{S_n} S_{in}^2 \tag{B.75}$$

Where:

P_{loss}	Power loss in the transformer [W]
S_n	Rating of the transformer [VA]
S_{in}	Input power to the transformer [VA]
P_0	Per unit no-load losses [-]
P_k	Per unit load losses [-]

As can be noticed from equation B.75, the no-load losses increases if the transformer is over-dimensioned, $S_n > S_{in,rated}$, compared to if it is not. On the other hand, the load losses decreases if the transformer is over-dimensioned.

B.5 Cables

In this section, loss models for AC and DC cables are derived, and also a loss model for the inductance used for compensating of the reactive power produced by long AC-cables. The information for the cable loss models is taken from [13], [12] and [11].

B.5.1 AC cable

In this work all AC cables are assumed to be three core cables with XLPE insulation. The parameters of the AC cables are taken from [13] and [12]. The parameters that are used for the loss models are the conductor resistance, the inductance, the capacitance and the dielectric loss angle. As normal, for cable parameters, they are given per km.

Due to the alternating electrical field inside the cable there are losses in the insulation. These losses are given as a loss angle in the data sheets and the equivalent resistance can be calculated with equation B.76.

$$R_{Dloss\ \ l} = \frac{1}{\omega C_l \tan\delta} \tag{B.76}$$

Where:

$R_{Dloss\ \ l}$	Dielectric loss resistance [ohm/km]
ω	Frequency of the electrical field [rad/s]
C_l	Capacitance of the cable [F/km]
$\tan\delta$	Loss angle $= 2 \cdot 10^{-4}$ for XLPE cables [-]

The conductor resistance in data sheets is often given in DC-resistance and for a conductor temperature of 20^oC. But in an electrical system, the cable is often dimension to have a conductor temperature of 60^oC and the frequency of the current is in this work 50Hz, when using an AC network. Therefore the resistance must be recalculated for these conditions, equation B.77 is used for the temperature correction and

equations B.78 and B.79 for the frequency corrections.

$$R_T = R_{T0}\frac{T+273}{T_0+273} \quad \text{(B.77)}$$

$$R_\omega \approx R_{DC}[1+\frac{1}{48}(\frac{r}{\delta})^4] \text{ if } \frac{r}{\delta} < 1.5 \quad \text{(B.78)}$$

$$R_\omega \approx R_{DC}[\frac{1}{4}+\frac{1}{2}\frac{r}{\delta}+\frac{3}{32}\frac{\delta}{r}] \text{ if } \frac{r}{\delta} > 3 \quad \text{(B.79)}$$

$$\delta = \sqrt{\frac{2}{\omega\sigma\mu}} \quad \text{(B.80)}$$

$$\delta_{Cu} = \sqrt{\frac{2}{2\pi 50 \cdot 59.88 \cdot 10^6 \cdot 4\pi \cdot 10^{-7}}} = 9.20\text{mm}$$

$$\delta_{Al} = \sqrt{\frac{2}{2\pi 50 \cdot 37.74 \cdot 10^6 \cdot 4\pi \cdot 10^{-7}}} = 11.59\text{mm}$$

Where:

T_0	Reference temperature $[^oC]$
T	Temperature of the conductor $[^oC]$
R_{T0}	Resistance at reference temperature $[\Omega]$
R_T	Resistance at temperature T $[\Omega]$
R_{DC}	Resistance for DC-current $[\Omega]$
R_ω	Resistance at frequency ω $[\Omega]$
r	Radius of the conductor [m]
δ	Skin depth [m]
ω	Frequency of the current [rad/s]
σ	Conductivity of the conductor [S/m]
μ	Permeability of the conductor [Vs/Am]
δ_{Cu}	Skin depth for copper conductor and 50 Hz
δ_{Al}	Skin depth for aluminium conductor and 50 Hz

For power cables, the conductor radius varies from approximate 6 to 56mm which gives a conductor area of 25 to 2000 square millimeters. From this it is noticed that the ratio between the conductor radius and the skin depth varies approximate from 0.5 to 5.8. This gives that for some values of conductor radius none of the two equations B.78 or B.79 are valid. For these cases a mixture of the two equations are used to construct a continuous function.

To compensate for the extra losses due to the reactive power production in long cables the long line equations are used, [7]

$$R_c + i\omega L_c = (R_l + i\omega L_l)\frac{\sinh(\sqrt{(R_l+i\omega L_l)(\frac{1}{R_{Dloss,l}}+i\omega C_l)}l)}{\sqrt{(R_l+i\omega L_l)(\frac{1}{R_{Dloss,l}}+i\omega C_l)}} \quad \text{(B.81)}$$

$$R_{Dloss} + i\omega C_c = (\frac{1}{R_{Dloss,l}}+i\omega C_l)\frac{\tanh(\sqrt{(R_l+i\omega L_l)(\frac{1}{R_{Dloss,l}}+i\omega C_l)}\frac{l}{2})}{\sqrt{(R_l+i\omega L_l)(\frac{1}{R_{Dloss,l}}+i\omega C_l)}} \quad \text{(B.82)}$$

Where:

R_l	Conductor resistance per km [Ω/km]
L_l	Inductance of the cable per km [H/km]
$R_{Dloss,l}$	Dielectric loss resistance per km [Ω/km]
C_l	Capacitance of the cable per km [F/km]
ω	Angular frequency of the grid [rad/s]
l	Length of the cable [km]

From equations B.81 and B.82 the parameters for the π-model of the cable in figure B.16 are taken.

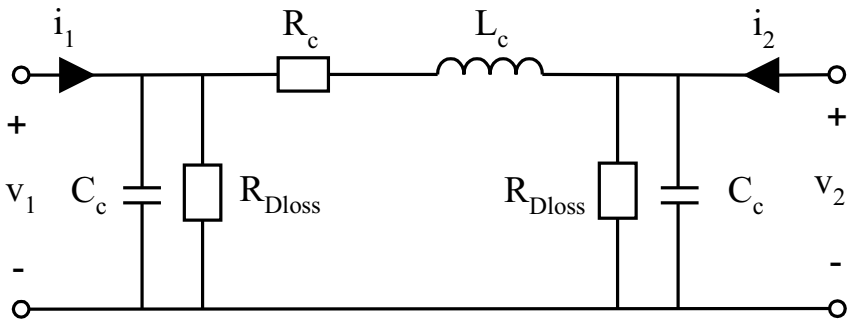

Figure B.16: Equivalent circuit of the cable for AC voltages.

If the model of the cable presented in figure B.16 and equations B.81 and B.82 are analyzed with the parameters given in [13] and [12] for sea cables the approximative loss model presented in equation B.83 can be delivered.

$$P_{loss} = P_0 l + C_0 l^3 + P_k l \frac{S_{in}^2}{S_n^2} \tag{B.83}$$

Where:

P_{loss}	Losses [W]
P_0 and C_0	No-load parameters
P_k	Load parameters
S_{in}	Input power [VA]
S_n	Rated power of the cable $= 3V_{rated}I_{rated}$ [VA]
l	Length of the cable [km]

From equation B.83 it can be noticed that the power losses at rated operation are independent of the rating of the cable, i.e for a given length and $S_{in} = S_n$ the power losses of the cable is independent of the rating, S_n, of the cable. This is due to the fact that the outer diameter of the cable does not change so much when the conductor area increases, increased rating, and therefore the cooling area of the cable is relative constant. This means that the same power loss can be cooled to keep the conductor temperature constant.

Another interesting result is that the no-load losses has two components, one that increases linearly with the cable length due to the fact that the resistance R_{Dloss} decreases inversely proportional to the cable length. The other term increases with the cube of the cable length. This can be explained if we for the moment describes the cable with a number of series connected π-models. When the cable is connected to an AC voltage, the cable capacitance will start to produce reactive power, which has to

go through the conductor resistance, R_c, and this gives a power loss. We know that the capacitance and the resistance increases linearly with the cable length. The load losses in the resistance, R_c, can be approximately described with $P_k S_{in}^2$. Due to that the reactive power production increases linearly, the input power, S_{in} increases linearly with the cable length and since the resistance increases linearly, the factor P_k increases linearly with the cable length. This gives that the losses in the conductor resistance increases with the cube of the cable length. Since this power loss arises as soon the cable is connected to an AC voltage this is modulated as a no-load loss.

In table B.1 the parameters of the approximative loss model of the AC cable are shown for the AC cables used in this work. As can be noticed from table B.1 the no-load losses are small compared to the load losses of the cable.

Table B.1: The parameters of the approximative loss model of the AC cables used in this work.

Voltage	P_0	C_0	P_k
11kV	5.01	0.0212	57656
22kV	13.08	0.0354	57656
33kV	21.48	0.0421	57656
45kV	38.40	0.0694	57656
66kV	70.71	0.1069	57656
132kV	200.87	0.1726	49470
220kV	530.30	0.2982	51211

B.5.2 DC cable

The cable for DC is constructed in similar way as an AC-cable, therefore the same model can be used for the DC-cable as for the AC-cable. But since the models in this chapter only is derived for steady state operations, the model for the DC-cable reduces to only the conductor resistance R_c as shown in figure B.17. The only correction

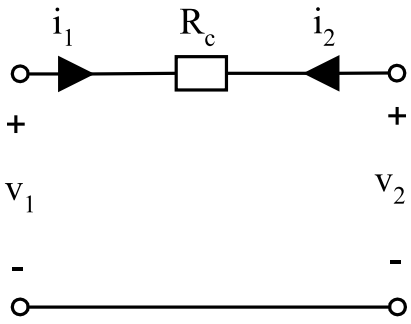

Figure B.17: Equivalent circuit of the cable for DC voltages.

that is needed for this model is to recalculate the resistance to the right temperature. Equation B.77 is used for this, the same as for the AC case.

In the same way as for the AC-cable an approximative loss model for the DC cable can be delivered. This model has only load-losses as can be seen in equation B.84

$$P_{loss} = P_k l \frac{P_{in}^2}{P_n^2} \tag{B.84}$$

Where:

P_k	Load parameter = 58742
P_{in}	Input power [W]
P_n	Rated power of the cable = $V_{rated}I_{rated}$ [W]
l	Length of the cable [km]

B.5.3 Cable compensating inductor

From appendix B.5.1 it is known that AC-cables has a large internal capacitance between the conductor and earth. This capacitance produces reactive power that has to be taken care of, especially if the cable is long. This is often done by inserting shunt inductances in both ends of the cable. These inductances are designed as three phases transformers but with only one winding per phase and with air gaps in the iron core. Because of the similarities between the transformer and the inductor these will be modulated in the same way, in figure B.18 the equivalent circuit of the inductor is shown. In figure B.18 the resistance R_1 is the winding resistance, R_{FE} is the iron loss

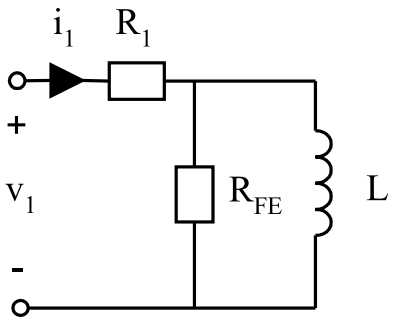

Figure B.18: Equivalent circuit of the compensating reactor for cables.

resistance and L is the inductance. The no-load losses of the reactor is set equal to the no-load losses of a transformer with the same VA rating. The load losses is set to half the load losses of a transformer with the same VA rating, since we only have a primary winding.

B.6 Converters

Converters is used to transform AC to DC, DC to AC or for transforming one DC voltage to another DC voltage. For rectifiers or inverters this can be done by using grid commutating converters or self commutating converters. The grid commutating converters uses diodes or thyristors as main components and the self commutating converters uses transistors, mosfet transistors, GTOs or IGBTs as main components. The self commutating converters offers much higher controllability over the voltages and currents, then the grid commutated converters do. This is due to the fact that in the self commutated converter the on and off switching of the valves are fully controllable but in the grid commutating converter none or one of these are controllable.

In this section the loss models of the converters used in this work are derived. The converters that will be treated are the diode rectifier, the IGBT inverter and the three DC/DC converters chosen in appendix A i.e boost, full bridge and full bridge isolated boost converter.

B.6.1 Diode rectifier

The diode rectifier will be modulated with a current stiff DC-side, as can be seen in figure B.19, assuming a large inductor. This is not true for all applications of the diode rectifier in this work, but the differences will be neglected. The current harmonics on the AC-side and the commutation time due to leakage inductances in the AC circuit will also be neglected. The losses in the rectifier will be modulated using conduction

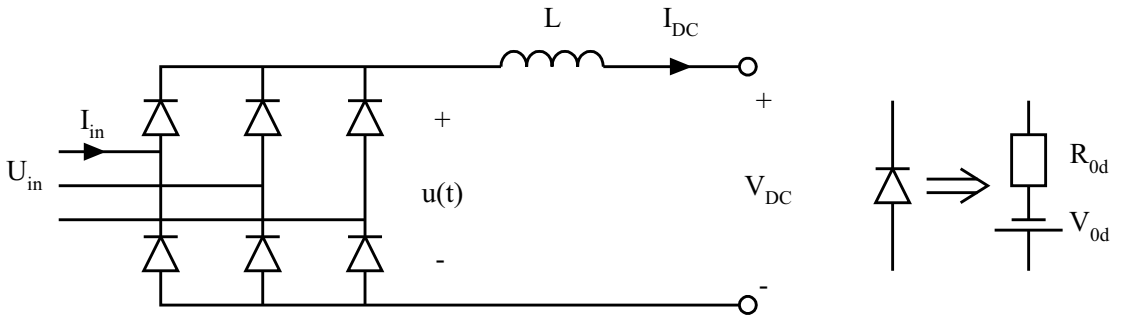

Figure B.19: Diode rectifier with a current stiff DC-side.

losses only, forward voltage drop and a resistance, as can be seen in figure B.19. The DC-voltage, V_{DC}, can be calculated as the mean value of the voltage $u(t)$ and with the current stiff DC-side the DC-current, I_{DC}, is assumed to be constant which gives

$$\begin{aligned} V_{DC} &= \frac{3}{\pi}\int_0^{\frac{\pi}{3}} \sqrt{\frac{2}{3}}U_{in}\cos(\nu) + \sqrt{\frac{2}{3}}U_{in}\cos(\nu - \frac{\pi}{3}) - 2R_{0d}I_{DC} - 2V_{0d}\frac{\mathrm{d}\nu}{\mathrm{d}t} \\ &= \frac{3\sqrt{2}}{\pi}U_{in} - 2(R_{0d}I_{DC} + V_{0d}). \end{aligned} \tag{B.85}$$

Where:

U_{in}	Line to line voltage [V]
V_{DC}	DC-voltage [V]
I_{DC}	DC-current [A]
R_{0d}	Conducting resistance for one diode [Ω]
V_{0d}	Threshold voltage for one diode [V]

With the given assumptions above, the power flow of the diode rectifier can be described as:

$$P_{loss} = 2R_{0d}I_{DC}^2 + 2V_{0d}I_{DC} \tag{B.86}$$

$$P_{out} = V_{DC}I_{DC} \tag{B.87}$$

$$P_{in} = \sqrt{3}U_{in}I_{in} = P_{loss} + P_{out} \tag{B.88}$$

$$Q_{in} = 0. \tag{B.89}$$

Where:

I_{in}	Fundamental phase current [A]
P_{loss}	Power loss in the diode rectifier [W]
P_{out}	Output power [W]
P_{in}	Input active power [W]
Q_{in}	Input reactive power [VAr]

The reactive power into the diode rectifier is assumed to be zero because the voltage and current are assumed to be in phase.

B.6.2 Hard-switched IGBT-inverter

In this section losses in rectifiers/inverters with IGBT valves are studied in detail, but the methods used is applicable to any self commutating converter with the same behavior. The theory used comes from articles [8],[9] and [33] and thesis [1]. IGBT converters are usually designed as in figure B.20 with a stiff DC-voltage which comes from the large capacitors on the DC-buss. This type of converter is therefore usually called VSI (Voltage Source Inverter).

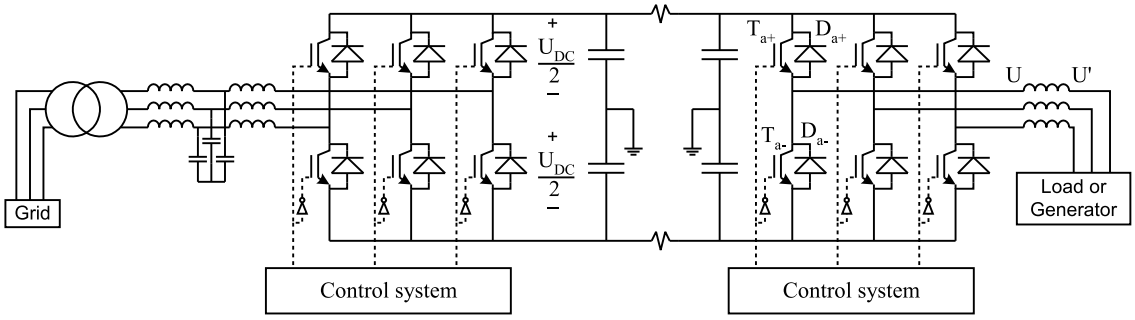

Figure B.20: VSI converter.

With the zigzag on the DC-bus means that the two sides of the converter can be placed with a short or long distance (millimeters to hundreds of km) between them and the two sides of the converter is connected together with DC-cables. With this technology, electric power can be transported over long distances. But if it is a back to back transistor converter with a short distance between the two bridges there is only one capacitor, on the DC-link and the two sides are usually in the same casing.

The filter inductances and capacitances on the grid and load side is to filter out the harmonics in the voltages. The filter to the grid is usually bigger and in more steps then on the load side, the reason for this is that the regulations regarding harmonics to the grid is more rigorous and the loads are usually machines which do not need such a clean voltage partly because they themselves comprise inductance. Often, in low-power applications, the converter is connected directly to the machine and the inductance in the machine is sufficient as a filter.

As seen in figure B.20 the anti-parallel diodes forms a three phase diode rectifier which means that the DC-voltage can not be lower than the peak value of the grid voltage. Usually it is desired that the DC-voltage is higher than this value because the controllability of the currents is better (faster) with a higher DC-voltage. This is due to that the derivative of the current through the filter inductance is dependent on the voltage over it and if the voltage over it is low, the currents are less controllable. By

having a higher DC-voltage, a high voltage can be applied over the filter inductance even when the AC voltage is at its peak value.

The following approximation can be derived for the active and reactive power from the load utilizing the magnitude and phase of the fundamental component of the voltages U and U'

$$\begin{aligned} P_l &= 3\frac{U_1' U_1 sin(\phi_1' - \phi_1)}{X} \\ Q_l &= 3\frac{U_1'(U_1' - U_1 sin(\phi_1' - \phi_1))}{X}. \end{aligned} \tag{B.90}$$

Where:

P_l	active power from the grid [W]
Q_l	reactive power from the grid [VAr]
U_1'	RMS-value of the fundamental component of the voltage U' [V]
U_1	RMS-value of the fundamental component of the voltage U [V]
ϕ_1'	phase angle of the fundamental component of the voltage U' [rad]
ϕ_1	phase angle of the fundamental component of the voltage U [rad]

From equations B.90 it can be noticed that the active power is approximate dependent on the phase difference between the voltages and the reactive power is approximative dependent on the difference between the voltage magnitudes. Observe that it is the neglecting of the transmission resistance that makes this assumption adequate. This means that with a higher voltage U_1, more reactive power can be produced to the load and to the grid and a higher voltage U_1 also means a higher DC-voltage. This means that with an increased DC-voltage the maximum produced reactive power increases and the speed of the current controller increases. But a higher DC-voltage demands that components with a higher rated voltage must be used, which increases the cost of the converter.

The maximum RMS-value of the output voltage is dependent on the DC-voltage but it is also dependent on which modulation technique that is used. There are two techniques that are commonly used, one uses a sine-wave as reference and the other uses a sine-wave added together with an appropriately selected zero sequence voltage, for instance a third harmonic. In equations B.91 the phase reference voltages for the sine modulation are shown and in equations B.92 the phase reference voltages for the sine with a third harmonic are shown.

$$\begin{aligned} U_{1ref}(t) &= M\sin(\omega t) \\ U_{2ref}(t) &= M\sin(\omega t + \frac{2\pi}{3}) \\ U_{3ref}(t) &= M\sin(\omega t + \frac{4\pi}{3}) \end{aligned} \tag{B.91}$$

$$\begin{aligned} U_{1ref}(t) &= M\{\sin(\omega t) + A_m\sin(3\omega t)\} \\ U_{2ref}(t) &= M\{\sin(\omega t + \frac{2\pi}{3}) + A_m\sin(3\omega t)\} \\ U_{3ref}(t) &= M\{\sin(\omega t + \frac{4\pi}{3}) + A_m\sin(3\omega t)\} \end{aligned} \tag{B.92}$$

Where:

$U_{xref}(t)$	reference for phase x
M	modulation index
A_m	modulation index for the third harmonic
ω	reference angular frequency [rad/s]
t	time [s]

When the reference voltage is equal to one, the converter produces its highest phase voltage which is equal to $\frac{U_{DC}}{2}$. This means that the magnitude of the reference voltage can not be higher then that one, since the converter will otherwise be over-modulated and produce a large amount of of low order harmonics. This also means that the modulation index for the sine modulated converter is limited to be in between zero and one. When setting the modulation index, M, to one, the converter will produce a phase voltage with a peak value of $\frac{U_{DC}}{2}$. Which means that the highest RMS phase voltage that this converter can produce is

$$U_{f,max} = \frac{U_{DC}}{\sqrt{8}}. \tag{B.93}$$

By setting the modulation index equal to zero the converter will produce a voltage with zero amplitude. This gives that the modulation index for the sine modulated converter can be expressed as

$$M = \frac{\sqrt{8}U_s}{U_{DC}} \quad \text{for} \quad U_s \leq U_{f,max}. \tag{B.94}$$

Where U_s is the RMS-value of the fundamental output phase voltage.

In figure B.21 the reference voltages for the sine and the sine added with a third harmonic are shown and the potential of the zero point relative the ground potential (the zero sequence component). In the left plot in figure B.21 the reference phase voltages for the three phases for the sine modulated converter are shown with M equal to 1/2. For the converter with the sine added with a third harmonic the same limit for the reference voltages holds, maximum amplitude equal to one. The modulation index for the third harmonic A_m can be set to almost any value, within reasonable limits, because the added third harmonic is a zero component which disappears in a three phase system with a floating zero point. The maximum modulation index, M, is dependent on the modulation index for the third harmonic, A_m, due to the limit on the reference voltage. The maximum modulation index is described in equation

$$\begin{aligned} M_{max} &= \frac{1}{1 - A_m} \quad \text{for} \quad 0 \leq A_m < \frac{1}{9} \\ M_{max} &= \frac{1}{8A_m}\left(\frac{12A_m}{1 + 3A_m}\right)^{\frac{3}{2}} \quad \text{for} \quad A_m \geq \frac{1}{9}. \end{aligned} \tag{B.95}$$

From equations B.92 it is noticed that higher modulation index, M, gives a higher fundamental voltage. From equation B.95 it can be found that $A_m = \frac{1}{6}$ gives the highest value of M_{max}, equal to $\frac{3}{\sqrt{3}}$. Another commonly used value of A_m is $\frac{1}{4}$ because this minimizes the torque ripple in electrical machines. But in this work A_m is set to $\frac{1}{6}$ in order to utilize the converter best. From this the highest RMS phase voltage that the converter can produce can be calculated to

$$U_{f,max,3} = \frac{U_{DC}}{2\sqrt{2}} M_{max} = \frac{U_{DC}}{\sqrt{6}} \tag{B.96}$$

and the modulation index for a given phase voltage can be calculated by

$$M = \frac{\sqrt{6}U_s}{U_{DC}} \quad \text{for} \quad U_s \leq U_{f,max,3}. \tag{B.97}$$

Where U_s is the RMS-value of the fundamental output phase voltage. In the right plot in figure B.21 the reference phase voltages for the three phases for the sine added with a third harmonic modulated converter are shown with $M = M_{max}$ and $A_m = \frac{1}{6}$. From

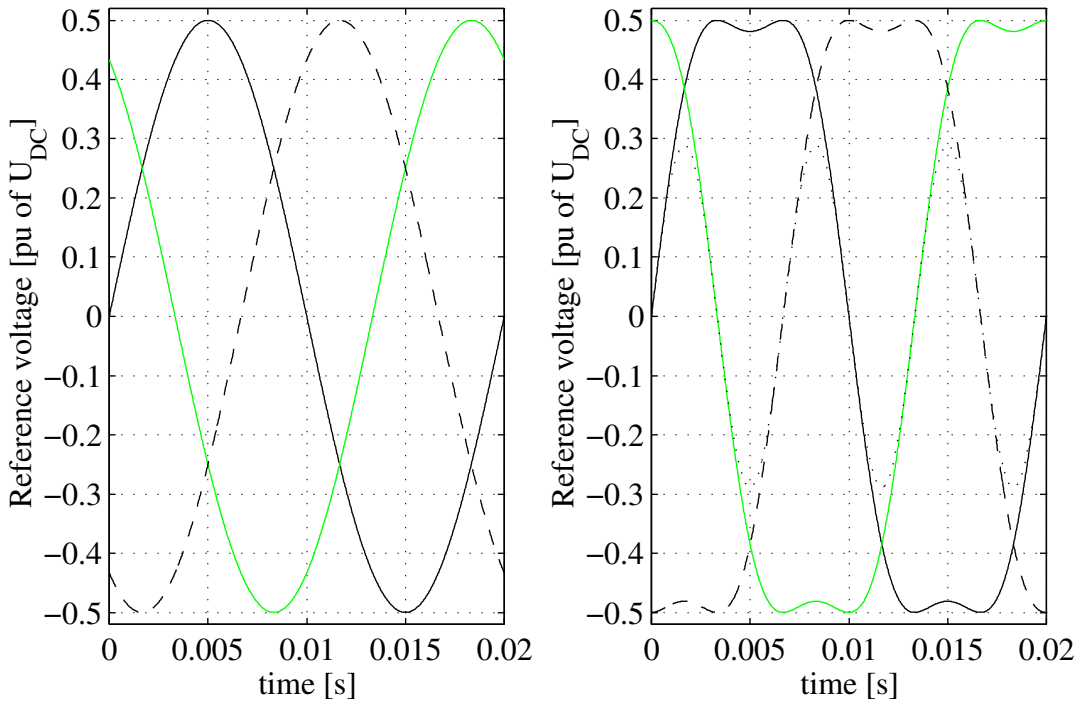

Figure B.21: Reference phase voltages, black phase 1, grey phase 2 and dashed phase 3. Left plot sine modulation and right sine with third harmonic $A_m = \frac{1}{6}$, dotted is the zero potential of a symmetrical three phase load connected to the converter.

the equations B.93 and B.96 it can be noticed that for the sine modulation, the DC-voltage needs to be higher to obtain the same output voltage as for the sine modulation with a third harmonic. This gives that components with a higher voltage rating must be used in this case to obtain a converter with the same rating as for a converter with sine and a third harmonic modulation.

The big disadvantage with the third harmonic modulation is that all the zero points must be floating which can cause problems with the protection of the converter and loads. In the right plot in figure B.21 the potential of the zero point of a symmetrical three phase load is shown, dotted curve, and from this it is obvious that this point can not be connected to ground potential. It is the same for the filter capacitors which can not be connected to ground without special arrangements. This can cause problems leading to additional costs when the filters are designed.

The phase voltages are created by pulse with modulation (PWM) technique. PWM-technique means that the potential rapidly (with the switching frequency) changes from $+\frac{U_{DC}}{2}$ to $-\frac{U_{DC}}{2}$ in such a way that the average value corresponds to the desired

reference voltage. In figure B.22 the PWM-pulses for one phase-leg in the converter shown in figure B.20 are shown, for sine modulation. In the top plot in figure B.22

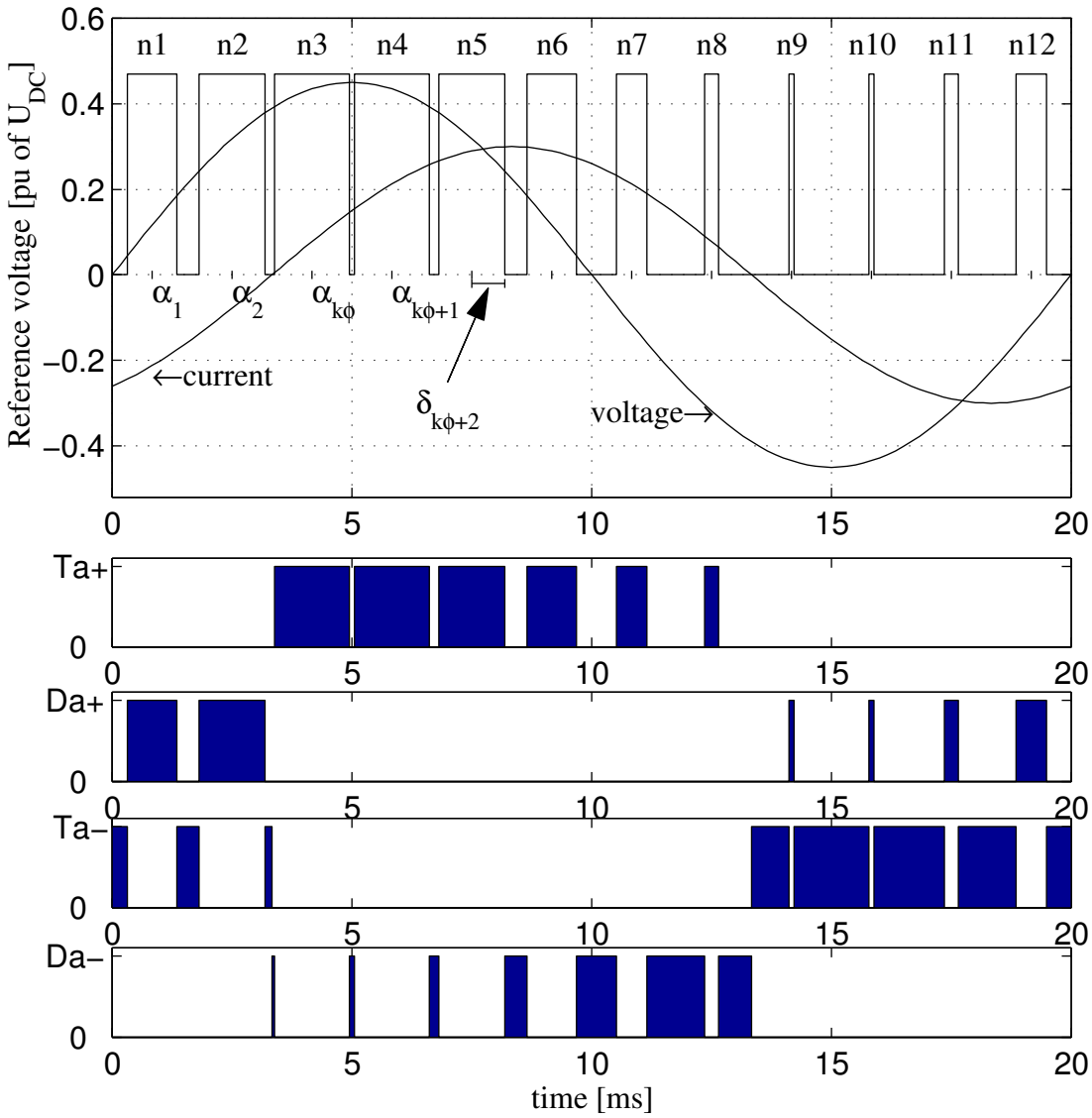

Figure B.22: Pulses of the PWM converter.

the fundamental phase voltage and current are shown together with the positive part of the instantaneous phase voltage. In this figure the switching frequency is very low in order to better illustrate what happens in the converter. The switching frequency is only 12 times higher than the fundamental, in a normal application this ratio is at least 20 times. In the lower plots in figure B.22 it is shown which of the components that is conducting the phase current. From these plots it is seen that when the phase current is positive it alternates between the IGBT T_{a+} and the diode D_{a-} and when the phase current is negative it alternates between T_{a-} and D_{a+}. The position of these components can be seen in figure B.20.

The losses in the components can be identified as conduction losses and switching

losses. The conduction losses for an IGBT or a diode can be expressed as [1]

$$P_{con} = \frac{1}{T}\int_0^T (u_{on}(t)i(t))\mathrm{d}t = \frac{1}{T}\int_0^T ((U_0 + r_0 i^{B_{con}}(t))i(t))\mathrm{d}t. \quad \text{(B.98)}$$

Where:

P_{con}	conduction losses [W]
$i(t)$	current through the component [A]
T	fundamental period [s]
$u_{on}(t)$	on-state voltage drop over the component [V]
r_0	dynamic conducting resistance [Ω]
B_{con}	curve fitting constant

In the last integral in equation B.98 the on-state voltage drop over the component has been expressed as a constant voltage drop and a dynamic resistance. This way of expressing the conducting losses gives a good agreement with measurements. The switching losses are not as simple to express as the conducting losses. It is possible to express them in means of collector-emitter voltage and collector current but this is not a very accurate method due to the need of approximations and because the switching characteristics are different and dependent on the component. The most accurate method is to measure the switching energy losses as function of the collector-emitter voltage and load current and then do a curve fitting of the measured switching energies according to equation B.99.

$$E_{sw} = A_{sw,on}U_{ce}(t)i^{B_{sw,on}}(t) + A_{sw,off}U_{ce}(t)i^{B_{sw,off}}(t) \quad \text{(B.99)}$$

Where:

E_{sw}	switching energy loss of the component [J]
$A_{sw,on}, B_{sw,on}$	turn-on curve fitting constants for the component
$A_{sw,off}, B_{sw,off}$	turn-off curve fitting constants
$U_{ce}(t)$	collector-emitter voltage [V]
$i(t)$	current through the component [A]

But since in this work there where no opportunity to measure the switching losses or the conduction losses on components that could be used in the converters used in this report, the component data will be taken from curves in data sheets. In figure B.23 the on-state voltage drop (left plot) and switching energies (right plot) from a data sheet for a IGBT and diode is shown. From the left plot in figure B.23 it can be noticed that the expression for the on-state voltage drop in equation B.98, grey curves, are good approximations for the voltage drops from data sheets, black curves. Even the more approximate curve, dashed, with $B_x = 1$ gives god agrement.

From the right plot it is noticed that the approximative equation B.99, grey curve, also follows the switching energies for the IGBT, black curve, with a good agrement and also the more approximative expression, dashed curve, with $B_x = 1$ follows the measured curve. For the diode, the recovery energy E_{rr} is only shown. The reason for this is that the on and off switching losses for the diode are insignificant compared with the recovery energy [1]. When the diode alternates from conducting to blocking it will lead current for a short while in the reverse direction. This is due to the fact that there are free charges in the barrier layer of the diode, and the energy needed to transport these charges away from the barrier layer is the recovery energy. It is noticed that

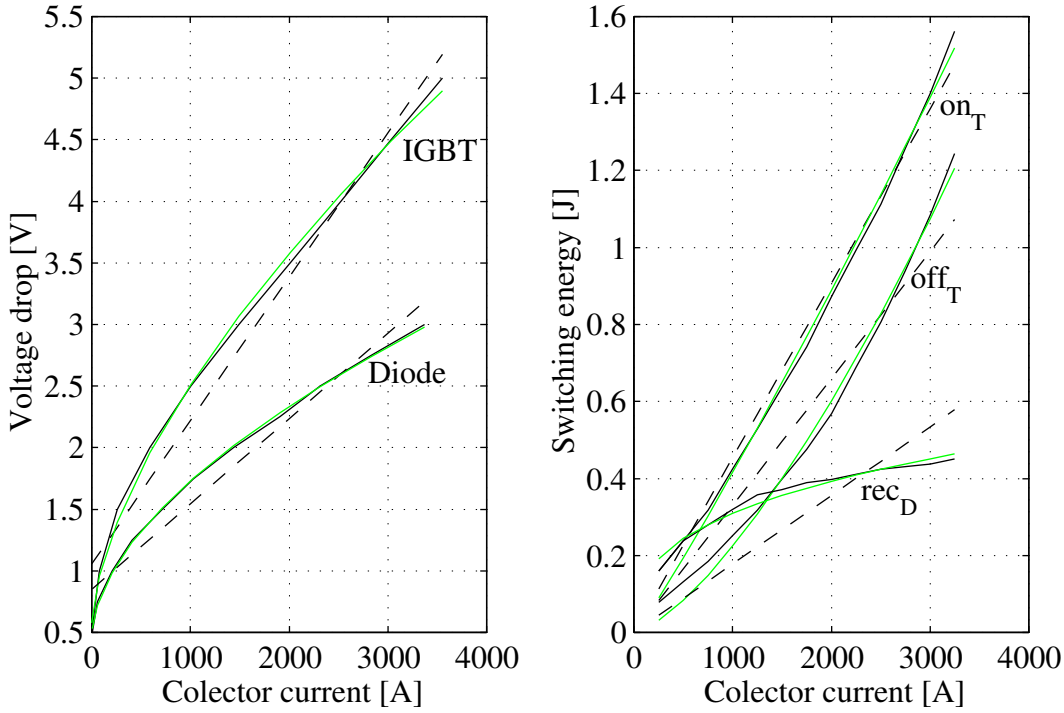

Figure B.23: Left plot the on-state voltage drop and the right plot the switching energies for a IGBT and diode. Black curve is from data sheet, grey is a first order curve fitting and the dashed is a simpler curve fitting with $B_- = 1$.

the model described in equation B.99 follows the measured curve, but for the simpler model with $B_x = 1$ the agrement is not very good.

In this work the linear expression for the conducting voltage drop over the IGBT and diode and for the switching energy losses are used, i.e $B_x = 1$.

To reduce the losses in the converters, the IGBT and diode that gives the lowest losses at rated operation for a given switching frequency are selected. The selected components are then down scaled to components with a rating of 1V and 1A. To obtain a IGBT and diode with a specified rating equations B.100 to B.104 are used.

$$v_0 = v_{0,bas} V_{DC} \tag{B.100}$$

$$r_0 = r_{0,bas} \frac{V_{DC}}{I_{DC}} \tag{B.101}$$

$$A_{sw,on} = A_{sw,on,bas} \tag{B.102}$$

$$A_{sw,off} = A_{sw,off,bas} \tag{B.103}$$

$$A_{sw,rec} = A_{sw,rec,bas} \tag{B.104}$$

Where:

v_0	Constant conducting voltage drop [V]
r_0	Resistance [Ω]
$A_{sw,on}$	turn-on switching loss parameter for IGBT
$A_{sw,off}$	turn-off switching loss parameter for IGBT
$A_{sw,rec}$	turn-off switching loss parameter for diode
$X_{,bas}$	Base quantity
V_{DC}	Wanted rated DC voltage of the component [V]
I_{DC}	Wanted rated DC current of the component [A]

For the converters used to control a machine, a switching frequency of 5kHz is used. For this converter, also called low voltage converter, the IGBT and diode in data sheet [19] is used. For the high voltage converters used in the transmission system the switching frequency is selected to 2kHz, the same as ABB uses in there HVDC-light A [53]. For the high voltage converter, an IGBT with a higher voltage rating is used. Therefore there is a possibility to reduce the losses due to the fact that the switching losses of the high voltage IGBT is higher. But the high voltage IGBT is used to reduce the numbers of series connected IGBT:s in the converter, which probably is the case for the real converters. The IGBT and diode in data sheet [18] is used for the high voltage converter.

In table B.2 the parameters of the down scaled IGBT and diode are shown. These parameters are used as base parameters for the equations B.100 - B.104 for the calculation of the parameters of the wanted IGBT and diode.

Table B.2: The parameters of the down scaled IGBT and diode.

	$v_{0,bas}$ [mV]	$r_{0,bas}$ [mΩ]	$A_{sw,on,bas}$ [10^{-7}]	$A_{sw,off,bas}$ [10^{-7}]	$A_{sw,rec,bas}$ [10^{-7}]
Low voltage					
IGBT	1.29	1.95	2.99	4.65	
Diode	1.07	1.12			1.94
High voltage					
IGBT	1.14	1.88	11.67	8.33	
Diode	0.83	1.08			5.42

As can be noticed from table B.2 the IGBT for the high voltage converter has lower conduction losses and higher switching losses then the IGBT for the low voltage converter. This is due to the fact, as mention before, that the IGBT for the high voltage converter is based on an IGBT with higher voltage rating then the IGBT used for the low voltage converter.

From the lower four plots in figure B.22 it is noticed that the current is always alternating between one transistor and one diode in a phase leg. This gives that the losses in one side of the converter, shown in figure B.20, can be determined by calculating the losses in one transistor and one diode and the multiply it by six to get the total losses. For example let us consider IGBT T_{a+} and diode D_{a-}. From figure B.22 it is seen that they conduct the current during a half of the fundamental period, starting on switching pulse $k\phi$. From this, the total losses for one half of the

converter in figure B.20 can be calculated as

$$P_{loss} = 6 \sum_{k=k\phi}^{k\phi+\frac{p}{2}-1} \{P_{conT_{a+}}(k) + P_{conD_{a-}}(k) + \frac{1}{T_s} E_{swT_{a+}}(k) + \frac{1}{T_s} E_{swD_{a-}}(k)\} \tag{B.105}$$

$$p = \frac{f_c}{f_s}. \tag{B.106}$$

Where:

$P_{loss\ \ conv}$	Total loses in one side of the converter [W]
$P_{conT_{a+}}(k)$	conduction losses in the IGBT for pulse k [W]
$P_{conD_{a-}}(k)$	conduction losses in the diode for pulse k [W]
$E_{swT_{a+}}(k)$	switch energies for the IGBT for pulse k [J]
$E_{swD_{a-}}(k)$	switch energies for the diode for pulse k [J]
T_s	fundamental period time [s]
p	frequency-ratio [-]
f_s	fundamental frequency [Hz]
f_c	switching frequency [Hz]

Now if only the sine modulation described in equation B.91 is taken into consideration the following relations can be formulated according to the references in figure B.22

$$\delta_k = \frac{1}{4f_c}(1 + M\sin(\omega_s \alpha_k)) \tag{B.107}$$

$$M = \frac{2\sqrt{2}U_s}{U_{DC}} \tag{B.108}$$

$$p = \frac{f_c}{f_s} \tag{B.109}$$

$$\omega_s = 2\pi f_s \tag{B.110}$$

$$i(t) = \hat{I}\sin(\omega_s t + \phi). \tag{B.111}$$

Where:

α_k	time at the middle of conducting pule number k [s]
δ_k	half of the conducting time of pulse k [s]
M	modulation index [-]
U_s	RMS-value of the fundamental phase voltage [V]
U_{DC}	DC-voltage [V]
$i(t)$	fundamental phase current [A]
$\hat{I}$	peak value of the current [A]
ϕ	phase angel between voltage and current [rad]

From these relations and equation B.105 the average conducting losses of the IGBT T_{a+} can be formulated as

$$P_{conT} = f_s \sum_{k=k\phi}^{k\phi+p/2-1} \int_{\alpha_k-\delta_k}^{\alpha_k+\delta_k} (v_{0T} i(t) + r_{0T} i^2(t))\mathrm{d}t = P_{conT1} + P_{conT2}. \tag{B.112}$$

From equation B.112 it is noticed that the conducting losses can be divided into two

parts. If the first part is considered, it can be evaluated as

$$\begin{aligned} P_{conT1} &= f_s \sum_{k=k\phi}^{k\phi+p/2-1} \int_{\alpha_k-\delta_k}^{\alpha_k+\delta_k} (v_{0T} i(t))\mathrm{d}t = f_s \hat{I} \sum_{k=k\phi}^{k\phi+p/2-1} \int_{\alpha_k-\delta_k}^{\alpha_k+\delta_k} (v_{0T}\sin(\omega_s t+\phi))\mathrm{d}t \\ &= \frac{v_{0T}\hat{I}}{2\pi} \sum_{k=k\phi}^{k\phi+p/2-1} \{2\sin(\omega_s\alpha_k+\phi)\sin(\omega_s\delta_k)\}\mathrm{d}t \\ &= \frac{v_{0T}\hat{I}}{2\pi} \sum_{k=k\phi}^{k\phi+p/2-1} \{2\sin(\omega_s\alpha_k+\phi)\sin(\frac{\pi}{2p}+\frac{\pi M}{2p}\sin(\omega_s\alpha_k))\}. \end{aligned}$$

Now set $\theta = \frac{\pi}{2p}$ and $x = M\theta$ which gives

$$\begin{aligned} P_{conT1} &= \frac{v_{0T}\hat{I}}{2\pi} \sum_{k=k\phi}^{k\phi+p/2-1} \{2\sin(\omega_s\alpha_k+\phi)\sin(\theta+x\sin(\omega_s\alpha_k))\} \\ &= \frac{v_{0T}\hat{I}}{\pi} \sum_{k=k\phi}^{k\phi+p/2-1} \{\sin(\theta)\sin(\omega_s\alpha_k-\phi)\cos(x\sin(\omega_s\alpha_k)) \\ &+ \cos(\theta)\sin(\omega_s\alpha_k-\phi)\sin(x\sin(\omega_s\alpha_k))\}. \end{aligned} \tag{B.113}$$

The sine of sine functions can be expressed with Bessel functions as

$$\begin{aligned} \cos(x\sin(\Psi)) &= J_0(x) + 2J_2(x)\cos(2\Psi) + 2J_4(x)\cos(4\Psi) + ... \\ \sin(x\sin(\Psi)) &= 2J_1(x)\sin(\Psi) + 2J_3(x)\sin(3\Psi) + 2J_5(x)\sin(5\Psi) + ... \quad . \end{aligned}$$

Where:
$J_n(x)$ the n:th order of the Bessel function

For $p > 10$ all Bessel functions of higher order than one are insignificant compared to the zero and first, this can be seen in figure B.24 where the ten first Bessel functions are shown with $x = \frac{pi}{2p}$. As seen in figure B.24 it is a god approximation to put all higher order of Bessel functions to zero for $p > 10$, as mention before p is usually greater then 20. With this approximation equation B.113 becomes

$$\begin{aligned} P_{conT1} &= \frac{v_{0T}\hat{I}}{\pi} \sum_{k=k\phi}^{k\phi+p/2-1} \{\sin(\theta)J_0(x)\sin(\omega_s\alpha_k-\phi) \\ &+ \cos(\theta)J_1(x)\cos(\phi) - \cos(\theta)J_1(x)\cos(2\omega_s\alpha_k-\phi)\}. \end{aligned} \tag{B.114}$$

Now change the summation variable k to n by the following substitution

$$\begin{aligned} \omega_s\alpha_{k\phi} &= (4k_\phi-2)\theta \\ \omega_s\alpha_{k\phi+n} &= (4k_\phi-2+4n)\theta \quad 0 \le n \le \frac{p}{2}-1. \end{aligned}$$

This gives that equation B.114 becomes

$$\begin{aligned} P_{conT1} &= \frac{v_{0T}\hat{I}}{\pi} \sum_{n=0}^{\frac{p}{2}-1} \{\sin(\theta)J_0(x)\sin(4\theta(k_\phi-\frac{1}{2}+n)-\phi) \\ &+ \cos(\theta)J_1(x)\cos(\phi) - \cos(\theta)J_1(x)\cos(8\theta(k_\phi-\frac{1}{2}+n)-\phi)\}. \end{aligned} \tag{B.115}$$

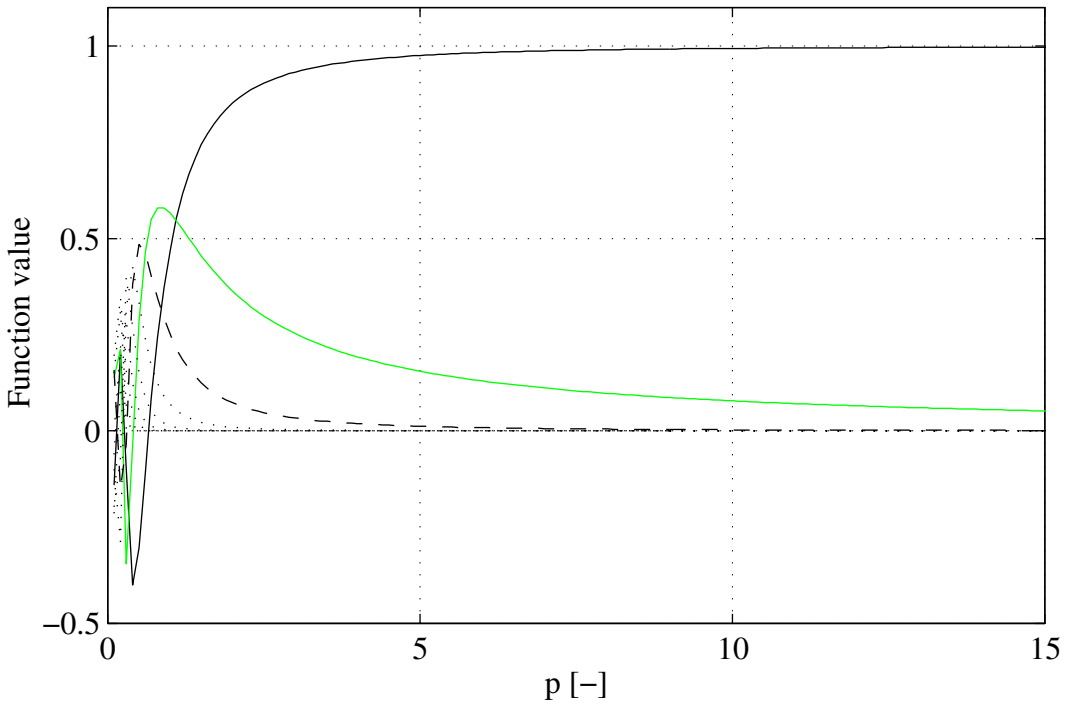

Figure B.24: The first ten order Bessel functions with $x = \frac{pi}{2p}$. Solid black J_0, grey J_1, dashed J_2 and dotted J_3 to J_9.

For summation of sine and cosine function the following holds

$$\sum_{k=0}^{N} \sin(k\alpha + \beta) = \frac{\cos(\frac{\alpha}{2} - \beta) - \cos(\frac{(2N+1)\alpha}{2} + \beta)}{2\sin(\frac{\alpha}{2})} \quad \text{(B.116)}$$

$$\sum_{k=0}^{N} \cos(k\alpha + \beta) = \frac{\sin(\frac{\alpha}{2} - \beta) + \sin(\frac{(2N+1)\alpha}{2} + \beta)}{2\sin(\frac{\alpha}{2})}. \quad \text{(B.117)}$$

With this equations equation B.115 can be expressed as

$$P_{conT1} = \frac{v_{0T}\hat{I}}{2\pi}(J_0(x)\frac{\cos(\theta(4 - 4k_\phi) + \phi)}{\cos(\theta)} + pJ_1(x)\cos(\theta)\cos(\phi)). \quad \text{(B.118)}$$

But $k\phi = 1 + \frac{\phi}{4\theta}$ which gives the final equation

$$P_{conT1} = \frac{v_{0T}\hat{I}}{2\pi}\{\frac{J_0(x)}{\cos(\theta)} + pJ_1(x)\cos(\theta)\cos(\phi)\}. \quad \text{(B.119)}$$

With the same procedure, the second part of the conduction losses for IGBT T_{a+} can be calculated as

$$\begin{aligned} P_{conT2} &= f_s \sum_{k=k\phi}^{k\phi+p/2-1} \int_{\alpha_k-\delta_k}^{\alpha_k+\delta_k} (r_{0T_{a+}} i^2(t))\mathrm{d}t \\ &= \frac{r_{0T}\hat{I}^2}{4}\{\frac{1}{2} + \frac{M}{p}\frac{\cos(\phi)}{\sin(2\theta)} + \frac{J_1(2x)\sin(8\theta)\cos(\phi)}{2\pi\sin(2\theta)\sin(6\theta)}\}. \end{aligned} \quad \text{(B.120)}$$

The conduction losses of IGBT T_{a+} is now the sum of equation B.119 and equation B.120, this becomes

$$\begin{aligned} P_{conT} &= \frac{v_{0T}\hat{I}}{2\pi}\{\frac{J_0(x)}{\cos(\theta)} + pJ_1(x)\cos(\theta)\cos(\phi)\} \\ &+ \frac{r_{0T}\hat{I}^2}{4}\{\frac{1}{2} + \frac{M}{p}\frac{\cos(\phi)}{\sin(2\theta)} + \frac{J_1(2x)\sin(8\theta)\cos(\phi)}{2\pi\sin(2\theta)\sin(6\theta)}\}. \end{aligned} \tag{B.121}$$

This equation can be simplified more by the following approximations

$$\cos(\theta) = \cos(\frac{\pi}{2p}) \rightarrow 1, \quad \text{when} \quad p \rightarrow \infty \tag{B.122}$$

$$J_0(x) = J_0(\frac{M\pi}{2p}) \rightarrow 1, \quad \text{when} \quad p \rightarrow \infty \tag{B.123}$$

$$J_1(x) \rightarrow \frac{x}{2}, \quad \text{when} \quad p \rightarrow \infty \tag{B.124}$$

$$\frac{\sin(Ax)}{Bx} \rightarrow \frac{A}{B}, \quad \text{when} \quad p \rightarrow \infty. \tag{B.125}$$

With these simplifications equation B.121 becomes

$$P_{conT} = \frac{v_{0T}\hat{I}}{2\pi}(1 + \frac{\pi}{4}M\cos(\phi)) + \frac{r_{0T}\hat{I}^2}{2\pi}(\frac{\pi}{4} + \frac{2}{3}M\cos(\phi)). \tag{B.126}$$

With the same technique, the conduction losses for the diode D_{a-} can be calculated but with different integration limits, the losses becomes

$$\begin{aligned} P_{conD} &= f_s \sum_{k=k\phi}^{k\phi+p/2-1} \{\int_{\alpha_k-\frac{1}{2f_c}}^{\alpha_k-\delta_k} (v_{0D}i(t) + r_{0D}i^2(t))\mathrm{d}t \\ &+ \int_{\alpha_k+\delta_k}^{\alpha_k+\frac{1}{2f_c}} (v_{0D}i(t) + r_{0D}i^2(t))\mathrm{d}t\}. \end{aligned} \tag{B.127}$$

This equation can be solved as the equation for the IGBT but a simpler solution is to integrate the conduction losses over a half of the fundamental period and subtract the losses from the equation B.121 with the parameters for the diode inserted instead of the parameters for the IGBT, this becomes

$$\begin{aligned} P_{conD} &= f_s \int_{\frac{\phi}{\omega_s}}^{\frac{\phi}{\omega_s}+\frac{1}{2f_s}} (v_{0D}\hat{I}\sin(\omega_s t - \phi) + r_{0D}\hat{I}^2\sin^2(\omega_s t - \phi))\mathrm{d}t \\ &- \frac{v_{0D}\hat{I}}{2\pi}\{\frac{J_0(x)}{\cos(\theta)} + pJ_1(x)\cos(\theta)\cos(\phi)\} \\ &- \frac{r_{0D}\hat{I}^2}{4}\{\frac{1}{2} + \frac{M}{p}\frac{\cos(\phi)}{\sin(2\theta)} + \frac{J_1(2x)\sin(8\theta)\cos(\phi)}{2\pi\sin(2\theta)\sin(6\theta)}\} \\ &= \frac{v_{0D}\hat{I}}{2\pi}\{2 - \frac{J_0(x)}{\cos(\theta)} - pJ_1(x)\cos(\theta)\cos(\phi)\} \\ &+ \frac{r_{0D}\hat{I}^2}{4}\{\frac{1}{2} - \frac{M}{p}\frac{\cos(\phi)}{\sin(2\theta)} - \frac{J_1(2x)\sin(8\theta)\cos(\phi)}{2\pi\sin(2\theta)\sin(6\theta)}\}. \end{aligned} \tag{B.128}$$

This equation can be simplified in the same way as the equation for the IGBT and the simplified equation becomes

$$P_{conD} = \frac{v_{0D}\hat{I}}{2\pi}(1-\frac{\pi}{4}M\cos(\phi)) + \frac{r_{0D}\hat{I}^2}{2\pi}(\frac{\pi}{4}-\frac{2}{3}M\cos(\phi)). \quad \text{(B.129)}$$

The switching losses for the IGBT T_{a+} can be calculated by summing up equation B.99 each time the current alternates between IGBT T_{a+} and diode D_{a-}. With the same procedure as for the conducting losses the switching losses becomes

$$\begin{aligned}
P_{swT} &= f_s \sum_{k=k_\phi}^{k_\phi+\frac{p}{2}-1} \{A_{sw,on}U_{DC}i(\alpha_k-\delta_k) + A_{sw,off}U_{DC}i(\alpha_k+\delta_k)\} \\
&= f_s \sum_{k=k_\phi}^{k_\phi+\frac{p}{2}-1} \{A_{sw,on}U_{DC}\hat{I}\sin(\omega_s\alpha_k-\phi-\theta-x\sin(\omega_s\alpha_k)) \\
&+ A_{sw,off}U_{DC}\hat{I}\sin(\omega_s\alpha_k-\phi+\theta+x\sin(\omega_s\alpha_k))\} \\
&= f_s\hat{I}U_{DC}A_{sw,on}\{J_0(x)\cos(\theta)\frac{\cos(4\theta(1-k_\phi)+\phi)}{\sin(2\theta)} \\
&- J_0(x)\sin(\theta)\frac{\sin(4\theta(1-k_\phi)+\phi)}{\sin(2\theta)} - J_1(x)\sin(\theta+\phi)\frac{p}{2}\} \\
&+ f_s\hat{I}A_{sw,off}U_{DC}\{J_0(x)\cos(\theta)\frac{\cos(4\theta(1-k_\phi)+\phi)}{\sin(2\theta)} \\
&- J_0(x)\sin(\theta)\frac{\sin(4\theta(1-k_\phi)+\phi)}{\sin(2\theta)} + J_1(x)\sin(\phi-\theta)\frac{p}{2}\} \\
&= \frac{f_s\hat{I}U_{DC}A_{sw,on}}{2}\{\frac{J_0(x)}{\sin(\theta)} - pJ_1(x)\sin(\theta+\phi)\} \\
&+ \frac{f_s\hat{I}U_{DC}A_{sw,off}}{2}\{\frac{J_0(x)}{\sin(\theta)} + J_1(x)p\sin(\phi-\theta)\}. \quad \text{(B.130)}
\end{aligned}$$

This equation can be simplified in the same way as before, it becomes

$$\begin{aligned}
P_{swT} &= \frac{f_s\hat{I}U_{DC}A_{sw,on}}{2}\{\frac{1}{\theta} - \frac{M\pi}{4}(\theta\cos(\phi)+\sin(\phi))\} \\
&+ \frac{f_s\hat{I}U_{DC}A_{sw,off}}{2}\{\frac{1}{\theta} - \frac{M\pi}{4}(\theta\cos(\phi)-\sin(\phi))\}. \quad \text{(B.131)}
\end{aligned}$$

The switching losses for diode D_{a-} is obtain if $A_{sw,on}$ is substituted against $A_{sw,rec}$ and $A_{sw,off}$ is put to zero. This assumption can be made because when the IGBT is turned off, the diode begins to conduct the current as seen in figure B.22. But as noticed before, the on and off switching energies for the diode are insignificant. It is only the recovery energy that is of importance and it can be treated as a switch off energy. This leads to that the switching losses of the diode becomes

$$P_{swD} = \frac{f_s\hat{I}U_{DC}A_{sw,rec}}{2}(\frac{J_0(x)}{\sin(\theta)} - J_1(x)p\sin(\theta+\phi)). \quad \text{(B.132)}$$

Which can be simplified to

$$P_{swD} = \frac{f_s\hat{I}U_{DC}A_{swrecT}}{2}(\frac{1}{\theta} - \frac{M\pi}{4}(\theta\cos(\phi)+\sin(\phi))). \quad \text{(B.133)}$$

The total losses of one side of the converter can now be calculated as

$$P_{lossconv} = 6(P_{conT} + P_{conD} + P_{swT} + P_{swD}). \quad \text{(B.134)}$$

Where as shown above:

$$P_{conT} = \frac{v_{0T}\hat{I}}{2\pi}(\frac{J_0(x)}{\cos(\theta)} + pJ_1(x)\cos(\theta)\cos(\phi)) + \frac{r_{0T}\hat{I}^2}{4}(\frac{1}{2} + \frac{M}{p}\frac{\cos(\phi)}{\sin(2\theta)} + \frac{J_1(2x)\sin(8\theta)\cos(\phi)}{2\pi\sin(2\theta)\sin(6\theta)})$$
$$P_{conD} = \frac{v_{0D}\hat{I}}{2\pi}(2 - \frac{J_0(x)}{\cos(\theta)} - pJ_1(x)\cos(\theta)\cos(\phi)) + \frac{r_{0D}\hat{I}^2}{4}(\frac{1}{2} - \frac{M}{p}\frac{\cos(\phi)}{\sin(2\theta)} - \frac{J_1(2x)\sin(8\theta)\cos(\phi)}{2\pi\sin(2\theta)\sin(6\theta)})$$
$$P_{swT} = \frac{f_s\hat{I}U_{DC}A_{sw,on}}{2}(\frac{J_0(x)}{\sin(\theta)} - J_1(x)p\sin(\theta+\phi)) + \frac{f_s\hat{I}U_{DC}A_{sw,off}}{2}(\frac{J_0(x)}{\sin(\theta)} + J_1(x)p\sin(\phi-\theta))$$
$$P_{swD} = \frac{f_s\hat{I}U_{DC}A_{sw,rec}}{2}(\frac{J_0(x)}{\sin(\theta)} - J_1(x)p\sin(\theta+\phi)).$$

Or with the simplified equations:

$$P_{conT} = \frac{v_{0T}\hat{I}}{2\pi}(1 + \frac{\pi}{4}M\cos(\phi)) + \frac{r_{0T}\hat{I}^2}{2\pi}(\frac{\pi}{4} + \frac{2}{3}M\cos(\phi))$$
$$P_{conD} = \frac{v_{0D}\hat{I}}{2\pi}(1 - \frac{\pi}{4}M\cos(\phi)) + \frac{r_{0D}\hat{I}^2}{2\pi}(\frac{\pi}{4} - \frac{2}{3}M\cos(\phi))$$
$$P_{swT} = \frac{f_s\hat{I}U_{DC}A_{sw,on}}{2}(\frac{1}{\theta} - \frac{M\pi}{4}(\theta\cos(\phi) + \sin(\phi))) + \frac{f_s\hat{I}U_{DC}A_{sw,off}}{2}(\frac{1}{\theta} - \frac{M\pi}{4}(\theta\cos(\phi) - \sin(\phi)))$$
$$P_{swD} = \frac{f_s\hat{I}U_{DC}A_{swrecT}}{2}(\frac{1}{\theta} - \frac{M\pi}{4}(\theta\cos(\phi) + \sin(\phi))).$$

For converters with a sine modulation and an additional third harmonic the losses can be derived in the same way but with the following relations to begin with

$$\delta_k = \frac{1}{4f_c}(1 + M(\sin(\omega_s\alpha_k) + A_m\sin(3\omega_s\alpha_k))) \quad \text{(B.135)}$$

$$M = \frac{2\sqrt{2}U_s}{U_{DC}}, \quad \text{for} \quad A_m = \frac{1}{6}. \quad \text{(B.136)}$$

Where:

α_k	time at the middle of conducting pule number k
δ_k	half of the conducting time of pulse k
M	modulation index
A_m	modulation index for the third harmonic
U_s	RMS-value of the fundamental phase voltage

With this relations and the introduction of $y = A_m x$ the conducting and switching losses of one side of the converter can be calculated in the same way as the losses for the converter with only sine modulation. The total losses of the converter with sine and a third harmonic modulation becomes

$$P_{lossconv} = 6(P_{conT} + P_{conD} + P_{swT} + P_{swD}). \quad \text{(B.137)}$$

Where:

$$
\begin{aligned}
P_{conT} &= \tfrac{v_{0T}\hat{I}}{\pi}\{\tfrac{J_0(x)J_0(y)}{2\cos(\theta)} - J_1(x)J_1(y)\sin(\theta)[\tfrac{\cos(4\phi)+\cos(2\phi)}{\sin(6\theta)} - \tfrac{\cos(2\phi)}{\sin(2\theta)} - \tfrac{\cos(4\phi)}{\sin(10\theta)}] \\
&+\tfrac{p}{2}J_1(x)J_0(y)\cos(\theta)\cos(\phi)\} + \tfrac{r_{0T}\hat{I}^2}{4\pi}\{\tfrac{\pi}{2} + \tfrac{2x\cos(\phi)}{\sin(2\theta)} + \tfrac{2y\cos(3\phi)}{\sin(6\theta)} \\
&+J_1(2x)J_1(2y)\sin(2\theta)\cos(2\phi) + J_0(2y)J_1(2x)\tfrac{\sin(8\theta)\cos(\phi)}{2\sin(2\theta)\sin(6\theta)} \\
&-J_0(2x)J_1(2y)\cos(2\theta)[\tfrac{1}{\sin(2\theta)} + \tfrac{1}{\sin(10\theta)}]\cos(3\phi)\} \\
P_{conD} &= \tfrac{v_{0D}\hat{I}}{\pi}\{1 - \tfrac{J_0(x)J_0(y)}{2\cos(\theta)} + J_1(x)J_1(y)\sin(\theta)[\tfrac{\cos(4\phi)+\cos(2\phi)}{\sin(6\theta)} - \tfrac{\cos(2\phi)}{\sin(2\theta)} - \tfrac{\cos(4\phi)}{\sin(10\theta)}] \\
&-\tfrac{p}{2}J_1(x)J_0(y)\cos(\theta)\cos(\phi)\} + \tfrac{r_{0D}\hat{I}^2}{4\pi}\{\tfrac{\pi}{2} - \tfrac{2x\cos(\phi)}{\sin(2\theta)} - \tfrac{2y\cos(3\phi)}{\sin(6\theta)} \\
&-J_1(2x)J_1(2y)\sin(2\theta)\cos(2\phi) - J_0(2y)J_1(2x)\tfrac{\sin(8\theta)\cos(\phi)}{2\sin(2\theta)\sin(6\theta)} \\
&+J_0(2x)J_1(2y)\cos(2\theta)[\tfrac{1}{\sin(2\theta)} + \tfrac{1}{\sin(10\theta)}]\cos(3\phi)\} \\
P_{swT} &= f_s\hat{I}U_{DC}A_{sw,on}\{\tfrac{J_0(x)J_0(y)}{2\sin(\theta)} - \tfrac{p}{2}J_0(y)J_1(x)\sin(\phi+\theta) \\
&+J_1(x)J_1(y)[\tfrac{\cos(2\phi+\theta)}{\sin(2\theta)} - \tfrac{\cos(2\phi-\theta)}{\sin(6\theta)} + \tfrac{\cos(4\phi-\theta)}{\sin(10\theta)} - \tfrac{\cos(4\phi+\theta)}{\sin(6\theta)}]\} \\
&+f_s\hat{I}U_{DC}A_{sw,off}\{\tfrac{J_0(x)J_0(y)}{2\sin(\theta)} + \tfrac{p}{2}J_0(y)J_1(x)\sin(\phi-\theta) \\
&+J_1(x)J_1(y)[\tfrac{\cos(2\phi-\theta)}{\sin(2\theta)} - \tfrac{\cos(2\phi+\theta)}{\sin(6\theta)} + \tfrac{\cos(4\phi+\theta)}{\sin(10\theta)} - \tfrac{\cos(4\phi-\theta)}{\sin(6\theta)}]\} \\
P_{swD} &= f_s\hat{I}U_{DC}A_{sw,rec}\{\tfrac{J_0(x)J_0(y)}{2\sin(\theta)} - \tfrac{p}{2}J_0(y)J_1(x)\sin(\phi+\theta) \\
&+J_1(x)J_1(y)[\tfrac{\cos(2\phi+\theta)}{\sin(2\theta)} - \tfrac{\cos(2\phi-\theta)}{\sin(6\theta)} + \tfrac{\cos(4\phi-\theta)}{\sin(10\theta)} - \tfrac{\cos(4\phi+\theta)}{\sin(6\theta)}]\}.
\end{aligned}
$$

Or with the simplified equations:

$$
\begin{aligned}
P_{conT} &= \tfrac{v_{0T}\hat{I}}{2\pi}\{1 + \tfrac{\pi}{4}M\cos(\phi)\} + \tfrac{r_{0T}\hat{I}^2}{2\pi}\{\tfrac{\pi}{4} + \tfrac{2}{3}M\cos(\phi) - \tfrac{2MA_m}{15}\cos(3\phi)\} \\
P_{conD} &= \tfrac{v_{0D}\hat{I}}{2\pi}\{1 - \tfrac{\pi}{4}M\cos(\phi)\} + \tfrac{r_{0D}\hat{I}^2}{2\pi}\{\tfrac{\pi}{4} - \tfrac{2}{3}M\cos(\phi) + \tfrac{2MA_m}{15}\cos(3\phi)\} \\
P_{swT} &= \tfrac{f_s\hat{I}U_{DC}A_{sw,on}}{2}\{\tfrac{1}{\theta} - \tfrac{M\pi}{4}[\theta\cos(\phi)+\sin(\phi)] + \tfrac{M^2A_m\theta}{6}[\cos(2\phi) - \tfrac{\cos(4\phi)}{5}]\} \\
&+\tfrac{f_s\hat{I}U_{DC}A_{sw,off}}{2}\{\tfrac{1}{\theta} - \tfrac{M\pi}{4}[\theta\cos(\phi)-\sin(\phi)] + \tfrac{M^2A_m\theta}{6}[\cos(2\phi) - \tfrac{\cos(4\phi)}{5}]\} \\
P_{swD} &= \tfrac{f_s\hat{I}U_{DC}A_{sw,rec}}{2}\{\tfrac{1}{\theta} - \tfrac{M\pi}{4}[\theta\cos(\phi)+\sin(\phi)] + \tfrac{M^2A_m\theta}{6}[\cos(2\phi) - \tfrac{\cos(4\phi)}{5}]\}.
\end{aligned}
$$

For the low voltage converters, the losses in the switches are only used to modulate the losses in the converter. The losses in filters, DC link etc are neglected. In figure B.25 the losses on one side of the converter in figure B.20 are shown, for the two types of modulating techniques described in this appendix. The two converters are operating at rated output voltage and rated current and the rating are the same for both converters. The losses are shown as function of the angle ϕ between the voltage and current. From figure B.25 it is seen that the switching losses for the converter with sine and third harmonic is lower then for the converter with only sine modulation. This is due to the fact that the DC-voltage is lower for this converter since the rated voltage is the same for both types, compare equations B.93 and B.96. But for the conduction losses the difference is not that big. It depends on the change of conducting time for the diode and IGBT. As can be seen from figure B.25 the total losses of the sine and third harmonic modulated converter is lower then for the converter with sine modulation. Therefore the converter with the sine and third harmonic is used in this work.

For the high voltage converter, used in the transmission system, the filter inductance nearest the valves and the transformer shown to the left in figure B.20 are included in the loss model of the converter, all other losses are neglected. The inductors are assumed to be loss-less and have a rating of 0.14p.u, as the inductor used in ABB:s HVDC-light converter. The transformer is modulated as in appendix B.4. In figure B.26 the losses of the converter station from AC to DC are shown in percent of

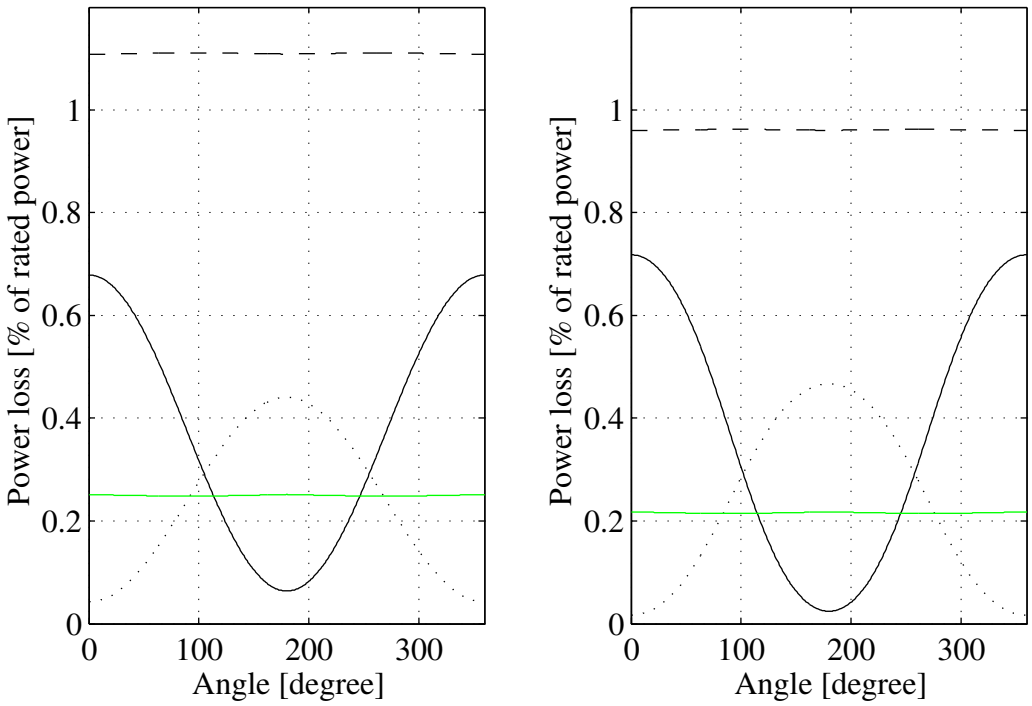

Figure B.25: Left plot losses for the sine modulated and right losses for the sine with a third harmonic modulated converter. Solid black is conduction losses for the IGBT, dashed switching losses for the IGBT, dotted conducting losses for the diode and solid grey switching losses for the diode.

the rated power. In this case, the consumed active power and produced reactive power are as in figure 4.2, active power solid and reactive power dashed. As can be seen in figure B.26 at rated operation, the switching losses are higher and the conducting losses are lower then for the low voltage converter in the right plot in figure B.25. It can be noticed that the high voltage station has an efficiency of approximately 97.8% at rated operation from AC to DC.

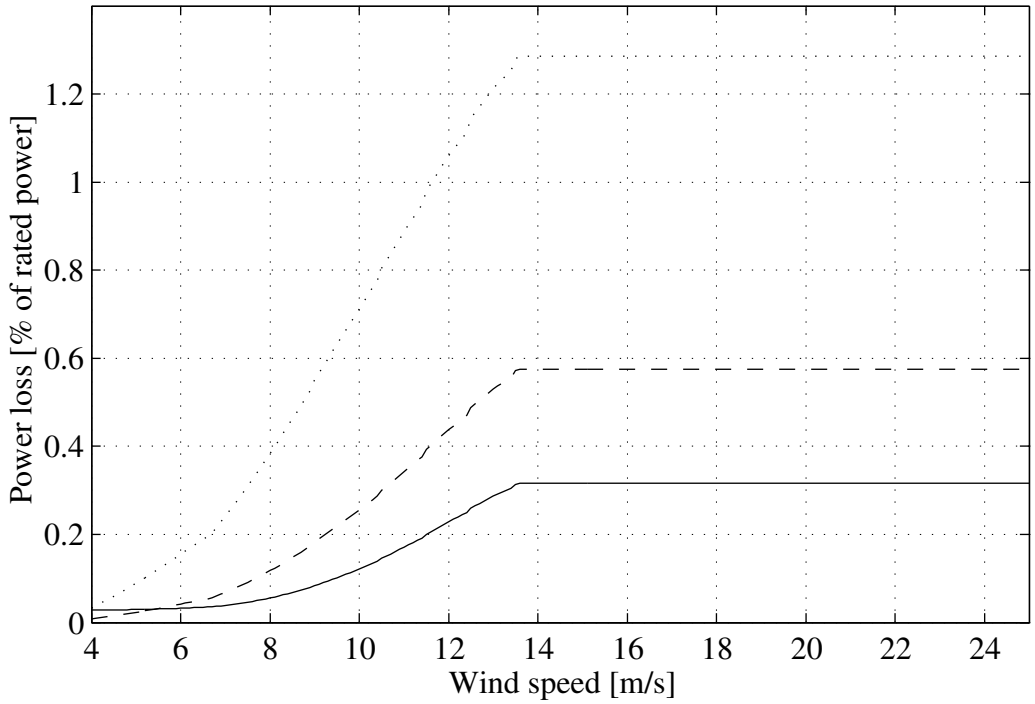

Figure B.26: Loses in the converter station. Solid transformer losses, dashed conduction losses in the valves and dotted switching losses in the valves.

B.6.3 Loss Model of the Boost Converter

For the loss calculations of the boost converter, presented in appendix A.2.1, the following assumptions are made:
The output capacitor, C_{out}, is lossless
Losses in the inductance ,L, can be represented by a resistance R_L
Conduction losses in the IGBT ,SW, can be represented by a resistance $R_{0,SW}$ and a voltage $V_{0,SW}$
The switch energies in the IGBT can be averaged to a power loss
Conduction losses in the diode ,D, can be represented by a resistance $R_{0,D}$ and a voltage $V_{0,D}$
The switch energies in the diode can be averaged to a power loss
The input and output voltages are smooth, V_{in} and V_{out}
The output current is smooth, I_{out}

With these assumptions the circuit scheme that includes the losses can be drawn as in figure B.27. In the figure, the scheme is drawn for the different conducting intervals of the boost converter. The last interval, $(D + D')T_s < t < T_s$, is when the current through the inductance is discontinuous, i.e equal to zero for a part of the switching period. The current source in figure B.27 expresses the switching losses for the diode and IGBT, where $D_{sw} = \frac{A_{on,SW}+A_{off,SW}+A_{rec,D}}{T_s}$ and A_x are described by equation B.99.

In the continuous current mode (CCM), $i_{in} > 0$, the ripple in the current through the inductance is assumed to be zero, which gives that $i_{in} = I_{in}$. This assumption gives that the voltage-second balance of the inductor can be expressed as

$$\begin{aligned} mean(v_L) &= (V_{in} - I_{in}(R_L + R_{0,SW}) - V_{0,SW})D \\ &+ (V_{in} - I_{in}(R_L + R_{0,D}) - V_{0,D} - V_{out})D' = 0. \end{aligned} \tag{B.138}$$

Where:
v_L Voltage over the inductor [V]
D Relative conducting time of the IGBT
D' Relative conducting time of the diode

This equation together with the fact that $D + D' = 1$, due to CCM, gives that the duty ratio can be express as

$$D = \frac{V_{out} - V_{in} - (R_L + R_{0,D})I_{in} + V_{0,D}}{V_{out} - (R_{0,SW} - R0, D)I_{in} - V_{0,SW} + V_{0,D}}. \tag{B.139}$$

In the same way, the actual ripple in the current through the inductor can be calculated according to

$$\Delta i_{in} = \frac{V_{in} - I_{in}(R_L + R_{0,SW}) - V_{0,SW}}{2L} DT_s. \tag{B.140}$$

Where:
T_s Switching period time [s]

If the current ripple Δi_{in} is greater then the mean value of the input current I_{in} the current through the inductance must be zero for a part of the switching period, se figure B.28. If this occurs the converter is operating in the discontinuous current mode (DCM) and for this the equation B.139 does not hold due to that $D + D' < 1$. As can

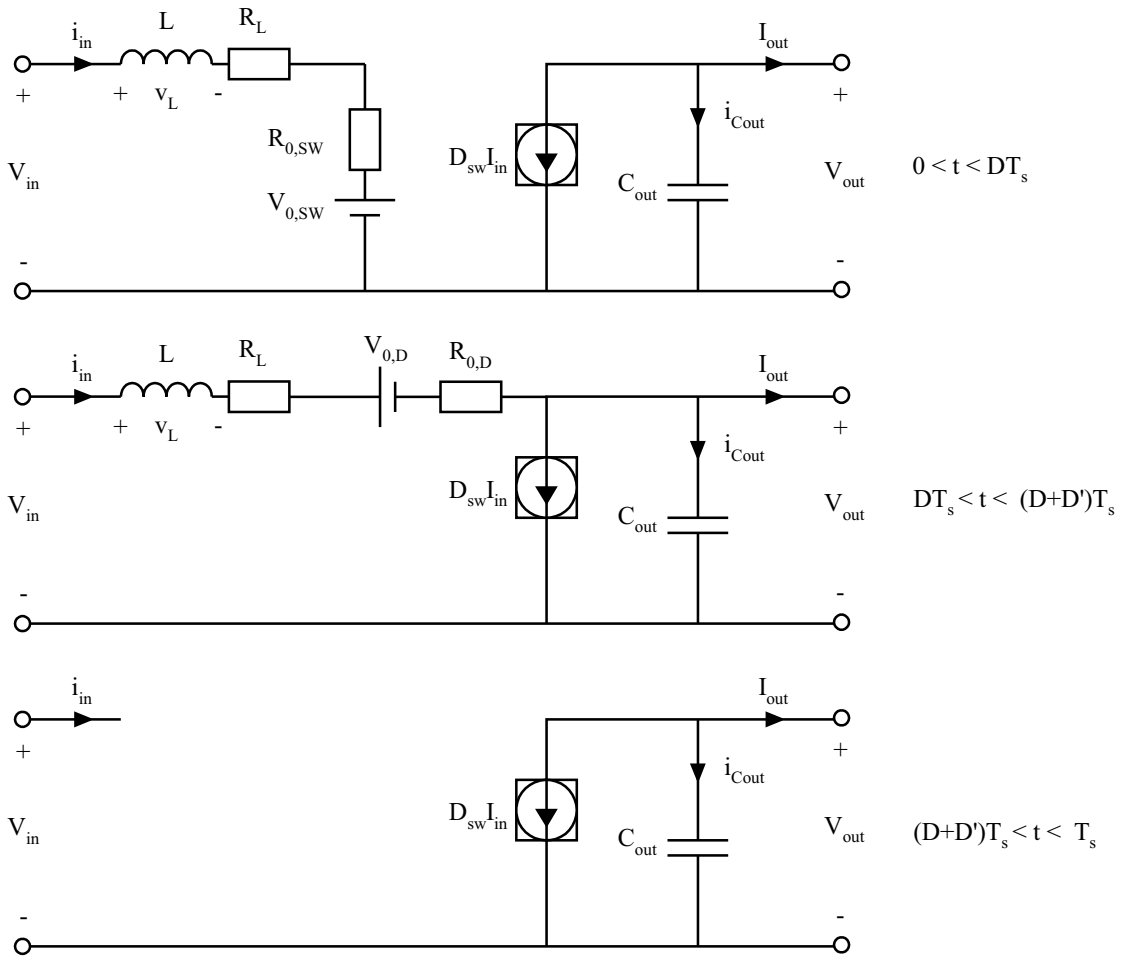

Figure B.27: The circuit scheme including the loss components for the boost converter.

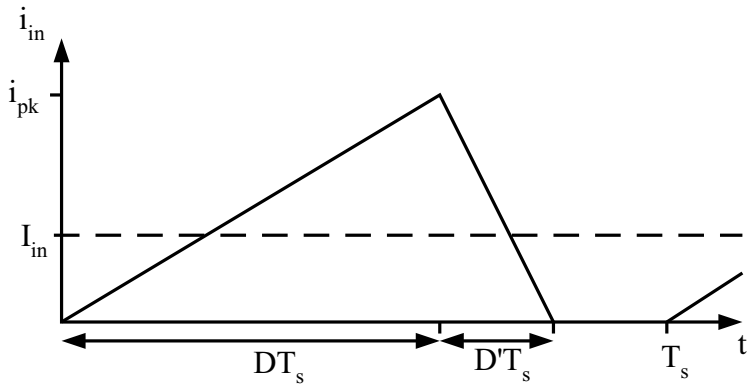

Figure B.28: The current through the inductance in DCM for the boost converter.

be noticed from figure B.28 the current trough the inductance can not be approximated to be smooth. But still the voltage drops over the loss resistances are approximated to be the resistance multiplied by the mean current through the inductance $V_x = R_x I_{in}$. This gives that the peak input current i_{pk}, the mean input current I_{in} and the mean

output current I_{out} can be expressed as

$$\begin{aligned} i_{pk} &= \frac{V_{in} - I_{in}(R_L + R_{0,SW}) - V_{0,SW}}{L} DT_s \\ I_{in} &= \frac{i_{pk}(D + D')T_s}{2} \frac{1}{T_s} = \frac{V_{in} - I_{in}(R_L + R_{0,SW}) - V_{0,SW}}{2L} D(D + D')T_s \end{aligned} \tag{B.141}$$

$$I_{out} = \frac{i_{pk} D' T_s}{2} \frac{1}{T_s} - I_{in} D_{sw} = I_{in}(\frac{D'}{D + D'} - D_{sw}). \tag{B.142}$$

Equation B.142 also holds for the mean output current in CCM, remember that $D + D' = 1$ for CCM. From equation B.141 and by setting up the volt-second balance of the inductor voltage the following equations are reached

$$\begin{aligned} D' &= \frac{2LI_{in}}{(V_{in} - I_{in}(R_L + R_{0,SW}) - V_{0,SW})DT_s} - D \\ mean(v_L) &= (V_{in} - I_{in}(R_L + R_{0,SW}) - V_{0,SW})D \\ &+ (V_{in} - I_{in}(R_L + R_{0,D}) - V_{0,D} - V_{out})D' = 0. \end{aligned}$$

These two equations gives that the duty ratio for DCM can be expressed as

$$D = \sqrt{\frac{2LI_{in}}{T_s} \frac{V_{out} - V_{in} + I_{in}(R_L + R_{0,D}) + V_{0,D}}{(V_{in} - I_{in}(R_L + R_{0,SW}) - V_{0,SW})(V_{out} + V_{0,D} - V_{0,SW} + I_{in}(R_{0,D} - R_{0,SW}))}}. \tag{B.143}$$

The losses in the components can be expressed as the integral of the voltage over the component multiplied with the current through it divided with the period time. This gives the following losses for both CCM and DCM

$$P_L = \frac{1}{T_s} \int_0^{(D+D')T_s} R_L I_{in} i_{in}(t) \mathrm{d}t = R_L I_{in}^2 \tag{B.144}$$

$$\begin{aligned} P_{con,SW} &= \frac{1}{T_s} \int_0^{DT_s} (V_{0,SW} + R_{0,SW} I_{in}) i_{in}(t) \mathrm{d}t \\ &= \frac{D}{D + D'} (V_{0,SW} + R_{0,SW} I_{in}) I_{in} \end{aligned} \tag{B.145}$$

$$\begin{aligned} P_{con,D} &= \frac{1}{T_s} \int_{DT_s}^{(D+D')T_s} (V_{0,D} + R_{0,D} I_{in}) i_{in}(t) \mathrm{d}t \\ &= \frac{D'}{D + D'} (V_{0,D} + R_{0,D} I_{in}) I_{in} \end{aligned} \tag{B.146}$$

$$P_{sw,SW} = \frac{A_{on,SW} + A_{off,SW}}{T_s} V_{out} I_{in} \tag{B.147}$$

$$P_{sw,D} = \frac{A_{rec,D}}{T_s} V_{out} I_{in}. \tag{B.148}$$

Where:

P_L	Losses in the inductor [W]
$P_{con,SW}$	Conduction losses in the IGBT [W]
$P_{con,D}$	Conduction losses in the diode [W]
$P_{sw,SW}$	Switching losses in the IGBT [W]
$P_{sw,D}$	Switching losses in the diode [W]

For the boost converter used in this work the switching frequency is set to 1kHz. In the same way as for the IGBT-converter in appendix B.6.2 a down-scaled model of the IGBT and diode is used. The same down-scaled parameters, base parameters, as used for the low voltage IGBT-converter are used for the boost converter in this work, the parameters are presented in table B.2. To obtain the parameters of the IGBT or diode with a specified rating equations B.100 - B.104 are used. In this work it is assumed that the losses in the inductance at rated operation of the boost converter are 0.1p.u.

With these assumptions and selections, the losses in the boost converter can be calculated. In figure B.29 the losses in the 2MW boost converter used in one of the DC wind turbines are shown. The converter has a fix output voltage of 5kV, an input voltage as the grey dashed line in the center plot of figure B.14 and an input power approximately as the dotted line in figure B.7.

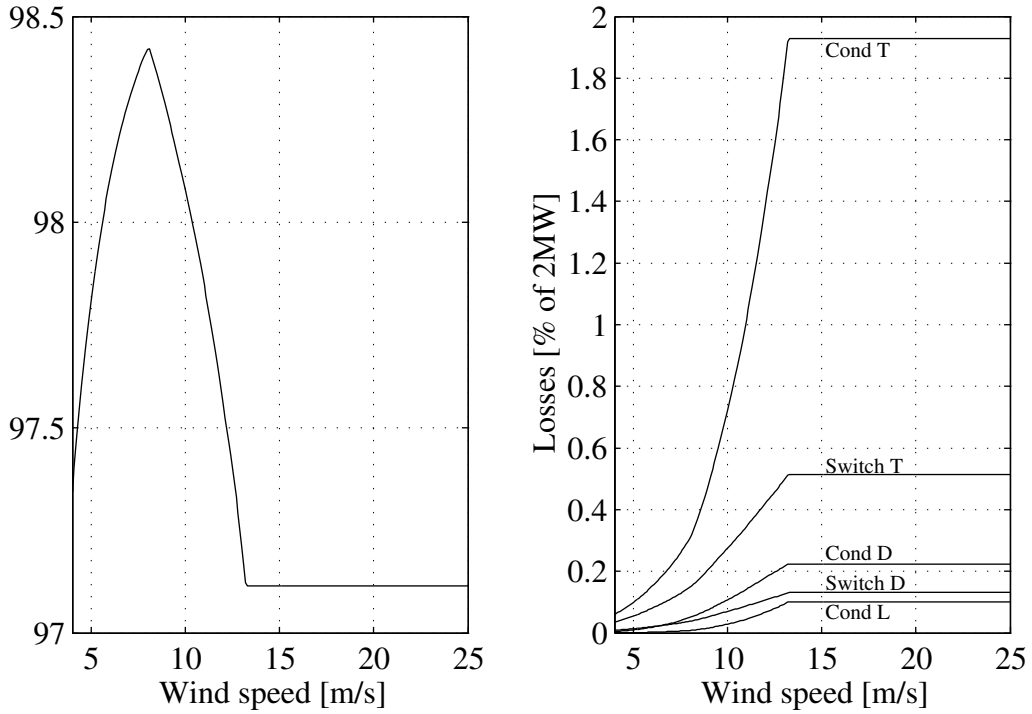

Figure B.29: Left plot shows the efficiency of the 2MW boost converter. The right plot shows the different losses in the converter. Cond stands for conduction losses, Switch for switching losses, T for IGBT, D for diode and L for the inductance.

B.6.4 Loss Model of the Full Bridge Converter

For the loss calculations of the full bridge converter, presented in appendix A.2.10, the following assumptions are made:

The output capacitor, C_{out}, is lossless
Losses in the inductance ,L, can be represented by a resistance R_L
Conduction losses in the IGBT ,SW, can be represented by a resistance $R_{0,SW}$
and a voltage $V_{0,SW}$
The switch energies in the IGBT can be averaged to a power loss
Conduction losses in the diode ,D, can be represented by a resistance $R_{0,D}$
and a voltage $V_{0,D}$
The switch energies in the diode can be averaged to a power loss
The leakage inductances in the transformer are neglected
The magnetizing current in the transformer is neglected
The conducting losses for the transformer are represented by
two resistances, R_{cu1} and R_{cu2}
The core losses are represented by a resistor R_{fe} parallel to
the magnetizing inductanse
The input and output voltages are smooth, V_{in} and V_{out}
The output current is smooth, I_{out}

With these assumptions the circuit scheme that includes the losses can be drawn as in figure B.30. In the figure the scheme is drawn for the different conducting intervals of the full bridge converter for the first half of the period. For the second half the scheme is identical. The last interval, $(D + D')T_s < t < \frac{T_s}{2}$, is for when the current through the inductance is discontinuous, equal to zero for a part of the switching period. The current sources in figure B.30 expresses the switching losses for the diode and IGBT. Where $D_{sw,SW} = 4\frac{A_{on,SW}+A_{off,SW}}{T_s}$, $D_{sw,D} = 4\frac{A_{rec,D}}{T_s}$ and A_x are described by equation B.99.

In the continuous current mode (CCM), $i_L > 0$, the ripple in the current through the inductance is assumed to be zero, which gives that $i_L = I_L$. This assumption gives that the voltage-second balance of the inductor can be expressed as

$$\begin{aligned} mean(v_L) &= (\frac{n_2}{n_1}V_{Lm,D} - V_{out} - 2V_{0,D} - I_L(R_{cu2} + R_{0,D} + R_L))2D \\ &- (V_{out} + 2V_{0,D} + I_L(R_L + R_{0,D}))2D' = 0 \qquad \text{(B.149)} \\ i_{Rfe,D} &= \frac{V_{Lm,D}}{R_{fe}} \qquad \text{(B.150)} \\ I_{SW,D} &= \frac{n_2}{n_1}I_L + i_{Rfe,D} \qquad \text{(B.151)} \\ V_{Lm,D} &= V_{in} - 2V_{0,SW} - (2R_{0,SW} + R_{cu1})I_{SW,D}. \qquad \text{(B.152)} \end{aligned}$$

Where:

v_L	Voltage over the inductor [V]
D	Relative conducting time of the IGBT
D'	Relative conducting time of the diode
$i_{Rfe,D}$	Current through the iron loss resistance under the conducting interval of the IGBT
$I_{SW,D}$	Current through the IGBT under the conducting interval of the IGBT
$V_{Lm,D}$	Voltage over the iron loss resistance under the conducting interval of the IGBT

This equation together with that $2D + 2D' = 1$, due to CCM, gives that the duty

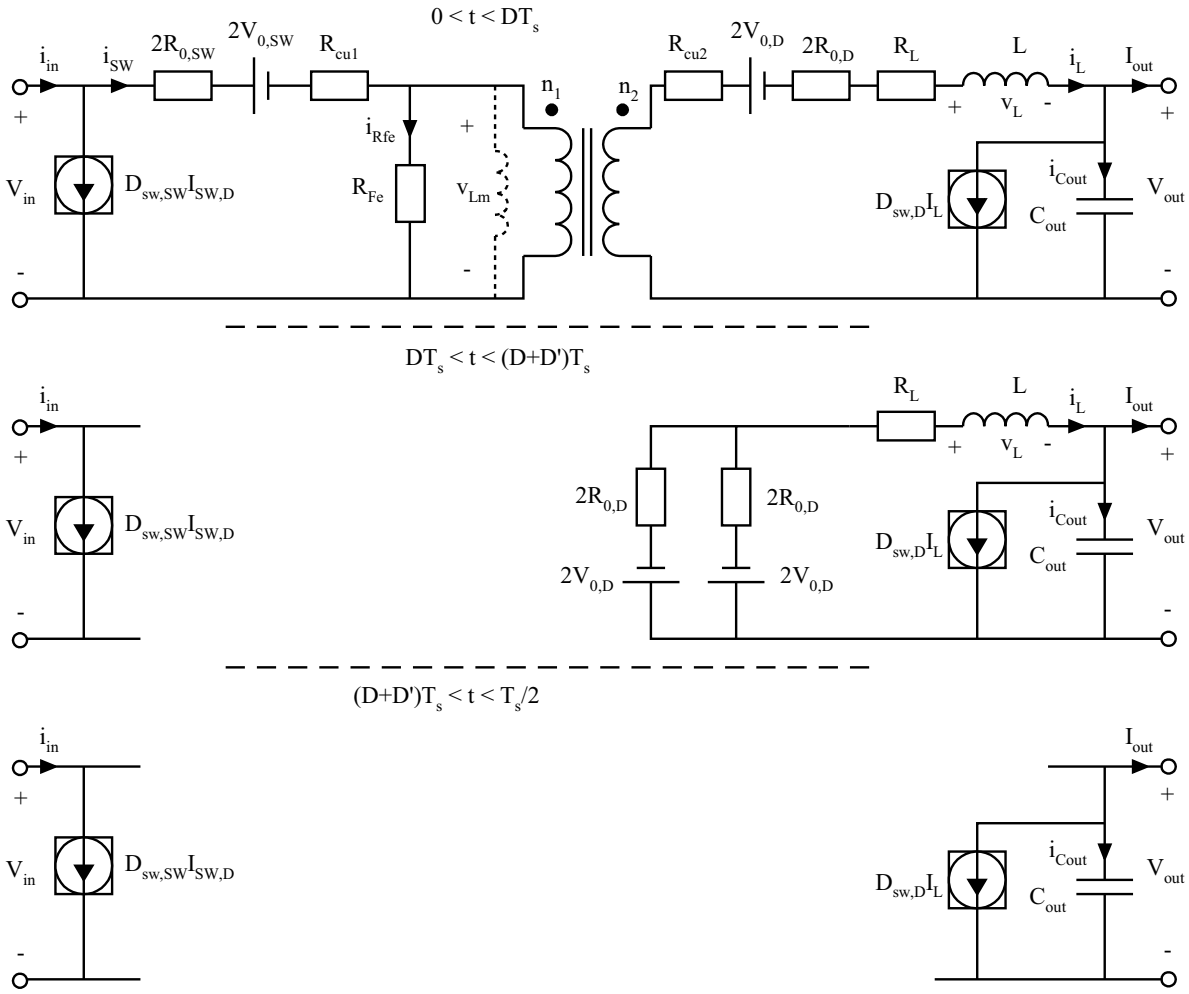

Figure B.30: The circuit scheme including the loss components for the full bridge converter.

ratio can be express as

$$2D = \frac{V_{out} + 2V_{0,D} + (R_L + R_{0,D})I_L}{\frac{R_{fe}}{R_{fe}+2R_{0,SW}+R_{cu1}}\frac{n_2}{n_1}(V_{in} - 2V_{o,SW}) - \frac{(2R_{0,SW}+R_{cu1})R_{fe}}{R_{fe}+2R_{0,SW}+R_{cu1}}(\frac{n_2}{n_1})^2 I_L - (R_{cu2} + R_{0,D})I_L}. \quad \text{(B.153)}$$

In the same way the actual ripple in the current through the inductor can be calculated to

$$\Delta i_L = \frac{V_{out} + 2V_{0,D} + I_L(R_L + R_{0,D})}{2L}(\frac{1}{2} - D)T_s. \quad \text{(B.154)}$$

Where:
T_s Switching period time [s]

If the current ripple Δi_L is greater then the mean value of the inductor current I_L the current through the inductance must be zero for a part of the switching period, se figure B.31. If this occurs, the converter is operating in the discontinuous current mode (DCM) and for this the equation B.153 does not hold due to that $2D + 2D' < 1$. As

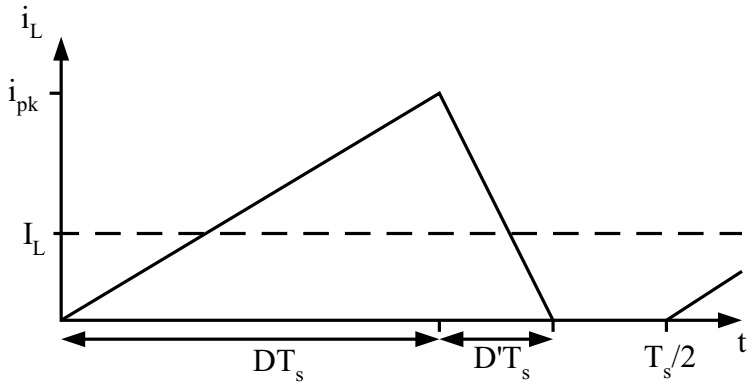

Figure B.31: The current through the inductance in DCM for the full bridge converter.

can be noticed from figure B.31 the current trough the inductance can not be approximated to be smooth. But the voltage drops over the loss resistances are approximated to be constant over the switching period. The voltage drop over the resistances are described by the following equations

$$V_{Rin} = (2R_{0,SW} + R_{cu1})I_{SW,D} \tag{B.155}$$
$$V_{Rout} = (R_{cu2} + 2R_{o,D} + R_L)I_L \tag{B.156}$$
$$I_{SW,D} = \frac{n_2}{n_1}I_L + i_{Rfe,D} \tag{B.157}$$
$$i_{Rfe,D} = \frac{V_{Lm,D}}{R_{fe}} \tag{B.158}$$
$$V_{Lm,D} = V_{in} - 2V_{0,SW} - V_{Rin}. \tag{B.159}$$

Where:

V_{Rin}	Voltage over the resistances on the input side [V]
V_{Rout}	Voltage over the resistances on the output side [V]
I_L	Mean value of the current through the inductor [A]
$i_{Rfe,D}$	Current through the iron loss resistance under the conducting interval of the IGBT
$I_{SW,D}$	Current through the IGBT under the conducting interval of the IGBT
$V_{Lm,D}$	Voltage over the iron loss resistance under the conducting interval of the IGBT

This gives that the peak inductor current i_{pk}, the mean inductor current I_L and the mean output current I_{out} can be expressed as

$$i_{pk} = \frac{V_{out} + 2V_{0,D} + I_L(R_L + R_{0,D})}{L}D'T_s$$
$$I_L = \frac{i_{pk}(D + D')T_s}{2}\frac{2}{T_s} = \frac{V_{out} + 2V_{0,D} + I_{in}(R_L + R_{0,D})}{L}D(D + D')T_s \tag{B.160}$$
$$I_{out} = I_L(1 - D_{sw,D}). \tag{B.161}$$

From equation B.160 and by setting up the volt-second balance of the inductor voltage

the following equations are reached:

$$\begin{aligned} D &= \frac{LI_L}{(V_{out} + 2V_{0,D} + I_L(R_L + R_{0,D}))D'T_s} - D' \\ mean(v_L) &= (\frac{n_2}{n_1}V_{Lm,D} - V_{out} - 2V_{0,D} - I_L(R_{cu2} + R_{0,D} + R_L))2D \\ &- (V_{out} + 2V_{0,D} + I_L(R_L + R_{0,D}))2D' = 0. \end{aligned}$$

These two equations gives that the duty ratio for the diodes for DCM can be expressed as

$$D' = \sqrt{\frac{LI_L}{T_s}} \cdot \sqrt{\frac{\frac{n_2}{n_1}\frac{R_{fe}}{R_{fe}+2R_{0,SW}+R_{cu1}}(V_{in}-2V_{0,SW})-V_{out}-2V_{0,D}-I_L(R_{cu2}+R_L+2R_{0,D}+(\frac{n_2}{n_1})^2\frac{R_{fe}(2R_{0,SW}+R_{cu1})}{R_{fe}+2R_{0,SW}+R_{cu1}})}{(V_{out}+2V_{0,D}+I_L(R_L+R_{0,D}))(\frac{n_2}{n_1}\frac{R_{fe}}{R_{fe}+2R_{0,SW}+R_{cu1}}(V_{in}-2V_{0,SW})+V_{0,D}-I_L(R_{cu2}+R_{0,D}+(\frac{n_2}{n_1})^2\frac{R_{fe}(2R_{0,SW}+R_{cu1})}{R_{fe}+2R_{0,SW}+R_{cu1}}))}}. \tag{B.162}$$

The losses in the components can be expressed as the integral of the voltage over the component multiplied with the current through it divided with the period time.

This gives the following losses for both CCM and DCM

$$\begin{aligned} I_{in} &= \frac{n_2}{n_1}\left(\frac{D}{D+D'} + D_{sw,SW} - (2D + D_{sw,SW})\frac{2R_{0,SW} + R_{cu1}}{R_{fe} + 2R_{0,SW} + R_{cu1}}\right)I_L \\ &+ (2D + D_{sw,SW})\frac{V_{in} - 2V_{0,SW}}{R_{fe} + 2R_{0,SW} + R_{cu1}} \end{aligned} \tag{B.163}$$

$$I_{out} = I_L(1 - D_{sw,D}) \tag{B.164}$$

$$P_L = \frac{2}{T_s}\int_0^{(D+D')T_s} R_L I_L i_L(t)\mathrm{d}t = R_L I_L^2 \tag{B.165}$$

$$\begin{aligned} P_{con,SW} &= \frac{2}{T_s}\int_0^{DT_s} (2V_{0,SW} + 2R_{0,SW} I_{SW,D}) i_{SW}(t)\mathrm{d}t \\ &= (2V_{0,SW} + 2R_{0,SW}(\frac{n_2}{n_1}I_L - \frac{2R_{0,SW} + R_{cu1}}{R_{fe} + 2R_{0,SW} + R_{cu1}}\frac{n_2}{n_1}I_L + \frac{V_{in} - 2V_{0,SW}}{R_{fe} + 2R_{0,SW} + R_{cu1}})) \\ &\quad (\frac{D}{D+D'}\frac{n_2}{n_1}I_L - 2D\frac{2R_{0,SW} + R_{cu1}}{R_{fe} + 2R_{0,SW} + R_{cu1}}\frac{n_2}{n_1}I_L + 2D\frac{V_{in} - 2V_{0,SW}}{R_{fe} + 2R_{0,SW} + R_{cu1}}) \end{aligned} \tag{B.166}$$

$$\begin{aligned} P_{con,D} &= \frac{2}{T_s}\int_0^{DT_s} (2V_{0,D} + 2R_{0,D} I_L) i_L(t)\mathrm{d}t + \frac{2}{T_s}\int_{DT_s}^{(D+D')T_s} (2V_{0,D} + R_{0,D} I_L) i_L(t)\mathrm{d}t \\ &= 2V_{0,D} I_L + R_{0,D}\frac{2D + D'}{D + D'} I_L^2 \end{aligned} \tag{B.167}$$

$$P_{sw,SW} = D_{sw,SW} V_{in}(\frac{n_2}{n_1}I_L - \frac{2R_{0,SW} + R_{cu1}}{R_{fe} + 2R_{0,SW} + R_{cu1}}\frac{n_2}{n_1}I_L + \frac{V_{in} - 2V_{0,SW}}{R_{fe} + 2R_{0,SW} + R_{cu1}}) \tag{B.168}$$

$$P_{sw,D} = D_{sw,SW} V_{out} I_L \tag{B.169}$$

$$\begin{aligned} P_{con,Tr} &= R_{cu1}(\frac{n_2}{n_1}I_L - \frac{2R_{0,SW} + R_{cu1}}{R_{fe} + 2R_{0,SW} + R_{cu1}}\frac{n_2}{n_1}I_L + \frac{V_{in} - 2V_{0,SW}}{R_{fe} + 2R_{0,SW} + R_{cu1}}) \\ &\quad (\frac{D}{D+D'}\frac{n_2}{n_1}I_L - 2D\frac{2R_{0,SW} + R_{cu1}}{R_{fe} + 2R_{0,SW} + R_{cu1}}\frac{n_2}{n_1}I_L + 2D\frac{V_{in} - 2V_{0,SW}}{R_{fe} + 2R_{0,SW} + R_{cu1}}) \\ &+ R_{cu2}\frac{D}{D + D'} I_L^2 \end{aligned} \tag{B.170}$$

$$P_{cor,Tr} = 2R_{fe}(\frac{V_{in} - 2V_{0,SW}}{R_{fe} + 2R_{0,SW} + R_{cu1}} - \frac{2R_{0,SW} + R_{cu1}}{R_{fe} + 2R_{0,SW} + R_{cu1}}\frac{n_2}{n_1}I_L)^2 D. \tag{B.171}$$

Where:

I_{in}	Expression for the input current, valid for CCM and DCM
I_{out}	Expression for the output current, valid for CCM and DCM
P_L	Losses in the inductor [W]
$P_{con,SW}$	Conduction losses in the IGBT [W]
$P_{con,D}$	Conduction losses in the diode [W]
$P_{sw,SW}$	Switching losses in the IGBT [W]
$P_{sw,D}$	Switching losses in the diode [W]
$P_{con,Tr}$	Copper losses in the transformer [W]
$P_{cor,Tr}$	Iron losses in the transformer [W]

For the full bridge converter the switching frequency is selected to be the same as for the boost converter, 1kHz. In the same way as for the boost converter a down-scaled model of the IGBT and diode is used. The down-scaled parameters, base parameters, are presented in table B.2. To obtain the parameters of the IGBT or diode given a

specified rating, equations B.100 - B.104 are used. In this work, the losses of the high frequency transformer are assumed to be equal to the losses of a 50Hz transformer with the same VA rating. In the same way as for the boost converter the losses in the inductance at rated operation are assumed to be 0.1p.u.

With these assumptions and selections the losses in the full bridge converter can be calculated. In figure B.32 the losses in the 2MW full bridge converter used in one of the DC wind turbines are shown. The converter has a fixed output voltage of 40kV, an input voltage as the grey dashed line in the center plot of figure B.14 and an input power approximately as the dotted line in figure B.7.

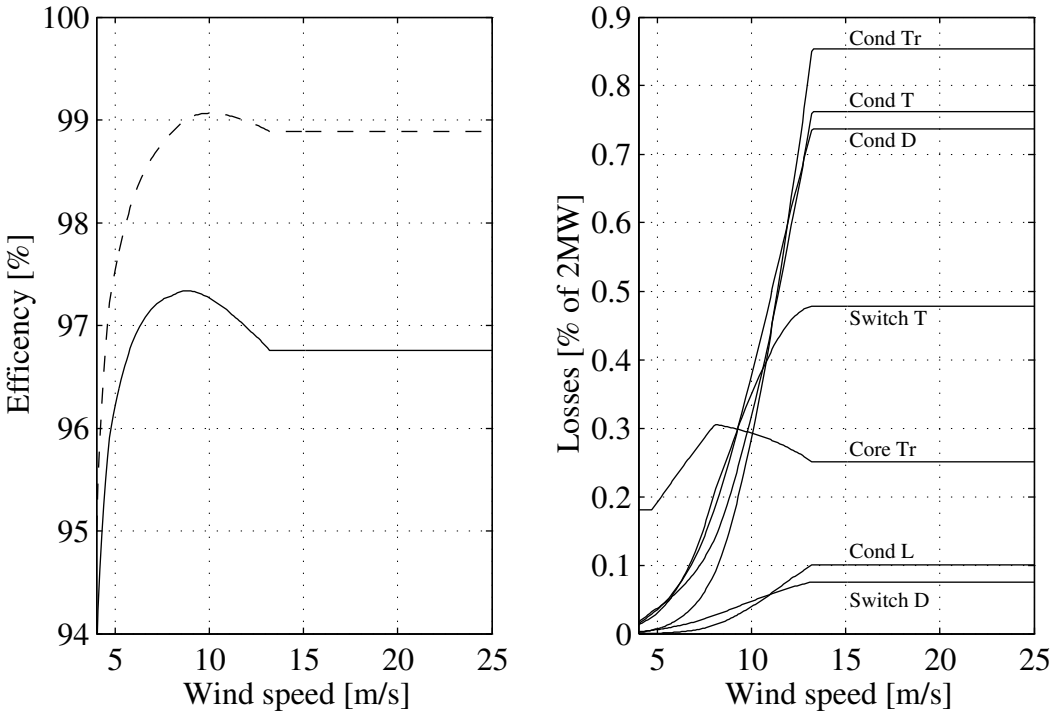

Figure B.32: The solid line in the left plot shows the efficiency of the 2MW full bridge converter and dashed line the efficiency for the transformer. The right plot shows the different losses in the converter. Cond stands for conduction losses, Switch for switching losses, Core for losses in the transformer core, T for IGBT, D for diode, Tr for transformer and L for the inductance.

B.6.5 Loss Model of the Full Bridge Isolated Boost Converter

For the loss calculations of the full bridge isolated boost converter, presented in appendix A.2.13, the following assumptions are made:

The output capacitor, C_{out}, is lossless
Losses in the inductance ,L, can be represented by a resistance R_L
Conduction losses in the IGBT ,SW, can be represented by a resistance $R_{0,SW}$ and a voltage $V_{0,SW}$
The switch energies in the IGBT can be averaged to a power loss
Conduction losses in the diode ,D, can be represented by a resistance $R_{0,D}$ and a voltage $V_{0,D}$
The switch energies in the diode can be averaged to a power loss
The leakage inductances in the transformer are neglected
The magnetizing current in the transformer is neglected
The conducting losses for the transformer are represented by two resistances, R_{cu1} and R_{cu2}
The core losses are represented by a resistor R_{fe} parallel to the magnetizing inductanse
The input and output voltages are smooth, V_{in} and V_{out}
The output current is smooth, I_{out}

With these assumptions, the circuit scheme that includes the losses can be drawn as in figure B.33. In the figure, the scheme is drawn for the different conducting intervals of the full bridge isolated boost converter and for the first half of the period. For the second half of the period, the scheme is identical. The last interval, $(D + D')T_s < t < \frac{T_s}{2}$, in figure B.33 is representing the situations when the current through the inductance is discontinuous, equal to zero for a part of the switching period. The current source in figure B.33 expresses the switching losses for the diode and IGBT. Where $D_{sw} = 4\frac{A_{on,SW}+A_{off,SW}+A_{rec,D}}{T_s}$ and A_x are described by equation B.99.

In the continuous current mode (CCM), $i_{in} > 0$, the ripple in the current through the inductance is assumed to be zero, which gives that $i_{in} = I_{in}$. This assumption gives that the voltage-second balance of the inductor can be expressed as

$$\begin{aligned} mean(v_L) &= 0 = (V_{in} - 2V_{0,SW} - I_{in}(R_L + R_{0,SW}))2D \\ &+ (V_{in} - 2V_{0,SW} - I_{in}(R_L + 2R_{0,SW} + R_{cu1}) - V_{Lm,D'})2D' \quad \text{(B.172)} \\ i_{Rfe,D'} &= \frac{V_{Lm,D'}}{R_{fe}} \quad \text{(B.173)} \\ V_{Lm,D'} &= \frac{n_1}{n_2}(V_{out} + 2V_{0,D} + (2R_{0,D} + R_{cu2})\frac{n_1}{n_2}(I_{in} - i_{Rfe,D'})). \quad \text{(B.174)} \end{aligned}$$

Where:

v_L	Voltage over the inductor [V]
D	Relative conducting time of the IGBT
D'	Relative conducting time of the diode
$i_{Rfe,D'}$	Current through the iron loss resistance under the conducting interval of the diode
$V_{Lm,D'}$	Voltage over the iron loss resistance under the conducting interval of the diode

This equation together with that $2D + 2D' = 1$, due to CCM, gives that the duty ratio can be express as

$$2D' = \frac{V_{in} - 2V_{0,SW} - I_{in}(R_L + R_{0,SW})}{\frac{R_{fe}}{R_{fe}+(2R_{0,D}+R_{cu2})(\frac{n_1}{n_2})^2}\frac{n_1}{n_2}(V_{out} + 2V_{0,D}) + (R_{0,SW} + R_{cu1} + \frac{R_{fe}(2R_{0,D}+R_{cu2})(\frac{n_1}{n_2})^2}{R_{fe}+(2R_{0,D}+R_{cu2})(\frac{n_1}{n_2})^2})I_{in}}. \quad \text{(B.175)}$$

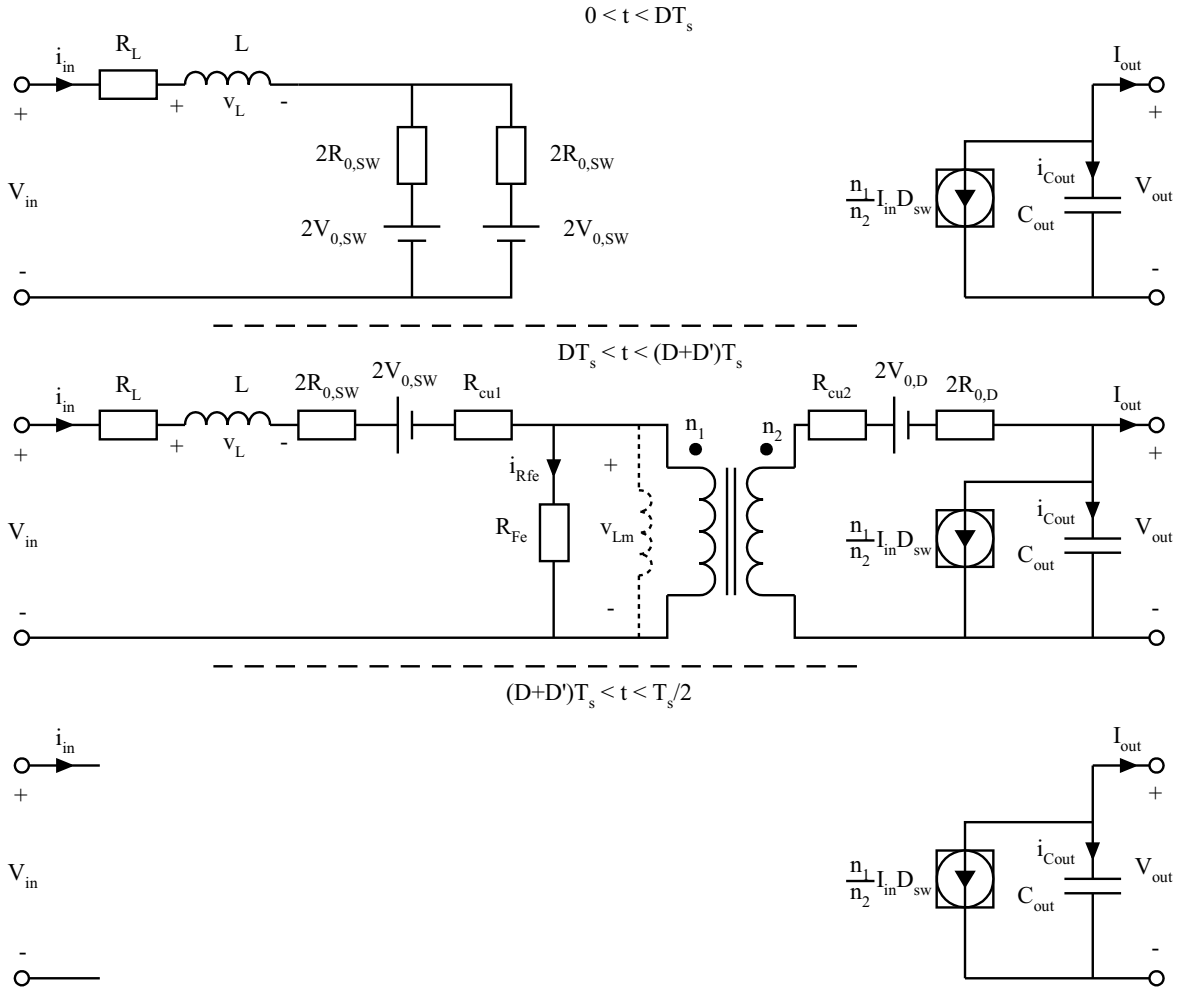

Figure B.33: The circuit scheme including the loss components for the full bridge isolated boost converter.

In the same way the actual ripple in the current through the inductor can be calculated to

$$\Delta i_{in} = \frac{V_{in} - 2V_{0,SW} - I_{in}(R_L + R_{0,SW})}{2L} DT_s. \tag{B.176}$$

Where:
T_s Switching period time [s]

If the current ripple Δi_{in} is greater then the mean value of the inductor current I_{in}, the current through the inductance must be zero for a part of the switching period, see figure B.34. If this occurs, the converter is operating in the discontinuous current mode (DCM) and for this the equation B.175 does not hold due to that $2D + 2D' < 1$. As can be noticed from figure B.34 the current trough the inductance can not be approximated to be smooth. But the voltage drops over the loss resistances are approximated to be constant over the switching period. The voltage drop over the resistances are

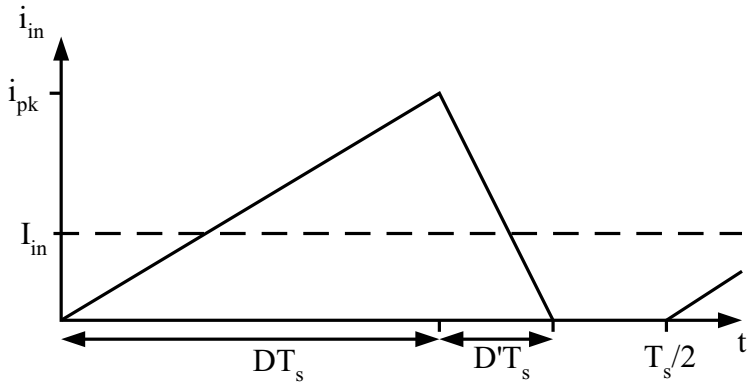

Figure B.34: The current through the inductance in DCM for the full bridge isolated boost converter.

described by the following equations

$$
\begin{aligned}
V_{Rin,D} &= (R_L + R_{0,SW})I_{in} && \text{(B.177)}\\
V_{Rin,D'} &= (R_L + 2R_{0,SW} + R_{cu1})I_{in} && \text{(B.178)}\\
V_{Rout} &= (R_{cu2} + 2R_{0,D})\frac{n_1}{n_2}(I_{in} - i_{Rfe,D'}) && \text{(B.179)}\\
i_{Rfe,D'} &= \frac{V_{Lm,D'}}{R_{fe}} && \text{(B.180)}\\
V_{Lm,D'} &= V_{in} - 2V_{0,SW} - V_{Rin}. && \text{(B.181)}
\end{aligned}
$$

Where:

$V_{Rin,D}$	Voltage over the resistances on the input side under the conducting interval of the IGBT [V]
$V_{Rin,D'}$	Voltage over the resistances on the input side under the conducting interval of the diode [V]
V_{Rout}	Voltage over the resistances on the output side [V]
$i_{Rfe,D'}$	Current through the iron loss resistance under the conducting interval of the diode
$V_{Lm,D'}$	Voltage over the iron loss resistance under the conducting interval of the diode

This gives that the peak inductor current i_{pk}, the mean input current I_{in} and the mean output current I_{out} can be expressed as

$$
\begin{aligned}
i_{pk} &= \frac{V_{in} - 2V_{0,SW} - I_{in}(R_L + R_{0,SW})}{L}DT_s\\
I_{in} &= \frac{i_{pk}(D + D')T_s}{2}\frac{2}{T_s} = \frac{V_{in} - 2V_{0,SW} - I_{in}(R_L + R_{0,SW})}{L}D(D + D')T_s.
\end{aligned}
\qquad \text{(B.182)}
$$

From equation B.182 and by setting up the volt-second balance of the inductor voltage

the following equations are reached

$$\begin{aligned} D' &= \frac{LI_{in}}{(V_{in} - 2V_{0,SW} - I_{in}(R_L + R_{0,SW}))DT_s} - D \\ mean(v_L) &= (V_{in} - 2V_{0,SW} - I_{in}(R_L + R_{0,SW}))2D \\ &+ (V_{in} - 2V_{0,SW} - I_{in}(R_L + 2R_{0,SW} + R_{cu1}) - V_{Lm,D'})2D' = 0. \end{aligned}$$

These two equations gives that the duty ratio for DCM can be expressed as

$$D' = \sqrt{\frac{LI_{in}}{T_s}} \cdot \sqrt{\frac{\frac{n_1}{n_2}\frac{R_{fe}}{R_{fe}+(2R_{0,D}+R_{cu2})(\frac{n_1}{n_2})^2}(V_{out}+2V_{0,D})-V_{in}+2V_{0,SW}+I_{in}(R_{cu1}+R_L+2R_{0,SW}+\frac{R_{fe}(2R_{0,D}+R_{cu2})(\frac{n_1}{n_2})^2}{R_{fe}+(2R_{0,D}+R_{cu2})(\frac{n_1}{n_2})^2})}{(V_{in}-2V_{0,SW}-I_{in}(R_L+R_{0,SW}))(\frac{n_1}{n_2}\frac{R_{fe}}{R_{fe}+(2R_{0,D}+R_{cu2})(\frac{n_1}{n_2})^2}(V_{out}+2V_{0,D})+I_{in}(R_{cu1}+R_{0,SW}+\frac{R_{fe}(2R_{0,D}+R_{cu2})(\frac{n_1}{n_2})^2}{R_{fe}+(2R_{0,D}+R_{cu2})(\frac{n_1}{n_2})^2}))}}. \quad \text{(B.183}$$

The losses in the components can be expressed as the integral of the voltage over the component multiplied with the current through it divide with the period time.

This gives the following losses for both CCM and DCM

$$
\begin{aligned}
I_{out} &= \frac{n_1}{n_2}\left(\frac{D'}{D+D'} - D_{sw,D} - 2D'\frac{(2R_{0,D}+R_{cu2})(\frac{n_1}{n_2})^2}{R_{fe}+(2R_{0,D}+R_{cu2})(\frac{n_1}{n_2})^2}\right)I_{in} \\
&- \left(\frac{n_1}{n_2}\right)^2\frac{2D'}{R_{fe}+(2R_{0,D}+R_{cu2})(\frac{n_1}{n_2})^2}(V_{out}+2V_{0,D}) \qquad \text{(B.184)} \\
P_L &= \frac{1}{T_s}\int_0^{T_s} R_L I_{in} i_{in}(t)\mathrm{d}t = R_L I_{in}^2 \qquad \text{(B.185)} \\
P_{con,SW} &= \frac{2}{T_s}\int_0^{DT_s}(2V_{0,SW}+R_{0,SW}I_{in})i_{in}(t)\mathrm{d}t + \frac{2}{T_s}\int_{DT_s}^{(D+D')T_s}(2V_{0,SW}+2R_{0,SW}I_{in})i_{in}(t)\mathrm{d}t \\
&= 2V_{0,SW}I_{in} + (1+\frac{D'}{D+D'})R_{0,SW}I_{in}^2 \qquad \text{(B.186)} \\
P_{con,D} &= \frac{2}{T_s}\int_{DT_s}^{(D+D')T_s}(2V_{0,D}+2R_{0,D}\frac{n_1}{n_2}(I_{in}-i_{Rfe,D'}))\frac{n_1}{n_2}(i_{in}(t)-i_{Rfe,D'})\mathrm{d}t \\
&= 2D'\frac{n_1}{n_2}\left(R_{0,D}\frac{n_1}{n_2}\frac{R_{fe}I_{in}-\frac{n_1}{n_2}(V_{out}+2V_{0,D})}{R_{fe}+(2R_{0,D}+R_{cu2})(\frac{n_1}{n_2})^2}\right) \\
&\left(\frac{I_{in}}{D+D'} - 2\frac{\frac{n_1}{n_2}(V_{out}+2V_{0,D})+I_{in}(2R_{0,D}+R_{cu2})(\frac{n_1}{n_2})^2}{R_{fe}+(2R_{0,D}+R_{cu2})(\frac{n_1}{n_2})^2}\right) \qquad \text{(B.187)} \\
P_{sw,SW} &= 4\frac{n_1}{n_2}\frac{A_{on,SW}+A_{off,SW}}{T_s}V_{out}I_{in} \qquad \text{(B.188)} \\
P_{sw,D} &= 4\frac{n_1}{n_2}\frac{A_{rec,D}}{T_s}V_{out}I_{in} \qquad \text{(B.189)} \\
P_{con,Tr} &= R_{cu1}\frac{D'}{D+D'}I_{in}^2 + R_{cu2}(\frac{n_1}{n_2})^2\frac{R_{fe}I_{in}-\frac{n_1}{n_2}(V_{out}+2V_{0,D})}{R_{fe}+(2R_{0,D}+R_{cu2})(\frac{n_1}{n_2})^2} \\
&\left(\frac{I_{in}D'}{D+D'} - 2D'\frac{\frac{n_1}{n_2}(V_{out}+2V_{0,D})+I_{in}(2R_{0,D}+R_{cu2})(\frac{n_1}{n_2})^2}{R_{fe}+(2R_{0,D}+R_{cu2})(\frac{n_1}{n_2})^2}\right) \qquad \text{(B.190)} \\
P_{cor,Tr} &= 2R_{fe}\left(\frac{\frac{n_1}{n_2}(V_{out}+2V_{0,D})+I_{in}(2R_{0,D}+R_{cu2})(\frac{n_1}{n_2})^2}{R_{fe}+(2R_{0,D}+R_{cu2})(\frac{n_1}{n_2})^2}\right)^2 D'. \qquad \text{(B.191)}
\end{aligned}
$$

Where:

I_{out}	Expression for the output current, valid for CCM and DCM
P_L	Losses in the inductor [W]
$P_{con,SW}$	Conduction losses in the IGBT [W]
$P_{con,D}$	Conduction losses in the diode [W]
$P_{sw,SW}$	Switching losses in the IGBT [W]
$P_{sw,D}$	Switching losses in the diode [W]
$P_{con,Tr}$	Copper losses in the transformer [W]
$P_{cor,Tr}$	Iron losses in the transformer [W]

The same assumptions and selections that was made for the full bridge converter in appendix B.6.4 are made for the full bridge isolated boost converter also. With these assumptions and selections, the losses in the full bridge isolated boost converter can be calculated. In figure B.35 the losses in the 2MW full bridge boost converter converter used in the series connected DC wind turbines are shown. The converter has a fix output voltage of 20kV, an input voltage as the grey dashed line in the center plot of

figure B.14 and an input power approximately as the dotted line in figure B.7.

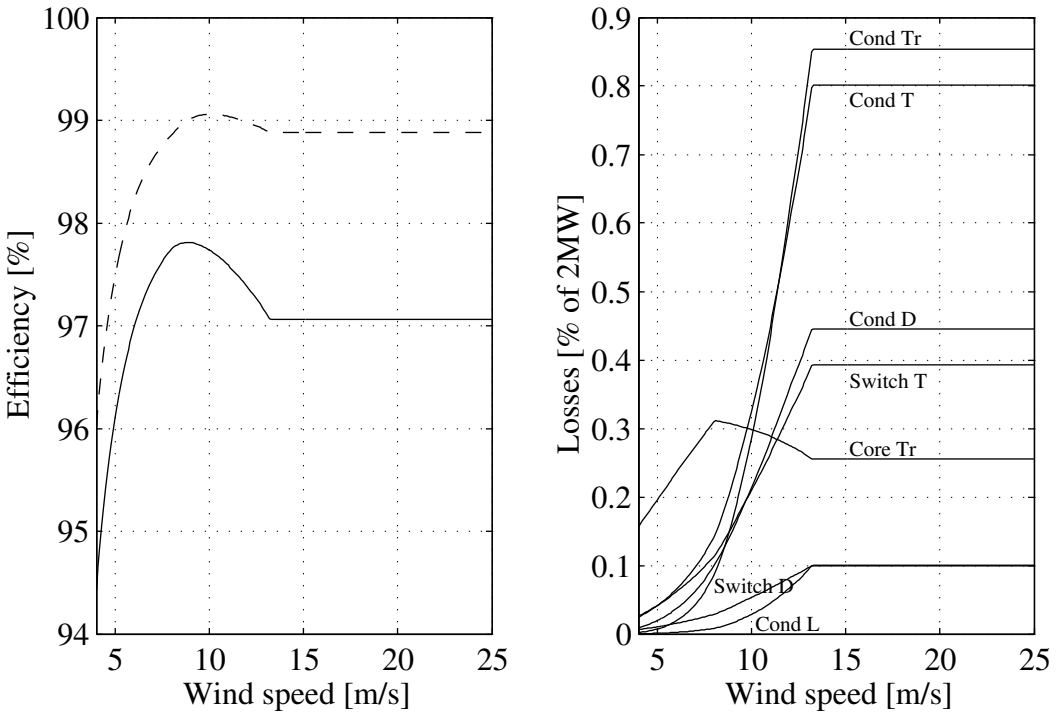

Figure B.35: Left plot shows the efficiency of the 2MW full bridge isolated boost converter, solid, and the efficiency for the transformer, dashed. The right plot shows the different losses in the converter. Cond stands for conduction losses, Switch for switching losses, Core for losses in the transformer core, T for IGBT, D for diode, Tr for transformer and L for the inductance.

Appendix C

Cost models

Due to that many of the sources who have help to contribute with cost information for different components in the wind park want to be anonymous, no references to these sources will be made. In some cases the information has been manipulated in order to hide its origin. In these cases it is described how the manipulation is done so that the reader will be able to critically check the information.

C.1 Energy production cost

The energy production cost is defined as how much it cost to produce and deliver a unit of energy to the grid, i.e to the PCC. This gives that the total investment cost of the wind farm is divided with the total energy delivered to the PCC. The total investment cost is calculated assuming that the whole investment is made in the first year and paid off during the life time of the wind farm. In addition, it is also assumed that some profit shall be made. The total energy that is delivered to the PCC is calculated by multiplying the average power delivered to the PCC with the average number of operational hours during one year multiplied with the lifetime of the wind park. The average power is calculated with equation 4.1. With these assumptions the energy production cost can be calculated as in equation C.1.

$$E_{cost} = \frac{\text{Invest}}{P_{out,AVG}T} \frac{r(1+r)^N}{(1+r)^N - 1} \frac{100}{100 - PR} = K \frac{\text{Invest}}{P_{out,AVG}} \tag{C.1}$$

Where:

E_{cost}	Energy production cost [SEK/kWh]
Invest	Investment [SEK]
$P_{out,AVG}$	Average output power [kW]
T	Average operational hour under one year [h]
r	Interest rate [-]
N	Lifetime of the wind farm [years]
PR	Profit in %
K	Constant

The life time of the wind farm is in this work set to 25 years, the interest rate to 4%, the profit to 3% and the average operational hours during one year is set to $365 \cdot 24 = 8760$. This gives that the production cost gets about 65% higher then

without profit and interest rate, ie. $K = 7.53 \cdot 10^{-6}$ with interest rate and profit and $K = \frac{1}{TN} = 4.57 \cdot 10^{-6}$ without.

As can be seen from equation C.1 the losses in the wind farm does not appear explicitly. Indirect they affects the production cost due to that an increase of the losses, decreases the average output power. To include the losses more directly in the energy production cost, an input power most be defined. The input power to the wind park is defined as the shaft power of a full variable speed wind turbine, described in chapter 3.4, multiplied with the number of wind turbines in the wind park. Note, that this way of defining the input power introduces extra power loss for fix speed wind turbines since these do not operate with the optimum λ value for low wind speeds, se chapter 3. The cost of the losses in the wind park is defined as the difference between the energy production cost calculated with equation C.1 with the average output power and the energy production cost calculated with equation C.1 with the average input power as P_{AVG}. With these definitions the energy production cost can be divided into two parts, as can be seen in equation C.2.

$$E_{cost} = E_{cost,invest} + E_{cost,loss} = K\frac{\text{Invest}}{P_{in,AVG}} + K\frac{\text{Invest}}{P_{in,AVG}}\frac{P_{loss,AVG}}{P_{out,AVG}} \tag{C.2}$$

Where:

E_{cost}	Energy production cost [SEK/kWh]
$E_{cost,invest}$	Energy production cost from the investment [SEK/kWh]
$E_{cost,loss}$	Energy production cost from the losses [SEK/kWh]
K	Constant, defined in equation C.1
Invest	Investment [SEK]
$P_{in,AVG}$	Average input power [kW]
$P_{out,AVG}$	Average output power [kW]
$P_{loss,AVG}$	Average losses in the wind park [kW]

From equation C.2 the contribution from each component in the wind park to the energy production cost can be defined. This is due to the fact that the investment, I, is the sum of the costs of all components and the mean power loss is the sum of the average power losses in each component. This gives that the contribution to the energy production cost from one component, $c1$, is defined as in equation C.3.

$$E_{cost,c1} = E_{cost,invest,c1} + E_{cost,loss,c1} = K\frac{I_{c1}}{P_{in,AVG}} + K\frac{\text{Invest}}{P_{in,AVG}}\frac{P_{loss,c1,AVG}}{P_{out,AVG}} \tag{C.3}$$

Where:

$E_{cost,c1}$	Contribution to the energy production cost from component $c1$ [SEK/kWh]
$E_{cost,invest,c1}$	Contribution from the cost of component $c1$ [SEK/kWh]
$E_{cost,loss,c1}$	Contribution from the losses in component $c1$ [SEK/kWh]
K	Constant, defined in equation C.1
Invest	Investment [SEK]
I_{c1}	Cost of component $c1$ [SEK]
$P_{in,AVG}$	Average input power [kW]
$P_{out,AVG}$	Average output power [kW]
$P_{loss,c1,AVG}$	Average losses in the component $c1$ [kW]

Equation C.3 will be used in this work, to divide the energy production cost into the contributions from different components and their cost and losses.

C.2 Wind turbine

The cost of the wind turbine includes a 20, 30 or 50kV transformer but does not include the foundation. The cost information that the cost model is based on comes from different wind turbine manufactures (six), in the power range from 0.5 to 2.5MW and with different electrical systems. The cost was assumed to be a linear function of the output power, as shown in equation C.4.

$$\text{Cost}_{WT} = A_p + B_p P_{rated} \tag{C.4}$$

Where:

Cost_{WT}	Cost of the wind turbine [MSEK]
P_{rated}	Rated output power [MW]
$A_p = -1.46$	Offset constant
$B_p = 8.38$	Slope constant

As seen from the equation C.4 the offset is negative which means that the model does not apply to wind turbines with an output power less the the smallest wind turbine used to derived the model. In figure C.1 the cost information given is shown after the output power is normalized to 2MW. The normalization was done in the following way: The difference between 2MW and the rated power of the wind turbine was multiplied with the slop constant B_p from equation C.4 and then added to the given price of the wind turbine. The circles in figure C.1 shows the cost information used to calculate the

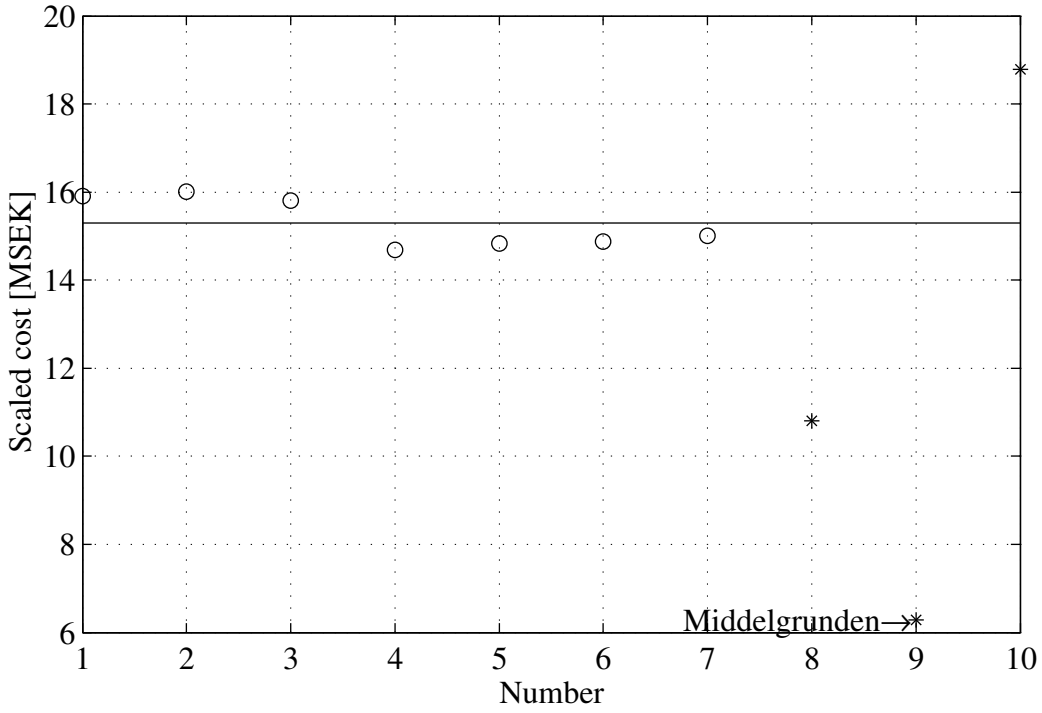

Figure C.1: The cost of the wind turbines after normalizing the output power to 2MW. Circles denotes the costs used to determine the constants in equation C.4, stars the costs that was not used and the solid line the cost for a 2MW wind turbine from the cost model.

constants in equation C.4 and the stars shows three outliers that was not used. From

equation C.4 and figure C.1 it can be observed that the cost of a 2MW wind turbine is approximately 15.3MSEK. The most interesting outlier denoted Middelgrunden in figure C.1 is the cost from the home page the Middelgrunden wind park [52].

The cost model for wind turbines presented in equation C.4 is used for all wind turbine types in this work. For the DC wind turbines in this work, it is assumed that they cost the same as a AC wind turbine with the same output power. This assumption is made based on the fact that an AC variable speed wind turbine has the same components as a DC variable speed wind turbine, compere figures 4.6 and 4.11.

C.3 Transformer

The model developed for the cost of transformers is based on the rated power. The cost information given is for transformers with rated power in the range 6.3 to 150MVA and high voltage side in the range 47 to 140kV and low voltages side in the range 10.5 to 77kV. The model developed is non-linear because it follows the given information best. The model is described as

$$Cost_{TR} = A_p + B_p P_{rated}^{\beta}. \tag{C.5}$$

Where:

$Cost_{TR}$	Cost of the transformer [SEK]
P_{rated}	Rated output power [VA]
$A_p = -1.208 \cdot 10^6$	Offset constant, if linear model $= 1.724 \cdot 10^6$
$B_p = 2143$	Slope constant, if linear model $= 0.04838$
$\beta = 0.4473$	Exponent if, linear model $= 1$

From equation C.5 it is noticed that the offset for the non-linear model is negative which gives that the model does not represent the cost for smaller transformers. In figure C.2 the information is represented by the circles and the model by the solid curve, the linear model is represented by the dashed line. From figure C.2 it is seen that the non-linear model represents the given information best.

C.4 Cables

The cable cost model is more detailed due to that more information about the cost as function of conductor area and rated voltage are known. The cost model of the AC cables is based on the rated power of the cables, as shown in equation C.6.

$$\text{Cost}_{AC} = A_p + B_p \exp(\frac{C_p S_n}{10^8}) \tag{C.6}$$

$$S_n = \sqrt{3} U_{rated} I_{rated} \tag{C.7}$$

Where:

Cost_{AC}	Cost of the AC cables [SEK/km]
U_{rated}	Rated voltage of the cable, line to line [V]
I_{rated}	Rated current of the cable [A]
A_p, B_p, C_p	Cost constants
S_n	Rated power of the cable [VA]

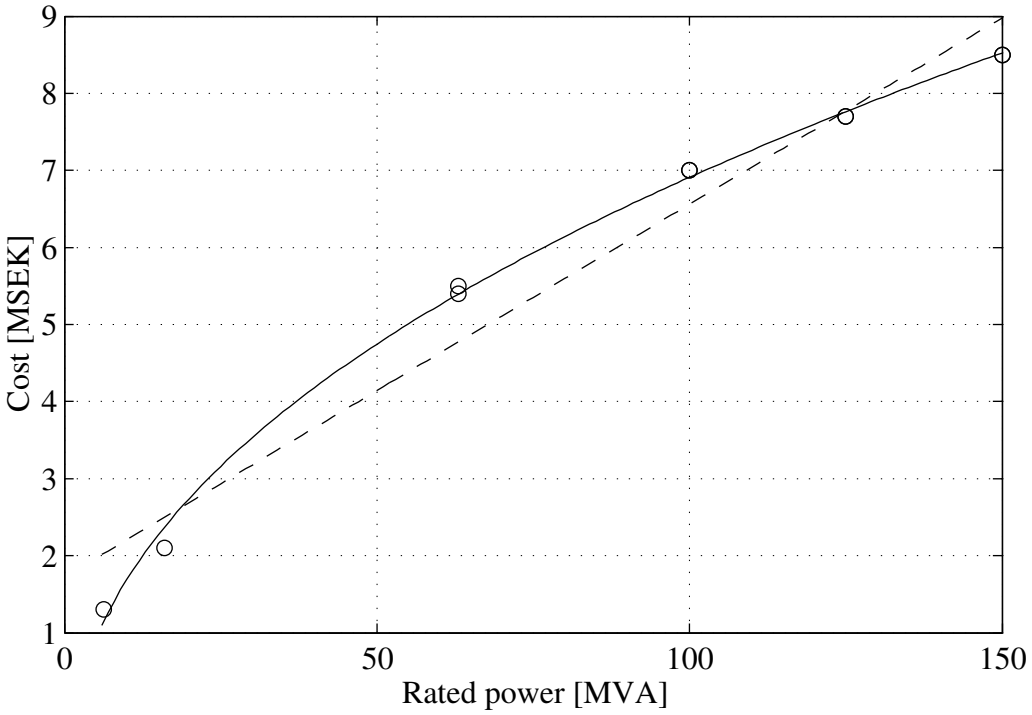

Figure C.2: The cost of the transformer, circles costs obtained, solid model in equation C.5 and dashed linear model ($\beta = 1$).

Table C.1: Cost parameters for AC cables, for different voltages.

Rated voltage [kV]	A_p $[10^6]$	B_p $[10^6]$	C_p
22	0.284	0.583	6.15
33	0.411	0.596	4.1
45	0.516	0.612	3
66	0.688	0.625	2.05
132	1.971	0.209	1.66
220	3.181	0.11	1.16

In table C.1 the parameters that are used in this work for the AC cable cost model are shown, for the different rated voltages. As can be noticed from equation C.6 and table C.1 the cost of the AC cables increases exponential with the rated power of the cable. It can also be noticed that the cost increases linearly with the cable length. In figure C.3 the cost model of the AC cables that are used in this work are shown, as solid lines, and the given costs as circles. The costs of the cables are shown for the rated powers that where available for each voltage level. As can be noticed from figure C.3 the cost model represents the given costs well.

In the same way as for the AC cables the cost model of the DC cables is based on the rated power of the cable. In equation C.8 the cost model is shown and as can be seen it is a linear model instead of the exponential used for the AC cables.

$$\text{Cost}_{DC} = A_p + B_p P_n \tag{C.8}$$

$$P_n = U_{rated} I_{rated} \tag{C.9}$$

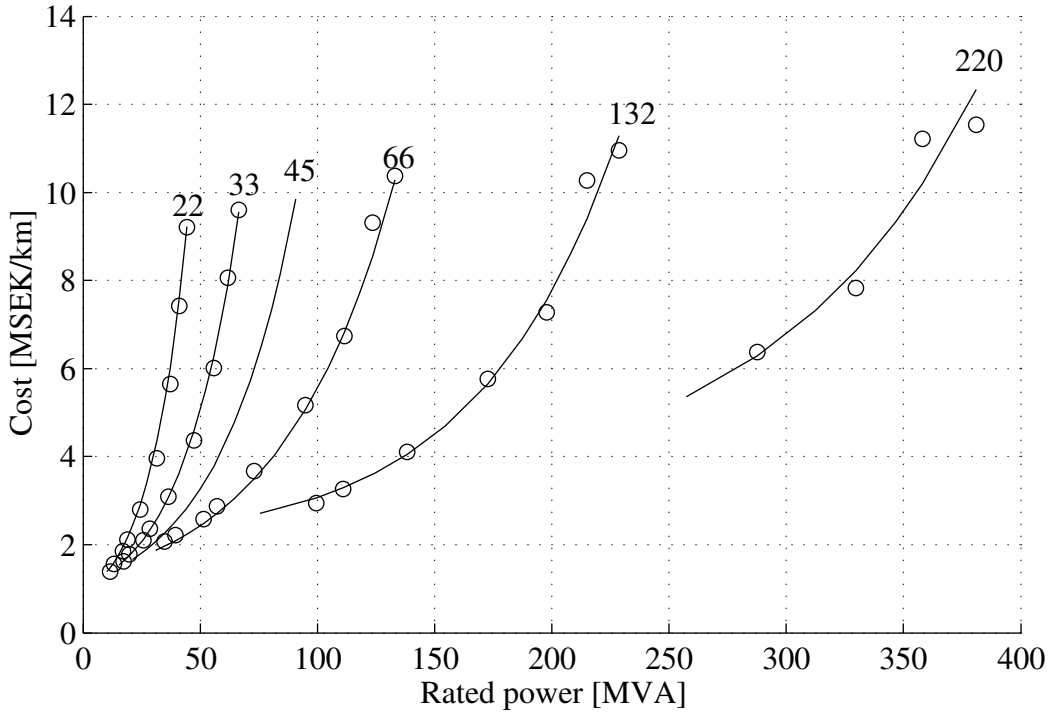

Figure C.3: The cost of the AC cables used in this work, circles costs obtained, solid model in equation C.6. The numbers in the figure indicates the rated line to line voltage of the cable in kV.

Where:

Cost_{DC}	Cost of the DC cables [SEK/km]
U_{rated}	Rated voltage of the cable, pole to pole [V]
I_{rated}	Rated current of the cable [A]
A_p, B_p	Cost constants
P_n	Rated power of the cable [W]

In table C.2 the parameters that are used in this work for the AC cable cost model are shown, for the different rated voltages. As can be noticed from equation C.8 and

Table C.2: Cost parameters for different voltages.

Rated voltage [kV]	A_p $[10^6]$	B_p
5	-0.346	0.408
40	-0.314	0.0618
160	-0.1	0.0164
230	0.079	0.0120
300	0.286	0.00969

table C.2 the cost of the DC cables increases linearly with the rated power of the cable and with the cable length. In figure C.4 the cost model of the DC cables that are used in this work are shown, as solid lines, and the given costs as circles. The costs of the cables are shown for the rated powers that where available for each voltage level. As can be noticed from figure C.4 the cost model represents the given costs well.

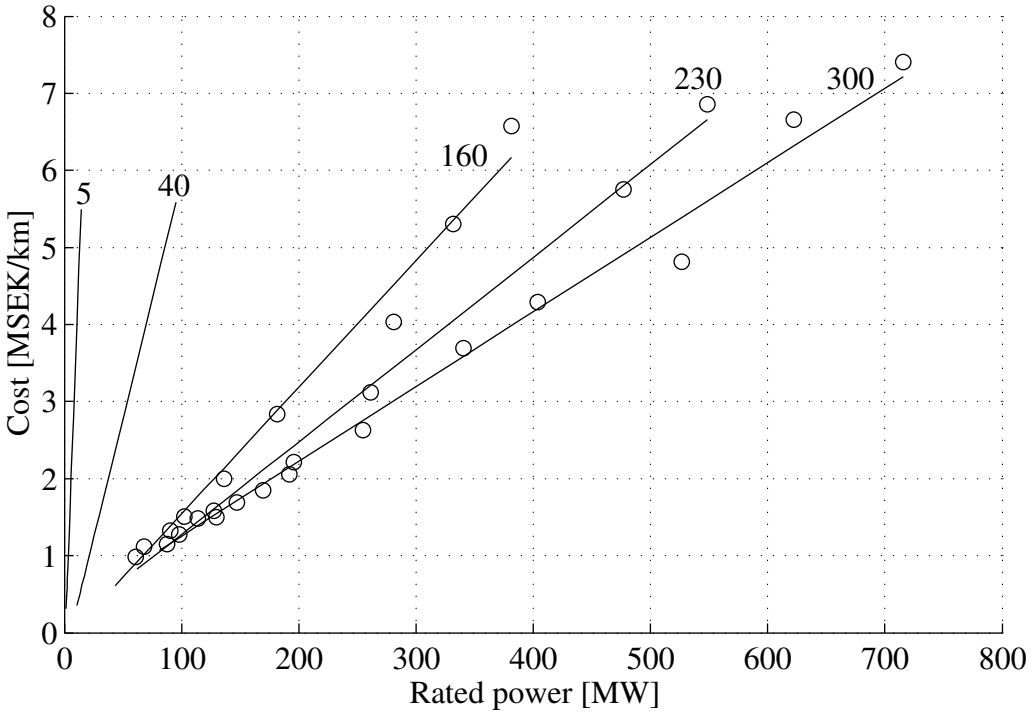

Figure C.4: The cost of the DC cables used in this work, circles costs obtained, solid model in equation C.8. The numbers in the figure indicates the rated pole to pole voltage of the cable in kV.

By comparing figure C.3 and figure C.4 it is seen that the DC cables are cheaper then the AC cables.

The installation cost for the cables are assumed to be $800SEK/m$ for land and $2400SEK/m$ for sea. DC-cables on land can be installed by ploughing. This technic is cheaper then the $800SEK/m$ mention before but it only works if there is now large stones or underearth rocks. Therefore the laying cost for land is assumed to be $800SEK/m$ for all cable types.

The cost for the cable compensating inductor is set to 2/3 of the cost for a transformer with the same VA rating. This is due to that cable compensating inductors only have one winding per phase compared to transformers that has at least two windings per phase.

C.5 Converters

The cost model for the different converters that are used in this work was difficult to obtain. The reason is that some of the converters (AC/DC) are still based on a young technics and some do not exist yet, DC/DC converters in the MW size. For the AC/DC converter, the cost will be set to 1SEK/VA. This cost is used for all the equipment between the AC connection to the DC connection and for a converter in the 150MVA size. But this cost will be used in this work for all AC/DC converters with a rating from 60MW and higher. In reality the cost of a smaller converter should be somewhat higher and for a bigger converter somewhat lower per VA.

For the DC/DC converters the same cost is used, 1SEK/VA. This is due to the fact that the total VA rating of the switches in the AC/DC converter is approximately the same for a DC/DC converter with the same rating as the AC/DC converter. This means that approximately the same amount of semiconductors are used. For the other components included in the cost of the AC/DC converter, transformer, inductors, filters etc. it has been noticed that these also are used in the large DC/DC converters, 60MW and higher, in this work. Due to this, the same cost as for the AC/DC converters are used for the DC/DC converters.

C.6 Switch gear

The cost model for the switch gear is approximated with a linear relation depending on the voltage level. In the left plot in figure C.5 the costs of the main components of the cubicles are shown, breakers (stars), disconnecters (circles) and sensors (plus signs). In the right plot the total cost of the cubicles are shown, circles, and the total component cost using the costs from the left plot are shown as stars. The lines in the two plots are least square approximations of the presented cost data. From the right

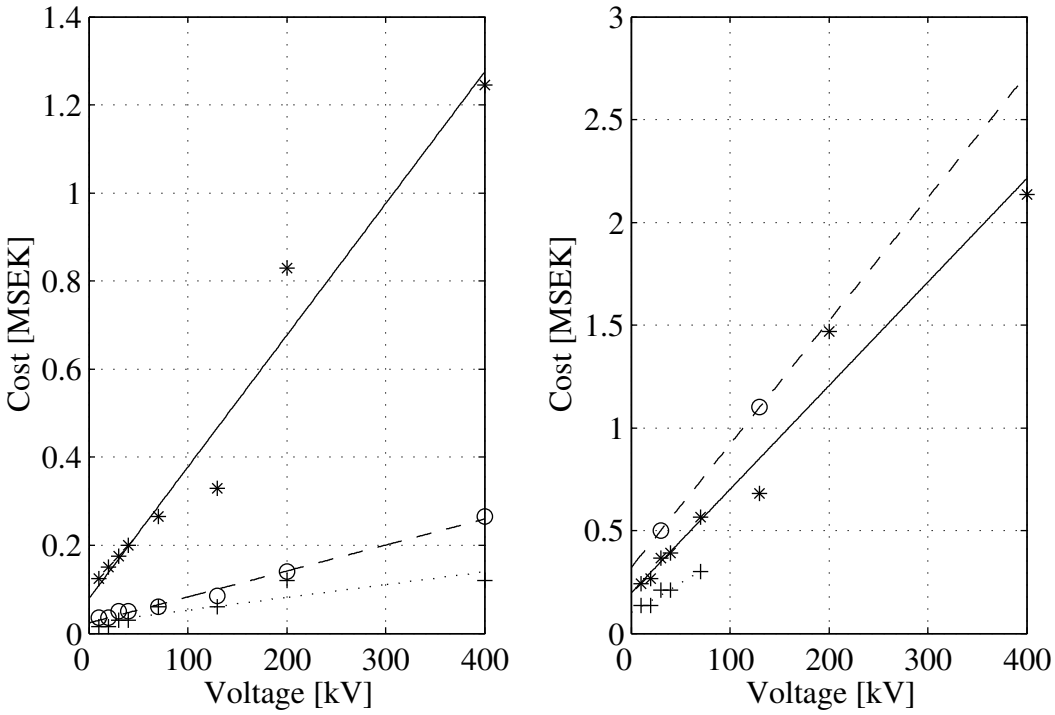

Figure C.5: In the left plot the component cost for breakers (stars), disconnecters (circles) and sensors (plus signs) are shown. The lines in the plot are least square approximations of the presented cost data. In the right plot the cost for cubicles, circles given cost data and stars the apparatus cost obtained from using the costs in the left plot. The plus signs are for the protections in the wind turbine. The lines in the plot are least square approximations of the presented cost data.

plot in figure C.5 it can be noticed that the cost models agrees well with the component costs. This is due to the fact that on top of the component cost a cost for the cabinets,

mounting and some peripheral equipment is added. The dashed line in the right plot in figure C.5 will be used to represent the cost for switch gear. The parameters for the dashed line are shown in equation C.10.

$$\text{Cost} = A_p + B_p U_{rated} \tag{C.10}$$

Where:

Cost	Cost of the cubical [SEK]
U_{rated}	Rated voltage of the switch gear, line to line [V]
A_p	Offset constant $= 320 \cdot 10^3$
B_p	Slope constant $= 6$

Of course, the cost for the transformer cubicle on the low voltage side, for example se figure 2.3, will be higher then the cost for the cubicles for the incoming lines due to the larger breaker and more protections for the transformer and busbars. But this higher cost for some of the cubicles is not taken into account in this work.

As can be noticed from the figures in chapter 4 some switch gear for the incoming lines to the wind turbines are needed. The component cost of this extra switch gear is shown in the right plot in figure C.5 as plus signs. The dotted line is the least square approximation of the presented cost data, which will be used to represent the cost for this equipment. In equation C.11 the parameters for this dotted line are shown.

$$\text{Cost}_{WT} = A_{p,WT} + B_{p,WT} U_{rated} \tag{C.11}$$

Where:

Cost_{WT}	Cost of the cubical [SEK]
U_{rated}	Rated voltage of the switch gear [V]
$A_{p,WT}$	Offset constant $= 100.33 \cdot 10^3$
$B_{p,WT}$	Slope constant $= 2.8726$

The cost functions presented in equations C.10 and C.11 are the ones used to represent the costs for switch gear in this work.

C.7 Other components

The other components in the wind farm that will have a cost in this work are the foundations for the wind turbines and in the cases it is needed, the offshore platform. For the components that have an equal cost in all wind turbine systems, the cost is neglected. This is because they are assumed to influence the result equally in all the cases and therefore they will not affect the comparison of the different cases.

In this work, all foundations for the wind turbines are assumed to be monopiles and the cost for these are set to 7.5MSEK independent of water depth and size and type of wind turbine.

The cost for the structure of the offshore platform is assumed to be described with equation C.12.

$$\text{Cost} = A_p + B_p P_{rated} \tag{C.12}$$

Where:

Cost	Cost of the structure of the offshore platform [SEK]
P_{rated}	Rated power of the wind farm [W]
A_p	Offset constant $= 20 \cdot 10^6$
B_p	Slope constant $= 0.7$

This cost model is for a quite sophisticated platform with living quarters for workers, heliport, low and high voltage switch gear and transformers or converters. Of course, in some cases a simpler platform can be sufficient. But in this work, the cost model presented in equation C.12 are used for all offshore platforms.